University of Liège

Faculty of Sciences, Department of Life Sciences

GIGA-Immunobiology, Laboratory of Virology and Immunology

Oncolytic HSV-1 armed with CXCR4-antagonist interferes with glioblastoma stem-like cells properties and disrupt pro-tumoral microenvironment

Maxime DUBOIS

Doctoral dissertation to obtain the grade of Doctor of Science in biochemistry and molecular and cellular biology.

Supervisor: Professor Catherine Sadzot

Co-supervisor: Professor Bernard Rogister

Academic year: 2025 – 2026

Acknowledgments

Nous sommes aujourd'hui le 7 mars 2026. Cette thèse est donc le fruit d'un peu plus de cinq années de travail, depuis le début de mon mémoire portant déjà sur le même sujet en janvier 2021. En réalité, mon histoire avec cette thèse est encore un peu plus longue. Je me souviens d'une visioconférence qui a dû avoir lieu courant 2020, impossible de me rappeler la date, durant laquelle différents sujets de mémoire nous avaient été présentés. Pendant longtemps, je ne me souvenais plus quel professeur avait évoqué l'idée de traiter les cancers du cerveau avec des virus oncolytiques, mais le sujet m'était resté en tête jusqu'au jour où nous avons enfin eu accès à la liste officielle des projets.

Je voudrais commencer par remercier ma promotrice de thèse, Catherine Sadzot, pour la confiance qu'elle m'a accordée en m'acceptant dans son laboratoire. Une confiance que j'espère avoir su entretenir, contre vents et marées, tout au long de cette thèse. Merci pour son soutien constant, son implication quotidienne dans mon travail, ses conseils, et ses nombreux rappels que le temps passe très, très, TRES vite. Merci également pour son écoute, pour les nombreuses discussions scientifiques et stratégiques, pour la possibilité d'argumenter d'égal à égal, et pour la grande liberté dont j'ai toujours bénéficié pour la décision finale.

Je remercie également Judit Sanchez Gil pour la dévotion avec laquelle elle a encadré le mémorant sans aucune expérience de laboratoire que j'étais. À l'époque, mon expérience se résumait à un seul stage… réalisé entièrement en télétravail à cause du Covid-19. Après quatre ans de thèse, trois mémorantes, et de nombreux stagiaires, je mesure aujourd'hui le temps et l'énergie nécessaires pour former un néophyte, ainsi que le stress supplémentaire que cela peut représenter, surtout en fin de thèse, surtout quand on sait qu'il ne travaillera jamais sur notre sujet à proprement parler. (Ah si, j'ai quand même aidé pour le reviewing du papier.)

Un grand merci également à Cédric Lassence, mon binôme, mon ombre, mon double (maléfique ?), pour les heures, les jours et les semaines passés assis côte à côte au laboratoire ou à l'animalerie, à réaliser des expériences beaucoup trop longues sur beaucoup trop d'échantillons, tout en discutant de tout et de rien. Merci pour tout le travail de fond : préparer les solutions, faire les manips dont je ne voulais plus, commander les réactifs au compte-gouttes. Merci aussi pour ses mille et une astuces : de la meilleure coupe de cheveux pour les souris de laboratoire, à la manière d'en recoudre trente avec un seul fil de suture, en passant par la technique consistant à utiliser deux gants gauches au cryostat pour en garder un chaud en permanence en s'asseyant dessus. Sans oublier les conseils pour choisir sa voiture… ou les pavés de sa terrasse.

Je tiens également à remercier Chloé Wilkin, qui a été ma véritable tutrice dans ce monde parfois hostile du doctorat. Petit à petit, elle a réussi à ouvrir quelques espaces dans ma carapace de solitaire, transformant ces cinq années d'un simple lieu de travail en un

endroit qu'on n'a finalement plus envie de quitter. Tellement que certains n'arrivent définitivement pas à se barrer… pour notre plus grand bonheur.

Merci à Marielle Lebrun pour son exaspérante énergie, à mille lieues de ma personnalité, qui aura pourtant eu tendance à me transmettre une certaine forme d'enthousiasme que je n'aurai su soupçonner chez moi. Merci aussi pour ses avis parfois divergents ou critiques sur certaines décisions, et pour son aide précieuse dans les nombreux domaines où j'étais totalement perdu. (Et merci pour les tampons de transfert, migration, etc., que je ne suis plus sûr d'en avoir déjà préparés moi-même…)

Merci également à tous les « petits nouveaux », Victoire, Manon, Marion, Florine, Lola, Clément, Sacha et Jérôme, qui ont progressivement fait de notre côté du bureau le plus stylé des deux. Grâce à vous, j'ai aussi pu, à mon tour, me sentir utile, apporter un peu d'aide et de soutien, et vraiment avoir le sentiment de faire partie d'un groupe dans mon laboratoire.

Je remercie évidemment aussi tous les membres des laboratoires de GEC et de Neurosciences pour leur aide toujours volontaire au moindre problème ou à la moindre demande. Je tiens particulièrement à remercier Bernard Rogister pour l'accueil dans son laboratoire ainsi que pour le prêt d'outils, de locaux et de réactifs chaque fois que j'en avais besoin. Merci également à Virginie Neirinckx pour ses conseils et pour son soutien apaisant tout au long de l'année.

Je remercie aussi Bénédicte Machiels pour l'apprentissage qu'elle m'a offert au sein de son laboratoire pour l'une des techniques principales de cette thèse, permettant d'isoler les cellules immunitaires du cerveau de souris. Merci également pour son apport scientifique crucial dans l'interprétation des résultats et dans ma compréhension du système immunitaire.

Je souhaite enfin remercier les membres du jury pour le temps qu'ils consacreront à la lecture et à l'évaluation de cette thèse, ainsi que pour leur présence et leurs questions lors de ma défense. Merci à vous : Giorgio Seano, Marta Alonso Roldan, Sylvie Legrand, Bénédicte Machiels, Virginie Neirinckx, Ingrid Struman, Bernard Rogister et Catherine Sadzot.

I would also like to thank the members of the jury for the time they will dedicate to reading and evaluating this thesis, and for their presence and questions during my defense. My sincere thanks to Giorgio Seano, Marta Alonso Roldan, Sylvie Legrand, Bénédicte Machiels, Virginie Neirinckx, Ingrid Struman, Bernard Rogister, and Catherine Sadzot.

Enfin, merci à mes parents, mes frères, ma sœur, mes grands-parents et mes amis pour leurs degrés divers d'intérêt pour mon travail. Merci pour la confiance qu'ils me transmettent par leur absence totale de doute en mes propres capacités, tout en me rappelant, assez souvent, que je suis très, très,… peu intelligent. Merci davantage encore

de m’avoir permis d’oublier instantanément ma thèse pendant quelques instants lorsque c’était nécessaire.

Merci à ma cohabitante légale, mon amour, oserais-je dire ma fiancée ? pour son soutien à toute épreuve. Merci, comme pour les autres, pour ta confiance, mais surtout parce que toi, mieux que quiconque, tu connais les moments de doute et de mutisme, de regret, de déprime et de nervosité. Merci pour ta présence quand il n’y a pas de mots à dire. Merci pour ta raison quand je ne veux plus entendre la mienne. Merci pour ta patience durant tous ces week-ends où il faut passer au laboratoire. Merci pour ton aide pendant l’écriture de cette thèse, alors que je ne trouve plus le temps pour rien. Merci aussi pour ton intérêt pour mon travail, que tu pourrais sûrement aller défendre à ma place, à condition de parler en métaphores de soldats russes (le cancer), allemands (le virus) et de résistants (le système immunitaire). Merci surtout parce que personne ne me rend heureux et ne me fait rire comme toi. Grâce à toi, aucun mauvais moment ne dure bien longtemps, et aucun problème ne paraît vraiment insurmontable.

Summary

Glioblastoma is the most frequent and aggressive primary brain cancer in adults, with a median overall survival of approximately 15 months. Despite extensive research efforts, no major therapeutic breakthrough has significantly improved patient prognosis over the past 25 years.

CXCR4/CXCL12 pathway plays a major role in glioblastoma aggressiveness, resistance to therapy, and recurrence. It promotes glioblastoma stem-like cells (GSCs) stemness and self-renewal, tumour invasiveness, angiogenesis, and the establishment of an immunosuppressive tumour microenvironment.

Virotherapy is a promising therapeutic strategy within the field of immunotherapy, which has shown success in several cancers but limited efficacy in glioblastoma. Oncolytic herpes simplex viruses (oHSVs) can selectively kill tumour cells while sparing healthy tissue thereby triggering a local immune response. Importantly, these viruses can also be "armed" with transgenes.

We engineered an oHSV expressing the CXCL12 antagonist CXCL12-P2G (oHSV/P2G) to simultaneously inhibit multiple pathways involved in tumour progression while stimulating anti-tumour immunity. *In* vitro, we confirmed P2G expression by oHSV/P2G infected cells, demonstrated inhibition of CXCR4 downstream signalling, and reduced CXCR4-dependent GSC stemness. Inhibition of invasiveness by oHSV/P2G was assessed both *in vitro* and in immunodeficient (athymic) orthotopic xenograft NUDE mouse models engrafted with human glioblastoma patient derived cell lines (GB138, T033).

In immunocompetent orthotopic syngeneic C57Bl6 mouse models engrafted with murine glioblastoma cell lines (GL261N4, 005-GSCs), oHSV/P2G triggered a strong immune response while impairing tumour angiogenesis. $CXCR4^+$ tumour-associated macrophages and microglia were significantly polarised to a pro-inflammatory phenotype, $CXCR4^+$ regulatory T cells were reduced, and other recruited lymphocytes (T and B cells) were increased. This resulted in a myeloid-to-lymphoid transition of the tumour microenvironment, associated with good prognosis. Notably, an indirect effect also promoted Th1 and cytotoxic profiles in $CD4^+$ and $CD8^+$ T cells, respectively, even though these populations exhibit low CXCR4 expression. Importantly, in poorly immunogenic mouse models (005-GSCs), oHSV alone did not improve median survival compared with controls, whereas oHSV/P2G significantly prolonged survival.

Future studies should investigate combination strategies with immune checkpoint inhibitors. Other immune populations, including dendritic cells, neutrophils, and natural killer cells, should also be examined, along with the specificity and memory development of the adaptive immune response. Finally, since virotherapy is currently considered a second-line treatment and the CXCR4/CXCL12 pathway contributes to tumour recurrence, relevant models should also be explored.

Résumé

Le glioblastome est la tumeur cérébrale primaire la plus fréquente et la plus agressive chez l'adulte, avec une survie globale médiane d'environ 15 mois. Malgré d'importants efforts de recherche, aucune avancée thérapeutique majeure n'a significativement amélioré le pronostic au cours des 25 dernières années.

La voie CXCR4/CXCL12 joue un rôle clé dans l'agressivité tumorale, la résistance aux traitements et les récidives. Elle favorise notamment l'auto-renouvellement et les propriétés des cellules de type souche du glioblastome (GSCs), l'invasivité, l'angiogenèse et l'établissement d'un microenvironnement tumoral immunosuppresseur.

La virothérapie constitue une approche prometteuse en immunothérapie. Elle a montré des résultats dans plusieurs cancers mais son efficacité reste limitée dans le glioblastome. Les herpès simplex virus oncolytiques (oHSV) peuvent détruire sélectivement les cellules tumorales tout en déclenchant une réponse immunitaire locale. Ils peuvent en outre être modifiés pour exprimer des transgènes.

Nous avons développé un oHSV exprimant un antagoniste de CXCL12, CXCL12-P2G (oHSV/P2G), afin d'inhiber simultanément plusieurs mécanismes impliqués dans la progression tumorale tout en stimulant l'immunité antitumorale. *In vitro*, nous avons confirmé l'expression de P2G, l'inhibition de la signalisation CXCR4 et la diminution des propriétés des GSCs, dépendantes de cette voie. L'effet anti-invasif d'oHSV/P2G a été démontré *in vitro* et dans des modèles murins NUDE orthotopiques immunodéficients greffés avec des cellules humaines de glioblastome (GB138, T033).

Dans des modèles murins orthotopiques syngéniques immunocompétents C57Bl6, greffées avec des cellules murines de glioblastome (GL261N4, 005-GSCs), oHSV/P2G a déclenché une forte réponse immunitaire tout en inhibant l'angiogenèse tumorale. Il a induit une polarisation pro-inflammatoire des macrophages et de la microglie associés à la tumeur, qui expriment CXCR4. Le nombre de lymphocytes T régulateurs $CXCR4^+$ a diminué, tandis que celui des autres lymphocytes recrutés (cellules T et B) a augmenté. Ceci a induit une reprogrammation du microenvironnement tumoral d'une majorité myéloïde à lymphoïde, associée à un meilleur pronostic. Un effet indirect a également favorisé des réponses Th1 et cytotoxiques des lymphocytes T $CD4^+$ et $CD8^+$, respectivement, qui n'exprime que faiblement CXCR4. Dans des modèles murins peu immunogènes (005-GSCs), oHSV/P2G, contrairement à oHSV seul, a significativement amélioré la survie médiane.

Des études futures devront explorer la combinaison avec des inhibiteurs de points de contrôle immunitaire. L'analyse d'autres populations immunitaires (neutrophiles, DC, NK), ainsi que de la spécificité et de la mémoire de l'immunité adaptative, sera également nécessaire. Enfin, des modèles de récidive devront être développés, compte tenu du rôle de la voie CXCL12/CXCR4 et de l'utilisation de la virothérapie en seconde ligne.

Index

Abbreviations

1p	Chromosome 1 short arm
19q	Chromosome 19 long arm
2-HG	2-Hydrocyglutarate
3-O-S HS	3-O-sulfated heparan sulphate
5-ALA	5-aminolevulinic acid
α-KG	α-Ketoglutarate
A2B5	A2b5 ganglioside epitope
AA	Amino acid
AC	Astrocyte
Ac	Adenylyl cyclase
ACK	Atypical chemokine receptor
ADAM	A disintegrin and metalloproteinase domain-containing proteins
ADCC	Antibody-dependent cellular cytotoxicity
AKT	Protein kinase
Angio-TAM	Pro-angiogenic TAM
ANXA1	Annexin A1
ALDH	Aldehyde dehydrogenase
ALKBH5	AlkB homolog 5, RNA demethylase
ANG	Angiopoietin
APC	Antigen-presenting cell
APC	Astrocyte precursor cell
ARG	Arginase
AS	Alternative splicing
ASCL	Achaete-scute family bHLH transcription
ABC	ATP-binding cassette
ATR	Ataxia telangiectasia and Rad3-related
ATM	Ataxia telangiectasia mutated
ATP	Adenosine Triphosphate
ATXR	Alpha thalassemia/mental retardation syndrome X-linked
BAC	Bacterial artificial chromosome
BAX	BCL2-associated X protein
BBB	Blood-brain barrier
BCAT	Branched-chain amino acid transaminase
BCL	B-cell lymphoma
BCLXL	B-cell lymphoma-extra large
BCR	B cell receptor
BCRP	Breast cancer resistance protein
BMDM	Bone marrow-derived macrophages
BMI	BMI1 proto-oncogene, polycomb ring finger
BRAF	Rapidly accelerated fibrosarcoma kinase
Bregs	Regulatory B cells

CAF	Cancer-associated fibroblast
CAMP	Cyclic adenosine monophosphate
CAR	Chimeric antigen receptor
CBX	Chromobox
CC	Corpus callosum
CCL	C-C motif chemokine ligand
CCN	Cellular communication network
CD	Cluster of differentiation
CDKN	Cyclin dependent kinase inhibitor
cDNA	Complementary DNA
CEBPB	CCAAT/enhancer-binding protein beta
CED	Convection-enhanced delivery
CHI3L1	Chitinase 3-like 1
CIITA	Class II transactivator
CL	Classical
CNS	Central nervous system
CNV	Copy number variation
COL	Collagen proteins
COX	Cyclooxygenase
CRMP	Collapsin response mediator protein
CSC	Cancer stem cell
CSF	Colony stimulating factor
CTL	Cytotoxic T lymphocyte
CXCL	CXC chemokine family ligand
CXCR	CXC chemokine family receptor
DAMP	Damage-associated molecular pattern molecule
DAG	Diacylglycerol
DC	Dendritic cell
DCX	Doublecortin
DDR	DNA damage response
DLL	Delta-like ligand
dsDNA	Double-stranded DNA
dsRNA	Double-stranded RNA
DSB	Double strand break
E	Early
EC	Endothelial cell
ECM	Extracellular matrix
EGFRv	Epidermal growth factor receptor variant
ELK	ETS transcription factor
EMT	Epithelial-to-mesenchymal transition
ENO	Enolase
EOR	Extent of resection
ETC	Electron transfer chain
ER	Endoplasmic reticulum
ER	Estrogen receptor
ERK	Extracellular signal-regulated kinase

EZH	Enhancer of zeste homolog
FABP	Fatty acid binding protein
FDA	Food and Drug Administration
FGS	Fluorescence-guided surgery
FGF	Fibroblast growth factor
FN1	Fibronectin
FOX	Forkhead box
frHMGB	fully reduced HMGB1
GABA	Gamma-aminobutyric acid
Gαi	G protein alpha subunits
Gβγ	G protein beta-gamma subunits
GABRA	Gamma-aminobutyric acid type A receptor subunit alpha
GBM	Glioblastoma
G-CSF	Granulocyte colony-stimulating factor
GDP	Guanosine diphosphate
GEM	Genetically engineered mouse
GFAP	Glial fibrillary acidic protein
GFP	Green fluorescent protein
GIC	Glioblastoma-initiating cells
GLI1/2	GLI family zinc ginger 1/2
GLICO	Cerebral organoid glioma
GLUT	Glucose transporter
GLS	Glutaminase
GPC	Glial progenitor cell
GPCR	G-protein-coupled receptor
GPDCL	Glioblastoma patient-derived cell line
G-protein	GTP-binding protein
GRC	Gordon Research Conference
GRK	GPCR kinase
GSC	Glioblastoma stem-like cells
GSH	(Reduced) glutathione
GSK	Glycogen synthase kinase
GSSG	(Oxidised) glutathione disulfide
GTP	Guanosine triphosphate
GTR	Gross-total resection
H3	Histone 3
HA	Hyaluronic acid
HA-tag	Hemagglutinin tag
HBD	Human beta-defensin
HCMV	Human cytomegalovirus
HIF1α	Hypoxia-inducible factor 1 α
HLDA	Human Leucocyte Differentiation Antigen
HILPDA	Hypoxia inducible lipid droplet associated
HMGB1	High Mobility Group Box 1

HSP	Heat-shock protein
HSPG	Heparan sulphate proteoglycans
HSV-1	Herpes simplex virus 1
HSPG	Heparan sulphate proteoglycan
HSPPC	Heat-shock protein peptide complex
HUVEM	Herpesvirus entry mediator
HVEM	Herpesvirus entry mediator
HSV-T	HSV-1 thymidine kinase
IAP	Inhibitor of apoptosis protein
IC	Immune checkpoint
ICAM	Intercellular adhesion molecule
ICD	Immunogenic cell death
ICI	Immune checkpoint inhibitor
ICP	Infected cell protein
IDH	Isocitrate dehydrogenase
IDO	Indoleamine dioxygenase
IE	Immediate early
IFNγ	Interferon gamma
IFNAR	Interferon receptor
IFN-TAM	Interferon-primed TAM
IgD-BCR	Immunoglobulin D B cell receptor
IGF2BP	Insulin like growth factor 2 mRNA binding protein
IL	Interleukin
Inflam-TAM	Inflammatory cytokine-enriched TAM
IMD	Intratumoral microdevice
iNOS	Inducible nitric oxide synthase
IP	Inositol trisphosphate
iPSC	Induced pluripotent stem cells
iRGD	Internalising Arginine–Glycine–Aspartic acid peptides
IRL	Inverted repeat long
IRS	Inverted repeat short
IV	Intravenous
JAK	Janus kinase
JNK	c-Jun N-terminal kinase
kDa	Kilodalton
kbp	Kilobase pairs
L	Late
L1CAM	L1 cell adhesion molecule
LAG	Lymphocyte activation gene
LA-TAMs	Lipid-associated TAM
LDHA	Lactate dehydrogenase A
LESTR	Leucocyte-derived seven-transmembrane domain receptor

LITT	Laser interstitial thermal therapy
lncRNA	long noncoding RNA
LV	Lateral ventricle
MAPK	Mitogen-activated protein kinase
MET	MET proto-oncogene, receptor tyrosine kinase
MCP	Monocyte chemoattractant family of proteins
MDM	Monocyte-derived macrophages
MDR	Multidrug resistance protein
MDSC	Myeloid-derived suppressor cell
MELK	Maternal embryonic leucine zipper kinase
MERTK	MER proto-oncogene, tyrosine kinase
MES	Mesenchymal
MET	Mesenchymal-to-epithelial transition
MEC	Major histocompatibility complexes
MGMT	O6-methylguanine-DNA methyltransferase
MIF	Macrophage migration inhibitory factor
MLH	MutL homolog
MLL	Mixed lineage leukaemia
MMP	Matrix metalloproteinases
MMR	DNA mismatch repair proteins
MRgFUS	MR-guided ultrasound
mRNA	messenger RNA
MMP	Matrix metalloproteinase
MSC	Mesenchymal stem cell
MSH2	MutS homolog 2
MSH6	MutS homolog 6
MSI	Musashi RNA binding protein
MTIC	Monomethyl-triazene-imidazole-carboxamide
MTOR	Mechanistic target of rapamycin
MGMT	O6-methylguanine-DNA methyltransferase
MYC	Myelocytomatosis oncogene
NEC	Nectin family receptor
NEFL	Neurofilament light chain
NF	Neurofibromin
NFκB	Nuclear factor kappa b
NLR	Nucleotide-binding oligomerisation domain-like receptors
NMHCIIA	Non-muscle myosin heavy chain IIA
NOD	Non-obese diabetic
NOS	Nitric oxide synthase
NPC	Neural progenitor cell

NK	Natural killer
NSC	Neural stem cell
N-ter	N-terminal
OB	Olfactory bulb
OCT	Octamer-binding transcription factor
OLIG	Oligodendrocyte transcription
OPC	Oligodendrocyte precursor cell
OS	Overall survival
OXPHOS	Oxidative phosphorylation
OV	Oncolytic virus
P	Proline
PAgs	Phosphoantigens
PAMP	Pathogen-associated pattern
PARP	Poly(ADP-ribose) polymerase
PBSF	Pre-B cell-stimulatory factor
PCV	Procarbazine, CCNU (Lomustine), Vincristine
PEG-PCL	Polyethylene glycol–polycaprolactone
PF	Platelet factor
PDGFRα	Platelet derived growth factor receptor alpha
PD	Programmed cell death protein
PDGF	Platelet-derived growth factor
PDH	Pyruvate dehydrogenase
PDK	Pyruvate dehydrogenase kinase
PDL	Programmed death ligand
PDT	Photodynamic therapy
PDX	Patient-derived xenograft
PFS	Progression-free survival
PGE	Prostaglandin
PHF5α	PHD finger protein 5 alpha
PIK3CA	Phosphatidylinositol-4,5-bisphosphate 3-kinase catalytic subunit alpha
PILRα	Paired immunoglobulin-like receptor alpha
PIP3	Phosphatidylinositol
POU3F2	POU class 3 homeobox 2
PLC	Phospholipase C
PMT	Proneural to mesenchymal transition
PN	Proneural
PpIX	Protoporphyrin IX
Prolif-TAM	Proliferating TAM
PRMT	Protein arginine methyltransferase
PRR	Pattern recognition receptor
PSP	Phosphoserine phosphatase
PTCH	Patched

pTERT	Promoter of telomerase reverse transcriptase
pTEN	Phosphatase and tensin homolog
PTPRC	Protein tyrosine phosphatase receptor type C
PTX	Plerixafor
PV	Polio virus receptor
RAF	Rapidly accelerated fibrosarcoma
RAS	Rat sarcoma
RB	Retinoblastoma
RBM11	RNA binding motif protein 11f
RBP	RNA binding protein
RC	Restriction cavity
RCD	Regulated cell death
RDC1	Receptor dog cDNA 1
Reg-TAM	Immune regulatory TAM
RELB	RELB proto-oncogene, NF-κB subunit
RFP	Red fluorescent protein
RMS	Rostral migratory stream
RNA	Ribonucleic acid
RORγ	RAR-related orphan receptor gamma
ROS	Reactive oxygen species
RR	Ribonucleotide reductase
RS	Replication stress
RSK	Ribosomal S6 kinases
RT	Radiotherapy
RTM-TAM	Resident tissue macrophage-like TAM
SALL2	Spalt like transcription
SARS2	Seryl-tRNA synthetase 2, mitochondrial
SCID	Severe combined immunodeficient
SDF1	Stromal cell-derived factor 1
SF3B1	Splicing factor 3b subunit 1
SHH	Sonic Hedgehog pathway
SHM	Somatic hypermutation
SGZ	Subgranular zone
SIRP	Signal regulatory protein
SLC12A5	Solute carrier family 12 member 5
SMAD5	SMAD family member 5
SOX	SRY-box transcription
SNAIL	Snail family transcriptional repressor
snRNA	Small nuclear RNA
snRNP	Small nuclear ribonucleoprotein
SR	Splicing regulatory proteins
STAT	Signal transducer and activator of transcription
STR	Subtotal resection
SVZ	Subventricular zone
SYT	Synaptotagmin

TAA	Tumour-associated antigens
TAM	Tumour associated macrophages and microglia
TAP1	Transporter associated with antigen processing 1
TCF	Transcription factor
TERT	Telomerase reverse transcriptase
Tfh	T follicular helper cells
TGFβ	Transforming growth factor beta
TGFBR	Transforming growth factor beta receptor
TGFBI	Transforming growth factor beta induced
TGN	Trans-golgi network
TH1	T helper 1
TIGIT	T cell immunoreceptor
TIME	Tumour immune microenvironment
TLR	Toll-like receptors
TLS	Tertiary lymphoid structures
TMB	Tumour mutation burden
TME	Tumour microenvironment
TNF	Tumour necrosis factor
TNFRSF1A	TNF receptor superfamily member 1A
TMZ	Temozolomide
TNC	Tenascin C
TOX	Thymocyte selection-associated high mobility group box
TP	Tumour Protein
TRADD	TNF receptor type 1-associated death domain protein
TRAIL	TNF-related apoptosis-inducing ligand
Treg	Regulatory T cell
TRL	Terminal repeat long
TRS	Terminal repeat short
TSA	Tumour-specific antigens
TSP1	Thrombospondin 1
TTF	Tumour treatment fields
UCHL	Ubiquitin C-terminal hydrolase
UL	Unique long
US	Unique short
VEGF	Vascular endothelial growth factor
VIM	Vimentin
VV	Viral vector
VZV	Varicella zoster virus
WHO	World Health Organisation
WNT	Wingless-related integration site
XIAP	X-linked inhibitor of apoptosis protein

Global Introduction

1. Central nervous system gliomas

1.1. Classification

Glioblastoma, sometimes abbreviated as GBM, is the most common primary brain tumour, accounting for about 60% of cases and affecting roughly 6 individuals per 100,000 each year. [1,2] The disease is highly aggressive and associated with a poor prognosis, with a median overall survival (OS) of 15 months, a progression-free survival (PFS) of approximately 7 months, and a 5-year survival rate of only 5%. [3–5]

The World Health Organization (WHO) revised the classification of central nervous system (CNS) tumours in 2021. Among these, the category of gliomas, glioneuronal, and neuronal tumours is divided into six subgroups: paediatric diffuse low-grade gliomas, paediatric diffuse high-grade gliomas, circumscribed astrocytic gliomas, glioneuronal and neuronal tumours, ependymomas, and adult-type diffuse gliomas. The latter are further classified into oligodendroglioma, astrocytoma, and glioblastoma. Gliomas display glial features, glial cells being the non-neuronal support cells of the CNS, which include astrocytes, oligodendrocytes, ependymal cells, and microglia. [1,2]

CNS tumours are graded from 1 to 4 based on histopathological features and biological aggressiveness rather than on invasiveness or metastatic potential, as in most cancers.

- **Grades 1 and 2** are classified as low-grade tumours and are characterised by low proliferative activity, limited infiltration, and mild cytological and nuclear atypia. Despite relatively favourable prognosis for low-grade tumours, recurrences are common and often involve progression to higher grades. [1,2]
- In contrast, **grades 3 and 4** are high-grade tumours, defined by marked anaplasia, pronounced nuclear atypia, and increased mitotic activity. [1,2]
    - **Grade 4** tumours are further distinguished histologically by the presence of microvascular proliferation and pseudopalisading necrosis. These tumours are highly aggressive, infiltrative, rapidly progressive, and associated with a poor prognosis and high mortality. [1,2]

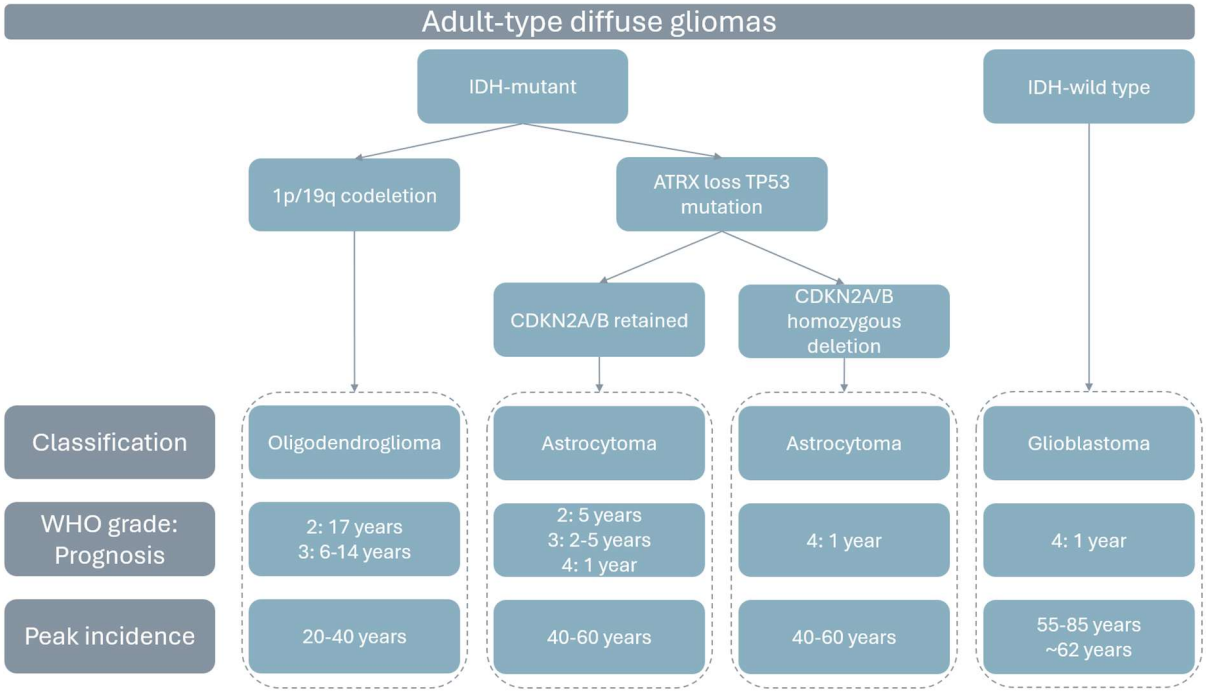

Figure 1. Adult-type diffuse gliomas classification. *This classification is based on key molecular features. IDH-mutant/1p19q-codeleted gliomas are oligodendrogliomas. IDH-mutant with ATRX loss/TP53 mutation are astrocytomas (CDKN2A/B deletion defines grade 4). IDH–wild-type gliomas are glioblastomas. This classification is associated with specific WHO grade, prognosis, and peak incidence. Inspired by Sanchez-Gil et al., 2022.*[6]

1.1.1. Oligodendroglioma and astrocytoma

Oligodendroglioma and astrocytoma can be distinguished from glioblastoma by the presence of isocitrate dehydrogenase (IDH) mutations. [1] IDH normally catalyses the conversion of isocitrate to α-ketoglutarate (α-KG). However, when mutated, it instead produces the oncometabolite 2-hydroxyglutarate (2-HG). 2-HG acts as a competitive inhibitor of α-KG-dependent dioxygenases, leading to disrupted histone demethylation and stabilisation of hypoxia-inducible factor-1α (HIF1α). IDH mutation also reduces glutamate production via α-KG-dependent *branched-chain amino acid transaminase ½ (*BCAT1/2), impairing branched-chain amino acid metabolism and creating a metabolic dependency on glutaminase. Collectively, these alterations promote gliomagenesis and impair cellular differentiation, while paradoxically conferring a less aggressive phenotype and increased sensitivity to therapy.[7]

Oligodendroglioma has the most favourable prognosis among adult-type diffuse gliomas, classified grade 2 or 3. It originates from the oligodendroglia lineage, with oligodendrocytes responsible for myelinating neural axons. It is often molecularly characterised by chromosome 1p/19q codeletion resulting from an unbalanced reciprocal translocation. [1,2,7] Oligodendroglioma exhibit relatively favourable prognosis, with OS of approximately 17 years for grade 2 and 6-14 years for grade 3 tumours **(Figure 1)**. [2,8]

Astrocytoma prognosis is poorer and depends on tumour grade, with OS of approximately 5 years for grade 2, 2-5 years for grade 3, and around 1 year for grade 4. [9] Astrocytoma is molecularly characterised by alpha thalassemia/mental retardation syndrome X-linked (ATRX) loss and tumour protein 53 (TP53) mutation, which are mutually exclusive with 1p/19q codeletion, while homozygous deletion of *cyclin dependent kinase inhibitor 2A/B* (CDKN2A/B) is sufficient to assign a grade 4 designation. Astrocytoma arises from the astrocytic lineage. Astrocytes, commonly described as star-shaped cells despite their diverse morphologies, provide structural support, organise the brain parenchyma, and regulate the microenvironment, including ion homeostasis, neurotransmitter clearance, and synaptic maintenance. [1,2] They also form the glia limitans, the outermost layer of the brain, which is of the blood-brain barrier (BBB) and has important implications for therapy resistance **(Figure 1)**. [7,10]

1.1.2. Glioblastoma

Glioblastoma is specifically defined as an IDH wild-type and histone 3 (H3) wild-type, grade 4 adult-type diffuse astrocytic glioma. Although historically considered to arise from the astrocytic lineage, the cell of origin is unclear. Glioblastoma is highly vascular, hypoxic, immunosuppressive, and exhibits pronounced inter- and intra-tumoral heterogeneity **(Figure 1)**. [1,2]

Although glioblastoma is considered of low tumour mutation burden (TMB), alterations in key regulatory genes have been identified, some of which are shared with oligodendroglioma and astrocytoma. These include mutations or deletions in the telomerase reverse transcriptase (TERT) promoter (pTERT[1]), PTEN[2], TP53, EGFR[3], NF1[4], RB1[5], and PIK3CA[6], as well as copy number variations involving MDM2[7], EZH2[8], CDKN2A/B, EGFR[9], PDGFRα[10] and CDK4. All these alterations converge on uncontrolled proliferation, enhanced survival, and overall tumour aggressiveness. This can arise from direct or indirect (1) activation of proteins that prevent senescence, or inhibition (2) of transcription factors, and (3) of upstream regulators involved in cell cycle arrest and growth control. Finally, (4) overexpression of growth factor receptors can promote cancer cell survival and proliferation **(Figure 2)**. [2,11–13]

1. TERT gene encodes telomerase reverse transcriptase, which preserves telomere stability. In normal physiology, TERT is expressed in cycling cells during embryonic

[1] Promoter telomerase reverse transcriptase
[2] Phosphatase and tensin homolog
[3] Epidermal growth factor receptor
[4] Neurofibromin 1
[5] Retinoblastoma 1
[6] Phosphatidylinositol-4,5-bisphosphate 3-kinase catalytic subunit alpha
[7] Mouse double minute 2 homolog
[8] Enhancer of zeste homolog 2
[9] Epidermal growth factor receptor
[10] Platelet derived growth factor receptor alpha

and foetal development and in self-renewing or progenitor adult cells. In cancer cells, **TERT promoter mutations** induce constitutive expression, enabling sustained proliferation. [2,11,13]

2. **TP53 mutations** result in loss of function, impairing cell cycle arrest and apoptosis in response to deoxyribonucleic acid (DNA) damage and stress. In glioblastoma, TP53 is also frequently degraded through MDM2 overexpression. Similarly, **RB1 mutations** disrupt its tumour suppressor function by preventing retinoblastoma protein binding and inhibition of E2F transcription factor, allowing S phase entry. Deletion of CDKN2A and CDKN2B, which normally inhibit CDK4, combined with CDK4 overexpression, increase RB1 phosphorylation, releasing E2F and promoting uncontrolled proliferation. [2,11,13]
3. **pTEN loss** often arises from chromosome 10 deletion. pTENα is a tumour suppressor gene that hydrolyses phosphatidylinositol 3,4,5-trisphosphate 3 (PIP3), inhibiting downstream phosphoinositide 3-kinase/protein kinase b/ mechanistic target of rapamycin (PI3K/AKT/mTOR) signalling, which promote survival, proliferation, invasion, and migration in glioblastoma cells. PIK3CA is frequently mutated in glioblastoma, resulting in constitutive PI3K activation. **NF1 loss-of-function mutation** has similar effects than pTEN loss but via the rat sarcoma/ mitogen-activated protein kinas (RAS/MAPK) pathway. [2,11,13,14]
4. Loss of chromosome 10 in glioblastoma is often accompanied by gain of chromosome 7 (+7/-10), which induces key oncogenes **overexpression** such as EZH2 methyltransferase and **EGFR**. EGFR is a transmembrane receptor tyrosine kinase that binds EGF and TGFα, promoting proliferation, angiogenesis, migration, survival, and differentiation. The most common oncogenic mutation is EGFRvIII, caused by deletion of exons 2-7, which prevents ligand binding resulting in constitutive activation. Co-expression of wild-type EGFR and EGFRvIII can create an autocrine loop, constitutively activating PI3K/AKT and RAS/MAPK signalling. Similarly, **PDGFRα amplification** drives glioblastoma progression via its ligand PDGF. [2,11,13,14]

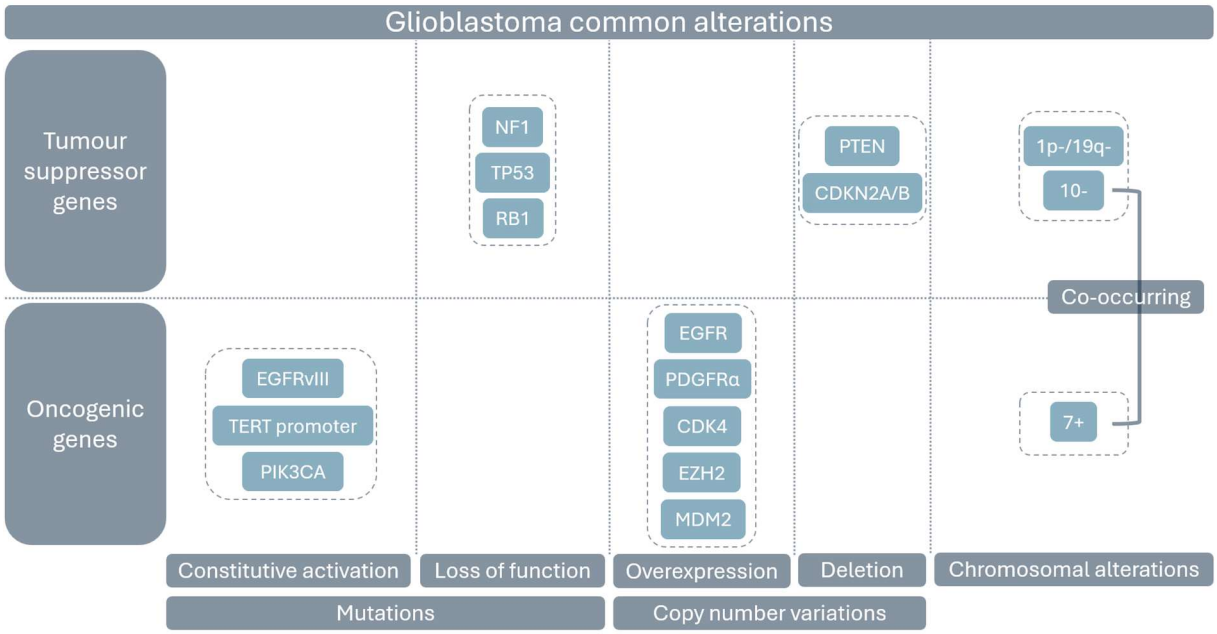

Figure 2. Glioblastoma common genetic alterations. *Cancers are often associated with alterations in tumour suppressor genes (loss-of-function mutations or deletions) and oncogenes (constitutive activation mutations or overexpression). In addition, chromosomal abnormalities may occur, including complete loss or gain of chromosomal regions. Glioblastoma exhibits all these types of alterations, involving specific recurrently affected genes and chromosomes. Original figure.*

1.2. Cell-of-origin theories

The cell-of-origin theory proposes that glioblastoma arises through the multistep accumulation of oncogenic driver mutations in normal cells, ultimately initiating tumour formation. Although the identity of the cell of origin in glioblastoma remains debated, it is clinically relevant, as inter-tumoral heterogeneity has been observed between patients, with lineage-specific gene expression signatures giving rise to distinct molecular features and prognostic outcomes, even in tumours harbouring the same initiating mutations.[13,15,16]

Candidates for the cell of origin include astrocytes (AC), astrocyte or oligodendrocyte precursor cells (APC, OPC), glial or neural progenitor cells (GPC, NPC), and neural stem cells (NSC). NSCs are present throughout the CNS during embryonic development and can initiate cell lineages. In adults, these populations arise from neurogenic niches such as the subventricular zone (SVZ) of the lateral ventricles and the subgranular zone (SGZ) of the dentate gyrus. Under physiological conditions, these regions are hierarchically organised: quiescent NSCs self-renew and occasionally generate, by asymmetric division, transient, highly proliferative progenitors (NPCs, GPCs), which differentiate into lineage-restricted precursors (neuroblasts, OPCs, APCs). The latter will then differentiate into mature astrocytes, oligodendrocytes or neurons that will usually migrate through the rostral migratory stream, along a high density of parallel blood vessels, into the olfactory

bulb, or locally within the dentate gyrus. The cell of origin likely arises from one of these populations, as proposed by two main theories: the astrocyte differentiation theory and the neural stem cell theory **(Figure 3)**. [13,16]

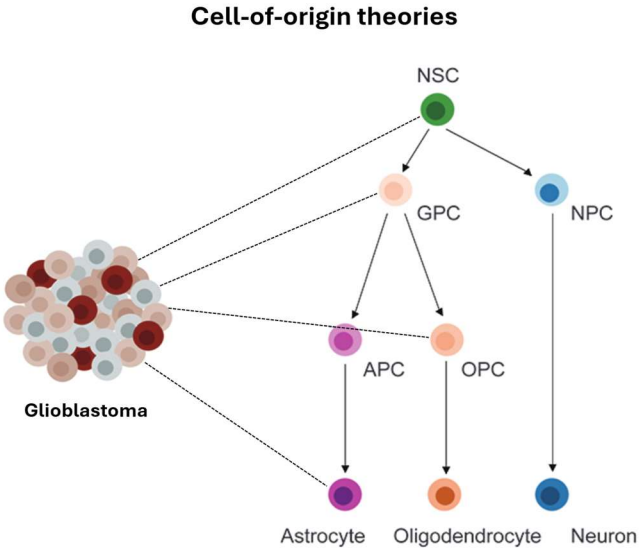

Figure 3. Cell-of-origin theories. *The glioblastoma cell of origin is still debated. Major theories point to astrocytes and neural stem cells, while highly proliferative glial progenitor cells and oligodendrocyte precursor cells are also potential candidates. NSC: neural stem cell, GPC: glial progenitor cell, NPC: neural progenitor cell, APC: astrocyte precursor cell, OPC, oligodendrocyte precursor cell. Adapted from Kim et al., 2021.*[13]

1.2.1. Astrocyte dedifferentiation theory

Historically, most cancers were thought to arise from somatic cells, with glioblastoma presumed to originate from astrocytes. For tumorigenesis, normal differentiated cells must acquire key abilities: autonomous growth, limitless replication, resistance to growth inhibition and apoptosis, sustained angiogenesis, and invasiveness. A critical step is the dedifferentiation of mature astrocytes promoting initiation of gliomagenesis. Mechanistically, this requires loss or inhibition of tumour suppressor genes (TP53, RB1, PTEN, NF1, CDKN2A/B, INK4α, ARF) alongside constitutive activation or overexpression of specific oncogenic factors (EGFR, PDGFRα, PIK3, AKT, RAS, MAPK, CDK4, MYC[11], SOX2[12], OCT4[13], KLF4[14]). [13,16,17]

1.2.2. Neural stem cell theory

A key argument for the NSC theory is that NSCs may need only oncogene activation or tumour-suppressor loss to initiate gliomagenesis. Indeed, NSCs already possess key cancer-like properties, including self-renewal and limited differentiation capacity.

[11] Myelocytomatosis oncogene
[12] SRY-box transcription factor 2
[13] Octamer-binding transcription factor 4
[14] Kruppel-like factor 4

Besides, malignant transformation through multi-step accumulation of driver mutations, which usually arise from DNA replicative errors, correlates with numerous cell divisions. Interestingly, NSCs from the subventricular zone (SVZ) has been shown to harbour low-level mutations also present in matching tumour tissue. [13,15]

1.2.3. Midway theory

Between the two extremes of mature astrocytes and undifferentiated NSCs, multipotent progenitor or precursor cells proliferate actively, possess limited self-renewal, and are committed to differentiation. These cells may acquire stem cell-like traits, including enhanced self-renewal, through oncogenic driver mutations. While malignant potential decreases with neural lineage restriction (NPCs, neuroblasts, neurons), OPCs are considered a key cell of origin, being broadly distributed beyond the SVZ and representing the most proliferative population within the brain. Moreover, PDGFRα, commonly overexpressed in glioblastoma, regulates OPCs proliferation and migration. Notably, the involvement of GPCs or APCs cannot be entirely ruled out. Alternatively, it has also been hypothesised that the cell of origin may differ from the cell in which the initial mutation occurs. [13,15,16]

2. Clinical course

2.1. Incidence

Peak incidence for adult-type diffuse gliomas varies by subtype, although they can occur at virtually any age. Oligodendroglioma is most common in young adults of 20-40 years, astrocytoma peaks between 40-60 years, and glioblastoma is most frequent between 55-85 years, with a mean age at diagnosis of 62 **(Figure 1)**. These tumours can relapse at a higher grade, partly explaining the gradual increase in peak incidence. [2]

Few predispositions have been described for glioblastoma. Nevertheless, there is a slight male predominance (approximately 1.35:1), and higher frequency of individuals of European ancestry. Most gliomas arise sporadically, while around 5% are associated with genetic syndromes such as Li-Fraumeni (germline TP53 mutation), Gardner (mutations in APC tumour suppressor gene, affecting wingless-related integration site (WNT) signalling), or Turcot (mutations in APC and DNA mismatch repair genes), or with a family history of malignant brain tumours. [2] Several negative prognostic factors exist, including increased age, corticosteroid use, and poor performance status, defined as limited work capacity, reduced ambulation or self-care ability, or confinement to bed or chair. [3,5]

2.2. Symptoms

Glioblastoma can cause headaches, nausea, vomiting, altered mental status, loss of consciousness, and, in severe cases, herniation, coma, and death. Focal neurological deficits and physical disability depend on tumour location and may include cognitive, behavioural and personality changes, depression, motor weakness, hemiparesis, or impairments in language and vision. Epileptic seizures are also common, particularly in low-grade gliomas, likely due to slower tumour growth, and lead to approximately half of initial diagnoses. [2,7]

These symptoms result from direct destruction or remodelling of the brain parenchyma by tumour growth. Hydrocephalus may also occur, arising from compression or obstruction of the ventricular system and disruption of cerebrospinal fluid flow. Pain is mainly caused by increased pressure on the vasculature, dura, or certain cranial nerves. Intracranial pressure often rises within the fixed-size skull due to the expanding tumour mass or associated oedema, which can be partially alleviated with glucocorticoids. [2]

2.3. Standard treatments

Standard treatment at diagnosis typically involves complete or partial resection of the macroscopic tumour. However, surgery is not feasible in some regions without causing significant disability, particularly in areas of the eloquent cerebral cortex, which govern essential functions such as language, motor, or sensory abilities. The brainstem is

another critical region, connecting the cerebrum and spinal cord, which controls vital autonomic functions, and serves as a major conduction pathway **(Figure 4)**. [2]

Subsequently, radiation therapy is administered (60 Gy/30 fractions, 5 fractions/week, 6 weeks) with concomitant chemotherapy using oral temozolomide (TMZ, 75 mg/m^2/day, 7 days/week). This is followed by six cycles of adjuvant TMZ at higher doses (150 mg/m^2 for 1 cycle, 200 mg/m^2 for 5 cycles of 28 days, 5 days/week). TMZ is an alkylating agent selected for its ability to cross the BBB and is converted *in vivo* to its active metabolite, monomethyl-triazene-imidazole-carboxamide (MTIC), which methylates DNA bases (O^6-guanine, N^7-guanine, N^3-adenine). O^6-methylguanine mispairs with thymine during DNA replication, activating the mismatch repair (MMR) pathway, which fails and ultimately leads to DNA strand breaks, cell-cycle arrest, and apoptosis in tumour cells **(Figure 4)**. [3,5]

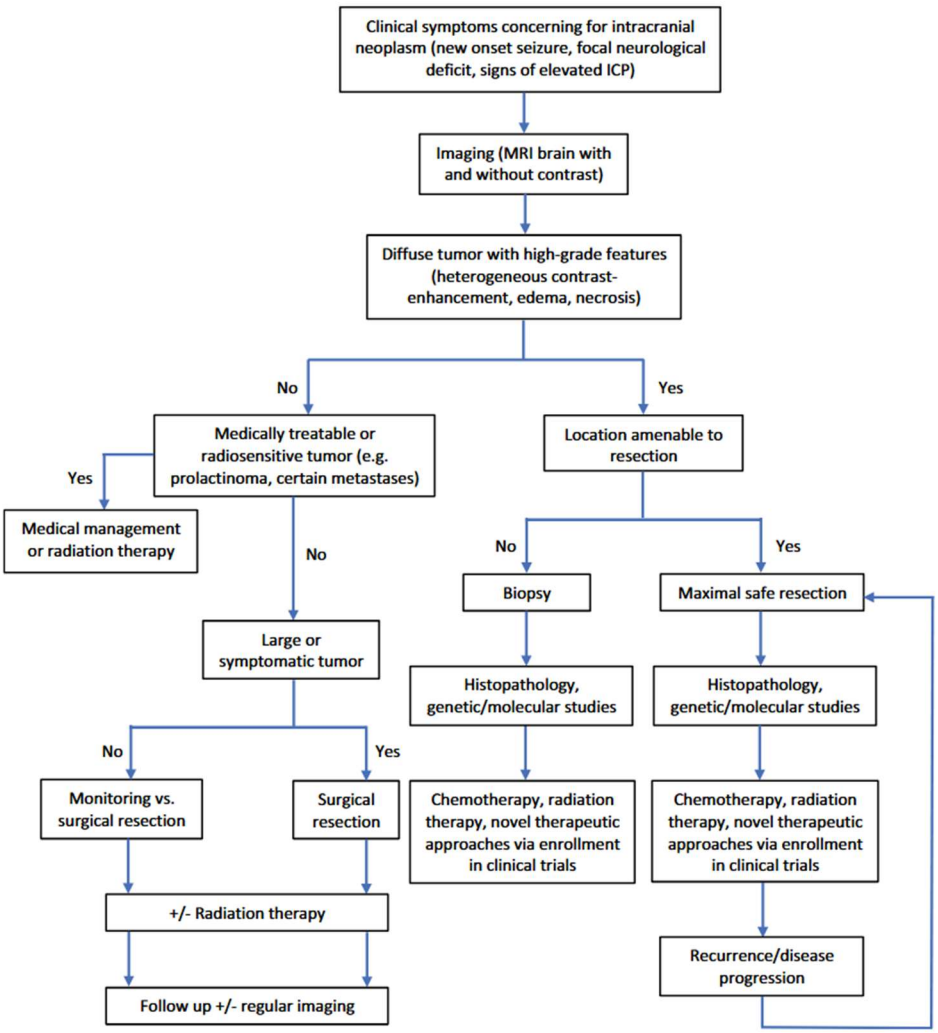

Figure 4. Standard diagnosis and treatment workflow for gliomas. *Clinical symptoms and imaging suggesting a diffuse high-grade brain tumour led to maximal resection if feasible, followed by histological and molecular diagnosis. Standard treatment is radiotherapy with chemotherapy, and clinical trial enrolment. At recurrence, management is similar and patient dependent. Unmodified from Wang et al., 2023.*[2]

2.4. Challenges for standard treatments

2.4.1. Surgical resection

Complete surgical resection is crucial, as higher extent of resection (EOR) correlates with improved outcomes. However, it is limited by tumour location and the infiltrative nature of glioblastoma, with invasive cells extending up to 2 cm beyond the macroscopic margin and migrating to distant neurogenic niches such as the SVZ. Strategies like fluorescence-guided surgery aims to maximise gross total resection (GTR, >95% removal) using fluorescent agents, such as fluorescein sodium or 5-aminolevulinic acid (5-ALA), which preferentially accumulate in malignant tissue and areas of the blood-brain barrier disruption and are visualised with adapted intraoperative microscopes. [2,11]

2.4.2. Blood-brain barrier

The blood-brain barrier poses a major challenge for intravenous drug delivery by restricting large-molecule transport and expressing efflux transporters, reducing therapeutic efficacy and increasing systemic toxicity. Strategies to improve CNS drug delivery include transiently increasing BBB permeability via MRI

[XV]-guided focused ultrasound driving microbubbles oscillation or using nanocarriers that cross the BBB via endocytosis. Alternative approaches involve intrathecal, intraventricular, or intranasal delivery (accessing the CNS via olfactory and trigeminal nerves), as well as local intra-tumoral administration through diffusion or convection-enhanced delivery. [2,11,18,19]

2.4.3. Intrinsic and treatment-induced alterations

Intrinsic and treatment-induced tumour cell alterations, distinct from canonical glioblastoma mutations, can drive resistance to standard therapies.

- First, **TMZ can induce hypermutation** through DNA repair defects, causing a ~10-fold increase in tumour mutation burden (TMB). Although elevated antigenicity may sensitise tumours to alternative therapies, hypermutated tumours are TMZ-resistant with increased proliferation, invasiveness, and immunosuppression. [11,12]
- **Epigenetic changes**, including DNA methylation, histone modifications, and chromatin remodelling, can modulate treatment response. Promoter hypermethylation of O-6-methylguanine-DNA methyltransferase (MGMT) and alkB homolog 5, RNA demethylase (ALKBH5) demethylases, limits their pro-oncogenic activity and TMZ resistance. However, promoter-independent MGMT expression sustains resistance despite specific inhibitors, and ALKBH5 silencing may also reduce anti-tumour immune responses. [11,20,21]
- **Alternative splicing (AS)** is dysregulated via protein arginine methyltransferase 5 (PRMT5) overexpression and alterations of serine and arginine rich splicing factor

[XV] Magnetic resonance imaging

3 (SRSF3) and splicing factor 3b subunit 1 (SF3B1), promoting spliceosome assembly, splice-site recognition, and oncogenic isoforms like EGFRvIII, which can further modulate AS of MYC-interacting proteins. Treatment-induced apoptosis may also trigger extracellular vesicle transfer of splicing regulators such as RNA binding motif protein 11 (RBM11), propagating AS-driven TMZ resistance. [12,20,22]

- **Post-transcriptional regulation** by long non-coding RNAs (lncRNAs) recruiting chromatin modifiers like EZH2, and microRNAs (miRNAs) further drives tumour aggressiveness and invasiveness. [12,20,22]
- Finally, radiotherapy and TMZ induce **metabolic reprogramming**, including the Warburg effect, upregulation of nutrient transporters and antioxidants, electron transport chain (ETC) remodelling, and increased reliance on fatty acids, collectively reducing reactive oxygen species (ROS) and supporting biosynthesis. Hypoxic, perivascular, and invasive tumour niches further shape these adaptations, contributing to therapeutic failure. [12,23]

2.5. Recurrence

Tumour recurrence occurs in most patients within 6-9 months after standard therapy, typically (approximately 80% of cases) at the margin of the original lesion within the resection cavity (RC). [7,12] Subtotal resection (STR) invariably leaves behind residual tumour cells, and infiltrative resistant cells may remain even after gross-total resection (GTR). [2] Then, resistance of residual cells to chemo- and radiotherapies, ultimately lead to recurrence, although the cell(s) of origin of recurrent tumours remain debated. Prognosis remains poor, with no global standard treatment beyond repeat surgery with contested benefits, chemotherapy, or radiotherapy. Patients are therefore encouraged to join clinical trials for novel therapies. [7,11,12]

2.5.1. Targeted therapies

Targeted therapies have long represented the main second-line option for recurrent tumours. Despite extensive research, clinical success remains limited due to BBB restrictions, tumour heterogeneity and niches, immunosuppression, pathway redundancy, and the absence of predictive biomarkers or personalised treatment strategies.

- These therapies target **oncogenic pathways and neoantigens**, using either FDA[XVI]-approved drugs or investigational agents. EGFR and EGFRvIII can be inhibited directly, via downstream PI3K/AKT/mTOR or RAS/MAPK/ERK[XVII] pathways, or through cytotoxic antibody-drug conjugates. Other targets include notch signalling pathway (NOTCH), WNT, and Sonic Hedgehog pathways (regulating

[XVI] Food and Drug Administration
[XVII] Extracellular signal-regulated kinase

stemness), TP53 activators (inducing apoptosis), TERT inhibitors (promoting senescence), and modulators of the RB/CDKN2A axis or CDK4 (controlling proliferation). [7,9,24,25]

- Besides, **biological features** of glioblastoma, such as invasiveness, hypoxia, and hypervascularisation, are commonly targeted. For example, bevacizumab, a humanized monoclonal immunoglobulin g1 (IgG1) antibody against vascular endothelial growth factor alpha (VEGFα), was developed to inhibit angiogenesis, although clinical benefits have been moderate. [7,9,24,25]
- Targeting less tumour-specific but **critical cancer cell functions** is also explored, including integrins (tumour-stroma interactions), tubulin and microtubules (mitosis), and nuclear/cytoplasmic transport proteins (regulating tumour suppressor localisation and drug efflux).[7,26]
- Some agents, such as vascular endothelial growth factor alpha (VEGFα), CXCR4, transforming growth factor beta (TGFβ) or transforming growth factor beta receptor 1 (TGFBR1) inhibitors, act at the **interface of targeted therapy and immunotherapy** by reducing tumour survival and immunosuppression. [27]

2.5.2. Cell-of-origin theories for recurrence

Cell-of-origin theories for recurrent tumours follow the same principles as for primary tumours, though the relationship between the initial tumour and its recurrence is of particular interest. [12] Recurrences typically arise within the resection cavity, implicating residual tumour cells, but oncogenic NSCs in the SVZ may also contribute (NSC cell-of-origin theory). Normally, NSCs migrate to the olfactory bulb via the rostral migratory stream while differentiating, but following brain injury (including tumour development or surgical resection), they can be redirected by chemokine/cytokines gradients such as tumour necrosis factor alpha (TNFα), interferon gamma (IFNγ), C-C motif chemokine ligand 2 (CCL2), and CXCL12. [28]

Hence, recurrent tumours are classified as primary- or SVZ-associated. Primary-associated tumours arise from residual infiltrative clones, sharing mutations with the original tumour in a linear evolutionary model. SVZ-associated tumours originate from NSCs carrying oncogenic mutations, migrating toward the resection cavity, and evolve independently in a branched/divergent model, sharing only SVZ mutations with the primary tumour. Alternatively, recurrence may derive from an early undetected subclone of the heterogeneous primary tumour that becomes dominant through treatment-driven selection. Notably, multifocal primary tumours may themselves follow a “multiverse” model, when seeded from distinct early clones. [28]

Clinically, knowing the cell of origin have the same importance than for primary tumours as it may impact the recurrence characteristics. Additionally, across linear, branched, and multiverse clonal evolution models, truncal mutations shared by most samples represent prime therapeutic targets. Conversely, targeting early subclone-specific

gatekeeper genes, essential for initiation but not maintenance, should be avoided. Subclones that drive tumour progression or shape the microenvironment, such as glioblastoma stem-like cells (GSCs), are also of interest. [28,29]

3. Tumour heterogeneity

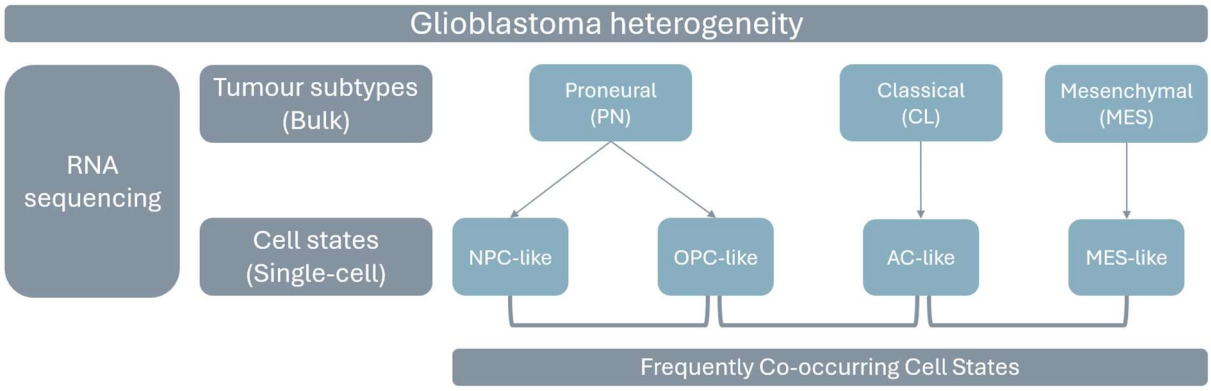

Figure 5. Glioblastoma heterogeneity. *Based on bulk RNA sequencing, three glioblastoma subtypes were identified: proneural, classical, and mesenchymal, each with distinct molecular and histological features. Single-cell RNA sequencing further resolved four tumour cell states with defined transcriptomic programs: neural progenitor cell (NPC)-like, oligodendrocyte precursor cell (OPC)-like, astrocyte (AC)-like, and mesenchymal (MES)-like. NPC- and OPC-like states are commonly enriched in proneural tumours, AC-like states predominate in classical tumours, and MES-like states are characteristic of mesenchymal tumours. OPC/AC and AC/MES also frequently co-exist within individual tumours.*[30,31] *Original figure.*

3.1. Subtypes of glioblastoma

Intra-tumoral heterogeneity in gliomas originates from early glioma clones that expand into multiple subclonal populations characterised by diverse mutation loads, CNVs, epigenetic alterations, and phenotypes. Under selective pressures such as nutrient limitation, therapeutic treatments, and external stresses, clonal competition shapes the tumour microenvironment (TME), where patient-specific subclones coexist in defined ratios, contributing to inter-tumoral heterogeneity. [12,31]

Despite the presence of numerous subclones in glioblastoma, bulk expression profiling has revealed that inter-tumoral heterogeneity is largely confined to three principal subtypes, each defined by predominant genetic mutation signatures: proneural (PN), classical (CL), and mesenchymal (MES) **(Figure 5)**. [12,30]

3.1.1. Proneural

The proneural subtype is characterised by enrichment of OPC or oligodendrocyte signatures (PDGFRα, OLIG1, OLIG2, CDK4, NKX2-2, OMG, PLP1, PLLP, TNR, ALCAM)[XVIII], overlapping with expression of developmental genes typical of NSC/NPC signatures

[XVIII] Oligodendrocyte transcription factor (OLIG), NK2 homeobox (KNX2-2), Oligodendrocyte myelin glycoprotein (OMG), Proteolipid protein (PLP), Plasmolipin (PLLP), Tenascin R (TNR), Activated leukocyte cell adhesion molecule (ALCAM)

(CD24, SOX2, SOX4, SOX11, CD133, DCX, DLL3, ASCL1, CBX1, UCHL1, CRMP1, TCF4)[XIX]. This subtype is further defined by TP53 and PIK3CA/PIK3R1 mutations associated with enhanced survival and proliferation, with a low frequency of chromosome +7/−10 events and reduced EFGR, glial fibrillary acidic protein (GFAP) and NESTIN expression. Phenotypically, proneural tumours display well-demarcated borders and are generally associated with a more favourable prognosis, despite their high proliferative potential. [15,26,30,31] *In vitro,* GSCs derived from PN glioblastoma tend to form small, tightly joined gliomaspheres. [32]

The neural subtype has occasionally been proposed as distinct from the proneural subtype. This transcription profile is associated with differentiated astrocytes, oligodendrocytes, and particularly neurons, and is characterised by enrichment of genes involved in neuronal projection and synaptic transmission neurofilament light chain (NEFL), gamma-aminobutyric acid type A receptor subunit alpha (GABRA1), synaptotagmin (SYT1), solute carrier family 12 member 5 (SLC12A5)). Its transcriptional profile most closely resembles that of normal brain tissue. [30]

3.1.2. Classical

The classical subtype is associated with an astrocytic signature (EGFR/EGFRvIII, GFAP, S100B, SLC1A3, GLAST, MLC1)[XX], a chromosome +7/−10 event, and deletion of CDKN2A/B, but not of other RB pathway components (RB1, CDK4, CCND2), and typically lacks TP53 mutations. It is also characterised by elevated expression of stem cell-related markers and activation of NOTCH (NOTCH3, JAG1, LFNG)[XXI] and Sonic Hedgehog (SMO, GAS1, GLI2)[XXII] signalling pathways. [12,30,31]

3.1.3. Mesenchymal

The mesenchymal subtype is reported as the most aggressive, with the shortest median OS, and associated with high expression of astrocytic (EGFR, GFAP) and microglial (CD68, PTPRC, TNF, MERTK)[XXIII] markers. Molecularly, it is primarily defined by NF1 mutation or deletion, frequently accompanied by PTEN mutation, implicated in RAS/MAPK and PI3K/AKT pathways. These tumours also exhibit mesenchymal markers (VIM, CHI3L1, MET, S100A4, ANXA1, SARS2, CD44, SMAD5, TGFBI)[XXIV] and increased expression of TNF

[XIX] Doublecortin (DCX), Delta-like ligand (DLL), Achaete-scute family bHLH transcription (ASCL), Chromobox (CBX), Ubiquitin C-terminal hydrolase (UCHL), Collapsin response mediator protein (CRMP), Transcription factor (TCF)

[XX] S100 calcium binding protein B (100B), Solute carrier family 1 member 3 (SLC1A3), Glutamate aspartate transporter (GLAST), Megalencephalic leukoencephalopathy with subcortical cysts (MLC)

[XXI] Jagged canonical notch ligand 1 (JAG), LFNG O-fucosylpeptide 3-beta-N-acetylglucosaminyltransferase (LFNG)

[XXII] Smoothened, frizzled class receptor (SMO), Growth arrest specific (GAS), GLI family zinc finger (GLI)

[XXIII] Protein tyrosine phosphatase receptor type C (PTPRC), Tumour necrosis factor (TNF), MER proto-oncogene, tyrosine kinase (MERTK)

[XXIV] Vimentin (VIM), Chitinase 3-like 1 (CHI3L1), MET proto-oncogene, receptor tyrosine kinase (MET), S100 calcium binding protein A4 (S100A4), Annexin A1 (ANXA1), Seryl-tRNA synthetase 2, mitochondrial (SARS2), SMAD family member (SMAD), Transforming growth factor beta induced (TGFBI)

family and nuclear factor kappa b (NFκB) pathway components (TRADD, RELB, TNFRSF1A)[XXV]. Histologically, they are highly invasive and hypoxic (HIF1α, HILPDA, ENO2, LDHA)[XXVI], display extensive necrosis, and show pronounced infiltration of tumour-associated macrophages and microglia (TAMs, via CSF2, IL3/4/5/13, CXCL14)[XXVII] [12,26,30,31] *In vitro*, GSCs derived from MES glioblastoma form larger, irregular, grape-like spheroids. [32]

3.2. Glioblastoma cell states

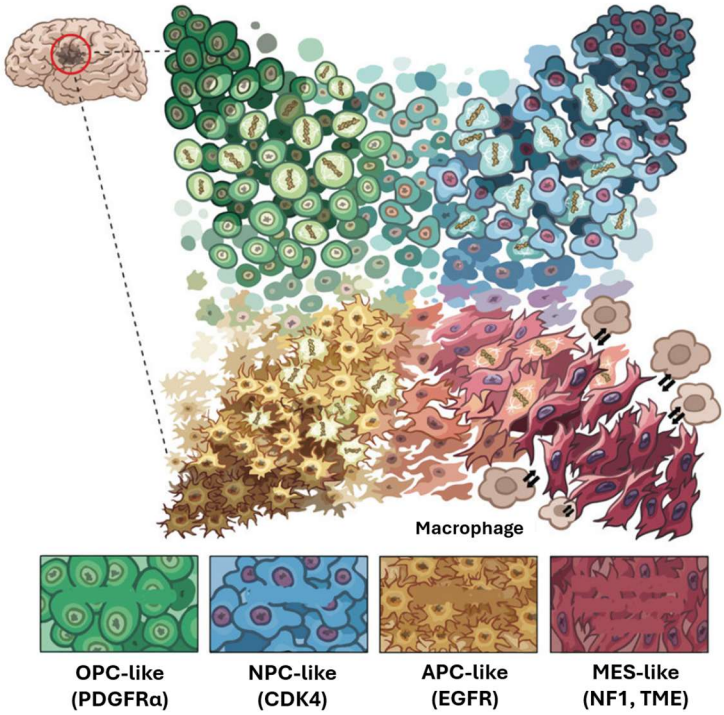

Figure 6. Glioblastoma cell states. *These cell states are dynamic and plastic but can be identified by transcriptomic markers and have distinct functional characteristics, leading to treatment resistance or differential responses to therapy.* CDK4 overexpression is associated with NPC-like states, PDGFRα with OPC-like states, and EGFR with AC-like states, while NF1 alterations and tumour microenvironment (TME) signals, particularly from TAMs, are linked to MES-like states. *Adapted from Neftel et al., 2019.*[31]

Single-cell RNA sequencing has revealed that the three principal glioblastoma subtypes correspond to distinct cellular states. The classical (CL) subtype is predominantly associated with the astrocyte-like (AC-like) state, while the PN subtype comprises two co-existing substates, OPC-like and NPC-like, which account for the overlapping transcriptional features observed in bulk RNA sequencing. The MES subtype corresponds

[XXV] TNF receptor type 1-associated death domain protein (TRADD), RELB proto-oncogene, NF-κB subunit (RELB), TNF receptor superfamily member 1A (TNFRSF1A)
[XXVI] Hypoxia inducible factor 1 subunit alpha (HIF1α), Hypoxia inducible lipid droplet associated (HILPDA), Enolase (ENO)
[XXVII] Tumour-associated macrophages (TAM), Colony stimulating factor 2 (CSF), Interleukin (IL)

to tumour cells in the MES-like state and a high abundance of myeloid cells. These cellular states correlate with characteristic genetic alterations: CDK4 overexpression with the NPC-like state, PDGFRα with OPC-like, EGFR with AC-like, and NF1 mutations with MES-like state. Such alterations preferentially promote the expansion and stabilisation of specific cell states and their associated TME, thereby driving tumour progression. However, cell-state identity is not strictly determined by genotype, and multiple states can coexist within a single subclone, contributing to intra-tumoral heterogeneity. This cellular plasticity may be influenced by tumour niches, with oxygen- and nutrient-rich vascularised regions favouring NPC-/OPC-like states, while hypoxic or necrotic regions promote MES-like profiles. Consequently, most glioblastoma encompass all four states, with every tumour containing at least two, most commonly AC-/MES-like, NPC-/OPC-like, or AC-/OPC-like **(Figure 5, 6)**. [12,31,33]

The interplay between subclone heterogeneity and cellular plasticity is a key driver of therapy resistance and relapse, highlighting the need for multimodal strategies targeting multiple subclones and states simultaneously. Subtypes differ in therapy sensitivity, as radiotherapy primarily affects PN tumours, whereas TMZ is more effective against CL tumours. Moreover, a single therapy may impact different pathways depending on the subclone. For example, integrin subunit alpha 6 (ITGA6) inhibition reduces stemness in PN tumours but alleviates radioresistance in MES-like tumours. Cellular plasticity can also drive treatment-induced transitions, such as proneural-to-mesenchymal shift after radiotherapy. [12,31,32]

Adding further complexity, ~15% of glioblastoma cells display hybrid PN-MES phenotypes, often associated with upregulated DNA damage repair, G2/M phase enrichment, reversible alterations, therapy resistance, recurrence, and poor prognosis. This hybrid subclones are highly responsive to microenvironmental cues. Indeed, cells near non-hypoxic tumour cores exhibit high proliferation, enlarged nuclei, resistance to cell death signals, enhanced nuclear import/export, and MYC activity, whereas vessel-co-opting cells are slow-cycling, invasive, angiogenic, stem-like, and senescent-like. [26,34]

3.3. GSCs

3.3.1. Definition

Glioblastoma stem-like cells (GSCs) share many features with hybrid cells. GSCs are multipotent, undifferentiated, self-renewing, stem-like cells, capable of forming gliomaspheres in serum-free conditions. Upon serial transplantation, GSCs initiate tumour formation and regenerate full tumour heterogeneity. Their proliferative or quiescent behaviour depends on their degree of differentiation, the microenvironment (which they actively modulate), and their transcriptional state with AC-like signatures promoting gliomagenesis and quiescence, and NPC-like supporting proliferation. Highly invasive and resistant to chemo- and radiotherapy, GSCs often persist post-surgery,

contribute to relapse, and are enriched in recurrent tumours, making them critical therapeutic targets. [20,35,36]

No single marker is entirely sensitive or specific for GSCs, though numerous proteins contribute to their maintenance, including surface markers (CD133, CD15, L1CAM, A2B5, CD90, CD44, CXCR4, ITGA6)[XXVIII], transcription factors (SOX2, SOX3, STAT3, SALL2, POU3F2, OLIG2, SNAIL, OCT4, MYC, ASCL1)[XXIX], epigenetic or post-transcriptional regulators (MSI1, RBPJ, IGF2BP2, BMI1, PHF5α, MELK, PSP, MLL5, ALKBH1/5)[XXX], transporters and metabolic regulators (ALDH, GLUT3, iron transporters)[XXXI], and functional proteins (NESTIN, SURVIVIN, MMP9)[XXXII]. Stemness-associated pathways include Sonic Hedgehog (SHH, PTCH, GLI1/2, NANOG)[XXXIII], WNT/βCATENIN, NOTCH, FOXM1, and NFκB, while canonical glioblastoma drivers such as EGFRvIII or PTEN also support GSC-state persistence. [20,23,37]

The origin of GSCs remains debated as they may arise from NSCs or through dedifferentiation of tumour cells that reacquire stem-like programmes via genetic alterations. Unlike NSCs, they follow abnormal multicellular development programmes, carry founder oncogenic mutations and arise during tumorigenesis, shaped by the TME. Although sometimes called glioblastoma-initiating cells (GICs) due to their tumour-initiating capacity, GSCs are distinct from cell of origin of the primary tumour, but may play a role in tumour recurrence. [23,38]

3.3.2. Contribution to heterogeneity

Beyond subclonal and cell-state diversity, glioblastoma exhibits a developmental hierarchy. The four mature tumour states (NPC-like, OPC-like, AC-like, MES-like) mirror neural and glial lineages, while GSCs constitute a heterogeneous subset of undifferentiated, NSC-like cancer stem cells.[13,31,32] GSCs drive heterogeneity and plasticity through high transcriptional entropy (oscillating, low-level expression of a broad gene set), and a permissive epigenetic landscape, enabling dynamic, stochastic occupation of diverse microstates in response to environmental stimuli, while maintaining multipotency.[20,36]

This hierarchical model of cellular differentiation suggests a unidirectional progression from GSCs to differentiated progeny with more restricted transcriptional programmes and

---

[XXVIII] L1 cell adhesion molecule (L1CAM), A2b5 ganglioside epitope (A2B5)

[XXIX] Signal transducer and activator of transcription (STAT), Spalt like transcription factor (SALL), POU class 3 homeobox (POU3F2), Snail family transcriptional repressor (SNAIL), Octamer-binding transcription factor (OCT),

[XXX] Musashi RNA binding protein (MSI), Ecombination signal binding protein for immunoglobulin kappa j region (RBPJ), Insulin like growth factor 2 mRNA binding protein 2 (IGF2BP2), Proto-oncogene, polycomb ring finger (BMI), PHD finger protein 5 alpha (PHF5α), Maternal embryonic leucine zipper kinase (MELK), Phosphoserine phosphatase (PSP), Mixed lineage leukaemia protein (MLL),

[XXXI] Aldehyde dehydrogenase (ALDH), Glucose transporter (GLUT)

[XXXII] Matrix metallopeptidase (MMP)

[XXXIII] Sonic hedgehog (SHH), Patched (PTCH), GLI family zinc finger (GLI),

reduced plasticity. However, interconversion between GSCs and differentiated cancer cells is also possible, potentially due to retained transcriptional entropy in the latter, or through series of reversible transitions among multiple microstates induced by microenvironmental or treatment-related cues.[20,36]

3.3.3. Niches

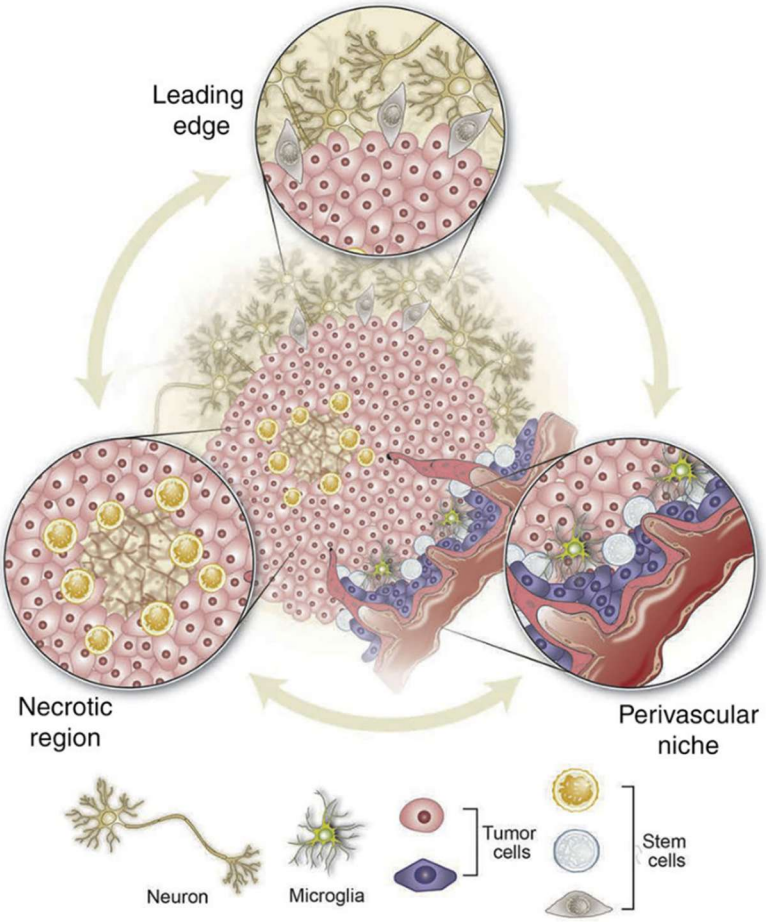

Figure 7. GSCs niches. *Glioblastomas exhibit three major interrelated regions that sustain GSCs and promote specific features: hypoxic, perivascular, and invasive niches. Neurons, microglia, stem cells, and tumour cells each contribute to the formation and maintenance of these niches, while their phenotypes are in turn shaped by the evolving microenvironment. Unmodified from Prager et al., 2020.*[36]

The concept of niches, originally used to describe regions where NSCs reside and remain self-renewing through local secreted factors, has been extended to areas of high GSCs density in glioblastoma. Three inter-related GSCs niches are described: the hypoxic-necrotic core, the perivascular niche, and the invasive edge. Each niche activates distinct transcriptional, epigenetic, and functional programmes in GSCs, which in turn remodel their microenvironment. Thereby, they constitute communication centres where cells interact by direct cell-cell contact, and by paracrine and autocrine loops **(Figure 7)**. [16,23,36]

- **Hypoxic-necrotic core:** Hypoxia is a common feature of glioblastoma arising from vascular occlusion or rapid tumour expansion outpacing angiogenesis, with normal brain and tumoral oxygenation around 40 and 10 mmHg, respectively. [12] Moreover, glioblastomas contain particularly hypoxic, necrotic cores surrounded by pseudopalisading tumour cells. Hypoxic stress in nutrient-restricted conditions is regulated by HIF1α and HIF2α, which are themselves regulated by the PI3K/AKT pathway and, thus, upregulated by PTEN loss. [12,23,36] HIF pathways drive metabolic and mesenchymal shifts in GSCs, including glucose (GLUT1/3) and ATP-binding cassettes (ABC) transporters upregulation, enhanced glycolysis, migration, quiescence, and therapy resistance. HIF2α, elevated under chronic hypoxia, promotes stemness through SOX2 and OCT4, while HIF1α regulates stemness, survival, invasion, and induces VEGFα to trigger angiogenesis, which initiates formation of the perivascular niche. [23,36,37]
- **Perivascular niche:** VEGFα receptors (VEGFRs) and co-receptors such as neuropilins (NRP1/2) are primarily expressed on endothelial cells (ECs), and their activation promotes ECs migration and proliferation, driving neoangiogenesis and contributing to the characteristic microvascular proliferation of glioblastoma. In perivascular niches, GSCs interact with endothelial cells (ECs) and astrocytes along capillaries and arterioles. GSCs proliferation displaces astrocytic end-feet and pericytes, further promoting angiogenesis. ECs, supported by pericytes and tumour-associated macrophages and microglia (TAMs), secrete factors sustaining GSCs stemness (NOTCH, SHH, NO, cGMP[XXXIV], ANGPT1/2[XXXV]), migration (via MMP9), DNA repair, and therapy resistance (TGFβ). ECs and pericytes also release CXCL12, which recruits $CXCR4^+$ GSCs (vascular co-option) and enhances their stemness, invasiveness, and resistance. In turn, GSCs maintain and amplify the niche by secreting high levels of VEGFα, and, by a paracrine and autocrine loop, can even acquire $VEGFR^+$ pericyte-like or endothelial-like phenotype (vascular mimicry), thereby supporting vessel stability, BBB integrity, tumour neovascularisation, and thus tumour growth. [16,20,36]
- **Invasive edge:** The hypoxic and perivascular niches together create a hypoxic periarteriolar microenvironment that enhances GSCs migration abilities and promotes their enrichment at the invasive edge, allowing them to evade from surgical resection. Their migration is further influenced by the extracellular matrix (ECM) composition and tissue stiffness, especially along blood vessels and white matter tracts. GSCs migration is driven by chemoattractant receptors such as CXCR4 and by high expression of MMPs (MMP2, MMP9, ADAMTS2[XXXVI]) that degrade and remodel the ECM. [36] Mechanistically, tumour cell migration relies on epithelial-to-mesenchymal transition (EMT), during which cells lose adhesion to

[XXXIV] Cyclic guanosine monophosphate
[XXXV] Angiopoietin
[XXXVI] ADAM metallopeptidase with thrombospondin

the ECM and to neighbouring tumour cells, enabling invasion, intravasation, and dissemination. Tumour cells undergoing EMT typically activate STAT3 which downregulates epithelial markers like epithelial cadherin (E-CADHERIN) and upregulates mesenchymal markers such as neural cadherin (N-CADHERIN), VIMENTIN, SNAIL, and snail family transcriptional repressor 2 (SLUG). After reaching a supportive niche, they can form secondary tumours through the reverse process, mesenchymal-to-epithelial transition (MET). [39,40]

Beyond these niches, additional ECM components and non-neoplastic cells, including neurons, astrocytes, ECs, mesenchymal stem cells, TAMs, and other immune cells, also contribute to GSCs maintenance. [20,36]

3.3.4. SVZ, a distant neurogenic niche

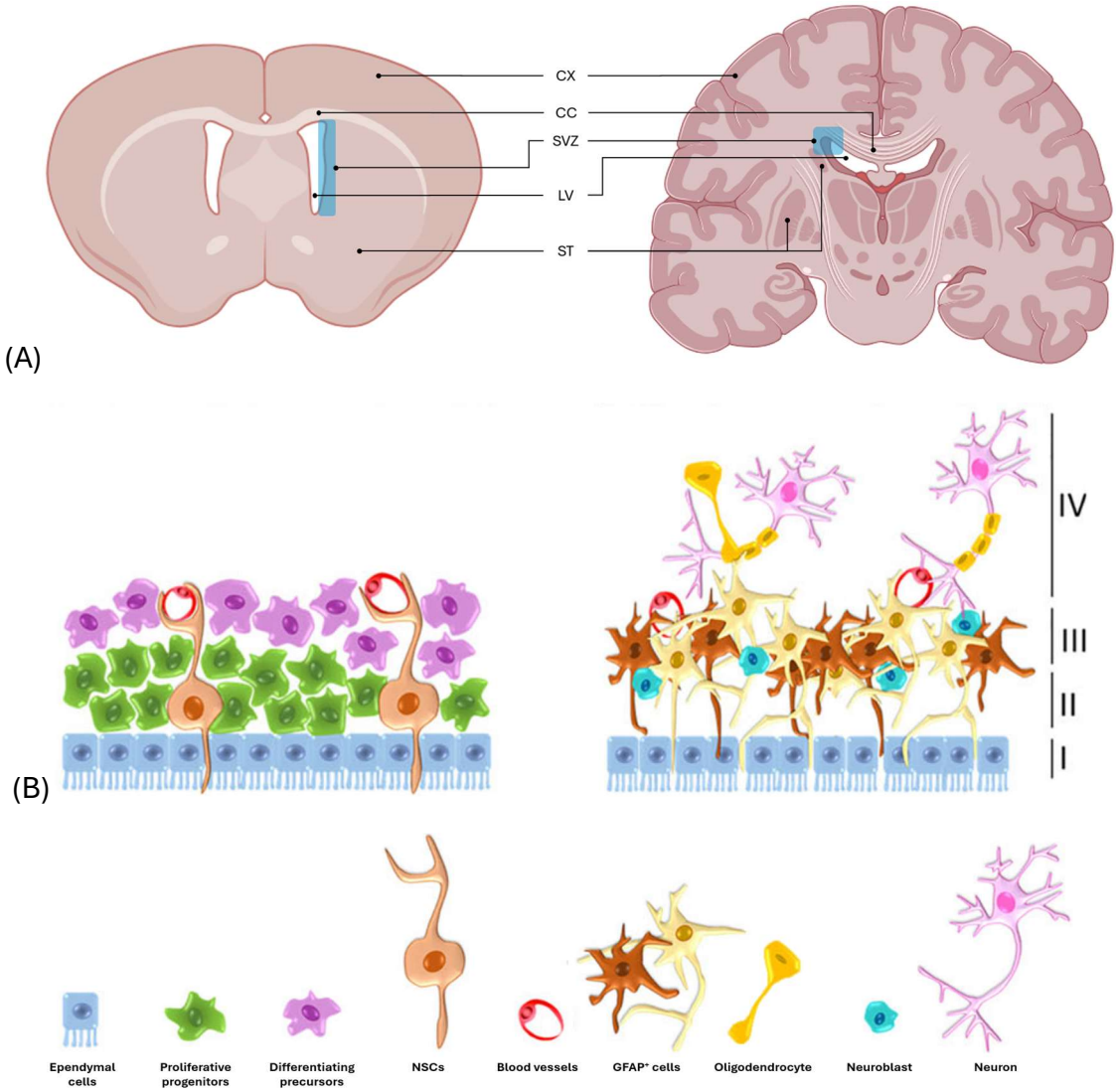

Figure 8. Mouse and human sub-ventricular zone. ***(A)*** *In both mouse and human, the SVZ is located along the lateral walls of the lateral ventricles, and right and left hemispheres SVZ are connected via the corpus callosum.* ***(B)*** *The SVZ is organized into several layers composed primarily of blood vessels, neural stem or progenitor cells, and*

supporting cells. SVZ: Subventricular zone; CC: Corpus callosum; LV: Lateral ventricles; CX: Cortex; ST: Striatum. ***(A)*** *Original figure created in BioRender.com.* ***(B)*** *Adapted from Lombard et al., 2021.*[37]

Two main neurogenic niches host and maintain self-renewing state of NSCs in the adult brain, the subventricular zone (SVZ) of the lateral ventricles and the subgranular zone (SGZ) of the dentate gyrus. The SVZ, located along the lateral wall of the lateral ventricles (LVs), is the largest and best-characterised neurogenic niche. In the human brain, it comprises four layers from the innermost to the outermost: a monolayer of ependymal cells, a hypocellular gap, an astrocytic ribbon containing ECs, microglia, NSCs and progenitor cells, and a transition zone adjacent to the parenchyma composed of myelinated axons and oligodendrocytes. In mice, the SVZ is denser but simpler in organisation, with a similar ependymal layer followed by several layers enriched in NSCs, progenitors, and differentiating neuroblasts and OPCs **(Figure 8)**.[37,41] SVZ microenvironment is shaped by specific secreted factors, ECM composition, and the availability of circulating nutrients and oxygen provided by the extensive vasculature and proximity to the BBB, collectively supporting NSCs quiescence and self-renewal. [37,42]

The SVZ contributes to glioblastoma initiation, maintenance, resistance, and recurrence, and tumour proximity to the LVs correlates with poor prognosis. This may reflect its function as a supportive niche for GSCs. Indeed, multiple SVZ-derived chemoattractants, including IL8/16, CCL2/3/12/19/20, CXCL1/12, and CX3CL1, direct GSCs migration from the invasive edge towards the ipsilateral and contralateral SVZ along the *corpus callosum* (white fibre tract connecting both hemispheres). Once there, GSCs definitely evade surgical resection and benefit from a microenvironment promoting survival, self-renewal, quiescence, migration, MES-like features, and therapy resistance. [37,41] Notably, GSC migration is bidirectional as they can follow NSC-like trajectories toward the olfactory bulb. Furthermore, oncogenic NSCs or GSCs may also deviate from these routes to migrate towards the tumour core or, post-surgery, into the resection cavity, thereby contributing to tumour recurrence. [41]

3.3.5. Resistance to therapy

GSC therapy resistance is primarily driven by their heterogeneity and plasticity, reinforced by distinct tumour niches. Accordingly, GSC populations fluctuate dynamically and adapt to treatment through metabolic and epigenetic remodelling, selection of pre-existing resistant subclones, or emergence of new resistant populations. For instance, RT induces a NFκB-driven MES-like signature, and anti-angiogenic therapies reorganise the tumour around hypoxic and invasive niches. TMZ and RT select for quiescent, highly DNA-repair-competent, and anti-apoptotic GSCs. Finally, TMZ-associated mutational signatures are enriched in recurrent tumours. [20,36]

Beyond plasticity, GSCs possess intrinsic resistance mechanisms. They upregulate pro-survival pathways (PI3K/AKT, SHH, NOTCH, WNT/βCATENIN), anti-apoptotic regulators

(FLIP, BCL2, BCLXL)[XXXVII], and inhibitor of apoptosis proteins (XIAP, cIAP1/2, NAIP, SURVIVIN)[XXXVIII], thereby blocking caspase activation. DNA repair capacity is enhanced through activation of ATR[XXXIX], ATM[XL], RAD17[XLI], CHK1/2[XLII], PARP1[XLIII], TIE2[XLIV], MGMT and KU70, the latter also inhibiting BAX[XLV]-mediated apoptosis. Specifically, chemoresistance arises through ABC transporters (BCRP1, MDR1)[XLVI], which efflux multiple drugs. Radioresistance involves CXCR4/CXCL12 signalling and constitutively elevated replication stress caused by transcription-replication collisions on large neural genes, forming R-loops, and activating fork-stabilising and DNA repair pathways. Resistance is also mediated by niche-induced quiescence (reduced DNA synthesis), MES-like state (AKT-dependent repair), and chronic hypoxia (with reduced reactive oxygen species generation, supressed electron transport chain activity, and increased antioxidants levels). [12,23,32,42–44]

Finally, GSCs actively establish an immunosuppressive microenvironment to evade the immune system. They downregulate innate immune sensors (TLRs) and antigen presentation (MHCs), polarise TAMs toward immunosuppressive phenotypes through secretion of anti-inflammatory cytokines (TGFβ, CXCL12, CSF1, MIC1, IL10)[XLVII], and upregulate immune checkpoints (PDL1) inhibiting cytotoxic T lymphocytes and activating regulatory T cells. [20]

[XXXVII] FLICE-like inhibitory protein (FLIP), B-cell lymphoma (BCL), -cell lymphoma-extra large (BCLXL)
[XXXVIII] X-linked inhibitor of apoptosis protein (XIAP), Cellular inhibitor of apoptosis protein (cIAP), NLR family apoptosis inhibitory protein (NAIP)
[XXXIX] Ataxia telangiectasia and Rad3-related
[XL] Ataxia telangiectasia mutated
[XLI] RAD17 checkpoint clamp loader component
[XLII] Checkpoint kinase
[XLIII] Poly(ADP-ribose) polymerase
[XLIV] TEK receptor tyrosine kinase
[XLV] BCL2 associated X protein
[XLVI] Breast cancer resistance protein (BCRP), multidrug resistance protein (MDR)
[XLVII] Colony stimulating factor (CSF), Macrophage inhibitory cytokine (MIC)

4. Tumour microenvironment

Glioblastoma tumour microenvironment (TME) plays a fundamental role in tumour development, survival, aggressiveness, and therapeutic resistance. It is composed of non-neoplastic healthy cells including neurons, astrocytes, oligodendrocytes, microglia, endothelial cells (ECs), mesenchymal stem cells (MSCs), cancer-associated fibroblasts (CAFs) and infiltrating immune cells, along with the extracellular matrix (ECM) and secreted or exosome-associated factors (proteolytic enzymes, growth factors, cytokines, chemokines). These components will be briefly described in the following section, with particular emphasis on the tumour immune microenvironment.

4.1. Extracellular matrix

The often overlooked ECM plays key roles in regulating tumour behaviour, progression, invasiveness, and therapeutic response by shaping the TME through physical support, biochemical signalling, and control of cell adhesion, migration, proliferation, and differentiation. ECM is composed of the basement membrane and stromal connective tissue matrix forming a complex and dynamic three-dimensional network. ECM complexity derives from heterogeneous composition, including small molecules and metabolites, growth factors, integrins, collagens, elastin, proteoglycans, and glycoproteins (tenascin C, fibronectin, thrombospondin 1, laminins), as well as glycosaminoglycans like hyaluronan ((Hyaluronan) HA, ligand for CD44). ECM dynamism results from continuous remodelling driven by growth factors, cytokines, as well as proteases, including cathepsins, serine proteases, matrix metalloproteinases (MMPs), ADAMs, and ADAMTSs, which alter ECM stiffness and composition, influencing tumour and immune cells recruitment, trafficking, proliferation, and function. Indeed, collagens, fibronectin, and tenascin C can have context-dependent pro- or anti-tumorigenic effects, modelling tumour immunity and metastasis. HA promotes Tregs recruitment, M2-TAMs polarisation, and survival of $CD44^+$ MES-like glioma cells, whereas thrombospondin 1 can maintain tumour dormancy by promoting M1-TAMs recruitment. Moreover, the ECM promotes hypoxia, angiogenesis, and immunosuppression by limiting oxygen and nutrient diffusion and favouring tumour cell-cell over cell-ECM adhesion. [39,45–47]

4.2. Secreted factors

Secreted factors are key regulators of the TME, promoting tumour growth, angiogenesis, invasion, and immune modulation. Growth factors are typical soluble factors including EGF, PDGF, fibroblast growth factor (FGF), hepatocyte growth factore (HGF), ANG1/2, TGFβ, and VEGFα. Cytokines and chemokines, including CSF1/2, colony stimulating fator (CCLs), CXCLs, and ILs, further modulate immune response and tumour growth. Besides, tumour cells secrete excess metabolites and ions because of metabolic reprogramming such as the Warburg effect, which enhances glycolysis and lactic acid production, also leading to TME acidosis promoting immunosuppression, aggressiveness, and resistance.

Finally, damage-associated molecular patterns (DAMPs) are released into the tumour microenvironment when tumour cells undergo DNA damage, replication or endoplasmic reticulum (ER) stress, endoplasmic reticulum (ROS) formation, Z-DNA binding protein (ZBP) activation, or stimulation by TNFα, FASL, or TRAIL. DAMPs include surface-exposed calreticulin, facilitating phagocytosis, and released constitutive intracellular molecules such as annexin A1, adenosine triphosphate (ATP), high mobility group box (HMGB1), heat shock protein (HSPs), RNA, and dsDNA. DAMPs are recognised by pattern recognition receptors (PRRs) expressed on tumour cells or antigen-presenting cells (APCs), including Toll-like receptors (TLRs; cellular and endosomal membranes), NOD-like receptors (NLRs; cytoplasm), cGAS/STING, formyl peptide receptor (FPR1), purinergic receptor (P2Y2), P2X7, and interferon alpha/beta receptor (IFNAR), thereby initiating anti-tumour responses through induction of IFNα/β and TNFα. [48–52]

4.3. Non-neoplastic non-immune cells

4.3.1. Neurons

Bidirectional communication between neurons and glioma cells has been described. Glioma cells enhance neuronal excitability and formation of functional synapses with and between neurons. In turn, neuronal activity, particularly optic nerve and olfactory bulb stimulation, promote glioma cells survival, proliferation and migration. These effects are thought to be mediated by neuron-derived brain-derived neurotrophic factor (BDNF) and neuregulin (NRG1), involved in neuronal development and synaptic structure and function, via PI3K/AKT/mTOR and MEK/ERK pathways. Additionally, direct electrochemical signalling from neurons induces neurotransmitter (glutamate, serotonin, gamma-aminobutyric acid (GABA), dopamine) receptor-mediated depolarisation of glioblastoma cell membranes and postsynaptic potentials that propagate through the tumour via gap junctions. Similarly, neurons influence ECs, thereby promoting angiogenesis and tumour growth. [49,51]

4.3.2. Astrocytes

Astrocytes are the most abundant glial cells in the CNS and regulate synapse formation and angiogenesis. Glioblastoma cells can activate astrocytes, which become hypertrophic with enlarged and irregular nuclei, as they release growth factors (TGFβ, VEGFα), cytokines (IL10), neurotrophic factors, and MMPs that modulate tumour growth, invasion, angiogenesis and immunosuppression. Additionally, astrocytes can form gap junctions with glioma cells, enabling the exchange of small molecules and toxins. [49,51,53]

4.3.3. Endothelial cells

Endothelial cells (ECs) play crucial roles in regulation of BBB permeability as well as in vessel formation and angiogenesis through autocrine and paracrine stimulation by high levels of pro-angiogenic factors such as VEGFα. Additionally, ECs express among other

immune regulators, CCL2, IL6, CXCL12, TGFβ, PDL1, MMPs, collectively promoting survival, immunosuppression, angiogenesis, migration, and therapy resistance. [53,54]

4.3.4. Mesenchymal stem cells and cancer-associated fibroblasts

Mesenchymal stem cells (MSCs), originating from bone marrow and adipose tissue, participate in tissue repair by differentiating into chondrocytes, adipocytes, osteoblasts, or fibroblasts. In the tumour context, they can transform into cancer-associated fibroblasts (CAFs), which are polarised by the TME into key stromal cells involved in structural support, tumour growth, ECM remodelling, angiogenesis, and immunosuppression through upregulation of VIMENTIN, fibroblast-specific protein (FSP), alpha smooth muscle actin (αSMA), CXCL12, TGFβ, IL6, CCL2, prostaglandin E2 (PGE2), and other factors. [40]

4.4. Tumour immune microenvironment

4.4.1. Hot, altered and cold tumours

Classification

In addition to tumour-intrinsic classifications, immune-based classifications enable prognostic prediction by defining three major tumour subsets: hot (immune-inflamed and infiltrated), altered (immune-inflamed but immune-suppressed or -excluded), and cold (immune-non-inflamed/desert/ignorant) tumours. This classification relies on several parameters, with a particular focus on $CD8^+$ cytotoxic T lymphocytes (CTLs) : (1) immune composition/nature, (2) function and polarisation, (3) spatial distribution, and (4) density within the tumour core/parenchyma, stroma, and invasive margin. [40,55–57] These immune subsets remain debated and lack strict definitions, particularly for altered tumours. Major limitations include incomplete consideration of heterogeneity, immune composition and spatial distribution, leading to poor crsoss-study comparability **(Figure 9)**. [55]

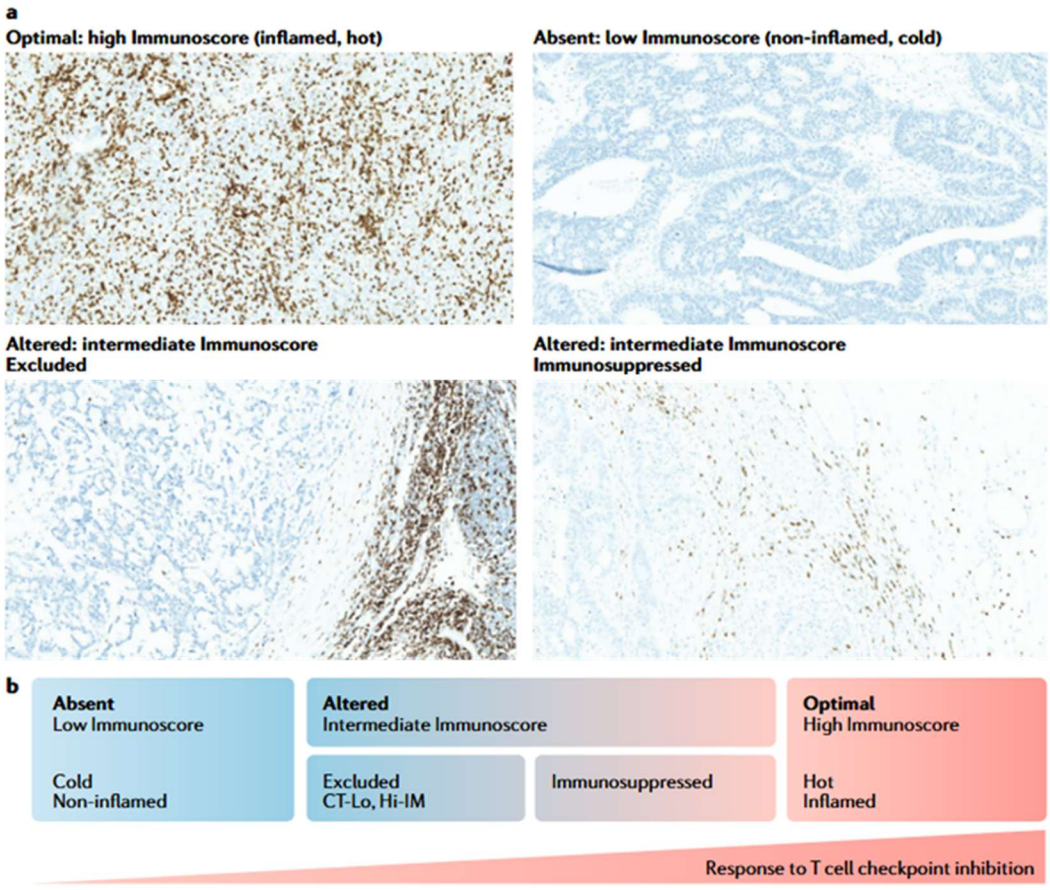

Figure 9. Cold, altered and hot tumour immune microenvironment. *They correspond to low, intermediate, and high immunogenic profiles, respectively. Cold tumours are non-inflamed and lack significant immune cell infiltration. Hot tumours are inflamed and rich in active immune cells. Altered tumours may exhibit two patterns: (1) either immune-excluded, with abundant immune cells restricted to the tumour periphery due to physical or functional barriers, or (2) immune-infiltrated with only few immunosuppressed cells due to a specific tumour microenvironment. Immune checkpoint inhibitor efficacy is inversely related to immune score and is highest in hot tumours. Indeed, pre-existing immune infiltration enables reactivation of exhausted T cells and restoration of anti-tumour immune responses. Adapted from Galon and Bruni, 2019.*[56]

- **Hot tumours** are characterised by inflamed, highly infiltrated tumour cores with elevated densities of effector immune cells, including CTLs, natural killer (NK) cells, dendritic cells (DCs), as well as pro-inflammatory tumour-associated macrophages and microglia (M1-TAMs) and $CD4^+$ T helper 1 (Th1) cells. These tumours exhibit high expression of IFNγ, granulysin, perforin, granzymes, T-box transcription factor (TBX21), STAT1/4, IRF1, CXCL9/10, CCL5, and other pro-inflammatory mediators. Interestingly, a hallmark of hot tumours is strong expression of immune checkpoints (ICs), including programmed cell death protein (PD1), cytotoxic T-lymphocyte-associated protein (CTLA4), lymphocyte-activation gene (LAG3), -cell immunoglobulin and mucin-domain containing-3 (TIM3), B7

homolog 3 protein (B7H3), and T cell immunoreceptor with Ig and ITIM domains (TIGIT), which are IFNγ-induced markers of late activation and exhaustion. These tumours are often responsive to immune checkpoint inhibitor (ICI). [52,56]

- At the opposite end, **cold tumours** lack immune inflammation and initiation of a tumour-specific immune response. This phenotype may result from potent physical barriers, or reduced tumour mutational burden (TMB), immunogenicity, and adjuvanticity, as well as defective MHC expression and antigen processing, leading to impaired T cell priming and activation. [18,56]
- **Altered tumours** represent intermediate and heterogeneous phenotypes and are subdivided into immune-suppressed and -excluded tumours. [18,56,57]
    - **Immune-suppressed** tumours are inflamed and infiltrated but display low immune-cell density and impaired immune function due to a strongly immunosuppressive microenvironment, characterised by specific soluble factors (IL10, TGFβ, VEGFα, ARG1)[XLVIII], upregulation of co-inhibitory molecules (CD47, ICs), as well as reduced expression of pro-inflammatory cytokines, chemokines, and co-stimulatory molecules (IL12α, CXCL9/10/11, CD28/80/86). Besides, the expression of chemokines such as CCL17/18/22 and CXCL1/2/3/12 promotes recruitment of immune suppressive cells such as myeloid-derived suppressor cells (MDSCs) and regulatory T cells (Tregs), while insufficient Th1 support further impairs function of CTLs and APCs (mostly DCs and TAMs). [18,56,57]
    - **Immune-excluded** tumours are inflamed but not infiltrated and may contain abundant potentially functional immune cells confined within healthy tissues or tumour invasive margin. This exclusion results from physical barriers such as ECM and tumour density, functional barriers including deficient chemokine gradients (CXCL9/10/11, CX3CL1, CCL2/5) and downregulation of chemokine receptors (CXCR3, CCR5), and dynamic barriers involving inhibitory tumour-T cell interactions that impair T cell survival. Additionally, hypoxia and abnormal tumour vasculature, characterised by disorganisation, leakiness and reduced expression of adhesion molecules (ICAM1, VCAM1)[XLIX], further limits T cell infiltration. [18,56,57]

Cold tumours are associated with poor prognosis and altered tumour with similar or worst prognosis. Cold and altered tumours are generally resistant to ICIs, as cold tumours lack inflammation, antigenicity and IC expression, while altered tumours have limited CTL infiltration or defective innate and adaptive immune response.[52,56,57]

[XLVIII] Arginase

[XLIX] Intercellular adhesion molecule 1 (ICAM), Vascular cell adhesion molecule (VCAM)

Cold-to-hot tumours transition and immunogenic cell death

The transition from cold to hot tumours depends primarily on immunogenic cell death (ICD), a form of regulated cell death (RCD) that induces immune responses through the simultaneous release of tumour neoantigens and adjuvant signals such as specific DAMPs and PAMPs. ICD is weakly induced by apoptosis due to rapid clearance of apoptotic bodies, compared to lytic RCDs such as necroptosis and pyroptosis, which promote DAMPs and cytokines release via membrane pore formation. Besides, unregulated lytic necrosis generally results in insufficient immunogenicity. ICD promotes recruitment of APCs, increase antigen uptake, processing, and expression on MHCs, along with expression of co-stimulatory molecules, type I IFN, and pro-inflammatory or Th1-associated mediators. Mature APCs migrate to secondary or tertiary lymphoid structures, where they cross-present tumour antigens to antigen-specific T cells. T cell priming occurs through TCR-MHC-antigen epitope interactions at the immunological synapse in the presence of co-stimulatory signals (CD28/80/86), CXCL9/10, interferon-stimulated genes (ISGs), IL1β/2/12α, IFNγ leading to expansion of effector and memory T cell populations. [48,50]

4.4.2. Glioblastoma TME

The complexity of the glioblastoma tumour microenvironment (TME) is partly driven by its localisation within the brain, an organ with distinctive and still debated immunological properties. CNS is considered as immune-privileged/distinct and relies primarily on resident innate immunity mediated by neurons, astrocytes, and microglia. Consequently, brain tumours preferentially recruit myeloid cells, which are commonly associated with immunosuppression. Nevertheless, adaptive immune responses can occur via the meningeal and glial lymphatic systems, as well as tertiary lymphoid structures. The latter consists of ectopically organised immune cell aggregates resembling lymph nodes and may provide alternative sites for T cell priming, B cell maturation, and lymphocyte infiltration. [51,58]

Glioblastoma exhibits feature of both cold/altered tumours. First, glioblastoma displays low TMB and limited neoantigen availability, resulting in low immunogenicity. Besides, immune exclusion is driven by the BBB, the glia limitans, abnormal vasculature, and hypoxia. Immunosuppression is further reinforced by secreted factors such as TGFβ, IL10, and VEGFα, and by the presence of immunosuppressive populations, including Tregs, MDSCs, M2-TAMs, resulting in reduced antigen presentation by APCs and scarce exhausted CTLs. Consistently, glioblastoma shows limited responsiveness to ICIs. [51,53,59,60]

The proportion of immune cells within the glioblastoma TME is highly heterogeneous across patients, ranging from approximately 6% to 70% of total cells, with an average of ~20%. Most of these immune cells are of myeloid origin (up to 90%), consisting predominantly of TAMs, mainly resident microglia and, to a lesser extent (2/3-fold), bone

marrow-derived macrophages (BMDMs), as well as neutrophils and MDSCs in lower comparable proportions. Tumour-infiltrating lymphocytes (TILs) constitute the remaining immune fraction (<10%) and include few NK cells (~1%), fewer B cells (~0.5%), and predominantly T cells, with in order of increasing abundance $CD4^+$ Tregs, $CD4^+$ T helper cells, and $CD8^+$ CTLs. [60]

Glioblastoma molecular subtypes further influence the TME. NF1 deficiency, characteristic of the MES subtype, is associated with increased infiltration of anti-inflammatory BMDMs, as well as neutrophil and TILs infiltration. This immune-rich profile results from higher TMB or treatment-induced hypermutation, increasing immunogenicity. As a compensation, immunosuppression is highly enhanced via TAMs and exhausted TILs, with high expression of ICs, such as TIM3 and PD1/PDL1[L], resulting in MES-like immune-rich tumours being associated with resistance, recurrence and poorer survival than myeloid-only tumours. In turn, this immunosuppressive microenvironment promotes the MES-like state. [59–61]

4.4.3. Tumour-associated macrophages and microglia

Origin and spatial distribution

In glioblastoma, tumour-associated macrophages and microglia (TAMs) are phagocytes and constitute the dominant immune population, representing up to half of cells within the tumour. They derive either from resident microglia, originating from $RUNX1^+$ yolk sac progenitors, or bone marrow-derived macrophages (BMDMs). The latter are recruited from circulating monocytes or skull bone marrow in response to monocyte chemoattractant family of proteins (MCPs), and differentiate into macrophages (CCR2 and Ly6C decrease, CXC3CR1 increase)[LI] upon infiltration. Microglia are the most abundant TAMs and are enriched at invasive margins where they promote tumour invasion through MMPs expression, whereas BMDMs preferentially localise to tumour core and perivascular regions, support GSCs maintenance, angiogenesis and immunosuppression. [59–62]

M1 vs M2 phenotypes

TAMs distribution and heterogeneous functions are further shaped by tumour cells and TME niches, through a phenomenon called polarisation reflecting TAMs high functional plasticity. [49,51,59,62,63]

- **M2-like phenotype:** Glioblastoma cells promote TAMs recruitment through secretion of chemokines including CCL2, CX3CL1, MCP1, MIC1, and CSF1, as well as hypoxia-inducible factor 1 alpha (HIF1α)-dependent upregulation of VEGFα and CXCL12 in hypoxic, perivascular and invasive regions. Immunosuppressive, pro-tumoral phenotypes are further driven by glioblastoma-derived anti-inflammatory

[L] Programmed death-ligand
[LI] C-C chemokine receptor type 2 (CCR2), lymphocyte antigen 6 complex, locus C (Ly6C)

cytokines like IL4/6/10/13, CSF1 and metabolites such as lactate, which acidify the TME and enhance HIF1α signalling in TAMs. Epigenetic reprogramming also contributes to TAM polarisation via glioma-derived exosomes enriched in non-coding RNAs (miR-1246, miR-6733-5p, miR-155-3p) acting through PI3K/AKT, STAT3, and inhibiting NFκB pathways. This glioblastoma-induced TAMs polarisation is commonly linked to poor prognosis and referred to as "altered activation", "pro-tumoral", "anti-inflammatory" or "M2" state. M2-TAMs should physiologically be involved in tissue repair, angiogenesis, and immune resolution post-injury/inflammation by promoting CTLs apoptosis and recruitment of Tregs and MDSCs. They are overrepresented in glioblastoma and contribute to metabolic dysregulation (ARG1, IDO), tumour growth (IGF1, EGF, PDGF, NGF, BDNF)[LII], invasion (MMPs, ADAMs), angiogenesis (HIF1α, VEGFα, IL1β/6/8), and immunosuppression (STAT3, PDL1, CD39/163/206, CCL17/22, IL4/10/13, TGFβ, MS4A7, CSF1). [49,51,59,62,63]

- **M1-like phenotype:** In contrast, the "classically activated", "anti-tumoral", "pro-inflammatory", or "M1" state is induced by DAMPs, PAMPs, Toll-like receptor (TLR4) ligands, IFNγ, LPS, or CSF2 and supports host defence through phagocytosis, APCs activity (upregulation of MHC, CD11b/c, Fc receptors), and promotion of Th1 responses via production of ROS, nitric oxide synthase (NOS2), C1q, IL1β/6/12, CXCL9/10/11, IFNγ, TNFα, and CSF2. [49,51,59,62,63]

However, the M1/M2 axis is criticised for oversimplifying TAMs heterogeneity and plasticity, as (1) TAMs frequently co-express M1 and M2 markers and can switch between states, (2) no discrete M1 or M2 populations were identified by transcriptomic analysis, (3) and several cytokines (IL1β/6, TNFα) display context-dependent pro- and anti-tumoral functions. Nevertheless, M1/M2 classification remains widely used in the literature and will still be used in this manuscript to facilitate comparison with previous studies and to broadly refer to pro- versus anti-inflammatory phenotypes or markers. Still, TAMs polarisation is now viewed as a continuum, and alternative functional states are being explored. [49,51,59,62,63]

Functional states of TAMs

Ma et al. (2022) proposed seven non-exclusive TAMs functional states: interferon-primed (IFN-TAMs), immune-regulatory (Reg-TAMs), inflammatory cytokine-enriched (Inflam-TAMs), lipid-associated (LA-TAMs), pro-angiogenic (Angio-TAMs), resident tissue macrophage-like (RTM-TAMs), and proliferating TAMs (Prolif-TAMs) **(Figure 10)**. [64]

- **Inflam-TAMs** promote immune cell recruitment and activation via NFκB-driven expression of IL1β/6, CXCL1/2/3/8, and CCL2/3/20.
- **IFN-TAMs**, driven by STAT1, express IFN-regulated and M1-associated genes (CXCL9/10/11, ISG15, CD68/80/86, MHCs, TLR4) but surprisingly also exert

[LII] Nerve growth factor (NGF), Brain-derived neurotrophic factor (BDNF)

immunosuppressive functions, via impaired antigen presentation, CTLs exhaustion, and Treg recruitment, stressing the inefficiency of the M1/M2 binary classification.

- **Reg-TAMs** resemble M2 macrophages and express ARG1, MRC1, CX3CR1, PDL1, IL10, TGFβ, CCL22 and TREM2, sharing immunosuppressive properties with LA-, RTM-, and Angio-TAMs.
- **Angio-TAMs** display combined pro-angiogenic (VEGFα, SPP1, VCAN, ANG2, IGFBP1) and anti-inflammatory (MRC1, CD163, CD44) signatures regulated by CEBPB, FOSL2, and HIF1α.
- **LA-TAMs** driven by ER stress and FOS/JUN proto-oncogene, AP-1 transcription factor subunit (FOS/JUN), HIF1α, MAF transcription factors, are specialised in lipid metabolism and oxidative phosphorylation, through apolipoprotein (APOC1), APOE, and fatty acid-binding protein 5 (FABP5), and promote immunosuppression (ARG1).
- **RTM-TAMs** largely correspond to microglia in glioblastoma purinergic receptor P2Y12 (P2RY12), transmembrane protein 119 (TMEM119) and accordingly participate in tissue remodelling and invasion through lymphatic vessel endothelial hyaluronan receptor E1 (LYVE1), hes family bHLH transcription factor 1 (HES1), folate receptor beta (FOLR2), macrophage receptor with collagenous structure (MARCO), V-set and immunoglobulin domain containing 4 (VSIG4), FLOR2, FABP4.
- **Prolif-TAMs** represent dividing macrophages characterised by cell-cycle and proliferation markers such as marker of proliferation 67 (MKI67), DNA topoisomerase 2A (TOP2A), cyclin A2 (CCNA2), cyclin-dependent kinase 1 CDK1, cell division cycle 45 (CDC45), HMGB1.

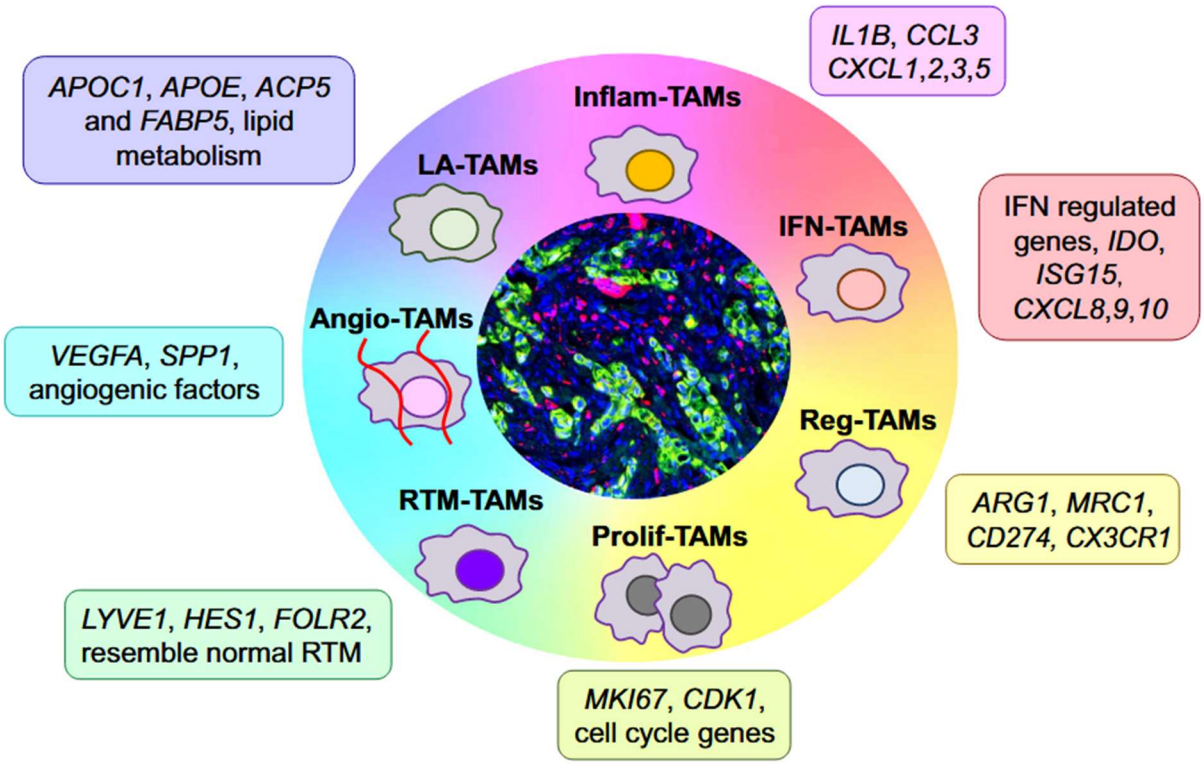

Figure 10. Classification of functional states of tumour-associated macrophages, *characterised by complex transcriptomic profiles along the M1-M2 axis. TAMs high plasticity makes discrete subpopulations difficult to identify. Nevertheless, certain states are consistently observed within tumours and are associated with distinct functions, prognoses, and transcriptomic signatures.* Ma et al. (2022) proposed seven non-exclusive states: interferon-primed (IFN-TAMs), immune-regulatory (Reg-TAMs), inflammatory cytokine-enriched (Inflam-TAMs), lipid-associated (LA-TAMs), pro-angiogenic (Angio-TAMs), resident tissue macrophage-like (RTM-TAMs), and proliferating TAMs (Prolif-TAMs). *Unmodified from Ma et al, 2022.*[64]

These functional states directly impact tumour features such as growth, invasiveness, angiogenesis, and immunosuppression.

- **Growth and invasiveness:** RTM-, LA-, and Angio-TAMs enhance tumour proliferation and invasion via secretion of growth factors (TGFβ, EGF, HGF, IL1β/6/8) and targeted release of MMPs (MMP2, MT1-MMP[LIII], MMP9) at invadopodia, facilitating ECM remodelling and brain parenchyma invasion. TGFβ plays a central role promoting EMT by increasing N-cadherin/E-cadherin ratio and activating αvβ5 integrin SRC/STAT3 signalling on GSCs, which maintains stemness through SOX9 stabilisation. [62]
- **Angiogenesis:** Angio-TAMs drive angiogenesis by localising to perivascular niches upon attraction by ECs-derived CXCL12 or CSF1, and in turn producing MMP9,

[LIII] Membrane-type 1 matrix metalloproteinase

VEGFα, CXCL12, IL1β/6/8, and IGFBP1, which activate PI3K/AKT and MAPK signalling in ECs promoting survival and proliferation. Via JAK[LIV]/STAT3 signalling, these factors also promote vascular mimicry by glioblastoma cells which adopt VEGFR$^+$ endothelial- or pericyte-like phenotypes with the ability to form vessel-like structures to sustain angiogenesis and tumour progression. [62,64]

- **Immunosuppression:** Immunosuppression represents a major function of Reg-TAMs and is shared by LA-, RTM-, and Angio-TAMs, contributing to the glioblastoma cold/altered immune phenotype. TAMs express already mentioned anti-inflammatory cytokines and ICs, while downregulating IL2, IL12α, TNFα, and IFNγ. Thereby, they specifically recruit and activate Tregs and MDSCs, while inhibiting or exhausting NK cells, CTLs and APCs. Additionally, TAMs exhibit high metabolic activity, consuming glucose and amino acids and releasing lactate and adenosine, thereby limiting nutrient and oxygen availability and lowering pH, which further limits T cell and NK cell anti-tumour responses. [62,64]

4.4.4. T cells

Origin

T lymphocytes are less abundant than TAMs but play a fundamental role. The thymus releases specific factors that recruit lymphoid progenitors from the bone marrow and induce their differentiation into immature TCR$^+$CD4$^+$CD8$^+$ T cells. Double-positive thymocytes undergo positive and negative selection to ensure recognition of either major histocompatibility complex class (MHCI) or MHCII molecules, becoming single CD8$^+$ or CD4$^+$ cells, respectively, without excessive self-antigen affinity. Naïve T cells then migrate to secondary and tertiary lymphoid structures, where they encounter APCs and, upon priming, differentiate into tumour-infiltrating lymphocytes (TILs) with effector or helper functions. In glioblastoma, these processes are impaired by low TMB and immunogenicity, innate immune dysfunction, immunosuppressive TME. Infiltration is also limited by aberrant leaky vasculature with reduced adhesion molecule expression, hypoxia due to nutrient and oxygen deprivation, and physical barriers such as the BBB and glia limitans. [65]

CD8$^+$ T cells

CD8$^+$ T cells are the most extensively studied and effective antitumour lymphocytes. Upon priming, they differentiate into memory cells or cytotoxic T lymphocytes (CTLs), a process driven by the master transcription factor TBX21. CTLs eliminate tumour cells through recognition of tumour-associated or -specific antigens (TAA, TSA)[LV] via FasL[LVI]/Fas[LVII]-mediated apoptosis or through secretion of cytokines (IFNγ, TNFα, nitric

[LIV] Janus Kinase
[LV] Tumour-associated antigen (TAA), Tumour-specific antigen (TSA)
[LVI] Fas ligand
[LVII] Fas receptor

acid (NO), CXCL9/10/11, IL2/12α) and cytotoxic granules containing granzyme, perforin, histone C, and granulysin, leading to membrane pore formation and cell lysis. Glioblastoma cells develop resistance to CTL-mediated killing through multiple mechanisms, including enhanced autophagy, altered regulated cell death pathways, membrane modification and accelerated repair, restriction and degradation of granzymes and perforin, as well as secretion of inhibitory factors and expression of co-inhibitory surface molecules. Nevertheless, increased $CD8^+$ T cell infiltration, proliferation, and activity are generally associated with improved prognosis, as are higher $CD8^+/CD4^+$ T helper and $CD8^+/CD4^+$ Treg ratios. [66,67]

A major challenge for $CD8^+$ T cells in immunologically cold or altered tumours is tolerance, defined as their inability to mediate tumour clearance.

- Tolerance may arise from **intrinsic genetic and epigenetic defects**, including hypermutation silencing IFNγ and TNFα promoters, defective TCRs, or reduced chromatin accessibility of effector genes. [65–69]
- **Extrinsic factors** within the TME can induce tolerance through mechanisms such as adaptive ignorance and clonal anergy. [65–69]
    - **Adaptive ignorance** results from insufficient antigen exposure due to low TMB, reduced neoantigen expression, impaired antigen processing and presentation, exclusion of T cells from the tumour core or brain parenchyma, and sequestration in the bone marrow mediated by forced S1P1 internalisation.
    - **Clonal anergy** occurs when T cell priming fails because of an altered co-stimulatory/co-inhibitory signals balance and the presence of inhibitory soluble factors produced by glioblastoma or immune cells.
- **Exhaustion** represents a distinct and physiologic form of tolerance, driven by chronic antigen stimulation, resulting in a decreased TBX21/EOMES[LVIII] ratio and upregulation of immune checkpoints (ICs), further enhanced by HIF1α-mediated hypoxia. ICs suppresses TCR signalling and CTL function, leading to reduced proliferation and survival, and increased autocrine stimulation by immunosuppressive cytokines such as IL-10 and TGFβ, ultimately promoting apoptosis. Negative paracrine feedback loops further exacerbate dysfunction, as IFNγ induces immunosuppressive mechanisms in Tregs, MDSCs, and glioblastoma cells, including IDO activity, PDL1 expression, and FasL release via exosomes. [65–69]

$CD4^+$ T cells

$CD4^+$ T cells are primarily recognised for their helper and regulatory roles mediated by cytokine secretion and co-stimulatory/co-inhibitory signals that shape APCs and $CD8^+$ T

[LVIII] Eomesodermin, T-box transcription factor

cells responses. However, they can also directly mediate tumour cell killing and function themselves as APCs. $CD4^+$ T cells display marked heterogeneity and plasticity, dependent on initial TCR priming and TME signals. [70]

- **Regulatory $CD4^+$ T cells (Tregs)** are generally considered pro-tumorigenic and are associated with poor prognosis and tumour growth. Although they account for only 5-10% of circulating $CD4^+$ T cells, they are enriched within tumours through recruitment, maintenance, activation, and expansion via the CCL2/CCR2, CCL22/CCR4, and CCL5/CCR5 axes. Physiologically, Tregs maintain tolerance to self-antigens and restore immune homeostasis after injury by suppressing pro-inflammatory cells such as CTLs, M1-TAMs, Th1 and NK cells, while promoting MDSCs, M2-TAMs. Their differentiation is driven by the transcription factor forkhead box P3 (FOXP3), which inhibits NFκB and nuclear factor of activated T cells (NFAT) signalling and activates STAT3, leading to reduced IL2/12α and co-stimulatory molecule expression and increased production of TGFβ, IL4/10, cytotoxic T-lymphocyte-associated protein (CTLA4), and PDL1. [68]
- **Th1 $CD4^+$ T cells** represent the most pro-inflammatory and anti-tumour subset and are associated with favourable prognosis. Their polarisation is induced by IL12α/IL18 through STAT1/4 signalling and TBX21 expression, promoting co-stimulatory interactions with APCs (CD40L/CD40), upregulation of IL12Rβ2, and secretion of IFNγ, TNFα and IL12α. These responses enhance CTL effector functions, drive M1-TAM polarisation, and inhibit tumour invasion, angiogenesis, and growth. Th1 cells can also directly kill tumour cells via granzyme and perforin release or through TRAIL- and FasL-mediated apoptosis. [68–70]
- **Th2** polarisation is induced by IL4 activating STAT5/6 pathways to upregulate GATA3 transcription factor. Th2-associated cytokines (IL4/5/9/10/13/25) promote granulocytes, Tregs and M2-TAMs recruitment and activity, humoral immunity, angiogenesis, while counteracting Th1 responses and antigen presentation. [70]
- **Th17** differentiation is induced by TGFβ and IL1β/6/10/21/23 and driven by retinoic acid receptor-related orphan receptor gamma (RORγ) transcription factor, leading to secretion of IL17/21/22/23 and IFNγ. Unlike GATA3 and TBX21, RORγ lacks stabilising positive feedback, which renders Th17 cells even more plastic and sensitive to TME cues, resulting in contradictory roles. While Th17 cells contribute to pathogen clearance, tumour cell killing, and recruitment of APCs, NK cells, and CTLs, they are frequently associated with poor prognosis. Indeed, IL17 also recruits MDSCs and Tregs, improves angiogenesis via VEGFα upregulation, facilitates invasion with MMPs-mediated ECM remodelling, promotes tumour growth via PI3K/AKT and STAT3 signalling in GSCs, and sustains chronic inflammation by inducing further cytokine release. [54,67,70,71]
- **T follicular helper (Tfh)** cells are characterised by the transcription factor Bcl6, induced via STAT3 following IL6/21 stimulation, resulting in CXCR5 upregulation

and support of B cell proliferation, somatic hypermutation, and class-switch recombination. Although typically confined to lymphoid organs, Tfh cells may contribute to ectopic tertiary lymphoid structures formation, supporting both humoral and cellular immunity and potentially improving prognosis. [70]

γδ T cells

γδ T cells are unconventional lymphocytes expressing γδ TCRs rather than αβ chains. They represent 1-5% of peripheral T cells but efficiently infiltrate tissues and can accumulate as TILs at comparable ratios as αβ T cells. They bridge innate and adaptive immunity through clonally rearranged TCR genes, MHC-independent antigen recognition, NK receptor expression, and cytotoxic molecule secretion. They can also activate other immune cells, act as APCs, and support B cell antibody production and antibody-dependent cellular cytotoxicity (ADCC). Overall, they are generally associated with favourable prognosis in cancer, although their role in brain tumours remains controversial.[72–74]

4.4.5. Less abundant immune cells

The following immune cell populations are briefly described to illustrate the diversity of leucocytes present in glioblastoma. They are not extensively analysed in the present manuscript.

Myeloid-derived suppressor cells (MDSCs) are immature monocytic and granulocytic cells derived from aberrant myeloid differentiation that promote immunosuppression, angiogenesis, invasion, and tumour growth, and are associated with poor prognosis. [49,51,62,75] Dendritic cells, although less abundant than TAMs, are the most potent APCs bridging innate and adaptive immunity. [49,51,52] Neutrophils display diverse functions but predominantly acquire pro-tumoral phenotypes in glioblastoma, with a high neutrophil-to-lymphocyte ratio correlating with poor survival. [49,51,61,75] Natural killer (NK) cells, though rare in tumours, are potent cytotoxic lymphocytes with complementary functions to CTLs. They can kill malignant cells that downregulate MHC I, restrict metastasis and improve survival. [49,51] B cells are the least abundant immune population. They contribute to antitumour immunity through antigen presentation, cytotoxicity, and secretion of tumour-specific antibodies. Conversely, regulatory B cells (Bregs) may instead promote tumour progression, immunosuppression, and angiogenesis via cytokine, antibodies and growth factors secretion. [53,69,76–78]

5. Models

Despite extensive research improving outcomes in many cancers, glioblastoma overall prognosis has changed little since Stupp protocol over 20 years ago due to CNS complexity, heterogeneity, TME, resistance and recurrence. Immunotherapies aiming to restore immune surveillance represent the principal hope, despite initially disappointing results, and will be addressed in the next section. Meanwhile, reconsideration of fundamental and preclinical models, which often yield promising results but fail clinically, has become crucial leading to their continuous evolution.

5.1. In vitro/Ex vivo (human glioblastoma *cultures)*

5.1.1. 2D cultures

Conventional glioblastoma cell lines were first established in the 1970s from patient samples, immortalized for indefinite proliferation, and grown in 2D on treated surfaces in serum-containing media. Common cell lines include U87-MG, U251-MG, T98G, LN229, and the more recent GB138 (established ~2010, *used in this thesis*). These cultures yield homogeneous monolayers with uniform access to nutrients and oxygen, consistent cell-cell interactions, and the possibility of co-culture with non-neoplastic cells. While these lines provide commercially available reproducible material for drug testing, they fail to replicate native tumour organisation and heterogeneity. Moreover, long-term culture, repeated passages, and artificial conditions induce genotypic and phenotypic drift, contributing to the poor translation of preclinical results. [41,79–82]

5.1.2. Spheroids

Since 2000-2010, glioblastoma patient-derived cell lines (GPDCLs) were developed by processing fresh biopsies within hours of resection, and subsequent culture in serum-free media supplemented with growth factors (EGF, (basic fibroblast growth factor) βFGF) and B27, thereby enriching GSCs cells ($CD133^+$, $NESTIN^+$, $NANOG^+$) and preserving genetic and histologic characteristics of the tumour of origin under 20 passages. *For this thesis*, T08, T013, T018, and T033(-LRLG) GPDCLs were established from residual tumour tissue by the Laboratory of Nervous system Disorders and Therapy, GIGA-Neurosciences, ULiège, Belgium, with the contribution of the University of Liège Hospital and Biobank. In these conditions, spontaneous aggregates are formed (spheroids, neuro-/glioma-spheres) upon cell-cell interactions and upregulation of adhesion molecules like cadherins and integrins. Spheroids organised 3D structures induce gradients of nutrients, metabolites, and oxygen, generating hypoxic/necrotic cores, quiescent intermediate layers, and proliferative outer layers. Approximation of the tumour microenvironment may be obtained through co-culture with TAMs, T cells, astrocytes, or neurons, as well as via the organotypic multicellular spheroid system which maintain stromal, vascular and immune cellular components from the tumour biopsy. [79–82]

5.1.3. Organoids

Organoids, derived from embryonic or induced pluripotent stem cells in Matrigel or ECM components, self-organize into layered 3D structures with high density of heterogeneous cell types in more physiological interactions with their microenvironment. Tumoroids may be derived from patient tumour tissue or from genetically engineered cerebral organoids via CRISPR/Cas9[LIX]. The glioblastoma integrated cerebral organoid model (GLICO) model integrates patient-derived GSCs into cerebral organoids, showing strong correlation with primary tumours, including gap-junction-mediated microtube networks supporting invasion, proliferation, and communication. Organoids that mimic the blood-brain barrier and develop immune-like cells (such as microglia) are under investigation. Nevertheless, vascular and immune systems remain rudimentary, organoid formation lacks standardised protocols, and reproducibility remains a major limitation. [80–83]

5.1.4. Scaffolds

Scaffold models were developed specifically to better replicate ECM composition and its roles in spatial organization, growth support, and the mediation of interactions with and between tumour and non-neoplastic cells.

- **Organotypic glioma slice** cultures involve seeding labelled glioblastoma cells onto thick slices of mouse or human brain tissue, which can be maintained for weeks to study tumour invasion and microenvironmental interactions. [79,81]
- Reproducibility and cost-effectiveness have been later improved using natural or synthetic **biomimetic ECM-like 3D scaffolds**, which offer relevant pore size and density, stiffness, and post-manufacturing adaptability that resembles ECM remodelling. [79,81]
- Further technological advances have led to the bioprinting of scaffolds using hyaluronic acid, gelatine methacrylate, or collagen bioinks. These **bio-printed miniature brain** models enable the generation of drug or bioactive gradients and support studies of niche organization, as well as TAMs recruitment, polarization, and their role in tumour invasiveness. [79,81]

5.1.5. Microfluidics and GB-on-a-chip

Microfluidic platforms simulate dynamic tumour microenvironments using submillimetre scaffolds embedded in brain-specific ECM and perfused with circulating media under laminar flow, allowing precise time-controlled composition and gradients. These systems enable long-term culture (>50 days) and facilitate the study of interstitial flow effects, BBB, and vascular network. [79,81,82]

[LIX] Clustered regularly interspaced short palindromic repeats / CRISPR-associated protein 9

Glioblastoma-on-a-chip models have emerged through the integration of microfluidics with 3D bio-printed scaffolds and co-culture of GPDCLs with non-neoplastic cells such as macrophages, astrocytes, endothelial cells, and pericytes. [79,81,82]

5.2. *In vivo* (Mouse models)

Despite ethical concerns, animal models remain essential as cost-effective and reproducible systems that conserve relevant developmental, genetic, and histological characteristics of the tumour of origin. They provide appropriate supplies and gradients of nutrients, growth factors, and oxygen within a functional vascular network, along with microenvironmental and ECM support and interactions, thereby enabling the recapitulation of tumour development, organization, heterogeneity, and responses to treatment.[80,81,84]

Paradoxically, most animals differ from humans in brain organization, gene expression, and ECM composition, introducing species-specific tumour development, treatment responses, and potential phenotypic drift. Among available models, mice are generally preferred over zebrafish or rats because of their closer biological similarity to humans and their relative ease of genetic manipulation and maintenance, although their small brain size can complicate stereotactic and surgical procedures. [80,81,84]

5.2.1. Immunodeficient orthotopic xenograft mouse models

Xenograft mouse model refers to human glioblastoma cells, preferentially GPDCLs, which are implanted into immunodeficient mice (athymic NUDE *used in this thesis*, severe combined immunodeficiency (SCID), non-obese diabetic mice (NOD), or NOD-SCID) to prevent graft rejection. These models maintain 3D tumour architecture, genetic and histological features, invasiveness, niches, and subtype-specific traits, enabling study of molecular pathways, hypoxia, angiogenesis, therapy, and relapse. Their main limitations are slow tumour growth, with experiments lasting several months, and absent or altered immune interactions.[81,82,84]

To overcome the latter, humanized mouse models are generated by engrafting human peripheral blood mononuclear cells, hematopoietic stem cells, or foetal liver/thymus tissue into immunodeficient mice, resulting in human $CD45^+$ cells representing most human immune cell types in the peripheral blood. However, humanized mice remain costly and time-consuming, and provide only transient human immunity, limited by incomplete or asynchronous immune cell functionality. Similarly, microbiota-humanized mice have been developed to address species-specific effects of the gut microbiome. [81,82,84]

5.2.2. Immunocompetent orthotopic syngeneic or allografts mouse models

Immunocompetent mouse models retain the advantages of xenograft models while also providing a fully functional immune system, lower maintenance costs, and rapidly

developing tumours, allowing experiments to last only several weeks to just over a month. Their main limitation is that both the murine immune system and the artificially developed murine glioblastoma cell lines may not fully recapitulate human tumour biology. [84] These models can be either syngeneic or allogeneic, depending on whether the host and donor share same genetic backgrounds or only same species, with C57Bl/6 strain being the most common (*used in this thesis*). [82,84]

Chemically induced models

Chemically induced models, first developed in the 1970s, generate genetically and histologically heterogeneous tumours with relevant microenvironments using mutagens such as methyl- or ethyl-nitrosourea (*in utero* of pregnant animals) or methylcholanthrene (intracranially in adults). To improve reproducibility while losing heterogeneity, cell lines were derived from these tumours. [81,82,84–88]

- The most widely used is **GL261** (*used in this thesis*), derived from intracranial methylcholanthrene-induced tumours in adult C57BL/6 mice, followed by serial injections and maintenance in 2D serum-containing cultures. GL261 tumours exhibit human-like genetic alterations (TP53 loss, rat sarcoma oncogene family (RAS) and MYC overexpression), invasiveness (VIMENTIN$^+$), angiogenesis (CD31$^+$), mesenchymal-like features (CD44$^+$), and a GSCs subpopulation (NESTIN$^+$, CD133$^+$, SOX2$^+$). However, they are considered immunogenic as they respond to immunotherapies such as ICIs, despite no clinical translation. This may be explained by high tumour mutation burden, as well as elevated MHC and Cd80/86 expression, although immunosuppression persists via upregulation of CXCR4 and VEGFα. [81,82,84–88]
- **CT2A** tumours share similar origin but demonstrates higher invasiveness, microvascular proliferation, pseudopalisading necrosis, faster tumour growth, and shorter survival. They exhibit stronger immunosuppression, with exhausted CTLs (ICs upregulation) and relatively few microglia compared to BMDMs. Notably, CT2A tumours remain responsive to immunotherapies, but pre-transplant culture in GSCs serum-free conditions increases ICI resistance *in vivo*, while paradoxically elevating the CTL/Treg ratio. [81,82,84–88]

Genetically engineered models

Genetically engineered mouse models (GEMs), developed in the 2000s, allow precise induction of somatic or germline mutations using Cre/loxP, CRISPR/Cas9, transposons, or viral vectors. They frequently incorporate hallmark human glioblastoma alterations, such as *Tp53* mutations and RAS/AKT pathway activation reflecting EGFR overexpression and PTEN loss. Compared to chemically induced models, GEMs offer tighter control over genomic loci, timing, and targeted cell type. GEM-derived cell lines are cultured as GPDCLs, preserving tumour or origin features, reducing genetic drift, and enriching for GSCs.[81,84]

- The **005-GSCs** model (*used in this thesis*) is derived from a GEM generated via an inducible Cre-loxP lentiviral vector injected in the hippocampus of p*Gfap*[LX]-Cre *Tp53*$^{+}$/$^{-}$ C57BL/6 mice, restricting Cre recombinase expression to GFAP^{+} cells, including potential glioblastoma cell-of-origin astrocytes and NSCs. Constitutively active *Ras* and *Akt* constructs (pCMV-loxP-RFP-loxP-Flag-H-*Ras*V12 and pCMV-loxP-RFP-loxP-HA-myr-*Akt*)[LXI] are introduced concurrently, with RFP acting as a stuffer fragment to prevent expression until Cre-mediated recombination **(Figure 11)**. [89] 005-derived tumours exhibit high stemness, MES-like phenotype, reduced immunogenicity, and resistance to ICIs, associated with absent MHCI, downregulated co-stimulatory molecules, and limited CTL activation, despite abundant activated microglia and Tregs. [82,88]

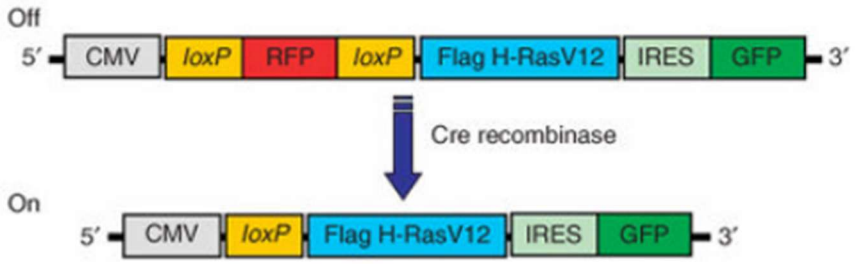

Figure 11. Constitutively active Ras constructs for 005-GSC engineering. *Lentiviral vectors carrying constitutively active Ras and Akt constructs (pCMV-loxP-RFP-loxP-Flag-H-RasV12 and pCMV-loxP-RFP-loxP-HA-myr-Akt) were introduced concurrently into the hippocampus of pGfap-Cre Tp53 $^{+}$/$^{-}$C57BL/6 mice. In GFAP $^{+}$cells (astrocytes and neural stem cells), Cre-mediated removal of RFP, which otherwise blocks RasV12 or myr-Akt expression, led to tumorigenesis. 005-GSCs were subsequently derived from these tumours. Unmodified from Marumoto et al., 2009.* [89]

- Another interesting model is based on tamoxifen-inducible CreER system, in which Cre recombinase is fused to the estrogen receptor (ER), enabling temporal control of locus of crossover in P1 (LoxP) recombination upon tamoxifen induction that triggers CreER nuclear translocation. Recently, a model was developed with (1) *Tp53* and *Pten* flanked by LoxP sites and (2) CreER under the NSC-specific *Tlx* promoter (p*Tlx*-CreERT2). Isolation, *in vitro* culture, and serial engraftment of mutant NSCs produced **mGB0/1/2** models, corresponding to classical, proneural, and mesenchymal subtypes respectively, based on genomic and transcriptomic profiles. Mouse glioblastoma 2 (mGB2) displays histopathologic and immunologic features most representative of poor-prognosis human glioblastoma, including a high myeloid-to-lymphoid cell ratio. [82,84,88,90]

[LX] Glial fibrillary acidic protein
[LXI] Cytomegalovirus promoter (pCMV), red fluroresenc protein (RFP), hemagglutinin tag (HA)

6. Immunotherapies

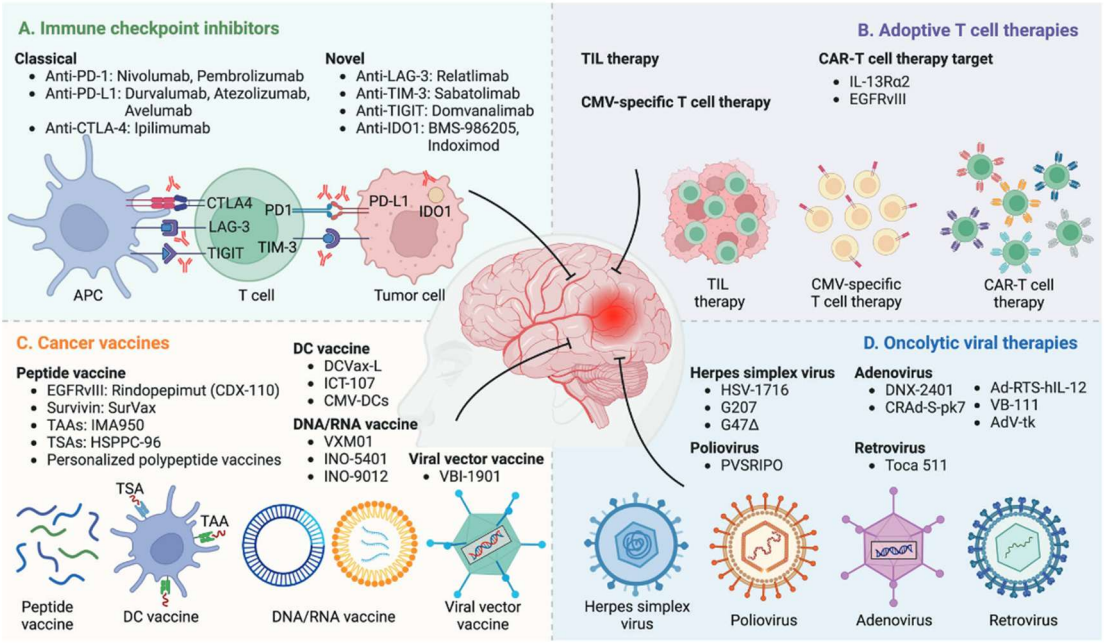

Figure 12. Immunotherapies for glioblastoma. *Four major immunotherapeutic strategies are under investigation, each comprising multiple treatments at different stages of clinical development: immune checkpoint inhibitors, adoptive T cells, cancer vaccines, and oncolytic viruses.* Immune checkpoint inhibitors block inhibitory pathways to restore T-cell activity. Adoptive T cells involve the transfer of engineered or expanded T cells to directly target tumour cells. Cancer vaccines aim to induce tumour-specific immune responses through antigen presentation. Oncolytic viruses selectively infect and lyse tumour cells while promoting local inflammation. *Unmodified from Liu et al., 2024.*[58]

Immunotherapies encompass a broad range of innovative strategies aimed at overcoming immune resistance in immunologically cold or altered tumours by restoring effective immunosurveillance, thereby achieving tumour clearance. Clinical outcomes of immunotherapies in glioblastoma remain modest, underscoring the need for novel, diversified, and more effective approaches and delivery routes (intracranial, intra-tumoral, intraventricular, intrathecal, resection cavity infusion). Currently, five immunotherapeutic strategies are under investigation, each comprising multiple treatments at different stages of clinical development: specific pathways inhibitors, immune checkpoint inhibitors, adoptive T cells, cancer vaccines, and oncolytic viruses. **(Figure 12)** [58,91]

Glioblastoma represents both an ideal target and a major challenge for such approaches due to a profoundly dysfunctional tumour microenvironment shaped by the immunologically distinct brain, exclusion by the blood-brain barrier, low tumour mutational burden (TMB) and antigenicity, related to limited inflammation and immune infiltration. These features result in a predominantly myeloid tumour characterised by

defective innate immune responses, reduced antigen processing and MHC expression, and strong immunosuppression mediated by soluble factors and specialised immune cells, ultimately driving exhaustion of antitumour immune cells, particularly cytotoxic T cells, through high immune checkpoint expression. In addition, tumour heterogeneity, GSCs, and resistant *mesenchymal glioblastoma subtype* further limit therapeutic efficacy. [58,91]

6.1. Pathways

At the interface between targeted therapies and immunotherapy, multiple signalling pathways, cytokines, chemokines, and growth factors can be selectively modulated to achieve synergistic effects by simultaneously limiting tumour growth and immunosuppression. Therapies have been developed using antagonists of TGFβR1, CSF1R, VEGFα, IL8, CXCR4/CXCL12, CCR5/CCL5, HIF1α, or agonists of TLRs, stimulator of interferon genes (STING), and CXCL9/10/11, as well as direct administration of pro-inflammatory molecules such as CSF2 or G-CSF. These strategies include monoclonal antibodies or nanobodies (bevacizumab), small molecules (AMD3100), with one specific target as well as microRNAs (miR-93) and long non-coding RNAs (lnc135528), which modulate the expression of multiple genes. Numerous combinations of these approaches with other immunotherapies, including immune checkpoint inhibitors, vaccines, adoptive cell, and oncolytic viruses, are currently under investigation. [49,92,93]

Notably, limited drug bioavailability at the tumour site remains a major challenge and may be addressed through nanoparticle-based delivery systems. For example, polyethylene glycol–polycaprolactone (PEG-PCL) micelles form a hydrophobic core-hydrophilic shell structure that enables encapsulation of hydrophobic drugs, improves systemic circulation, and prevents degradation. Coupling PEG-PCL nanoparticles to internalising arginine-glycine-aspartic acid (iRGD) peptides allows binding to alpha-v beta-3 integrin (αvβ3) integrins on brain microvascular endothelial cells and tumour cells, facilitating BBB crossing and tumour internalisation. [49,92,93]

6.2. Immune checkpoint inhibitors

Immune checkpoints (ICs) are physiological regulators of the immune system, primarily surface molecules upregulated upon activation of T cells or APCs, that maintain immune homeostasis, promote resolution of immune responses, ensure self-tolerance, and prevent autoimmune damage by inducing T cell anergy, exhaustion, and apoptosis. Several ICs are aberrantly upregulated in cancer, including PD1/PDL1, CTLA4, LAG3, TIGIT, V-domain Ig suppressor of T cell activation (VISTA), IDO1, thymocyte selection-associated high mobility group box protein (TOX), and TIM3. [53,94–99]

Immune checkpoint inhibitors (ICIs), mainly monoclonal antibodies that block extracellular ligand-receptor interactions, were developed to counteract these mechanisms. ICIs reactivate tumour-specific exhausted T cells, which subsequently

infiltrate the tumour, exert effector functions and produce IFNγ, promoting DCs recruitment, enhanced antigen processing, and increased pro-inflammatory cytokine production, in turn amplifying T cell responses. Neoadjuvant ICI administration, defined as treatment prior to standard therapy, may elicit stronger immune responses than adjuvant ICIs. Neoadjuvant treatment may induce tumour downsizing facilitating gross total resection with reduced damage to surrounding parenchyma, improve eradication of micrometastatic disease tissues, and limit exhaustion of treatment-induced immune response. Additionally, neoadjuvant therapy occurs while lymphatic and vascular connections between the tumour and regional lymph nodes are not yet disrupted by aggressive standard therapies. Nevertheless, following ICI treatment, ICs are markedly upregulated, and the glioblastoma microenvironment remains dominated by immunosuppressive $CXCR4^+$ myeloid populations, including TAMs and MDSCs, which limit immunosurveillance, prevent complete tumour clearance, and reduce overall survival. [53,94–99]

ICIs have demonstrated major clinical success in melanoma and non–small cell lung cancer (NSCLC), with phase III trials showing improved overall survival median from months to ~2-3 years in melanoma and ~1-2 years in NSCLC. However, clinical trials in glioblastoma have not shown benefit. Anti–PD-1 alone or with anti–CTLA-4 has not improved outcomes in recurrent glioblastoma compared with bevacizumab. In newly diagnosed glioblastoma, adding ICIs to standard therapy has also not improved survival. [53,94–99]

6.3. Vaccines

Cancer vaccines can be prophylactic, as demonstrated by reduced incidence of hepatocellular carcinoma and cervical cancer following vaccination against hepatitis B virus and human papillomavirus. However, most cancer vaccines, including those targeting glioblastoma, are therapeutic and aim to (re)stimulate immune responses against established tumours by enhancing antigen presentation by APCs to prime naïve or memory T cells, thereby inducing tumour regression and durable immune memory. A major challenge lies in identifying homogeneous tumour-associated antigens (TAAs) or, preferentially, tumour-specific antigens (TSAs) and neoantigens, which are not necessarily related to tumorigenesis and vary between patients and tumour cells, potentially requiring personalised approaches based on whole-genome sequencing. In some cases, antigens may be exogeneous, derived from prior infections, and overexpressed in tumours, such as human cytomegalovirus (HCMV), detected in more than 90% of glioblastomas. [58,95,100]

Vaccine platforms include synthetic TSA-derived peptides, bacterial DNA plasmids, mRNA, viral vectors, and DC-based vaccines, often combined with adjuvants.

- **Bacterial DNA plasmids** encode for TSAs enabling presentation via both MHC I and II pathways, and stimulate by themselves innate immunity through PAMPs/DAMPs such as CpG motifs, dsDNA, and encoded immune-stimulatory cytokines.
- **mRNA vaccines** are relatively easy to manufacture, enabling scalable production, can be efficiently delivered via lipid nanoparticles, and offer several safety advantages, including the absence of infectivity, rapid physiological degradation, no requirement for nuclear entry, and an inability to integrate into the host genome.
- Unexhaustive list of glioblastoma **TSA-derived peptides vaccines** includes (1) rindopepimut (CDX-110), an EGFRvIII-specific peptide vaccine with keyhole limpet hemocyanin adjuvant, (2) the IMA950 multipeptide vaccine combined with CSF2, polyinosinic-polycytidylic acid stabilized with poly-L-lysine and carboxymethylcellulose (poly-ICLC), and anti-PD1, and (3) VXM01, a DNA plasmid encoding VEGFR2.
- **Viral platforms**, such as VBI-1901 targeting cytomegalovirus (CMV) antigens, may simultaneously function as vectors, adjuvants and vaccines.
- Finally, autologous dendritic (**DC) vaccines** derived from peripheral blood monocytes or pluripotent stem cells can be loaded with TSA-derived peptides (e.g. cytomegalovirus phosphoprotein 65 (CMVpp65 RNA-pulsed DCs) or whole-tumour lysates (DCVax-L), although the latter may induce responses against self-antigens. [58,100–103]

6.4. Adoptive cells

Adoptive cell therapy involves the isolation of immune cells from patients, primarily T cells but also NK cells, B cells, and γδ T cells, followed by *ex vivo* expansion, activation, and selection in the presence of high cytokines concentrations, and subsequent reinfusion after lymphodepleting patient conditioning. Clonal selection can be achieved by culturing peripheral blood mononuclear cells with TSAs.

- T cell receptor-engineered **T cell therapies** were developed to improve antigen specificity, while chimeric antigen receptor (CAR) technologies bypass MHC restriction by coupling antibody-derived antigen-binding domains to intracellular co-stimulatory signalling domains (CD3ζ, CD28, 4-1BB). Nevertheless, CAR-T cells are restricted to surface antigens, require high epitope density, and their high affinity can reduce serial killing while promoting exhaustion. In glioblastoma, CAR-T cells have primarily targeted IL13Rα2, EGFRvIII, B7H3, human epidermal growth factor receptor 2 (HER2) and human cytomegalovirus (HCMV). CAR-T cell therapy has shown significant clinical success in B-cell malignancies, particularly through CD19 targeting, achieving high overall response rates (~70–90%) and durable remissions that led to multiple FDA approvals. However, early-phase trials in glioblastoma and other solid tumours have shown limited clinical benefit. Major

barriers include (1) impaired trafficking and persistence, (2) an immunosuppressive TME with elevated IC expression, and (3) limited tumour-specific antigens alongside tumour heterogeneity and antigen escape.[58,95,104]

- **CAR-NK cells** offer several advantages over CAR-T cells, including improved safety, reduced risk of cytokine release syndrome or graft-versus-host disease, and preservation of native NK receptor function, limiting immune escape through antigen loss. NK cells can be derived from autologous peripheral blood or tumours, or, as MHC-independent lymphocytes, from induced pluripotent stem cells or NK-92 cell lines, enabling off-the-shelf allogeneic therapies. Notably, CAR-NK-92 cells are irradiated prior to infusion to prevent proliferation while retaining cytotoxicity. [58,105,106]
- **B cell-based therapies** (BVax) employ autologous 4-1BBL^{+} B cells expanded with CD40 agonists and IFNγ, which differentiate into antibody-secreting plasmoblasts targeting tumour and ECM components (impairing tumour invasion), function as APCs, and traffic between tumour and lymphoid tissues. [58,105,106]

6.5. Virotherapy

Virotherapy principally relies on three main mechanisms: **(Figure 13)**

- **Transgene expression:** Virotherapy involves the use of genetically engineered viral vectors (VVs) or oncolytic viruses (OVs) to deliver immunotherapeutic transgenes. These viruses enable sustained expression of pathway inhibitors, immune checkpoint inhibitors, or TSA. [6,53,58,91,95,98,107]
- **Selective replication:** A key feature of commonly used viruses is their natural or engineered tropism for cancer cells, enabling targeted delivery and release of therapeutic agents while limiting toxicity. Viral platforms also differ in replication capacity, ranging from completely replication-deficient vectors to viruses capable of replicating in all cells. Alternatively, retargeted or replication-selective (naturally occurring or genetically attenuated) viruses can replicate only in cancer cells. A key distinction exists between VVs and OVs, as OVs have the additional ability to induce direct tumour cell lysis while sparing healthy tissues. [6,53,58,91,95,98,107]
- **Immune activation:** VVs and OVs induce a strong anti-tumour immune response by acting as adjuvants through PAMPs and DAMPs resulting from the infection. In addition, OVs only trigger immunogenic cell death, already described in the *tumour immune microenvironment* section as a critical driver of immunologically cold-to-hot tumour transition. [6,53,58,91,95,98,107]

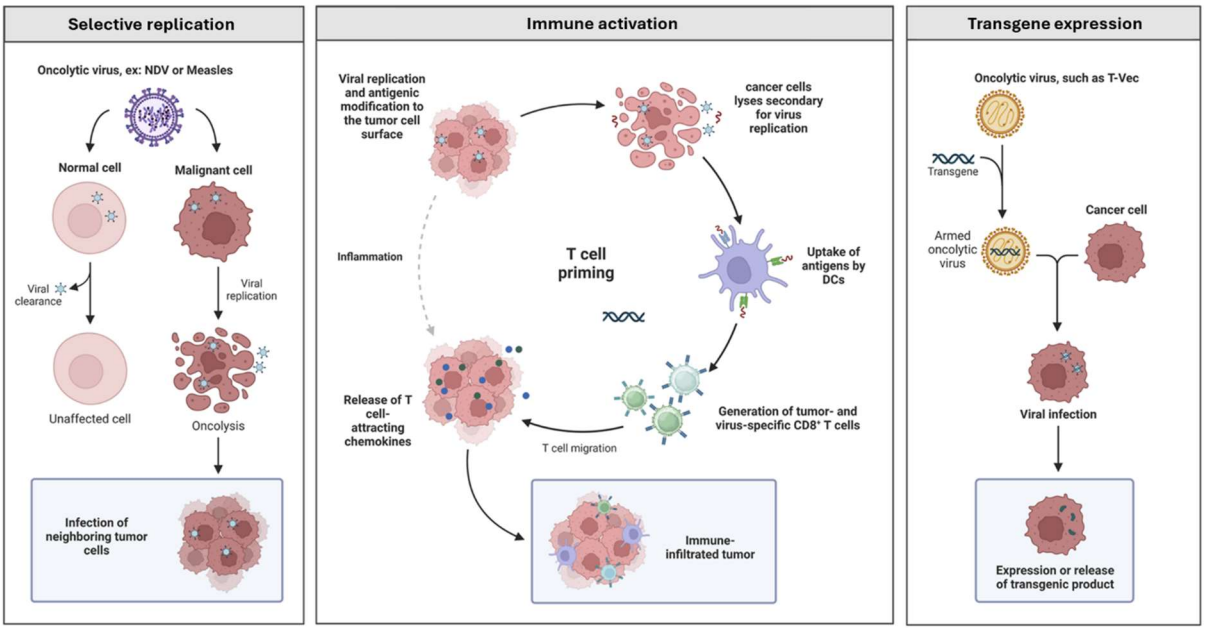

Figure 13. Mechanisms of Action of Oncolytic Virotherapy. *Oncolytic viruses selectively infect and lyse tumour cells. They promote local immune activation through immunogenic cell death, with subsequent antigen uptake by dendritic cells and T-cell priming, leading to tumour inflammation. Current oncolytic virotherapy also commonly includes transgene expression, enabling infected tumour cells to locally produce and secrete anti-oncogenic proteins. Adapted from Al-Shammari et Piccaluga, 2023.*[108]

Numerous VVs and OVs are under investigation for glioblastoma, including dsDNA viruses (adenovirus, herpes simplex virus, bovine herpesvirus, vaccinia virus), ssDNA viruses (adeno-associated virus, parvovirus), dsRNA viruses (reovirus), positive-sense ssRNA viruses (zika virus, poliovirus, alphaviruses), and negative-sense ssRNA viruses (Newcastle disease virus, Sendai virus, measles virus, vesicular stomatitis virus). [6,53,58,91,95,98,107]

Despite extensive fundamental, preclinical and clinical development to understand every aspect of this complex therapy involving viral infection, spread, replication, transgene expression, and cytotoxicity as well as innate and adaptive immune response, and tumour-specific oncogenic pathways, only four oncolytic viruses have been approved for cancer treatment worldwide. These include a selective unattenuated picornavirus for melanoma (Rigvir®, 2004, Latvia), a genetically engineered adenovirus targeting TP53-deficient tumour cells in head and neck cancer (Oncorine®, 2005, China), and two attenuated herpes simplex virus type 1 (HSV-1): Talimogene laherparepvec for unresectable metastatic melanoma (T-VEC, Imlygic™, 2015, USA/EU), and Teserpaturev for residual and recurrent glioblastoma (G47Δ, Delytact®, 2021, Japan). The attenuations in T-VEC (Δ34.5Δ47) and G47Δ (Δ34.5Δ47Δ6), restrict replication to dividing, PKR-deficient cancer cells while enhancing immune recognition, and will be described in the next section. [6,53,58,91,95,98,107]

7. Oncolytic Herpes Simplex Virus 1

7.1. Herpes simplex virus 1

7.1.1. Structure and genome

Herpes simplex virus type 1 (HSV-1) is a member of the human *Alphaherpesvirinae* subfamily, alongside HSV-2 and varicella-zoster virus (VZV). Alphaherpesviruses are neurotropic viruses characterised by rapid lytic replication in epithelial cells and the establishment of lifelong latency in sensory neurons, with periodic reactivation. *Alphaherpesviridae* are 150-200 nm viruses composed of an icosahedral nucleocapsid enclosing the genome, surrounded by a tegument of regulatory proteins and enzymes, and an envelope derived from the host lipid bilayer embedded with viral glycoproteins essential for attachment and entry. The 120-160 kbp double-stranded DNA genome is organized into unique long (UL) and unique short (US) regions flanked by long and short inverted repeats (TRL-UL-IRL-IRS-US-TRS). [6,109,110]

HSV-1 envelope carries ~20 viral proteins, including 13 glycoproteins, of which glycoprotein B (gB), gC, gD, gH, and gL are essential for viral entry, while its tegument contains 20-25 proteins. HSV-1 capsid consists of 162 capsomeres formed by six viral proteins, including VP5 (major component) and UL6 (portal protein). Finally, the 152 kbp genome encodes ~80 genes, that can be designated by their loci UL1-UL56, US1-US12, and RL1-RL2/RS1. [6,109,110]

7.1.2. Infectious cycle

Initial contact and attachment

Initial contact of HSV-1 with the host cells is mediated via gB/C interactions with heparan sulphate proteoglycans (HSPGs), followed by specific gD binding to herpesvirus entry mediator (HVEM), NECTIN, or 3-O-sulfated heparan sulphate (3-O-S HS). The first two are type 1 transmembrane glycoproteins widely expressed across cell types. HVEM belongs to the TNF receptor superfamily (TNFRSF14) with functions related to immune regulation and NECTIN is a member of the membrane immunoglobulin superfamily and is involved in cell adhesion. 3-O-S HS, present on most cell surfaces, is a heparan sulphate glycosaminoglycan that consists of a linear polysaccharide composed of repeating disaccharide units of glucosamine and uronic acid residues. Notably, 3-O-S HS serves as initial attachment receptor for many viruses, although it is a less efficient/essential receptor for HSV-1 than HVEM and NECTIN. [6,111]

Entry

Upon binding, gD conformational changes engage the fusion-mediator gH/gL complex. gB pre-fusion trimer interacts simultaneously with gD/gH/gL complex and its own receptors

(NMHCIIA, PILRα, MAG)[LXII]. 3-O-S HS may be involved by binding both gD and gB. Subsequently, gB undergoes structural rearrangements to expose hydrophobic fusion loops, enabling envelope-host membranes fusions or endocytosis. Simultaneously, gH/gL interaction with alpha-v beta-3 and beta-8 integrins (αvβ3/8) integrins triggers calcium release and PI3K/AKT signalling, stimulating cell survival. [6,111]

Replication and Egress

Upon entry, HSV-1 capsid-tegument complexes recruit dynein for retrograde microtubule transport to the nuclear envelope, delivering viral DNA through nuclear pores. Tegument proteins induce host-mediated transcription of immediate early (IE) genes, regulating immune evasion and transcription of early (E) and late (L) genes. E genes control nucleotide metabolism as well as viral DNA repair and replication, the latter triggering L genes expression involved in virion structure, assembly and egress. Capsids bud through inner and outer nuclear membranes into the cytosol. Meanwhile, *de novo* synthesised tegument and envelope proteins are processed via the ER to the trans-Golgi network (TGN) or plasma membrane. Cytosolic capsids recruit kinesin for anterograde transport and acquire tegument and envelope proteins by budding into TGN vesicles or plasma membrane endosomes, forming organelle-associated enveloped virions ultimately released by exocytosis. [6,112,113]

7.2. Construction of oncolytic herpes simplex virus 1

HSV-1 is well suited for oncolytic virotherapy. [6,114,115]

- It has a large, **fully sequenced** double-stranded DNA **genome** and **well-characterized life cycle** with known essential genes, enabling efficient genetic engineering.
- Moreover, approximately 30 kbp of **nonessential genomic regions** can be replaced with transgenes or bacterial artificial chromosome (BAC) components, facilitating further viral engineering and laboratory use.
- In addition, HSV-1 infection can be controlled with **antiviral agents** such as acyclovir, a deoxyguanosine analogue lacking a 3'-OH group that, following phosphorylation by viral thymidine kinase (HSV-TK) and host kinases, is incorporated by the viral DNA polymerase, thereby blocking further DNA synthesis.
- HSV-1 also exhibits a **high global prevalence** (~64%), resulting in pre-existing host immune memory that can limit uncontrolled viral spread while enhancing antitumour immune responses.

[LXII] non-muscle myosin heavy chain IIA (NMHCIIA), paired immunoglobulin-like type 2 receptor alpha(PILRα), myelin-associated glycoprotein (MAG)

- Nevertheless, the **broad tropism of HSV-1**, which allows infection and replication in most human cell types, necessitates genetically engineered attenuation to reduce neurovirulence.

Oncolytic HSV-1 (oHSV) typically incorporates three principal modifications, which will be described following the chronological progression of the viral infectious cycle **(Figure 14)**:

- **US12 IE gene (ICP[LXIII]47):** ICP47 binds and inhibit the transporter associated with antigen processing 1 (TAP1), preventing recruitment of peptides into the ER and their subsequent loading and presentation onto MHC molecules. oHSV-Δ47 immune recognition is thus enhanced, limiting uncontrolled spread through infected tumour cells lysis and **promoting tumour inflammation**.
- **UL39 Early gene (ICP6)**: ICP6, the large subunit of the viral ribonucleotide reductase (RR), is essential for viral DNA synthesis in non-dividing cells, lacking sufficient functional cellular RR. oHSV-Δ6 replication is thus **restricted to dividing cells**, including cancer cells.
- **RL1 Late gene (ICP34.5)**: ICP34.5 counteracts translational shutoff mediated by the kinase PKR, by interacting with the phosphatase PP1α and their common target eIF2α. oHSV-Δ34.5 is thus unable to trigger protein synthesis and virion assembly in healthy cells with functional translational control, thereby **limiting neurovirulence.** To improve viral spread in partially protein kinase R (PKR)-deficient tumours, single-copy deletions or tumour-specific expression (pNestin in rQNestin34.5) are sometimes used. Furthermore, US12 deletion (oHSV-Δ47) partially restores viral protein translation by placing the late US11 gene under the IE US12 promoter, as unique short region 11 (US11) inhibit PKR by binding to its major activation ligand, dsRNA.

[LXIII] Infected cell protein

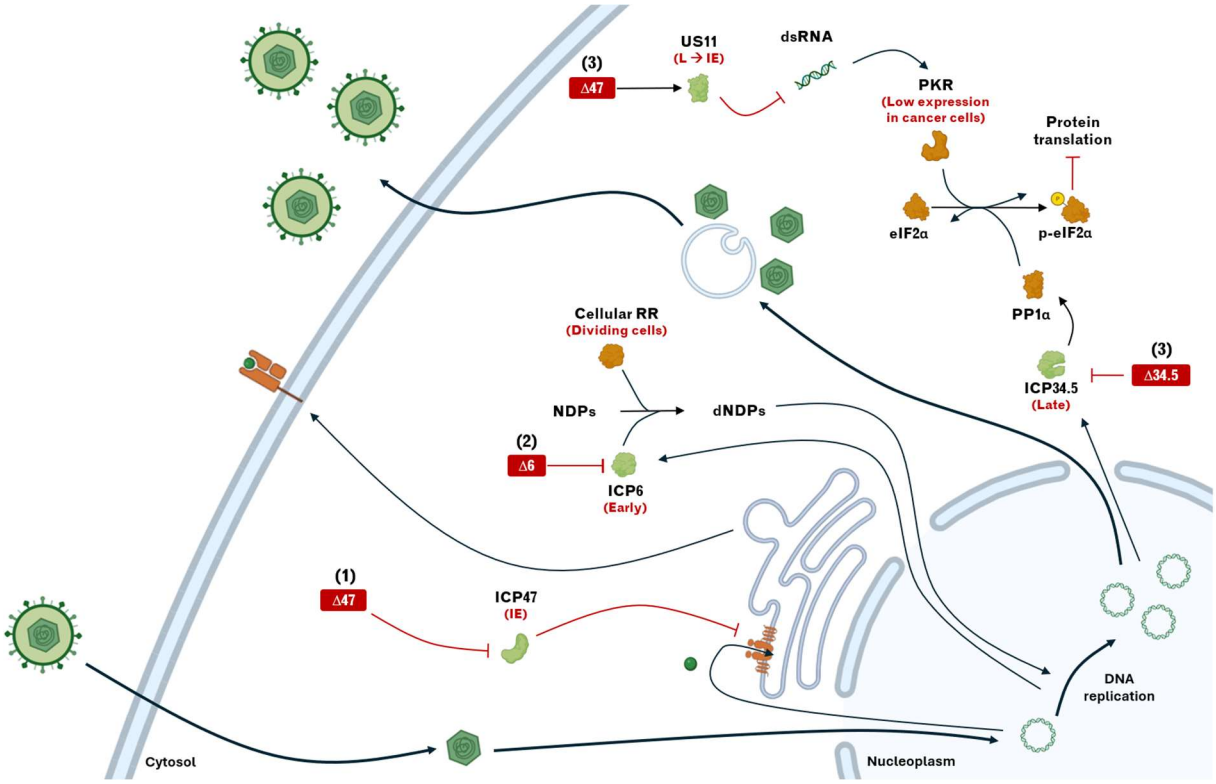

Figure 14. Oncolytic HSV-1 three main genetic alterations along the infectious cycle. *(1) Upon entry, in the immediate early phase, HSV-1 expresses ICP47, which blocks antigen loading by TAP1 and subsequent MHC class I antigen presentation. Δ47 deletion improves immune recognition of infected cells. (2) During the early phase, the viral ribonucleotide reductase (RR), ICP6, supports viral DNA synthesis. Δ6 restricts replication to dividing cells with active cellular RR. (3) During virion assembly, in the late phase, ICP34.5 prevents eIF2α-mediated translational shutdown via PP1 activation. Δ34.5 viruses are attenuated but can replicate in tumour cells with low PKR activity. Δ47 also drives US11 expression under ICP47 gene's immediate early promoter. US11 inhibits PKR by binding dsRNA, restoring protein synthesis and balancing Δ34.5 mutation.*

7.3. Construction of oHSV armed with a CXCR4 antagonist

Transgene insertion is now standard in virotherapy, commonly encoding pro-inflammatory cytokines (IL12/15/18, CSF2), suicide genes (HSV-TK, CYP2B1)[LXIV], pro-apoptotic molecules (TRAIL), anti-angiogenic factors (PF4), tumour suppressors (PTEN), tumour-associated antigens (EphA2), extracellular matrix modulators (MMP9), and inhibitors of immune checkpoints (PD1) or oncogenic pathways (VEGFα). Additional engineering strategies include retargeting glycoprotein D to tumour-specific receptors (IL13Rα2, EGFR, HER2, CXCR4) by replacing receptor-binding domains with single-chain fragment antibodies or nanobodies.[6,116–125]

[LXIV] cytochrome P450 family 2 subfamily B member 1 (CYP2B1)

We engineered an armed oHSV encoding a CXCR4 antagonist (oHSV/P2G), based on a mutated form of its ligand CXCL12 (CXCL12-P2G or P2G, described in the next section). The oHSV/P2G construct was generated by inserting the CXCL12-P2G sequence under the EF1α promoter into the green fluorescent protein (GFP)⁺ oHSV-Δ47Δ6Δ34.5 backbone. The P2G gene was fused to an IL-2 signal peptide to promote secretion and to an emagglutin epitope tag (HA-tag) to enable detection. **(Figure 15)**[117]

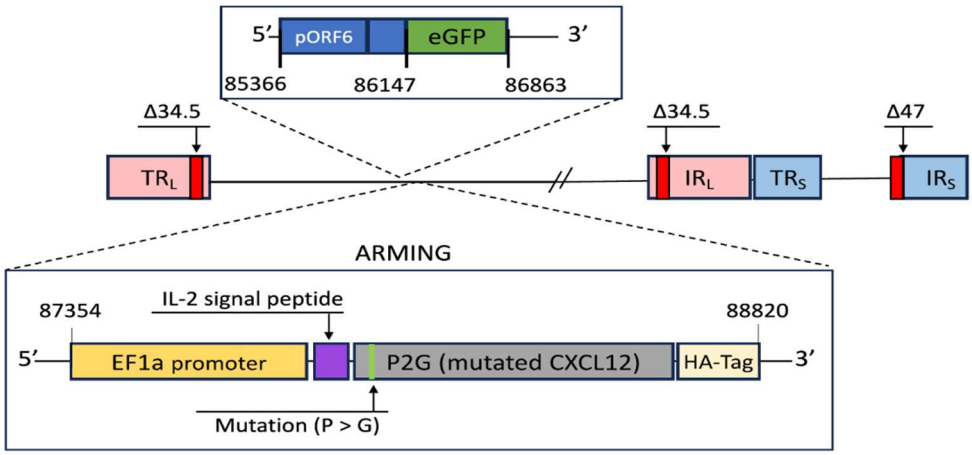

Figure 15. oHSV/P2G genome construction. *The oHSV backbone is derived from HSV-1 (Δ47, Δ6 Δ34.5)*. The 120-160 kbp double-stranded DNA genome is organized into unique long (UL) and unique short (US) regions flanked by long and short inverted repeats (TRL-UL-IRL-IRS-US-TRS). *The eGFP cassette, downstream of pORF6, replaces ICP6 expression. The pEF1α–IL-2 signal peptide–CXCL12-P2G–HA tag transgene was inserted downstream of the GFP cassette. Unmodified from Paolo D'Arrigo, Maxime Dubois et al.*[117]

The potential of CXCR4 inhibition in glioblastoma is detailed in the next section, focused on the CXCR4/CXCL12 pathway. The rationale for combining CXCR4 blockade with virotherapy is presented in the subsequent "aim of the thesis" section. Briefly, viral vectors bypass the blood–brain barrier, ensure sustained local production, and avoid systemic CXCR4 inhibition. Oncolytic virotherapy induces local inflammation, while CXCR4 inhibition enhances anti-tumour immune response. This work provides a comprehensive overview and characterisation of the effects of oHSV/P2G compared to oHSV on key biological functions in glioblastoma.

8. CXCR4/CXCL12 pathway

8.1. Discovery

8.1.1. CXCR4

One of the earliest mentions of CXCR4 was as leukocyte-derived seven-transmembrane receptor (LESTR), related to IL8Rs and isolated from a human monocyte cDNA library. [126] It was later named Fusin for its role as a co-factor in HIV-1 fusion and entry into $CD4^+$ T cells. [127] LESTR was characterised as a seven-transmembrane, guanosine triphosphate (GTP)-binding protein (G-protein)-coupled receptor (GPCR) of the Gαi subtype (352 AA, ~39.7 kDa). [126] LESTR/Fusin was subsequently designated CXCR4 and CD184 according to the chemokine-receptor nomenclature (GRC, 1996) and the cluster-of-differentiation nomenclature (7th HLDA Workshop, 2001). [128,129]

8.1.2. CXCL12

CXCR4 ligand is a cytokine containing four conserved cysteines forming two disulfide bonds and belonging to the CXC subfamily, in which the two N-terminal cysteines are separated by one amino acid, unlike the CC, CX3C, and XC subfamilies. [126] The ligand was identified as stromal cell-derived factor 1 (SDF1), later termed pre-B cell-stimulatory factor (PBSF) and CXCL12, a CXC cytokine isolated from a bone-marrow stromal cell cDNA library and shown to promote B cell progenitor proliferation and immune cell chemotaxis. [129–131] CXCL12 is considered a primordial chemokine, as it is essential for embryogenesis and organogenesis, [63] displays equal similarity to both CXC and CC chemokines despite its two N-ter cysteines, and is highly conserved across species, differing by only one AA between mouse and human. [132] CXCL12 comprises seven isoforms (α, β, γ, δ, ε, θ, and iso7) occurring as monomers or dimers, differing in the fourth exon, while sharing the first 67 N-terminal (N-ter) residues. [133–135] Two CXCR4-binding sites lie in CXCL12(1-17), KPVSLSYR-CPC-RFFESH. The RFFESH motif mediates initial N-ter CXCR4 contact, enabling access to a shallow receptor site, while N-ter residues, particularly lysine at position 1 (K1) and proline at position 2 (P2), induce CXCR4 conformational change and signalling **(Figure 16)**. [133]

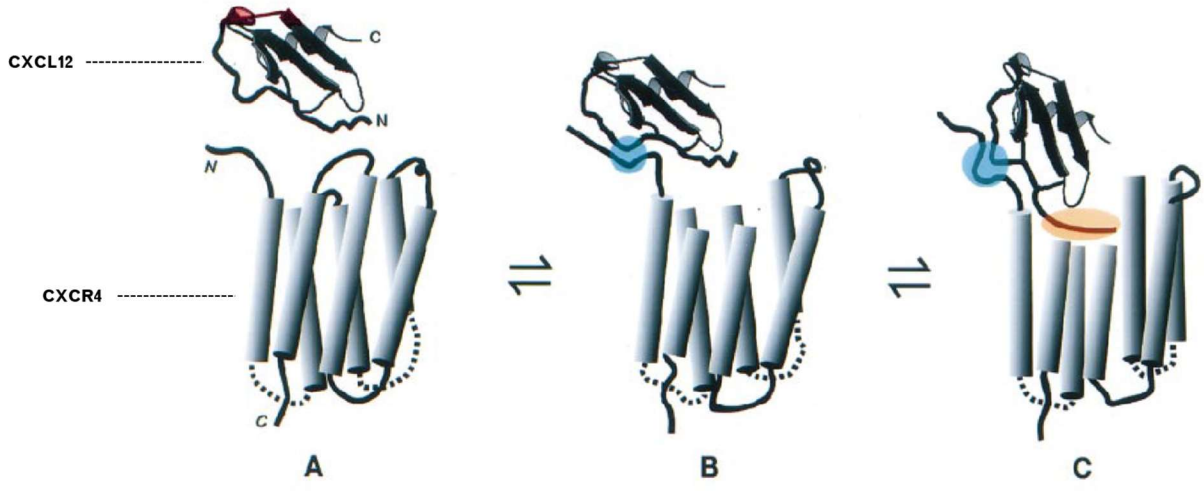

Figure 16. Two-step CXCR4/CXCL12 interaction. *Two CXCR4-binding sites lie in CXCL12(1-17), KPVSLSYR-CPC-RFFESH. **(B)** The RFFESH motif mediates initial N-ter CXCR4 contact, **(C)** enabling access to a shallow receptor site, while KPVSLSYR N-ter residues, particularly K1 and P2, induce CXCR4 conformational change and signalling. Adapted from Crump et al., 1997.*[133]

8.2. Distribution and roles

CXCR4 is broadly expressed, especially in stem cells, as well as vascular, immune and central nervous systems, and is upregulated in hypoxic, damaged, and neoplastic tissues, especially cancer stem cells, where it correlates with poor prognosis. [136–138] CXCL12 is likewise constitutively expressed in most organs and increased in injured tissues. [136,137] Early discoveries showed that CXCL12 participates in myelopoiesis and B cell lymphopoiesis, [139] acts as a chemoattractant responsible for B cell and granulocytic precursor retention in the bone marrow, [140] as well as for T lymphocyte chemotaxis [141] and $CD34^+$ hematopoietic progenitor mobilisation to peripheral blood. [142] CXCR4/CXCL12 axis is also essential for vascular, cardiac, immune and CNS development and regeneration, mainly through ECs and neuroblast differentiation and migration. [140,143]

8.3. Signalling

Upon ligand binding, CXCR4 undergoes a conformational change that activates its associated G proteins, as the Gα subunit exchanges guanosine diphosphate (GDP) for guanosine triphosphate (GTP) and dissociates from the G protein beta-gamma subunits (Gβγ) complex.[137,144] **(Figure 17)**

- Gαi inhibits **adenylyl cyclase** (Ac), thereby reducing cyclic adenosine monophosphate (cAMP) levels and protein kinase A (PKA) activity.
- Gαq or Gβγ activates phospholipase (**PLC)**, converting phosphatidylinositol 4,5-bisphosphate (PIP2) into DAG and inositol 1,4,5-trisphosphate (IP3), increasing protein kinase C (PKC) activity and cytosolic calcium ion (Ca^{2+}) release.

- Gβγ or Gαi also promotes RAS activation leading to **RAS/RAF[LXV]/MEK/MAPK** (ERK1/2, p38, JNK) phosphorylation, and PI3K activation producing PIP3 to recruit PDK1 and activate **PI3K/AKT/mTOR**.

CXCR4 activation may also trigger G-protein-independent signalling pathways. **(Figure 17)**

- GPCR kinase (GRK) promote **βARRESTIN** recruitment, leading to G-protein signalling inhibition, MAPK activation, CXCL12 scavenging and receptor desensitisation via clathrin-mediated internalisation, followed by CXCR4 recycling or degradation. [137,145]
- CXCR4 can also signal via **JAK/STAT3** pathways and activate **NFκB**. [146,147]

CXCR4 exists as monomers, homodimers, heterodimers, oligomers, or nanoclusters in the plasma membrane. CXCR4 homodimer signalling has been well characterised (see above), whereas signalling mediated by heterodimers remains incompletely understood. Notably, heterodimers can form with several receptors, including CXCR7, the T-cell receptor (TCR), CCR5, and CCR2. CXCR4-CXCR7 heterodimers favour βARRESTIN recruitment over G-protein-dependent CXCR4 signalling, but can also activate Ca^{2+} mobilisation and chemotaxis. Heterodimer signalling is thought to involve receptor crosstalk. CXCL12 may therefore activate signalling pathways of the CXCR4-associated receptor or, conversely, ligands of these receptors (such as CXCL11, peptide–MHC complexes, or CCL2/3/4/5/7/8/13) may trigger CXCR4 downstream signalling. **(Figure 17)** [63,148,149]

[LXV] Rapidly accelerated fibrosarcoma kinase

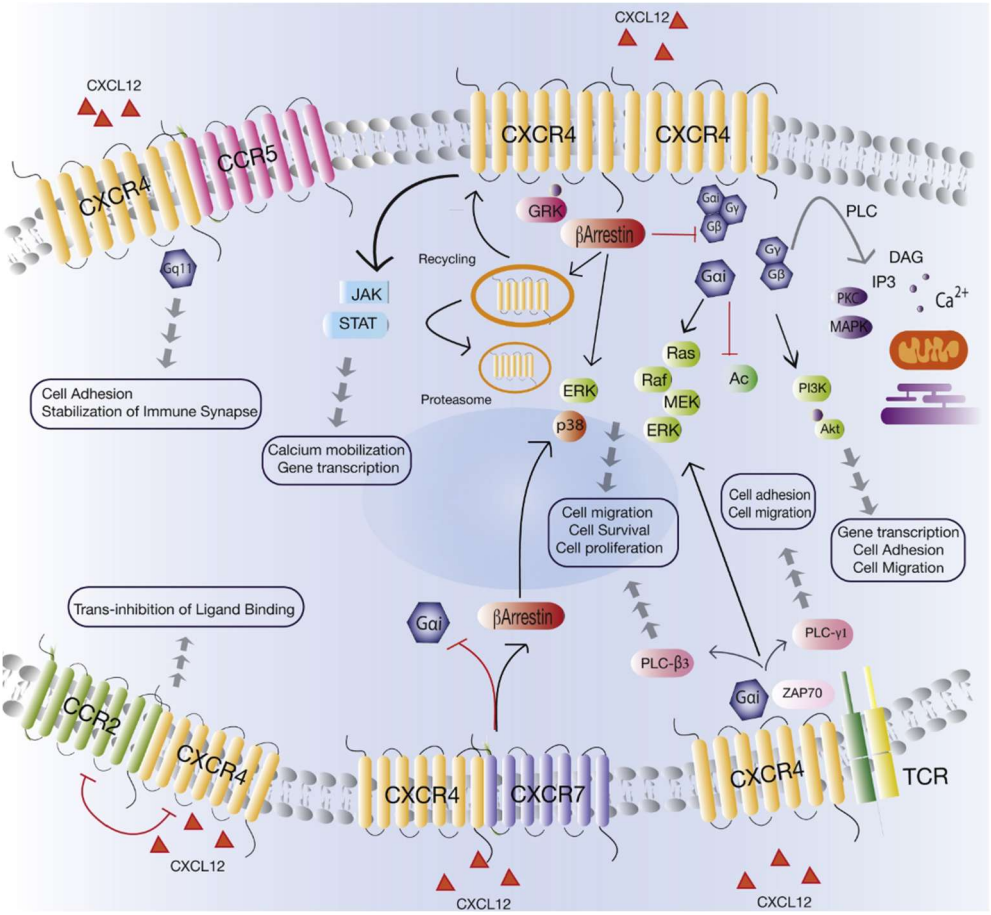

Figure 17. CXCL12 downstream signalling. *CXCR4 activation triggers G-protein and downstream signalling pathways including PLC/PKC/Ca²⁺, RAS/RAF/*MEK/MAPK *and* PI3K/AKT/mTOR. *It can also activate β-arrestin–dependent signalling leading to receptor internalisation and G-protein inhibition. Furthermore, it can engage JAK/STAT and NFκB signalling. CXCR4 forms homo- and heterodimers which modulate signalling outcomes and enable receptor crosstalk. Unmodified from Pozzobon et al., 2016.*[149]

8.1. Alternative ligands

Unlike most chemokine-receptor pairs with promiscuous binding, CXCL12 and CXCR4 were long considered monogamous. [63] This selectivity was supported by the surprisingly equivalent phenotypes of CXCR4- and CXCL12-deficient mice. [140] However, receptor dog cDNA 1 (RDC1), later named CXCR7/ACKR3, was isolated in 1989 from a dog thyroid cDNA library. It was long viewed a conserved orphan receptor, and eventually identified as a receptor for CXCL12 and CXCL11, a CXCR3 ligand. [150–152] CXCR7 is prominently expressed in vascular, neoplastic, and brain tumour-associated astrocytes. [153] CXCL12 binds CXCR7 with ~10-fold higher affinity than CXCR4, although CXCR4 is kinetically favoured due to faster association-dissociation rates. [63] CXCR7 cannot couple to G-proteins owing to the altered DRYLAIV (DRYLSIT) motif and might function as a CXCR4 antagonist by scavenging CXCL12 or signalling through βARRESTIN and chemokine internalisation. [137,150] Interestingly, CXCR7 may also synergise with CXCR4 by internalising

or degrading CXCL12. Indeed, it can prevent CXCR4 downregulation under high ligand concentrations, reduce CXCR4$^+$ cell retention in bone marrow or perivascular niches during inflammation, and enhance CXCR4-dependent migration via its upregulation behind the invasive front.[150]

New CXCR4 ligands continue to be identified, including high mobility group box 1 (HMGB1), macrophage migration inhibitory factor (MIF), extracellular ubiquitin (eUb), human beta-defensin 3 (HBD3), and others. [145] Notably, HMGB1 is a nonhistone nuclear protein that functions as a DNA chaperone in the nucleus and promotes autophagy in the cytosol. Upon injury, necrosis, or severe stress, HMGB1 is released as a DAMP, triggering inflammation via its disulfide form, which binds TLR4 or receptor for advanced glycation end products (RAGE). [134,154,155] In contrast, fully reduced fully reduced high mobility group box 1 (frHMGB1) binds CXCR4 with ~10-fold higher affinity than CXCL12, either directly or by forming a heterodimer with CXCL12. Reduced HMGB1 synergizes with CXCL12, by acting itself as a chemoattractant to promote tissue repair, as well as by inducing CXCL12 transcription via autocrine loop, preventing CXCL12 degradation via heterodimeric stabilisation.[134,155,156]

8.2. CXCR4/CXCL12 axis in glioblastoma

CXCR4 is overexpressed in many cancers, including glioblastoma, and correlates with poor prognosis by supporting tumour growth, angiogenesis, invasiveness immunosuppression, and therapeutic resistance [63,136,137] TP53 mutations, common in cancer, contribute to CXCR4 overexpression, while CXCR4/CXCL12 signalling upregulates MDM2, further degrading TP53, in a positive feedback loop.[157] The roles of CXCR7 remain controversial and will not be extensively addressed. [135,145,157]

8.2.1. Role in tumorigenesis and maintenance

CXCR4/CXCL12 promotes proliferation and survival via PI3K/AKT/mTOR, ERK/MAPK and JAK/STAT3. AKT, ERK, and STAT3 enhance anti-apoptotic factors (BCLXL, SURVIVIN) while inhibiting pro-apoptotic proteins (BAD, BIM)[LXVI] and glycogen synthase kinase 3 beta (GSK3β), thereby stabilizing βCATENIN and driving cell cycle progression. MAPKs translocate to the nucleus, activating proliferation factors such as ELK1, ribosomal S6 kinases (RSKs), and MYC, which is involved in a positive feedback loop increasing CXCR4 expression. NFκB activation destabilizes inhibitor of NFκB alpha (IκBα), inducing SHH secretion and stimulating CXCL12 production in surrounding PTCH$^+$ stromal cells.[135,157,158] CXCR4 overexpression in GSCs also promotes self-renewal and stemness marker expression. [40,159]

[LXVI] BCL2-associated agonist of cell death (BAD), BCL2-interacting mediator of cell death (BIM)

8.2.2. Role in angiogenesis

Under HIF1α-mediated hypoxia or injury, endothelial cells (ECs) and GSCs secrete CXCL12, promoting angiogenesis through ECs recruitment, reassembly, and proliferation, as well as enhancing VEGFα upregulation via PI3K/AKT, JAK/STAT3. Less potent pro-angiogenic factors, like βFGF, cyclooxygenase-2 (COX2), IL6, IL8, and TNFα, may contribute. [135,145]

8.2.3. Role in invasion

CXCR4/CXCL12 drives invasion and metastasis primarily via EMT, by activating JAK/STAT3, and NFκB pathways, which regulate adhesion molecules (laminin, fibrinogen, CD44, cadherins, integrins) and actin cytoskeletal reorganization. PI3K/AKT and MAPK upregulate MMPs and SURVIVIN, facilitating migration. [135,157] CXCR4/CXL12 axis is involved in crucial steps of metastasis as CXCL12 gradients to distant organs guide metastatic seeding. CXCL12 also supports extravasation and trafficking within vascular tissues. Moreover, CXCL12 drives $CXCR4^+$ GSCs homing and retention to their niches, including bidirectional migration from the tumour to the SVZ and then to the olfactory bulb. [41,160] Similarly, $CXCR4^+$ NSC differentiation into OPCs and their migration to the resection cavity rely on localized CXCL12 release by GSCs, ECs and astrocytes. [28]

8.2.4. Role in immunosuppression

CXCL12 both mediates retention of hematopoietic progenitors and stem cells in bone marrow, and facilitates immune cell trafficking into tumours. [63] In glioblastoma, ECs, cancer-associated fibroblasts (CAFs), astrocytes, and GSCs secrete CXCL12, recruiting $CXCR4^+$ immunosuppressive cells (TAMs, Tregs, MDSCs, Bregs). CXCR4 signalling impairs $CD8^+$ T cells differentiation and DCs antigen presentation. Finally, CXCR4/CXCL12 promotes M2-TAMs polarisation via upregulation of IL10, TGFβ, PDL1, CXCL12 upon JAK/STAT3/6 activation, whereas CXCL12/CXCR7 may promote pro-inflammatory M1-TAMs profiles (iNOS, class II major histocompatibility complex transactivator (CIITA), CCR7, IL1β, IL6, IL12) through STAT1 and NFκB. [63,146,158]

8.2.5. Role in immune surveillance

Intriguingly, CXCR4 may exhibit potential overlooked anti-tumour roles. First, CXCR4 may support immunosurveillance via “immunogenic surrender”. CXCR4 forms complexes with CD47 (“don’t eat me” signal), highly expressed on cancer cells, which co-internalize upon CXCL12 binding independently of downstream signalling. This prevents CD47/SIRPα[LXVII] interaction and enables TAMs-mediated phagocytosis, followed by antigen presentation and tumour-specific T cell priming. [63] Besides, CXCR4 interacts with immunoglobulin D B-cell receptor (IgD-BCR) and TCR, enabling essential cross-

[LXVII] Signal regulatory protein alpha

signalling. Consequently, TCR functions may depend on CXCR4/CXCL12, while TCR ligation can activate CXCR4 to induce cytokine secretion and T cell migration. [63]

8.3. CXCR4/CXCL12 antagonists

The most widely used CXCR4 antagonist is AMD3100, a bicyclam small molecule (0.83 kDa). AMD3100 irreversibly blocks CXCL12 binding and signalling without activating CXCR4. [161] AMD3100 limits cancer invasion, metastasis, angiogenesis, and tumour growth via downregulation of MMP2/9, VEGFα, and PI3K/AKT or RAS/RAF/MAPK signalling, [162–165] while reducing MDSC and Tregs recruitment and promoting CTL and M1-TAMs activity. AMD3100 combined with G-CSF is FDA-approved for mobilizing $CD34^+$ hematopoietic progenitor cells into the peripheral blood for collection and subsequent autologous transplantation in patients with non-Hodgkin lymphoma. [166] AMD3100 may also function as an allosteric agonist of CXCR7, as it can induce βARRESTIN recruitment to CXCR7 in the absence or presence of CXCL12.[167] Contrasting with strong preclinical glioblastoma data, plerixafor (AMD3100) has only reached Phase I trials, combined with standard treatments or bevacizumab, for newly diagnosed or recurrent glioblastoma. These treatments aimed at reducing tumour perfusion and growth. They showed safety and biological activity but no survival or tumour control benefit.[168,169]

BoxA, the first HMG-box domain of HMGB1, binds CXCR4 with similar affinity as HMGB1 and acts as a competitive inhibitor. It inhibits CXCR4 signalling and downstream functions while enhancing the above mentioned “immunogenic surrender” via signalling-independent co-internalization of CXCR4/CD47 complexes, promoting CXCR4 antitumour activity. [134,156]

The inhibitor CXCL12-P2G or simply P2G (*used in this thesis*), is a mutated CXCL12 peptide that can be delivered via viral vector. Substituting proline with glycine at position 2 abolishes receptor activation while retaining approximately one third of the native binding affinity, exploiting the importance of the N-terminal residues for activation rather than binding. Mechanistically, the receptor conformational change required for signalling is likely prevented by increased conformational flexibility of the glycine or loss of proline side-chain interactions. [133] The anti-cancer effect of P2G has been described in breast cancer and osteosarcoma murine models, with various impact on metastasis formation. [170,171]

Aim of the thesis

Glioblastoma is the most common central nervous system malignancy, with relatively high incidence and poor prognosis. Standard, targeted, and immune therapies have failed to improve overall survival for nearly 25 years. Treatment resistance arises from tumour-intrinsic features including aggressiveness, invasiveness, hypervascularisation, recurrence, heterogeneity, and plasticity, all largely driven by glioblastoma stem-like cells (GSCs). Moreover, treatment efficacy is limited by brain-specific constraints as surgical resection is rarely complete or repeatable, the blood–brain barrier is restrictive, and the brain is immune-privileged. The latter, together with GSCs, low tumour mutation burden and limited immunogenicity, promotes a profoundly pro-tumoral microenvironment characterised by anti-inflammatory factors, exhausted cytotoxic T cells, and immunosuppressive populations such as regulatory T cells and tumour-associated macrophages and microglia (TAMs).

The CXCR4/CXCL12 pathway correlates with tumour growth and poor prognosis. It supports hypervascularisation, invasiveness, as well as GSCs properties, especially in hypoxic, perivascular and invasive niches. CXCL12 also enhances immunosuppression by recruiting $CXCR4^+$ immunosuppressive cells and reprogramming immune populations toward anti-inflammatory phenotypes, increasing suppressive effector functions and cytokine secretion.

Intra-tumoral delivery of oncolytic herpes simplex virus type 1 (oHSV) is one of the few potent immunotherapies under investigation and received time-limited approval in Japan for residual and recurrent glioblastoma (teserpaturev, oHSV Δ34.5Δ47Δ6, 2021). Despite this important milestone, research continues to optimise understanding and efficacy of virus delivery, retargeting, spread, induction of immunogenic cell death, transgene expression, and modulation of tumour-specific pathways and features, particularly in the immune microenvironment.

This thesis aims to develop and characterise an oHSV armed with the CXCL12 antagonist P2G (oHSV/P2G) to disrupt CXCR4/CXCL12 signalling. This approach was designed to enable tumour infection and killing, triggering inflammation, while simultaneously inhibiting various key glioblastoma features and alleviating immunosuppression.

oHSV/P2G efficacy was compared with unarmed oHSV and PBS control. First, we used human glioblastoma cell lines (GB138) and patient-derived cells lines (T08, T013, T018, T033), *in vitro*, and in orthotopic xenografts in immunodeficient athymic NUDE mice, to demonstrate reduced GSCs stemness and migration. Subsequently, immune cell recruitment and polarisation were assessed in orthotopic syngeneic immunocompetent C57Bl6 mouse models (GL261N4, 005-GSCs). Finally, tumour- and TAMs-mediated angiogenesis was evaluated in the latter models and *in vitro* using GB138 cells, human monocyte-derived macrophage and a microglia cell line (HMC3).

Results

oHSV/P2G disrupts GSCs stemness and migration. (Molecular therapy, Oncology, 2025 Nov 3, 33(4), 201083[117])

An oncolytic herpesvirus expressing a CXCR4 antagonist interferes with Glioblastoma cells stemness features and migration.

D'ARRIGO Paolo[1, 6], DUBOIS Maxime[1, 6], SANCHEZ GIL Judit[1], LASSENCE Cédric[1], HEGO Alexandre[2], BROUWERS Benoit[3], LOMBARD Arnaud[3,4], ROGISTER Bernard[3,5], NEIRINCKX Virginie[3], LEBRUN Marielle[1, 7], SADZOT-DELVAUX Catherine[1, 7]

[1] Laboratory of Virology and Immunology, GIGA-Immunobiology, University of Liège, 4000 Liège, Belgium

[2] Laboratory of Nervous system Disorders and Therapy, GIGA-Neurosciences, University of Liège, Belgium

[3] GIGA-Cell Imaging Platform, GIGA, University of Liège, 4000 Liège, Belgium

[4] Neurosurgery Department, CHR Citadelle, 4000 Liège, Belgium

[5] Neurology Department, University Hospital, 4000 Liège, Belgium

[6] Equal contributions as first co-authors

[7] Equal contributions as last co-authors

Summary

The following introductory section does not add substantial new information beyond the global introduction of the thesis. It addresses the role of GSCs in glioblastoma, and their self-renewal and migratory capacities, which depend on the CXCR4/CXCL12 axis. The inhibition of this pathway using AMD3100 and CXCL12-P2G is also described, along with the therapeutic potential of oHSVs. The subsequent results section aims to describe the construction of oHSV/P2G, validate viral replication, transgene expression, and pathway inhibition. Then, it assesses oHSV/P2G inhibition of GSC stemness, self-renewal, and migratory abilities. The discussion first focuses on technical aspects of the results before addressing the clinical relevance of CXCR4 inhibition in tumour recurrence. Finally, it addresses the potential of this strategy to enhance standard treatments such as surgical resection, radiotherapy, and immunotherapy.

The following paper was published in *Molecular Therapy Oncology* in November 2025.

Molecular Therapy
Oncology
Original Article

An oncolytic herpesvirus expressing a CXCR4 antagonist interferes with glioblastoma cells' stemness features and migration

Paolo D'arrigo,[1,6] Maxime Dubois,[1,6] Judit Sanchez Gil,[1] Cédric Lassence,[1] Alexandre Hego,[2] Benoit Brouwers,[3] Arnaud Lombard,[3,4] Bernard Rogister,[3,5] Virginie Neirinckx,[3] Marielle Lebrun,[1,7] and Catherine Sadzot-Delvaux[1,7]

[1]Laboratory of Virology and Immunology, GIGA-Immunobiology, University of Liège, 4000 Liège, Belgium; [2]GIGA-Cell Imaging Platform, GIGA, University of Liège, 4000 Liège, Belgium; [3]Laboratory of Nervous System Disorders and Therapy, GIGA-Neurosciences, University of Liège, 4000 Liège, Belgium; [4]Neurosurgery Department, CHR Citadelle, 4000 Liège, Belgium; [5]Neurology Department, University Hospital, 4000 Liège, Belgium

Glioblastoma (GBM) is one of the most aggressive brain tumors. Despite the standard therapy, the survival from diagnosis remains dramatically low, especially due to tumor recurrence. Glioblastoma stem-like cells (GSCs) have been implicated in this tumor relapse, e.g., based on their capacity to escape the tumor and to migrate through the brain via CXCR4-dependent mechanisms. CXCR4 regulates biological features associated with tumor progression, including self-renewal, migration, and radio resistance. Importantly, its expression correlates with severity and poor prognosis of several cancers including GBM. The CXCR4/CXCL12 pathway therefore appears as an interesting potential therapeutic target. We have generated an oncolytic herpes simplex virus (oHSV) expressing HA-P2G, a mutated form of CXCL12 previously described as a CXCR4 competitive inhibitor. We demonstrate that, *in vitro*, oHSV/P2G impairs human GSC stemness marker expression, self-renewal, and migration. In two orthotopic xenograft murine models, oHSV/P2G intratumor injection limits tumor growth through the brain parenchyma and GSC migration through the *corpus callosum*. The ability of P2G to interfere with major GSC features demonstrates the interest in considering oHSV/P2G as a promising new therapeutic approach for GBM patients.

INTRODUCTION

Glioblastoma (GBM) is one of the most malignant brain tumors. Despite aggressive standard therapy, consisting in surgical resection followed by radio and chemotherapy, the current overall survival is only 15–16 months from the diagnosis,[1] due to a high recurrence rate. Recurrent tumors usually display poor sensitivity to standard therapies and high infiltrative capacity.[2]

Several studies have identified glioblastoma stem-like cells (GSCs) as partially responsible for GBM aggressiveness and recurrence.[3] Identified for their self-renewal abilities and the expression of neural stem cell (NSC) markers, GSCs have also been linked with increased invasive properties. In an orthotopic xenograft murine model, GSCs have been shown to escape the tumor, to invade the subventricular zone (SVZ) via the *corpus callosum*, and to be resistant to radio- or chemotherapy in a CXCR4/CXCL12-dependent manner,[4,5] properties that have been confirmed in humans.[6,7] In addition, they maintain an immune-suppressive microenvironment that is beneficial for the tumor growth.[8]

C-X-C chemokine receptor type 4 (CXCR4) and its ligand "Stromal cell-derived factor 1" (SDF1, better known as CXCL12) activate signaling pathways able to sustain stemness, proliferation, survival, and migration of tumor cells but also angiogenesis and immune response modulation.[9] Most GSCs highly express CXCR4 and produce CXCL12, revealing an autocrine signaling loop.[10] CXCR4, which emerges as a new marker of GSCs, is over-expressed in many cancers including GBM, and its expression usually correlates with tumor aggressiveness.[11–13] In addition, NSCs in the SVZ have recently been shown to harbor cancer-driving mutations and to participate to recurrence in a CXCR4/CXCL12-dependent manner.[14] In a mouse model, NSCs harboring p53 and PTEN (phosphatase and tension homolog) mutations have indeed been shown to be able to migrate into the cavity created by the primary tumor resection, differentiate into Olig2+ oligodendrocyte progenitors, and form a recurrent tumor, all of which being dependent on the CXCR4/CXL12 pathway.[14]

Preclinical studies have shown that inhibition of CXCR4 is able to alter GBM characteristics of aggressiveness.[15,16] Recently, a systemic delivery of nanoparticles coated with an iRGD peptide and in which a CXCR4 antagonist (AMD3100 or Plerixafor) is encapsulated resulted in the inhibition of GBM growth and activation of an anti-tumor microenvironment, thus confirming the importance of the

Received 2 October 2024; accepted 29 October 2025;
https://doi.org/10.1016/j.omton.2025.201083.

[6]These authors contributed equally

[7]These authors contributed equally

Correspondence: Sadzot-Delvaux Catherine, Laboratory of Virology and Immunology, GIGA-Immunobiology, University of Liège, 4000 Liège, Belgium.
E-mail: csadzot@uliege.be

CXCL12/CXCR4 pathway as a therapeutic target.[15] Several other CXCR4 antagonists have been evaluated in clinical trials for the GBM treatment, showing promising results when combined with standard therapies.[17] Among the CXCR4/CXCL12 inhibitors, mutated forms of CXCL12 have been shown to efficiently antagonize CXCR4 signaling pathway. Crump et al. demonstrated that switching the second amino acid of CXCL12 from a Proline to a Glycine (for that reason, called "P2G" in this manuscript) allows the mutated cytokine to bind CXCR4 while acting as a potent antagonist.[18] The anti-cancer effect of P2G has been described in breast cancer and osteosarcoma murine models, with various impact on metastasis formation[19,20] but so far not in GBM.

Oncolytic herpes simplex viruses (oHSVs) represent one of the most promising anti-cancer tools in the evolving landscape of virotherapy. Deep knowledge of HSV genome and a relative flexibility for genetic modifications have led to the engineering of a triple-mutated generation of oHSVs that has demonstrated its safety and is currently involved in clinical trials for the treatment of different tumors, including GBM.[21,22] In 2021, the Japanese Pharmaceuticals and Medical Devices Agency conditionally approved the first oHSV treatment (Delytact, G47Δ) for adult GBM.[23] However, in many cases, oHSVs alone are not sufficient to counteract GBM malignancy. For this reason, they are either used as part of combination therapies or engineered to express a transgene that can enhance their anti-tumor activity, both approaches being promising avenues.

We have engineered an oHSV armed with P2G (called oHSV/P2G), which can replicate in the tumor and locally induce the production and secretion of P2G. This approach combines thereby the well-described effects of oHSV virotherapy with the inhibition of a crucial signaling pathway, while avoiding side effects of a systemic administration of a CXCR4 antagonist. The current study focuses on oHSV/P2G impact on both GSCs' self-renewal and migration abilities, two important intrinsic GBM properties linked with GSC functions. These features have been addressed both *in vitro* in human patient-derived GSCs and *in vivo* in two murine orthotopic xenograft GBM model.[4]

RESULTS

Human GSCs express CXCR4 and CXCL12 at various levels

Five patient GSC cultures derived from newly-diagnosed (T08, T013, T018, and GB138[24]) or recurrent GBM (T033) have been used in this study. Considering the heterogeneity of patient-derived GSCs, these cell lines have been characterized for their capacity to express both CXCR4 and its ligand CXCL12. Flow cytometry analysis revealed that, apart from T08 that is barely positive for CXCR4 expression, the other GSC lines express CXCR4 at different levels (Figure S1A), with a very high expression in GB138 and T033 cells. The amount of CXCL12 produced in the supernatant and measured by ELISA showed that GB138 and T033 cells highly express CXCL12 while T08 cells secrete CXCL12 at a very low level (Figure S1B). T013 and T018 cells express both CXCR4 and CXCL12 at an intermediate level. To demonstrate the dependency of P2G effect on CXCR4 expression, most *in vitro* experiments aiming to evaluate oHSV/P2G impact have been carried out in parallel on GB138 and T08 cells, which respectively express high and low CXCR4 levels.

oHSV/P2G can antagonize CXCR4 signaling

oHSV/P2G has been engineered as follows. P2G coding sequence, under the EF1α promoter, has been inserted in the ΔICP34.5/ΔICP6 herpes simplex virus 1 (HSV-1) backbone, just after the pICP6-EGFP coding sequence (fQuick, kindly provided by Prof. EA Chiocca, Brigham and Women's Hospital, Boston, MA, USA). Moreover, P2G gene has been flanked by the interleukin-2 (IL-2) signal peptide and hemagglutinin (HA)-tag coding sequence, to promote its secretion and allow its detection, respectively (Figure 1A). To ensure its replication in GSCs, U_S12 gene coding for ICP47, which interferes with peptide presentation, has been deleted in the oHSV backbone. This deletion places the U_S11 gene, normally expressing a late protein, under the control of the U_S12 promoter, allowing thereby its expression as an immediate-early protein, partly restoring the infectivity of the oncolytic virus.[25] All constructs were verified by PCR and sequencing.

Western blot (WB) analysis of oHSV- or oHSV/P2G-infected GB138 or T08 cells revealed that, as expected, oHSV/P2G infection led to the expression and secretion of HA-tagged P2G by both GSC lines (Figure 1B).

Quantification of HA-tagged P2G in the supernatant of oHSV/P2G-infected GB138 cultures confirmed that P2G-HA is increasingly secreted up to 48 h after infection (Figure 1C). Filtration (0.1 μm filter) of the supernatant, previously proved effective in removing the viral particles without affecting the proteins in the medium,[26] did not affect the amount of P2G-HA (* in Figure 1C), making it possible to evaluate P2G impact independently of the viral infection or virus-induced cell death. Importantly, the amount of P2G detected in the supernatant (±1 ng/10^6 GB138 cells) was in the same range as the amount of CXCL12, the endogenous ligand of CXCR4 (±0.6 ng/10^6 GB138 cells) (Figure S1B).

Insertion of P2G transgene into the oHSV backbone did not impair the capacity of the virus to replicate in human GBM (Figure S2A), and, importantly, oHSV or oHSV/P2G infection has a similar impact on cell proliferation (Figure S2B). Culture in the presence of oHSV- or oHSV/P2G-conditioned medium (cm) did not affect cell proliferation either (Figure S2C). Finally, cell death upon infection was similar with both viruses (Figure S2D).

CXCR4 activation by CXCL12 triggers intracellular pathways, whose activation can lead to the ERK (extracellular signal-regulated kinase) or STAT3 (signal transducer and activator of transcription 3) phosphorylation, in a G-protein-dependent or -independent manner, respectively.[27] To confirm that P2G can antagonize CXCR4 signaling pathway, GB138 cells have been cultured in the presence of non-infected (NI), oHSV-, or oHSV/P2G-conditioned media, and the levels of phosphorylation of ERK and STAT3 were evaluated by WB (Figure 2). The densitometric quantification indicated that, contrary to oHSV(cm), oHSV/P2G(cm) significantly impaired the

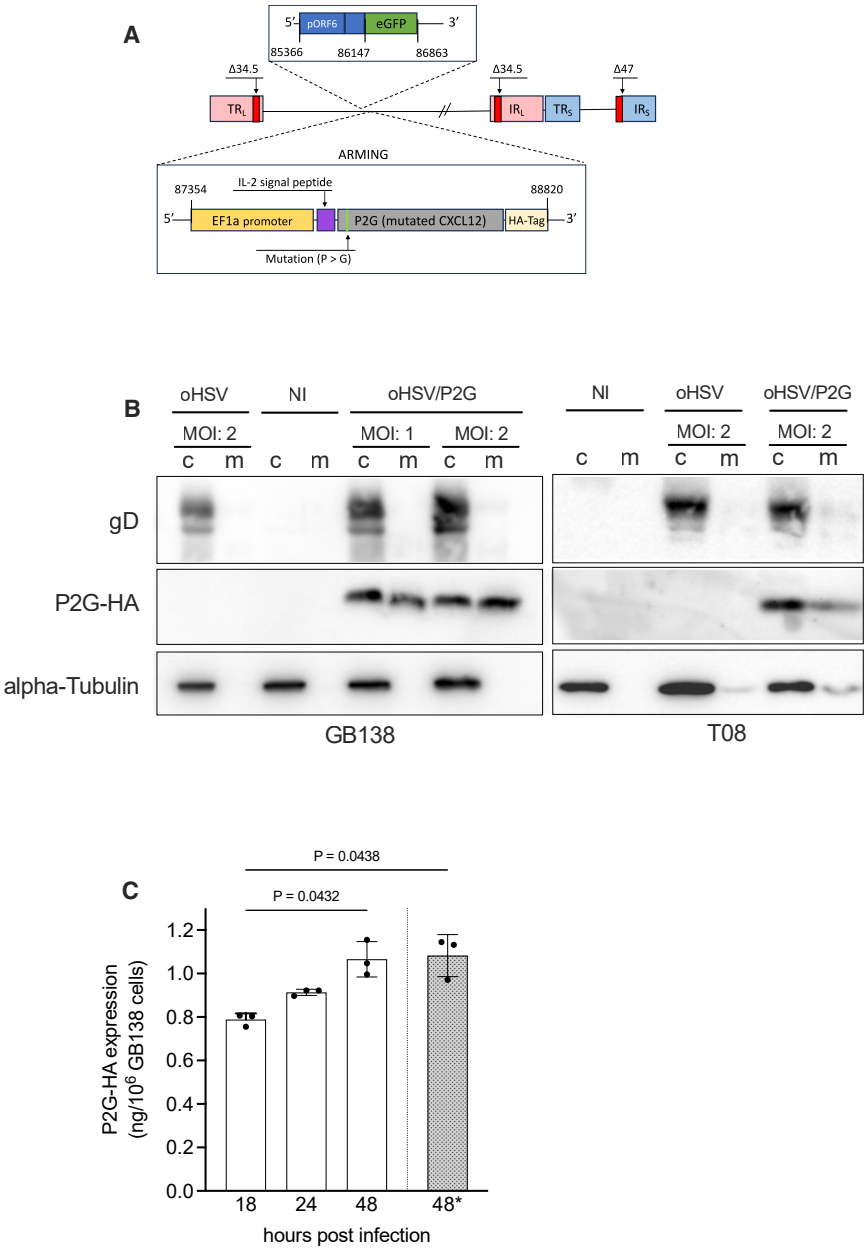

Figure 1. Construction and characterization of oHSV/P2G

(A) Schematic representation of oHSV/P2G genome. (B) P2G-HA expression by human GB138 (left panel) and T08 (right panel) primary cells was analyzed by western blot analysis performed on non-infected (NI), oHSV- or oHSV/P2G-infected cells lysates (c), and supernatant (m) (multiplicity of infection-MOI: 1 or 2). HSV glycoprotein D and α-tubulin detection were used as infection and loading control, respectively. (C) P2G-HA secretion in the supernatant was quantified by ELISA. Human GB138 cells were infected with oHSV or oHSV/P2G (MOI: 1), and the supernatant was harvested 18, 24, or 48 hours post-infection (hpi). In addition, the supernatant harvested 48 hpi was filtered to eliminate viral particle (0.1 μm filtration indicated by *). Bars represent the mean (SD) of 3 independent experiments. Statistical significance was determined by one-way ANOVA, with Tukey's multiple comparisons test with individual variances computed for each comparison.

phosphorylation of ERK, confirming the antagonistic properties of P2G on this signaling pathway. The phosphorylation of STAT3 followed the same trend with oHSV/P2G leading to a lower phosphorylation level of STAT3, but this effect was not statistically significant. AMD3100, a well-described CXCR4 inhibitor, led to decreased phosphorylation of both ERK and STAT3 without being statistically significant.

oHSV/P2G decreases GSC stemness marker expression and counteracts GSC self-renewal abilities

To investigate the effects of oHSV/P2G on GSCs key features, we first analyzed its impact on the expression of several markers, whose concomitant expression is generally linked to stem-like cell profile of GSCs.[28] Although oHSV infection of GB138 cells increased INTα6 and CD44 or decreased SOX2, OCT7, and SALL2 expression, oHSV/P2G infection led to a significant decrease of all these stemness markers' expression except for SALL2 expression, which decreased but not significantly (Figure 3A). Conversely, oHSV/P2G infection of T08 ($CXCR4^{low}$) cells had no significant effect on the expression of any of the analyzed stemness markers (Figure 3B). In line with these observations, infection of GB138 cells by oHSV/P2G significantly decreased the CD133 expression level compared to NI cells as analyzed by flow cytometry (Figure 3C).

The self-renewal ability of GB138 cells was then evaluated by either clonogenic or tumorsphere formation assays,[29] which respectively reflect the capacity of a single cell to form a colony by clonal expansion or to form spheres, two key features of GSCs. To limit the effect of the virus itself and to prevent virus-induced cell death from interfering with the observation of P2G effect, cells were infected at a low MOI (MOI: 0.1). The clonogenic assay revealed that, after 6 days of culture, the number of colonies was lower in the oHSV- or oHSV/P2G-infected cells than in the control condition, indicating that, despite the low MOI, the infection itself impairs the self-renewal capacity of GB138 cells, which nevertheless was even significatively more affected upon oHSV/P2G infection (Figure 3D).

To evaluate their capacity to form tumorspheres, GB138 cells were infected and cultured for 6 days in sphere-forming conditions.

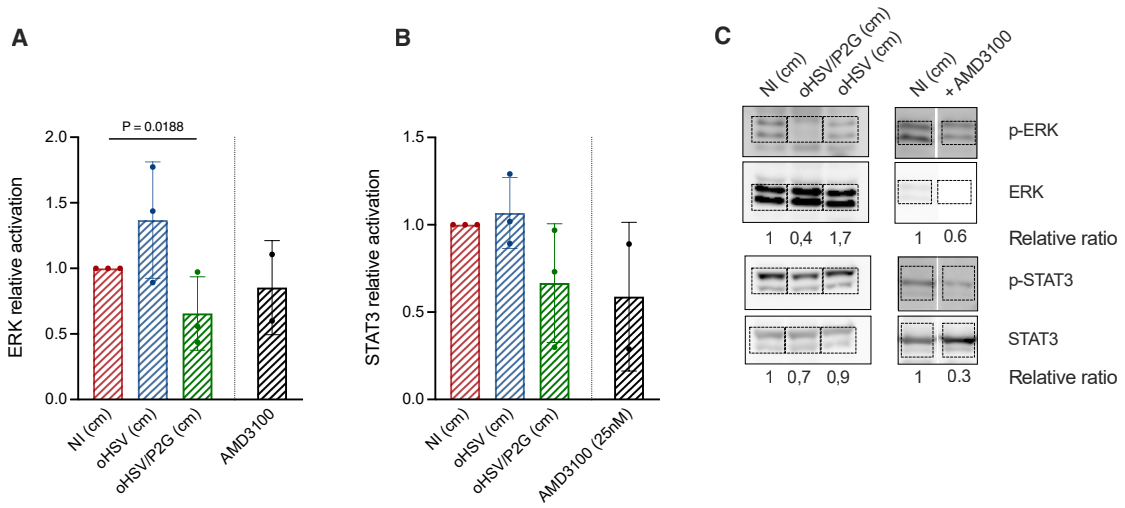

Figure 2. P2G impairs CXCR4 signaling pathway

P2G effect on CXCR4 signaling pathway was evaluated by western blot (WB) quantification of ERK (A) and STAT3 (B) phosphorylation in GB138 cells cultured with oHSV- or oHSV/P2G-conditioned media (cm) or AMD31000 (Plerixafor; 25 nM) used as a control of CXCR4 pathway inhibition. p-ERK/ERK and pSTAT3/STAT3 ratios were quantified by band densitometry after western blotting and expressed as the relative ratio with the ratio in cells cultured with NI(cm) considered as 1. Bars represent the mean (SD) of 3 independent experiments (2 for AMD3100). Statistical significance was determined by unpaired *t* test analyses. Representative pictures of a WB are shown in (C). Bands analyzed by densitometry for quantification are delineated by dotted lines.

Again, the infection itself had an impact on the capacities of GB138 cells to form tumorspheres, but the number of tumorspheres observed in oHSV/P2G-infected cells was even lower than that in oHSV-infected cells, demonstrating a significant effect of P2G itself (Figure 3E). This assay, repeated in the presence of conditioned media or AMD3100, confirmed that, contrary to oHSV(cm), which did not affect the tumorsphere formation, oHSV/P2G(cm) or AMD3100 significantly impaired the number of tumorspheres as compared to NI(cm) (Figure 3F). Interestingly, no significant difference was observed between oHSV/P2G(cm) and AMD3100 ($p = 0.958$). These results were confirmed for the other GSCs, except for T08 ($CXCR4^{low}$) cells for which a slight but not significant decrease was observed upon oHSV/P2G infection (Figure 3G).

oHSV/P2G counteracts GSC migration *in vitro*

Another important feature of GSCs previously observed *in vivo* is their capacity to escape the tumor mass and to migrate to a stem cell niche by a CXCR4/CXCL12-dependent mechanism. The migration of GSCs can be observed in the *corpus callosum,* through which they can eventually reach the SVZ.[4,30] This invading capacity of GSC is pointed as one of the mechanisms underlying GBM recurrence. The capacity of oHSV/P2G to impair GSC migration was first evaluated *in vitro* by transwell or sprouting assays.

GB138 tumorspheres were infected for 18 h with oHSV or oHSV/P2G (MOI: 0.1) before being dissociated and seeded onto laminin-coated transwells. Counting of cells that had migrated throughout the membrane over a 48 h period showed that the capacity of GB138 cells to invade the membrane was significantly impaired upon oHSV/P2G infection (Figure 4A left and middle panels). This observation was confirmed by quantification of the crystal violet released after lysis of cells that have migrated through the membrane (Figure 4A, right panel). In line with these results, the invasion ability of GB138 cells, cultured with oHSV/P2G(cm) or with AMD3100, was significantly lower than that in the presence of NI(cm) or oHSV(cm) (Figure 4B).

To confirm the ability of oHSV/P2G to impair GSC migration, sprouting assays were performed with T013 ($CXCR4^{medium}$) and T08 ($CXCR4^{low}$) tumorspheres previously infected or not with oHSV or oHSV/P2G. Twenty-four hours after seeding, migration of T013 cells was clearly impaired by oHSV/P2G infection while the effect on T08 cells was very limited (Figures 4C and 4D). Sprouting assay performed on cells cultured with conditioned media or media supplemented with AMD3100 confirmed these observations (Figures 4E and 4F). Although oHSV(cm) increased T013 cell migration, the presence of P2G significantly decreased it. AMD3100 tended to impair T013 cell migration as well, but its effect was not significantly different when compared to NI ($p = 0.167$) (Figure 4E). Conversely, migration of T08 cells was not affected neither by P2G nor by AMD3100 (Figure 4F). In these two assays, effects of P2G and AMD3100 were not significantly different.

Finally, both the transwell and the spouting assays were repeated in the presence of purified CXCL12 or AMD3100. In GB138 and T013 cells, CXCL12 significantly increased cell migration whereas AMD3100 tended to decrease it although its effect was not significant when compared to non-treated cells. On the contrary, CXCL12 or AMD3100 had no effect on T08 cells, confirming that GSC migration depends on the CXCR4/CXCL12 signaling (Figure S3).

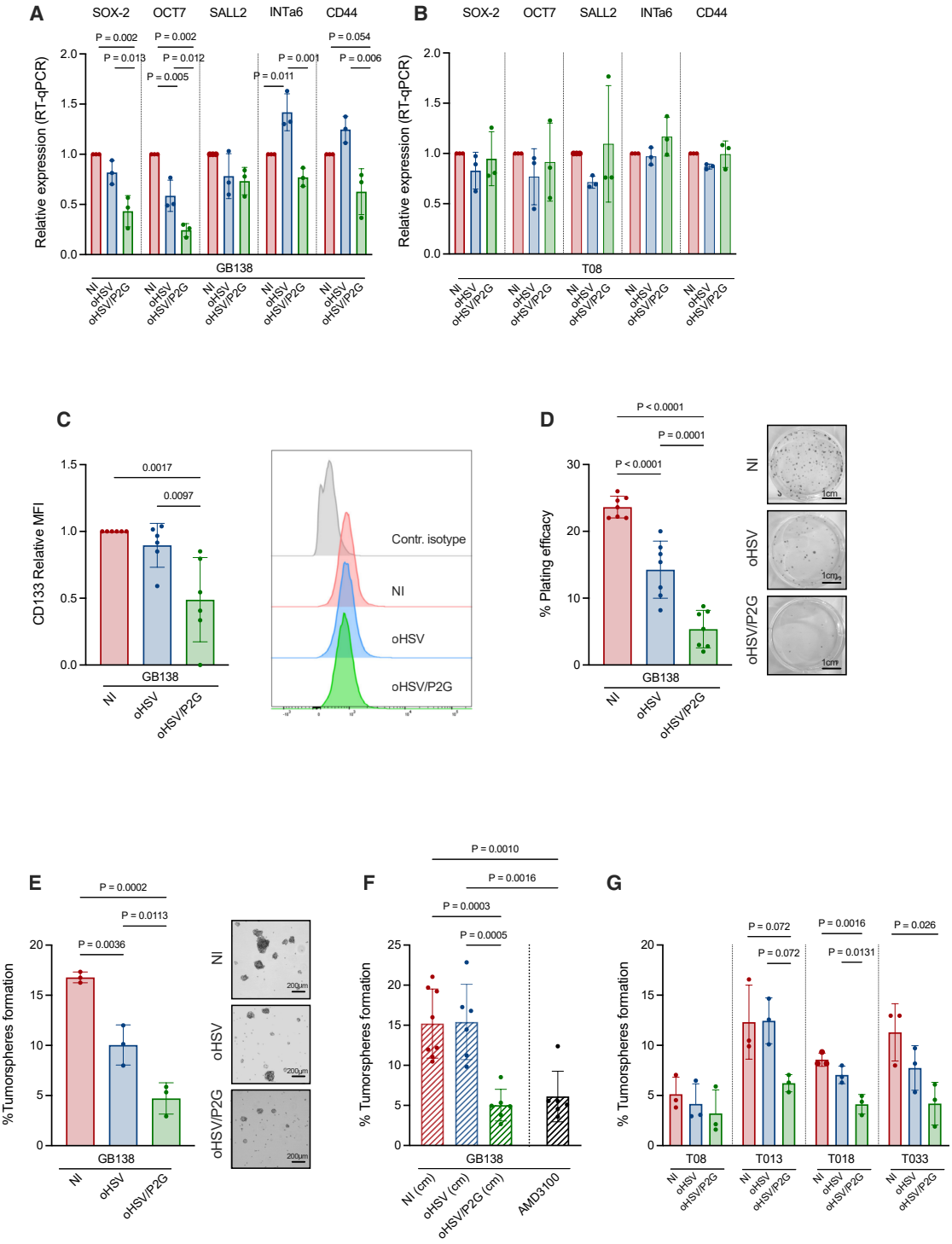

Figure 3. oHSV/P2G impacts stemness marker expression and GSC capacity to self-renew and to form tumorspheres

(A–C) Human GB138 (A and C) or T08 (B) cells were cultured as tumorspheres and infected with oHSV or oHSV/P2G (MOI: 0.1). Expression of stemness markers (SOX2, OCT7, SALL2, INTα6, and CD44) was evaluated 6 days post-infection by RT-qPCR and expressed relative to the level of expression in non-infected cells considered as 1 (A and B). Bars represent the mean (SD) of 3 (RT-qPCR) independent analyses. Statistical significance was determined for each gene by ordinary one-way ANOVA with Tukey's multiple comparisons test, with a single pooled variance. In parallel, GB138 cells were dissociated, and the median fluorescence intensity (MFI) of cells expressing CD133 at the plasma membrane was evaluated by flow cytometry (C). The MFI of 6 independent experiments is shown as relative to the MFI in the NI cells considered as 1 for each

(legend continued on next page)

oHSV/P2G impairs tumor growth and GB cell migration *in vivo*

The capacity of oHSV/P2G to interfere with tumor development and tumor cell migration was evaluated *in vivo* in two orthotopic xenograft murine models, with engraftment of GB138-RFP$^+$Luc$^+$ (Figure 5) or T033-LRLG (dsRed$^+$) (Figure 6), two GSC lines modified to express fluorescent marker.

A first experiment (Exp1) was performed in the GB138 model. For technical reasons, this experiment has been performed in two times with nine (3 in each experimental group) and twenty mice (6 for PBS or oHSV and 8 for oHSV/P2G treatments) (Figure 5A). Briefly, GB138-RFP$^+$Luc$^+$ cells were engrafted into the right striatum of *nude* mice (day 0). On day 19, *in vivo* bioluminescence imaging was performed to monitor tumor growth. Statistical differences between experimental groups were analyzed by R to take into consideration the potential bias resulting from pooling two independent sets of data (R script in supplemental material) and showed that all groups harbor a comparable bioluminescence signal intensity, without reaching statistical significance (Figure 5B). On day 20, PBS, oHSV, or oHSV/P2G (1×10^6 plaque-forming units [PFUs], 2 μL) was injected into the tumor mass. Mice were sacrificed on day 47, and brains were cleared for light-sheet microscopy analysis. The tumor volume estimation after 3D reconstruction clearly indicated that tumors in the oHSV- and oHSV/P2G-treated mice were smaller than those in the PBS group although the differences were not statistically significant (Figure 5C, statistical analysis in supplemental material). Importantly, while all PBS- or oHSV-treated mice harbored tumors, two oHSV/P2G-treated mice did not present any tumors at the end of the experiment.

After manual annotation of individual serial light-sheet images, the *corpus callosum* was 3D-reconstructed (representative pictures on Figure 5D; all pictures in Figure S4; exemplative 3D reconstruction in Video S1). Although tumors remain quite compact and did not invade the healthy surrounding tissue, we identified GBM cells escaping the tumor mass and migrating through the *corpus callosum*, in line with previous studies. These cells were highlighted using fire statistical colors, reflecting migration distance relative to the tumor axis, and the volume of the infiltrative tumoral tissue was measured. While migrating cells were observed in all PBS-treated tumors, they were observed in 66% of the oHSV- and only in 44% of the oHSV/P2G-treated groups (Figures 5E and S4). Moreover, the volume corresponding to cells migrating toward the *corpus callosum* was extremely low in oHSV- or oHSV/P2G-treated mice and significantly lower in oHSV/P2G-treated mice than in the control group (Figure 5F). The decrease of migration was even more marked considering the ratio between the volume of migrating cells and the whole tumor volume (Figure 5G), showing a clear and significant decrease in oHSV/P2G mice compared to control mice.

To evaluate the capacity of oHSV or oHSV/P2G to limit tumor growth, a long-term experiment was then performed in the same GB138 model (Exp 2). Briefly, 28 mice were engrafted with GB138-RFP$^+$Luc$^+$ cells and treated twice (day 20 and 42) with PBS (9 mice), oHSV (9 mice), or oHSV/P2G (10 mice) (Figure 5A). By day 139, none of the mice in any of the experimental groups had died nor exhibited abnormal behavior that would have warranted euthanasia. Mice were then sacrificed, and immunostaining on serial brain sections was performed to evaluate tumor size (Figures 5H and 5I). While most tumors of the PBS-treated mice were massive, some of them occupying almost the entire hemispheres, tumors in mice treated with oHSV or oHSV/P2G were either completely absent (3/9 and 4/10 in oHSV- and oHSV/P2G-treated mice, respectively) or very small, demonstrating the basal effect of virotherapy on the tumor growth. At this long-term experiment, no significant difference in tumor volume was observed between oHSV and oHSV/P2G, 139 days post-infection.

The capacity of oHSV/P2G to interfere with tumor development and tumor cell migration was also assessed in a more invasive T033-LRLG model.[31] As a prerequisite, we confirmed that T033 cells, isolated from a recurrent tumor and expressing CXCR4 at a high level, were able to migrate *in vitro* and that this migration was impaired upon oHSV/P2G infection (Figure S5A).

Mice were then engrafted with T033-LRLG cells expressing dsRed. Based on the tumor growth observed in previous experiments, PBS, oHSV, or oHSV/P2G (5 mice in each group) was administered by intratumor injection on day 14 and 21 from the engraftment (Figure 6A). One mouse did not receive any treatment and was considered as a control to evaluate the invasiveness of the T033-derived tumor about 2 months after engraftment (day 63). At this late time point, tumor cells were observed invading not only the right hemisphere in which the engraftment was done but also the left hemisphere, which was invaded mainly through the corpus callosum (Figure 6B, left panel). Tumor cells were detected on 8 serial sections (covering the distance from −2 to +2 mm around the bregma on the antero-posterior axis) confirming the capacity of T033-LRLG cells to

experiment (C, left panel), and histograms of a representative sample analysis are shown (C, right panel). Statistical significance was determined by ordinary one-way ANOVA with Tukey's multiple comparisons test, with a single pooled variance. (D) The capacity of GB138 cells to self-renew upon oHSV or oHSV/P2G infection (MOI: 0.1) was measured by a clonogenic assay. Bars represent the mean (SD) of 7 wells (3 independent experiments; 1 to 3 wells/condition in each experiment). Statistical significance was determined by one-way ANOVA with Tukey's multiple comparisons test, with a single pooled variance. A representative picture of each experimental condition is shown in parallel. Scale bar represents 1 cm. (E–G) The capacity of GB138 cells to form tumorspheres upon oHSV or oHSV/P2G infection was expressed as a percentage of plated cells forming spheres 18 h after plating. Representative pictures of tumorspheres upon mock (NI), oHSV, or oHSV/P2G infection are shown in parallel. Scale bar represents 200 μm (E). The experiment was repeated with GB138 cells cultured in the presence of NI-, oHSV-, oHSV/P2G-conditioned media or NI media supplemented with AMD3100 (40 nM) (F). Finally, 4 other patient-derived primary GSCs (T08, T013, T018, and T033) were mock-infected or infected with oHSV or oHSV/P2G (G). Bars represent mean (SD) of 3 (E and G) or 6 (F) independent analyses. Statistical significance was determined by one-way ANOVA with Tukey's multiple comparison test with a single pooled variance.

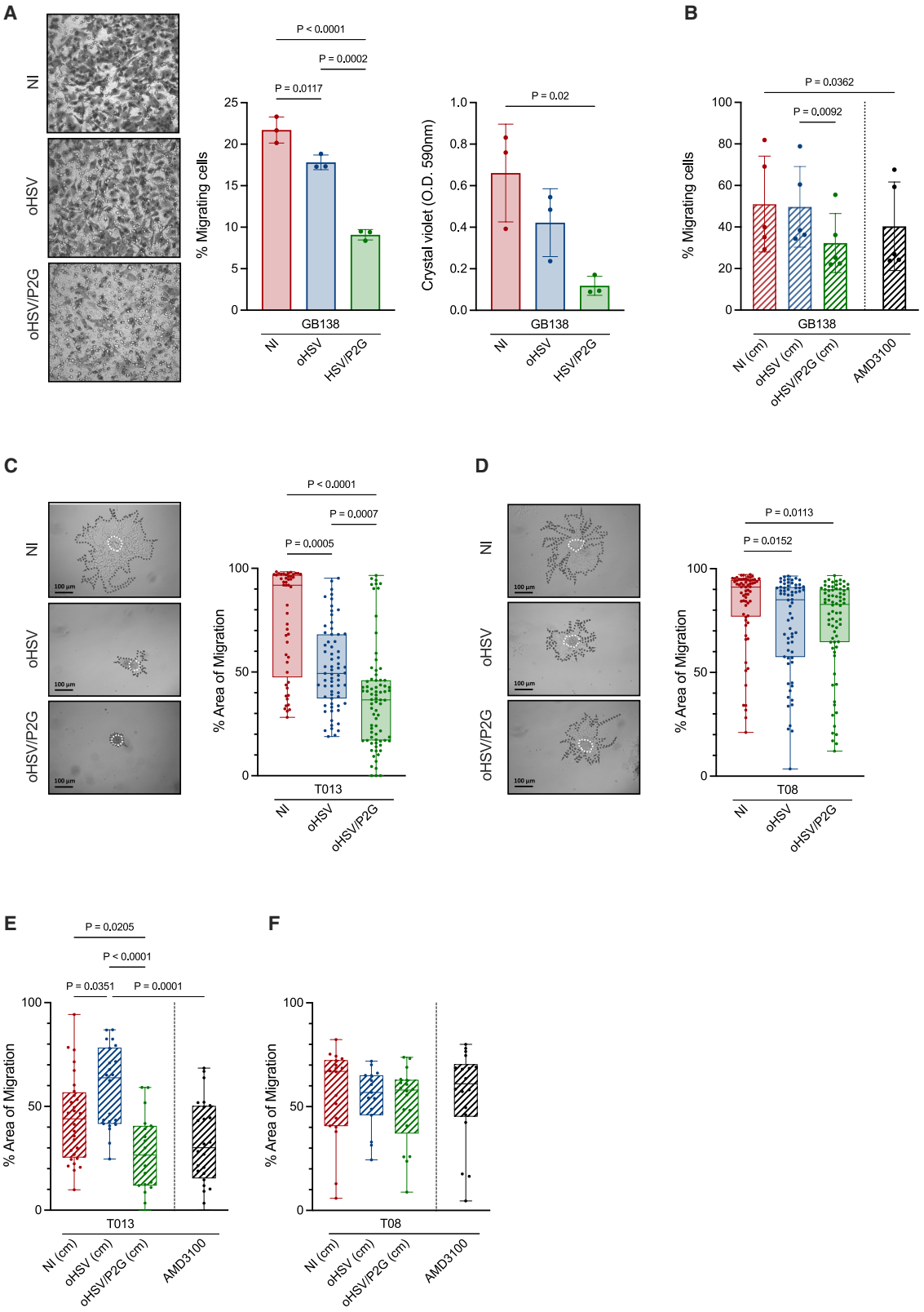

(legend on next page)

invade the whole hemisphere and to form a highly invasive tumor (Figures 6D and S5B, gray bar).

Analyses of the area of dsRed^{+} cells on each section using a machine learning-based pixel classifier revealed that the tumor area was significantly smaller in mice treated with oHSV or oHSV/P2G (Figures 6D and S5B) compared to PBS.

Quantification of the mean distance between the centroids of all annotated grid elements revealed that the capacity of tumor cells to migrate and infiltrate the surrounding healthy tissue was significantly reduced upon oHSV/P2G injection compared to PBS and to oHSV alone (Figures 6E and S5C), which highlights the interest of arming the virus with a CXCR4 inhibitor. Importantly, beside the basal effect of the virotherapy, which limits tumor size, arming the virus with P2G has a strong impact on cell migration, allowing to maintain the tumor in a more spatially defined area. These results were in line with the observations made in the GB138 model.

DISCUSSION

GBM is the most aggressive form of adult brain cancer and remains associated with poor prognosis mostly due to therapeutic failure and recurrences.[1] GSCs that express stemness markers, display strong self-renewal abilities, and are generally resistant to most therapies have been identified as contributing to GBM recurrence.[32] Moreover, GSCs participate to the establishment of an immune-suppressive microenvironment sustaining tumor growth.[8] As shown in previous studies, some GSC features such as self-renewal and capacity to form tumorspheres or to migrate are mediated by the CXCR4/CXCL12 pathway.[10,11,33] In many cancers including GBM, CXCR4 expression is correlated with poor prognosis, highlighting its inhibition as a potential therapeutic strategy.[12,13] Numerous preclinical studies have investigated the efficacy of systemic delivery of CXCR4 inhibitors with encouraging outcomes. However, systemic administration of CXCR4 inhibitors leads to side effects and poor pharmacokinetics properties.[34]

In addition to the side effects that can result from a systemic administration of any drug, the blood-brain barrier (BBB) further complicates the targeting of brain tumors. Therefore, many technical approaches are being considered to either allow the drug to be transported by a carrier capable of crossing the BBB or deliver the drug directly to the tumor.

A very promising technical approach is the use of nanoparticles to deliver drugs that can target either the tumor itself or the microenvironment and the immune cells in particular.[35] Synthetic protein nanoparticles coated with a cell-penetrating iRGD peptide and encapsulating small interfering RNA against STAT3, a major transcription factor associated with GBM progression, AMD3100, or immune checkpoint inhibitor have proven their efficacy to inhibit GBM proliferation to modify the microenvironment and to sensitize the tumor to radiotherapy.[15,36,37] Although able to cross the BBB upon systemic delivery, which constitutes an important step, nanoparticles were detected in various organs and in the liver in particular,[36] potentially leading to side effects, depending on the drug. More recently, extravesicular vesicles shown to play a role in various pathogenesis including cancer have been evaluated for their capacity not only to be loaded with drugs but also to be modified to specifically target a cell or a tissue. Although very novel and requiring deeper characterization, this approach using extravesicular vesicles derived from mesenchymal stem cells has been shown to cross the BBB more easily than synthetic nanoparticles and to be less immunogenic and appear thus as promising.[38]

Virotherapy and in particular herpes simplex virus virotherapy, which has proven its safety for GBM treatment, constitutes another powerful approach to ensure a localized administration while limiting the side effects on other organs. Many oHSVs have been developed to treat GBM and to target GSCs.[22] Many of those have been armed with transgene coding for cytokine, chemokine, cytotoxic, anti-apoptotic, anti-angiogenic transgene that will interfere with one or several biological processes involved in the tumor development. With their capacity to replicate in tumor cells and kill them while sparing healthy cells, they directly participate in the tumor size decrease. In addition, independently of the transgene, they can trigger the local and systemic immune response, which plays a crucial role in controlling the tumor.

We have engineered an oncolytic HSV-1 (Δγ34.5/ΔICP6/ΔICP47) armed with a mutated form of CXCL12 (called P2G) described in

Figure 4. oHSV/P2G impacts GB cell migration

(A and B) Transwell assay: GB138 cells infected or not with oHSV or oHSV/P2G (MOI: 0.1) were cultured in the upper insert of a two-compartment culture device (Transwell), and their capacity to migrate through the transwell membrane was evaluated after 48 h. Representative picture of each condition is shown in the left panel (magnification: 20x) while migration is represented either as the percentage of cells that have migrated through the transwell membrane (middle panel) or by the measure of the crystal violet released after the lysis of cells that have migrated (right panel) (A). The same experiment was performed with cells cultured in the presence of non-infected (NI), oHSV- or oHSV/P2G-conditioned media (cm), or NI-conditioned media supplemented with AMD3100 (40 nM) (B). Bars represent the mean (SD) of 3 (A) or 5 (B) independent experiments. Statistical significance was determined by one-way ANOVA, with Tukey's multiple comparisons test, with individual variance computed for each comparison. (C–F) Sprouting assay: T013 (CXCR4^{medium}) (C) and T08 (CXCR4^{low}) (D) GSCs cultured as tumorspheres were either non-infected or infected with oHSV or oHSV/P2G. Representative pictures are shown in parallel (left panels). The sphere areas were measured at 1 hpi (hours post-infection, white dotted lines) and 24 hpi (dark dotted line), and the percentage of migration (right panels) was expressed as follows: (*Total area at 24h-Area at 1h*)/*Total areaat 24h*. Scale bar represents 100 μm. The same experiment was repeated with T013 (E) or T08 (F) cells cultured with NI-, oHSV- or oHSV/P2G-conditioned media or NI-conditioned media supplemented with AMD3100 (40 nM). Boxplots represent the repartition of the values of each dataset, each dot representing one sphere. Area of migration has been measured in 4 (C and D) or 3 (E and F) independent experiments. Whiskers represent the maximum and minimum values. Statistical significance was determined by Kruskal-Wallis test (C and D) or ordinary one-way ANOVA (E and F), depending on the normality evaluated with the Shapiro-Wilk normality test.

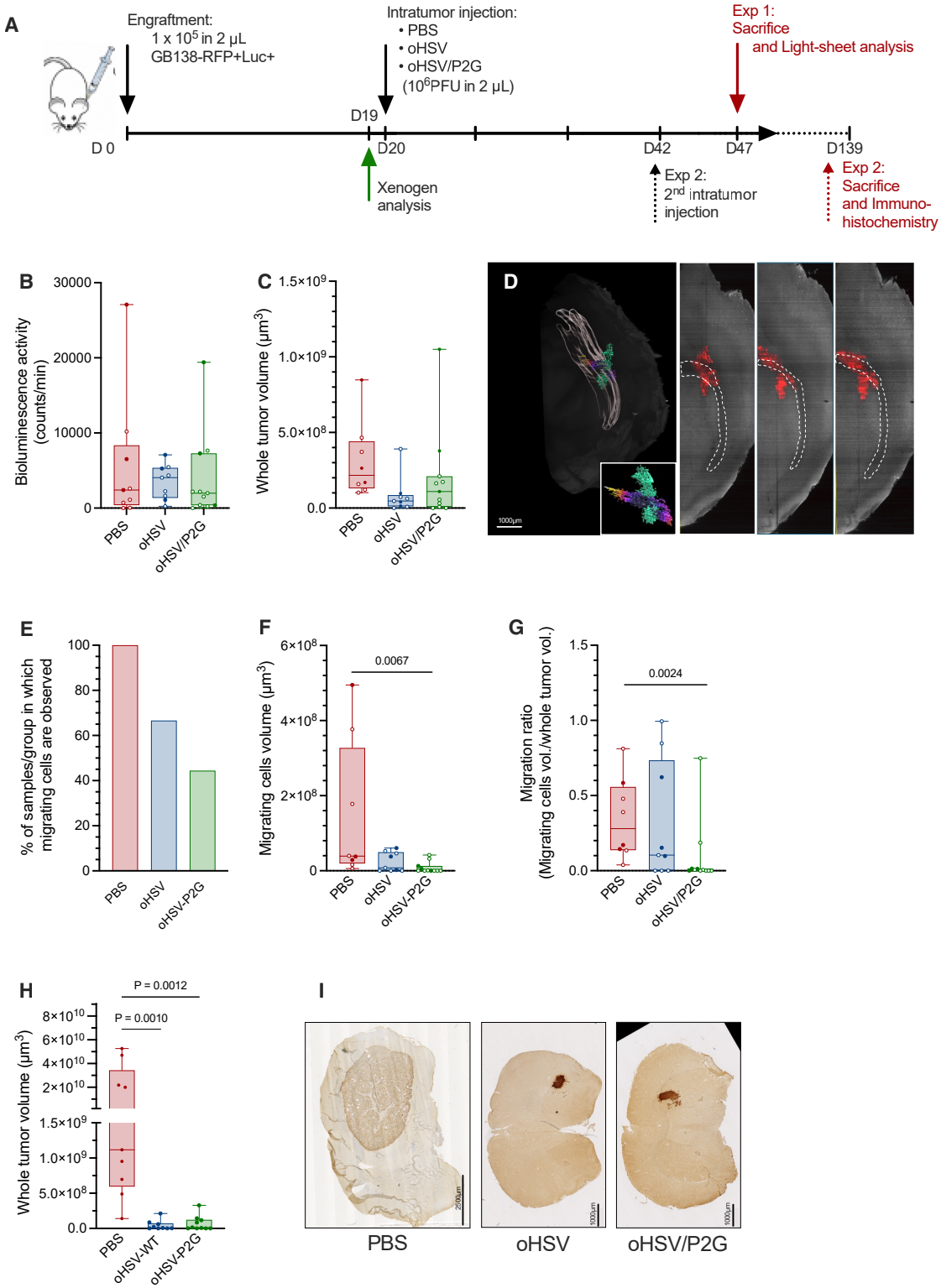

Figure 5. oHSV/P2G impairs GB cell migration in a GB138 cell orthotopic xenograft *in vivo* model

(A) Experimental settings of the orthotopic xenograft model. (B) to (G) correspond to Exp1 (short-term) results while (H) and (I) correspond to Exp 2 (long-term). (B) Size of the tumor evaluated by bioluminescence imaging on day 19. For technical reason, Exp 1 (B–G) was performed in two consecutive series, and two dataset were thus obtained

(legend continued on next page)

the literature as a potent CXCR4 inhibitor.[18] Considering that the CXCR4/CXCL12 pathway controls many biological mechanisms involved in cancer progression, we hypothesize that P2G might have a very broad effect not only on GBM cells, which are the focus of this work, but also on the microenvironment.

The insertion of P2G does not impair virus replication and leads to the secretion of P2G by the infected cells. Furthermore, the amount of P2G secreted by the infected GBM cells is shown to be similar to the amount of endogenous CXCL12.

Although the virus itself influences human GSC phenotype and even though arming does not induce additional cell death compared to the virus itself, the presence of P2G has a significant impact on GSC features as compared to the non-armed virus. Arming with P2G, indeed, significantly decreases stemness markers' expression and impairs self-renewal and migration capacities of GSCs as confirmed by culture with conditioned media devoid of viral particles. Importantly, the effect of P2G depends on the level of CXCR4 in patient-derived GSCs and is therefore very low in GSCs with low levels of CXCR4 expression.

In a GB138 orthotopic xenograft murine model, intratumor injection of either oHSV or oHSV/P2G reduces tumor size, as estimated by 3D-reconstructed light-sheet microscopy images and immunohistochemical staining. It should be noted that in Exp 1 (short-term experiment), one of the oHSV/P2G-treated mice harbors a huge tumor, comparable to the tumors usually observed in the PBS group. This could account for technical issues, in particular to the difficulties to ensure the virus injection into the tumors, which grow slowly and are very small at the time of treatment. Interestingly, while all PBS- or oHSV-treated mice developed a tumor, two (out of 11) oHSV/P2G-treated mice did not, as observed in light-sheet microscopy analysis carried out at the end of the experiment (day 47, Figure S4). Importantly, in a long-term experiment (Exp 2) in which mice were treated twice (3 weeks apart) and sacrificed about 100 days after the second treatment, tumors in the PBS group were huge, occupying a large part of the hemisphere while tumors in both oHSV- and oHSV/P2G-treated mice were very small and even undetectable in 33% (3 out of 9) and 25% (4 out of 10) in oHSV- and oHSV/P2G-treated mice, respectively. These observations demonstrate that virotherapy could lead to a long-lasting impact despite the absence of adaptive immune response in *nude* mice. Surprisingly, despite the size of the tumors, none of the PBS-treated mice lost weight or displayed abnormal behavior. However, for ethical reasons, all mice were sacrificed on day 139, and no survival assay was performed.

Although presenting GSC features and being able to migrate, GB138 cells lead to tumors that grow quite slowly and remain in a relatively defined region with tumor cells migrating quite exclusively through the corpus callosum. To confirm the capacity of oHSV/P2G to limit GSC migration, another *in vivo* model was thus set up. After only 2 months, T033 tumor cells were detected not only all over the right injected hemisphere but also in the left hemisphere, reflecting high invasiveness. Once again, both oHSV and oHSV/P2G were able to reduce tumor size.

Notwithstanding encouraging results demonstrating the capacity of oHSV/P2G to significantly impair stemness features *in vitro*, we could not demonstrate *in vivo* a clear-cut improvement upon oHSV/P2G treatment compared to non-armed oHSV regarding the capacity to kill the tumor cells and to clear the tumor *in vivo*. Considering that, *in vitro*, oHSV and oHSV/P2G lead to cell death with the same efficacy and impact similarly cell proliferation, it is not surprising that, *in vivo*, in absence of adaptive immune response known to play a critical role in the virotherapy efficacy, no significant differences of tumor size could be observed about 100 days after the viral injection. However, it is important to note that, while most *in vitro* experiments were performed with a low MOI (0.1), a high dose of virus (10^6 PFU) was injected in the tumor to ensure the virotherapy efficacy. Although impossible to evaluate, the MOI at the site of injection is thus probably much higher than that in *in vitro* experiments. We could not rule out that, *in vivo*, the viral infection itself has such a strong impact on tumor growth that the impact of P2G is underestimated. It would be worth evaluating whether a lower MOI would have a less drastic effect on the tumor size while sustaining a stronger and long-lasting production of P2G that would highlight its impact.

GSCs can escape the tumor in a CXCR4-dependent manner and migrate through the *corpus callosum*, potentially to the SVZ,[4,39] which could participate to treatment failure and recurrence. In

(plain dot: first series, circle: second series). Statistical significance (for B–G) was determined in R (R script available in supplemental material) to verify whether any bias might result from differences between the two datasets. (C) Whole tumor volume measured on tumor 3D reconstruction (Imaris) of brains recovered on day 47. Despite the trend showing a reduction of the tumor volumes in the oHSV and oHSV/P2G mice, no statistical difference with the control group was observed (R script available in supplemental material). (D) Representative picture of the 3D reconstruction of the tumor mass (green) and of cells migrating (statistically fire-colored according to their distance to the central tumor mass) through the *corpus callosum* (gray). Scale bar represents 1 mm. 3D reconstruction of the tumor mass and of migrating cells is shown independently of the *corpus callosum* in the insert. Three individual images of that specific sample are shown on the right panels. Cancer cells (RFP^+) and the *corpus callosum* (manually annotated) appear in red and white dotted lines, respectively. Pictures of Imaris 3D modelization of all brains are shown in Figure S4. A movie allowing to visualize the steps of the 3D reconstruction and to turn it at 360° is available in the supplemental information (Video S1). (E) Percentage of mice for which cells migrating through the *corpus callosum* were observed. (F and G) Volume of cells migrating through the *corpus callosum* (F) or ratio of migrating cells regarding the volume of the whole tumor (G). Boxplots represent the repartition of the measures carried out on 8 (PBS), 9 (oHSV), and 11 (oHSV/P2G) mice with whiskers representing the maximum and minimum values. (H and I) Long-term experiment (Exp 2). Whole-tumor volume of brains recovered on day 139 (H). Boxplots represent the repartition of the measures form 9 (PBS and oHSV) and 10 (oHSV/P2G) mice with whiskers representing the maximum and minimum values. Statistical significance was determined with a Kruskal-Wallis test after Shapiro-Wilk normality test. A presentative picture of one section is shown for each experimental group (I). Scale bar represents 2.5 mm (oHSV) or 1 mm (oHSV and oHSV/P2G).

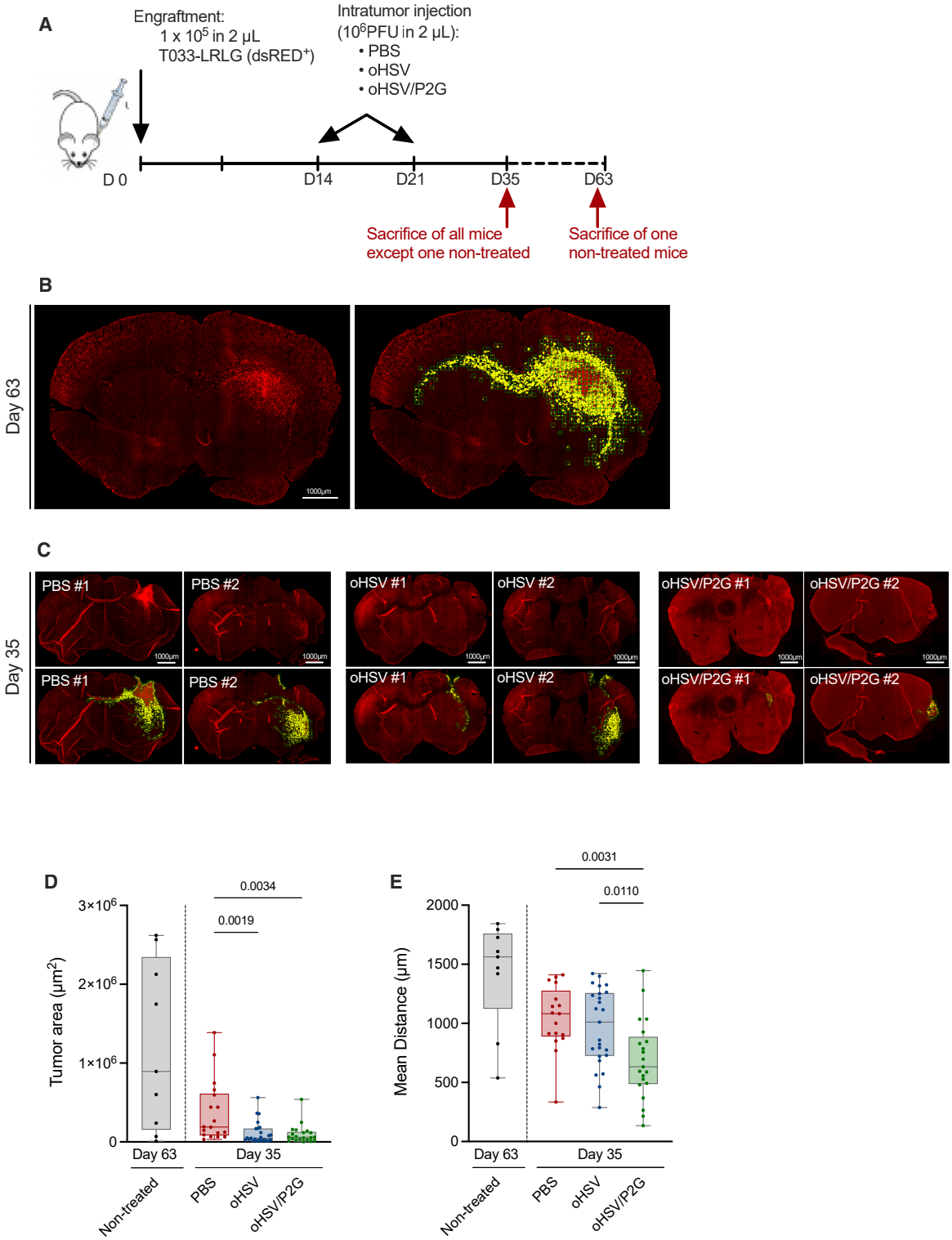

Figure 6. oHSV/P2G impairs GB cell migration in a T033 cell orthotopic xenograft *in vivo* model

(A) Experimental settings of the orthotopic xenograft model. (B) Representative picture of brain sections of the mice sacrificed on day 63 (non-treated mice). Images were with obtained with a Zeiss Axioscan 7 slide scanner (20× objective) (left panel) and analyzed for quantification (right panel). Scale bar represents 1 mm. Image analysis was

(legend continued on next page)

addition, CXCR4 is also involved in the differentiation of NSCs harboring cancer-driving mutations into Olig2$^+$ oligodendrocyte progenitors and of their migration into the cavity created by primary tumor resection where they can form a recurrent tumor.[14] It should therefore be considered that inhibiting cell migration by inhibiting CXCR4 could be beneficial, particularly by reducing the ability of tumor cells to give rise to recurrences. We clearly showed that P2G arming impairs cell migration, both *in vitro* and in two different *in vivo* models. Importantly, in the GB138 model, no tumor cell migration was observed in 5 mice (out of 9; 55%) in the oHSV/P2G group while observed in all PBS- and in 3 (out of 9; 33%) oHSV-treated mice. Moreover, considering the size of the tumors, cell migration was extremely limited in all oHSV/P2G samples. These observations were confirmed in the T033 model. In this model, which harbors more invading capacities, oHSV/P2G, in contrast to oHSV, significantly impaired tumor cell migration distance, resulting in less infiltrative tumors. These observations highlight the capacity of a CXCR4 inhibitor locally expressed by an armed oncolytic virus to restrain tumor cell migration. Impairing tumor cell migration is certainly of high interest, not only because it limits the capacity of the GSCs to reach the SVZ or other niche where they could hide and acquire treatment resistance[5] but also because consequently the tumor mass remains more compact, thereby facilitating the possibility of further surgical resection.

While the SVZ constitutes an important niche for GSCs, it is not the only niche where they can hide. Hira and colleagues have indeed shown that hypoxic peri-arteriolar tissue constitutes a GSC niche similar to the hypoxic peri-arteriolar hematopoietic stem cell niches[40] and that CXCR4 antagonists may mobilize GSCs from this niche and sensitize them to therapy.[41] Surgical resection and radiotherapy, considered as first-line treatment, are usually followed by vasculogenesis promoted by a CXCR4-dependent recruitment of bone marrow-derived cells (BMDCs), which can be inhibited by CXCR4 inhibitors. Although not investigated in the current study, it would really be worth investigating tumor vasculogenesis and mobilization of both GSCs and BMDCs, which would reinforce the rationale of oHSV/P2G administration after the current treatment.

Besides their capacity to lyse tumor cells, oncolytic viruses can also impact the tumor microenvironment (TME). They can trigger the production of cytokines and thereby recruit immune cells.[42–44] CXCR4 inhibitors have also been shown to reshape the TME and to potentiate immunotherapy in melanoma,[45] in ovarian cancer,[46] and in GBM.[37,47] In preclinical models, they have been shown to switch macrophages from a pro-tumor M2-like to an anti-tumor M1-like phenotype.[48] Of note, pro-tumoral macrophages, particularly abundant in GBM, correlate with faster progression and therapy resistance. In addition, CXCR4 inhibition has recently been shown to decrease regulatory T cells (Treg) recruitment, to impair their functions and more generally to counteract immunosuppressive properties of the TME.[49] It is thus crucial to evaluate the oHSV/P2G effect on the immune response. Characterization of oHSV/P2G in an immunocompetent syngeneic model will allow to confirm that, in GBM, CXCR4/CXCL12 inhibition not only modifies GSC phenotype and capacity to migrate but also modulates the TME, thereby controlling tumor growth as described for other cancers.

In conclusion, our results demonstrate that oHSV/P2G has a significant impact on GSCs, reducing their stemness marker expression and significantly impairing their self-renewal and migration capacity both *in vitro* and *in vivo*.

oHSV/P2G virotherapy, whose impact on CXCR4$^+$ cells of the TME needs to be further evaluated, could thus be considered as an add-on to the first-line treatment, to limit the risk of relapse and improve GBM prognosis.

MATERIALS AND METHODS

Cell lines

Vero cells (ATCC, #CCL-81) and patient-derived human GBM GB138 cells,[24] were maintained in Dulbecco's modified Eagle's minimal essential medium high glucose (DMEM HG, Lonza, Verviers, Belgium) supplemented with 10% fetal bovine serum (FBS). GBM patient-derived cultures (T08, T013, T018, and T033[24]) were established from residual tumor tissue after surgical resection (Neurosurgery department, Liège University Hospital -CHU- and University Hospital Biobank -BHUL-, Liège, Belgium), in accordance with the legal regulations on residual human body material. GB138 RFP$^+$ Luc$^+$ and T033-LRLG[31] cells expressing RFP and dsRed, respectively, were used for follow-up in *in vivo* experiments. All GSCs were cultured as tumorspheres in stem cell medium (DMEM/F12 with GlutaMAX [Gibco] supplemented with B27 [1/50] without vitamin A [Gibco], 1% penicillin-streptomycin [Lonza, Verviers, Belgium], 1 μg/mL of heparin [n 7692.1, Carl Roth, Belgium], recombinant human epidermal growth factor [20 ng/mL], and recombinant human

performed with QuPath using a machine learning-based pixel classifier to identify dsRed$^+$ signal (yellow pixels, right panel). A 100 × 100 μm grid was overlaid on each image, and only grid elements containing tumor annotations were retained for further quantification (green, right panel). (C) Pictures of brain sections from PBS-, oHSV-, or oHSV/P2G-treated mice (2 mice/experimental condition as representative example; day 35) and of the analysis performed for quantification (yellow: dsRed$^+$ signal detection; green: 100 × 100 μm overlaid grid). Scale bar represents 1 mm. (D) Tumor area estimated on each brain section from one non-treated or 5 PBS-, oHSV-, or oHSV/P2G-treated mice. Tumor area corresponds to the cumulative area of tumor cells detected in QuPath (yellow pixels). Boxplots represent the repartition of the values of each dataset, each dot representing the quantification on one slide. Tumor area estimated on each section from a single brain is represented in Figure S5B. Whiskers represent the maximum and minimum values. Statistical significance of day 35 data was determined by Kruskal-Wallis test after Shapiro-Wilk normality test. (E) Tumor cell spread estimated on brain sections from one non-treated or 5 PBS-, oHSV-, or oHSV/P2G-treated mice. Cell spread is estimated by the mean distances between the centroids of annotated grid elements. Boxplots represent the repartition of the values of each dataset, each dot representing the quantification on one slide. Mean distance estimated on each section from a single brain is represented in Figure S5C. Whiskers represent the maximum and minimum values. Statistical significance of day 35 data was determined by Kruskal-Wallis test after Shapiro-Wilk normality test.

fibroblast growth factor 2 [20 ng/mL] [Peprotech]). When indicated, GB138 were cultured as monolayers.

Construction of recombinant oHSVs

Recombinant viruses were engineered in fHsvQuik-1 bacterial artificial chromosome (BAC) containing an attenuated HSV-1 (strain F) (Δγ34.5, ΔUL39, GFP^+; kind gift from A. Chiocca, Brigham and Women's Hospital, Boston, MA, USA). Further ICP47 deletion was done as described by Todo et al.[50] Recombinants were obtained by the two-step Red recombination technique "en passant."[51] The sequence of human mutated CXCL12 sequence (second amino acid mutated P to G) flanked by the IL-2 signal peptide and HA tag in 5′ and 3′, respectively, and controlled by the EF1a promoter was inserted just after the EGFP gene (Figure 1A). Vero cells seeded in 6-well plates were transfected with this construct using jetPEI (Polyplus, Illkirch – FRANCE). Virus stocks were produced as previously described.[52] Viral particles were then ultracentrifuged, resuspended in PBS with 10% glycerol, and stored at −80°C. Virus titration was performed in Vero by plaque assay.[53]

Virus and cm production

GB138 cells were grown in DMEM HG 10% FBS. At confluence, the culture medium was removed and replaced by DMEM/F12 (without added growth factors), and cells were mock-infected or infected with oHSV or oHSV/P2G (MOI: 1). After 48 h, media were collected, centrifuged (260*g*, 5 min), filtered with 0.1 µm filter (Pall Life Sciences 4611 Acrodisc syringe filters with Supor membrane, 25 mm, 0.1 µm, sterile), aliquoted, and stored at −80°C.

Viral growth assay

50K GB138 cells were seeded in 24-well plate for 24 h and then infected with oHSV or oHSV/P2G (MOI 0.1 and 1). Virus replication was measured by recording GFP signal for 48 h (Incucyte S3). Total green object area (μm^2/well) was used to assess virus replication. Total object area measured with contrast imaging was recorded in parallel and expressed relative at T0 to evaluate the cell proliferation.

Detection of P2G-HA by WB

400K cells were seeded for 24 h before being infected with oHSV or oHSV/P2G (MOI: 1 or 2). Supernatant and cells were harvested 18 h post-infection (hpi).

Cells were lysed using modified RIPA buffer (Tris-HCl 50 mM pH 7.5, NaCl 150 mM, EDTA 1 mM, NP40 1%, and deoxycholate 0.25%) supplemented with proteases inhibitors (cOmplete, Roche).

Supernatants were diluted in acetone (1:4) to precipitate the proteins and further centrifuged at 13,000 rpm for 30 min.

After electrophoresis and transfer onto polyvinylidene fluoride membrane (GE Healthcare), membranes were incubated overnight at 4°C with anti-gD (ref. sc-21719, Santa Cruz; dilution 1:1,000), and anti-HA (ref. ab9110, Abcam; 1:1000) antibodies. Mouse anti-alpha-tubulin (ref. T6199, Sigma; 1:2,000) was used as loading control. HRP-conjugated anti-mouse immunoglobulin G (IgG) (ref. 7076, Cell Signal; dilution 1:2,500) or horseradish peroxidase (HRP)-conjugated-anti-rabbit IgG (ref. 7074, Cell Signal; 1:2,500) was used as secondary antibodies. After incubation with enhanced chemiluminescence (ECL) solution (luminol: 25 mg/100 mL in Tris-HCl pH 8.6 0.1 M; para-hydroxy coumaric acid 11 mg/10 mL DMSO; H_2O_2 35%), chemiluminescence signals were recorded with LAS4000 CCD camera (GE Healthcare).

pERK and pSTAT relative quantification

125K GB138 cells were seeded in T25 in stem cell culture medium. After 6 days, the culture medium was replaced by conditioned media supplemented with CXCL12 (80 pM) to induce CXCR4 signaling pathway. After 30 min, cells were harvested, lysed using modified RIPA buffer, and analyzed by WB with anti-ERK (#9102, Cell Signal; dilution 1:2,000), anti-pERK (#9106S, Cell Signal, 1:2,000), anti-STAT3 (#9139 Cell Signal, 1:1,000), or anti-pSTAT3 (#9145, Cell Signal, 1:1,000) antibodies. Mouse anti-alpha-tubulin (#T6199, Sigma; 1:2,000) was used as a loading control. HRP signals were revealed using ECL and imaged with LAS4000 CCD camera (GE Healthcare). Band densitometry was analyzed using ImageJ.

P2G-HA quantification by ELISA

P2G-HA quantification in the culture supernatants was performed by ELISA with the HA tag ELISA kit (ref MBS3802035, MyBioSource), according to the manufacturer protocol.

Resazurin assay

50K GB138 cells were seeded in 24-well plate for 24 h and then infected with oHSV or oHSV/P2G (MOI: 1). After 24, 48, or 72h, culture medium was removed, cells were washed with PBS, and medium were replaced by 300 µL of resazurin solution (1/5 resazurin +4/5 DMEM/F12). After 4 h, resazurin was transferred into a 96-well black opaque plate. Fluorescence was measured using FilterMax F5 multi-mode microplate reader and expressed as relative fluorescent units (Ex = 530–570 nm, Em = 590–620 nm).

RT-qPCR

Cells were seeded in 6-well plates (400K cells/well) for 24 h before being infected with oHSV or oHSV/P2G (MOI: 0.1) for 18 h and kept growing as tumorspheres.

Tumorospheres were then dissociated with Accutase (Biowest, Nuaillé, France), and 125K cells were seeded in T25 in stem cells medium. Six days after plating, the spheres were collected and total RNA was purified (Nucleospin kit, Macherey-Nagel, according to the manufacturer's protocol). One µg of RNA was reverse-transcribed using RevertAid H Minus First Strand cDNA Synthesis Kit (Thermo Scientific) with random primers. TATA-Box binding protein (TBP) transcripts or 18S rRNA were used as controls. qPCR reaction samples were prepared as follows: 4 µL of the diluted cDNA (10 ng in total) were mixed with 5 µL of SYBR green (TAKYON, Eurogentec, Liege, Belgium) and 0.5 µL of each primer (4 µM each) in a final volume of 10 µL. Primers used for transcript detection

Table 1. Primers used for RT-qPCR

	Forward	Reverse
SOX2	AGTCTCCAAGCGACGAAAAA	TTTCACGTTTGCAACTGTCC
OCT7	CTGACGATCTCCACGCAGTA	GGCAGAAAGCTGTCCAAGTC
SALL2	ACTCCTCTGGGGTGACCTTT	GGAGTGGTAGTGGAGGTGGA
Intα6	TTCCTGTTTCCTAGCTGTGT	ACTCTTTGGCCTGTTAGTCA
CD44	TCCAACACCTCCCAGTATGACA	GGCAGGTCTGTGACTGATGTACA
18S	AACTTTCGATGGTATCGCCG	CCTTGGATGTGGTAGCCGTTT
hTBP	ACAGCCTGCCACCTTACG	TGCCATAAGGCATCATTGGACTA

are described in Table 1. RT-qPCR was performed using the Roche LightCycler 480 (3 min at 95°C of activation; 45 cycles: denaturation 95°C, 3 s, hybridization and elongation 60°C 25 s).

Flow cytometry

Tumorspheres or cells cultured as monolayers were washed with PBS and dissociated by incubation during 10 min at 37°C with Accutase or trypsin-EDTA (Biowest), respectively, then centrifuged (350*g*, 5 min, 4°C), and washed with flow buffer. 5 μL of APC-conjugated anti-CXCR4 (1/20; BioLegend, Amsterdam, the Netherlands) or BV421-conjugated anti-CD133 antibody (1/25; BioLegend, Amsterdam, the Netherlands) was added to 1×10^5 cells in 100 μL of flow buffer and kept at 4°C for 1 h in the dark. Cells were then washed and centrifuged at 400*g* for 4 min at 4°C. After a second wash, cells were resuspended in 200 μL of flow buffer and analyzed with the FACSCanto II (BD Biosciences). Data were analyzed with FlowJo software.

Clonogenic assay

GB138 cells were seeded in 6-well plates (400K cells/well) for 24 h. Cells were then mock-infected or infected with oHSV or oHSV/P2G (MOI: 0.1) for 18 h before being harvested and counted. 500 cells were re-seeded in 6-wells plates for 7 days. They were then fixed with paraformaldehyde (4%, 10 min, room temperature [RT]) and stained with crystal violet (10 min, RT). After a final wash, colonies were counted, and the plating efficiency was expressed as the number of colonies/the number of plated cells × 100. Finally, cells were lysed with 0.1% SDS, and crystal violet absorbance was measured to confirm the colonies count.

Tumorspheres assay

GB138 cells were seeded in 6 wells-plates in DMEM HG media + 10% FBS (400,000 cells/well) for 24 h before being infected (MOI: 0.1). T08, T013, T018, and T033 cells were seeded in T25 in stem cell media (250K cells/flask). As spheres reach sufficient size, they were infected (MOI: 0.1). After 18 h of infection, cells were either harvested with trypsin-EDTA or dissociated using Accutase. 125K cells were transferred to a T25 in stem cell media. Alternatively, non-infected cells were seeded (125K cells in a T25) in stem cell media in the presence of conditioned media. Tumorsphere formation efficiency was evaluated after 6 days and expressed as the number of tumorspheres/the number of plated cells × 100.

Migration quantification by transwell assay

The upper chambers of ThinCerts transwells (pore size: 8 μm; Greiner Bio-One, CELLSTAR) placed in a 24-well plate (Greiner Bio-One) were filed with 60 μL of laminin (20 μg/mL in PBS) and incubated for 24 h at 37°C. Excess laminin was removed, 25K cells were plated in a final volume of 200 μL of conditioned media without growth factors, and 300 μL of complete medium were added. After 48 h, the medium was removed, and inserts were washed with PBS. Cells were then fixed with 4% paraformaldehyde for 10 min and washed with PBS, before being stained with crystal violet for 10 min. Non-migrating cells were removed from the transwell with a cotton swab, and invading cells were counted with ImageJ on five pictures taken randomly (magnification X20). The percentage of migrating cells is expressed as the number of invading cells/the number of plated cells × 100.

Sprouting assay

Tumorspheres were either infected with oHSV or oHSV/P2G or cultured with conditioned media for 24 h. They were then seeded into wells of a 96-well plate previously coated with 50 μL hydrobromide poly-D-lysine (10 μg/mL) for 30 min, washed with sterile water, and left to dry overnight under the hood. If infected, tumorspheres were kept in DMEM media without growth factors, while, if pretreated with conditioned media, they were kept in DMEM supplemented with conditioned media (50/50).

Pictures of the tumorspheres were taken with an optical microscope 1 h after plating and after 24 h of incubation. The migration level is measured using ImageJ and expressed as the percentage of migration regarding the tumorspheres area 1 h after plating (*Area at* 24*h-area at* 1*h* * 100).

In vivo experiments

All *in vivo* experiments were performed as previously approved by the Animal Ethical Committee of the University of Liège, in accordance with the Declaration of Helsinki and following the guidelines of the Belgium Ministry of Agriculture in agreement with European Commission Laboratory Animal Care and Use Regulation. Six-week-old female immunodeficient Crl:NU-Foxn1nu mice (Charles River Laboratories, Brussels, Belgium) were used for xenograft experiments. They were housed at the Animal Facility, University of Liège,

in sterilized, filter-topped cages (controlled temperature: 22°C, controlled lighting: 12h day/night). After 1 week acclimatization period, intra-striatal grafts were performed following the previously described procedures.[24] Briefly, 100K GB138-RFP$^+$Luc$^+$ or T033-LRLG cells resuspended in 2 μL of PBS were injected into the right striatum (stereotactic coordinates: 0.5 mm anterior and 2 mm lateral from the bregma and at a depth of 2.5 mm) of mice previously anesthetized with an intraperitoneal injection (intraperitoneal [i.p.]) of a Rompun (Sedativum 2%, Bayer, Brussels, Belgium) and Ketalar (Ketamin 50 mg/mL, Pfizer, Brussels, Belgium) solution (V/V) prepared just before injection. For GB138 RFP$^+$Luc$^+$ experiments, PBS (control) or oncolytic viruses (oHSV or oHSV/P2G; 10^6 PFU in 2μL of PBS) were injected on day 20 within the tumor, under anesthesia, and using the same stereotactic coordinates. For the long-term experiment (Exp 2), a second intratumor injection of PBS, oHSV, or oHSV-P2G was done on day 42. Mice were sacrificed on day 47 (Exp 1 and 2; light-sheet microscopy) or on day 139 (Exp 3, long-term experiment).

For T033-LRLG experiments, treatments were injected on day 14 and 21 and mice were sacrificed on Day 35. One non-treated mouse was sacrificed on day 63 to observe long-term development of T033-LRLG tumors. Mice health status (weight and behavior) was evaluated daily.

ARRIVE 2.0 (Animal Research: Reporting of *In vivo* Experiments) reporting guideline was used to assure the adequate management of animals.[54]

Bioluminescence activity

Mice engrafted with GB138-RFP$^+$Luc$^+$ were injected i.p. with Beetle Luciferin potassium salt (ref. E1605, Promega) (150 mg/kg) and imaged (under 2.5% isoflurane anesthesia) with camera-based bioluminescence imaging system (Xenogen IVIS 50; exposure time 1 min, 15 min after intraperitoneal injection). Regions of interest were defined manually, and images were processed using Living Image and Igor Pro software (version 2.60.1). Raw data were expressed as total counts/min.

Brain tissue clarification and light-sheet microscopy acquisition and analysis

Mice were euthanized with i.p. injection of Euthasol Vet (140 mg/kg), followed by an intracardiac perfusion of ice-cold saline solution. Brains were further clarified to remove lipids and replace them with polyacrylamide. Afterward, brains were incubated for 6 h at RT in 50% RIMS solution (#D2158, Sigma-Aldrich; Refraction index: 1.46; 50% in water). 50% RIMS solution (Refractive Index Matching Solution) was then discarded and replaced by 100% RIMS solution for an overnight incubation at RT.

Eventually, brains were imaged using light-sheet microscopy. Images were acquired with 5X objective (zoom = 0.6; pixel size = 1.52; light-sheet 5.826 μm; center thickness = 12.4; image size = 2,922.4 × 2,922.4 μm^2) and processed to obtain one merged image per plane and 3D reconstruction using Zeiss Arivis software.

Tumors were visualized thanks to the RFP signal while the *corpus callosum* was annotated on each individual image based on the brain autofluorescence signal. Tumor and *corpus callosum* 3D modeling were performed on Imaris Image Analysis software and allowed whole tumor volume and migrating cells volume measurements.

Brain tissue processing and tumor volume measurement

Mice were euthanized with i.p. injection of Euthasol Vet (140 mg/kg) and intracardiac perfusion of ice-cold saline solution, followed by paraformaldehyde 4% in PBS (for histology). Brains were incubated in sucrose 30% (Fisher Chemical; 48 h, 4°C) for tissue cryopreservation, and sectioned into 14 μm-thick serial sections using a cryostat. On a single SuperFrost (Thermo Scientific) adhesive slide, two consecutive brain sections are separated by 420 μm (=14 μm × 30 sections) of tissue thickness, with the 29 intermediate sections distributed across 29 other SuperFrost slides.

Tumor volume analysis was performed either after immunohistochemical staining in the GB138 model or based on the dsRed fluorescence in the T033-LRLG model.

In the GB138 model, tumor cells were detected by immunohistochemical detection of human vimentin (Mouse anti-human vimentin, MAB3400, Merck, 1:200) with PolyviewPlus HRP-DAB kit (Enzo Life Sciences, Brussels, Belgium). The tumor was delineated in QuPath based on anti-human vimentin positivity. On each slide, whole tumor volume was calculated by summing the volumes between consecutive sections, using the truncated cone volume formula: $V = \text{height} \times \pi^3 \times (R1^2 + R2^2 + R1 \times R2)$ where height is the distance between two consecutive slices (420 μm) and R1 and R2 are their radii, determined by treating their areas (μm^2) as circles using the formula: $R = SQRT(Area/\pi)$.

For tumor detection in the T033 model, sections were permeabilized with 0.1% Triton X-100 (VWR) in PBS, and nuclei were counterstained with Hoechst (Sigma-Aldrich). Whole-slide images were acquired using a Zeiss Axioscan 7 slide scanner (20× objective). Tumor cell detection was performed in QuPath using a machine learning-based pixel classifier to identify dsRed$^+$ signal. A 100 × 100 μm grid was overlaid on each image, and all grid elements containing tumor annotations were retained as regions of interest. Tumor area was quantified on each brain section as the cumulative area of all annotated tumor elements on this section. Tumor spread was quantified as the cumulative area of annotated grid elements (10,000 μm^2 × number of elements). To evaluate dispersion, mean distances between the centroids of annotated grid elements were calculated. No volume or 3D reconstruction was attempted for this model because of the absence of a delineated tumor mass.

Statistical analysis

All statistical analyses were performed using GraphPad Prism 10. Data are displayed as mean ± SD or as boxplot with the whiskers representing the minimum and maximum values. When appropriate, normality was evaluated using Shapiro-Wild test. Depending on

the experiments, one-way ANOVAs or Kruskall-Wallis tests were performed as indicated in the figure legends. For *in vivo* experiments 1 and 2 (Figures 5B–5G), statistical significance was analyzed with R to take into consideration the putative experimental bias. R script is available in supplemental material.

DATA AND CODE AVAILABILITY

All original data shown in the figures and supplemental figures are available upon reasonable request.

ACKNOWLEDGMENTS

D.P. and S.G.J. have benefited respectively from a postdoctoral and doctoral fellowship from TELEVIE-FNRS, Belgium. D.M. is a Research Fellow of the FNRS, Belgium. This work was supported by grants from the National Fund for Scientific Research (FNRS, Télévie); the Special Funds of the University of Liège; and the Leon Fredericq Foundation, Liège, Belgium. The authors would like to thank Prof. A. Chiocca (Brigham and Women's Hospital, Boston, MA, USA) for fHsvQuik-1 BAC; C. Desmet (GIGA, University of Liège) for his help for R-statistical analysis; and all the members of the GIGA Viral Vector, Imaging and Flow Cytometry, Genomics platforms, and animal facilities for valuable technical support. We warmly thank Adeline Deward (www.illuminesciences.be) for the graphical abstract.

AUTHOR CONTRIBUTIONS

Conceptualization: D.P., D.M., and S.-D.C. Virus engineering: S.G.J., D.M., and D.P. with the help of L.M. *In vitro* experiments: D.P. and D.M. *In vivo* experiments: D.M. with the help of L.A., L.C., and B.B. Image analysis: D.M. with the help of H.A. Manuscript writing: D.M., D.P., and S.-D.C. Scientific discussions during the project: D.P., D.M., R.B., N.V., L.A., L.M., and S.-D.C. All authors critically reviewed and edited the manuscript. Funding acquisition: S.-D.C. D.P. and D.M. contributed equally as first authors. L.M. and S.-D.C. contributed equally as last authors. All authors approved the final manuscript.

DECLARATION OF INTERESTS

S.G.J. is currently a Postdoctoral Research Fellow at the Brain Tumor Research Center, Massachusetts General Hospital (MGH), Boston, MA, USA.

D.P. is currently a scientist at Janssen Vaccines and Prevention B.V., Leiden, the Netherlands.

DECLARATION OF GENERATIVE AI AND AI-ASSISTED TECHNOLOGIES IN THE WRITING PROCESS

During the preparation of this work, the author(s) used the Pixel Classifier AI-assisted module of QuPath in order to perform semi-automated identification of $dsRed^{+}$ cells based on manual annotations provided by the author(s). Each resulting image was subsequently reviewed and manually corrected by the author(s).

In addition, the author(s) used ChatGPT (OpenAI) to assist in the development of QuPath scripts for the generation of grid elements and the measurement of distances between them. All generated grid elements and corresponding distance measurements were manually checked and validated for each image.

After using these tools, the author(s) reviewed and edited the content as needed and take(s) full responsibility for the content of the published article.

SUPPLEMENTAL INFORMATION

Supplemental information can be found online at https://doi.org/10.1016/j.omton.2025.201083.

REFERENCES

1. Abedi, A.A., Grunnet, K., Christensen, I.J., Michaelsen, S.R., Muhic, A., Møller, S., Hasselbalch, B., Poulsen, H.S., and Urup, T. (2021). A Prognostic Model for Glioblastoma Patients Treated With Standard Therapy Based on a Prospective Cohort of Consecutive Non-Selected Patients From a Single Institution. Front. Oncol. *11*, 597587. https://doi.org/10.3389/fonc.2021.597587.
2. Goenka, A., Tiek, D., Song, X., Huang, T., Hu, B., and Cheng, S.Y. (2021). The many facets of therapy resistance and tumor recurrence in glioblastoma. Cells *10*, 484. https://doi.org/10.3390/cells10030484.
3. Yi, Y., Hsieh, I.Y., Huang, X., Li, J., and Zhao, W. (2016). Glioblastoma stem-like cells: Characteristics, microenvironment, and therapy. Front. Pharmacol. *7*, 477. https://doi.org/10.3389/fphar.2016.00477.
4. Goffart, N., Kroonen, J., Di Valentin, E., Dedobbeleer, M., Denne, A., Martinive, P., and Rogister, B. (2015). Adult mouse subventricular zones stimulate glioblastoma stem cells specific invasion through CXCL12/CXCR4 signaling. Neuro Oncol. *17*, 81–94. https://doi.org/10.1093/neuonc/nou144.
5. Goffart, N., Lombard, A., Lallemand, F., Kroonen, J., Nassen, J., Di Valentin, E., Berendsen, S., Dedobbeleer, M., Willems, E., Robe, P., et al. (2017). CXCL12 mediates glioblastoma resistance to radiotherapy in the subventricular zone. Neuro Oncol. *19*, 66–77. https://doi.org/10.1093/neuonc/now136.
6. Piccirillo, S.G., Spiteri, I., Sottoriva, A., Touloumis, A., Ber, S., Price, S.J., Heywood, R., Francis, N.J., Howarth, K.D., Collins, V.P., et al. (2015). Contributions to drug resistance in glioblastoma derived from malignant cells in the sub-ependymal zone. Cancer Res. *75*, 194–202. https://doi.org/10.1158/0008-5472.CAN-13-3131.
7. Lara-Velazquez, M., Al-Kharboosh, R., Jeanneret, S., Vazquez-Ramos, C., Mahato, D., Tavanaiepour, D., Rahmathulla, G., and Quinones-Hinojosa, A. (2017). Advances in brain tumor surgery for glioblastoma in adults. Brain Sci. *7*, 166. https://doi.org/10.3390/brainsci7120166.
8. Johnson, A.L., Laterra, J., and Lopez-Bertoni, H. (2022). Exploring glioblastoma stem cell heterogeneity: Immune microenvironment modulation and therapeutic opportunities. Front. Oncol. *12*, 995498. https://doi.org/10.3389/fonc.2022.995498.
9. Shi, Y., Riese, D.J., and Shen, J. (2020). The Role of the CXCL12/CXCR4/CXCR7 Chemokine Axis in Cancer. Front. Pharmacol. *11*, 574667. https://doi.org/10.3389/fphar.2020.574667.
10. Gatti, M., Pattarozzi, A., Bajetto, A., Würth, R., Daga, A., Fiaschi, P., Zona, G., Florio, T., and Barbieri, F. (2013). Inhibition of CXCL12/CXCR4 autocrine/paracrine loop reduces viability of human glioblastoma stem-like cells affecting self-renewal activity. Toxicology *314*, 209–220. https://doi.org/10.1016/j.tox.2013.10.003.
11. Richardson, P.J. (2015). CXCR4 and Glioblastoma. Anti Cancer Agents Med. Chem. *16*, 59–74. https://doi.org/10.2174/1871520615666150824153032.
12. Stevenson, C.B., Ehtesham, M., McMillan, K.M., Valadez, J.G., Edgeworth, M.L., Price, R.R., Abel, T.W., Mapara, K.Y., and Thompson, R.C. (2008). CXCR4 expression is elevated in glioblastoma multiforme and correlates with an increase in intensity and extent of peritumoral T2-weighted magnetic resonance imaging signal abnormalities. Neurosurgery *63*, 560–570. https://doi.org/10.1227/01.NEU.0000324896.26088.EF.
13. Isci, D., D'uonnolo, G., Wantz, M., Rogister, B., Lombard, A., Chevigné, A., Szpakowska, M., and Neirinckx, V. (2021). Patient-oriented perspective on chemokine receptor expression and function in glioma. Cancers *14*, 130. https://doi.org/10.3390/cancers14010130.
14. Li, X., Kim, H.J., Yoo, J., Lee, Y., Nam, C.H., Park, J., Lee, S.-T., Kim, T.M., Choi, S.H., Won, J.-K., et al. (2025). Distant origin of glioblastoma recurrence: neural stem cells in the subventricular zone serve as a source of tumor reconstruction after primary resection. Mol. Cancer *24*, 64. https://doi.org/10.1186/s12943-025-02273-2.
15. Alghamri, M.S., Banerjee, K., Mujeeb, A.A., Mauser, A., Taher, A., Thalla, R., McClellan, B.L., Varela, M.L., Stamatovic, S.M., Martinez-Revollar, G., et al. (2022). Systemic Delivery of an Adjuvant CXCR4-CXCL12 Signaling Inhibitor Encapsulated in Synthetic Protein Nanoparticles for Glioma Immunotherapy. ACS Nano *16*, 8729–8750. https://doi.org/10.1021/acsnano.1c07492.
16. Luo, Z., Wang, B., Chen, Y., Liu, H., and Shi, L. (2020). Novel CXCR4 Inhibitor CPZ1344 Inhibits the Proliferation, Migration and Angiogenesis of Glioblastoma. Pathol. Oncol. Res. *26*, 2597–2604. https://doi.org/10.1007/s12253-020-00827-x.
17. Huynh, C., Dingemanse, J., Meyer zu Schwabedissen, H.E., and Sidharta, P.N. (2020). Relevance of the CXCR4/CXCR7-CXCL12 axis and its effect in pathophysiological conditions. Pharmacol. Res. *161*, 105092. https://doi.org/10.1016/j.phrs.2020.105092.
18. Crump, M.P., Gong, J.H., Loetscher, P., Rajarathnam, K., Amara, A., Arenzana-Seisdedos, F., Virelizier, J.L., Baggiolini, M., Sykes, B.D., and Clark-Lewis, I.

(1997). Solution structure and basis for functional activity of stromal cell-derived factor-1; dissociation of CXCR4 activation from binding and inhibition of HIV-1. EMBO J. *16*, 6996–7007. https://doi.org/10.1093/emboj/16.23.6996.

19. Williams, S.A., Harata-Lee, Y., Comerford, I., Anderson, R.L., Smyth, M.J., and McColl, S.R. (2010). Multiple functions of CXCL12 in a syngeneic model of breast cancer. Mol. Cancer *9*, 250. https://doi.org/10.1186/1476-4598-9-250.

20. Neklyudova, O., Arlt, M.J.E., Brennecke, P., Thelen, M., Gvozdenovic, A., Kuzmanov, A., Robl, B., Botter, S.M., Born, W., and Fuchs, B. (2016). Altered CXCL12 expression reveals a dual role of CXCR4 in osteosarcoma primary tumor growth and metastasis. https://doi.org/10.1007/s00432-016-2185-5.

21. Russell, S.J., Peng, K.W., and Bell, J.C. (2012). Oncolytic virotherapy. Nat. Biotechnol. *30*, 658–670. https://doi.org/10.1038/nbt.2287.

22. Kardani, K., Sanchez Gil, J., and Rabkin, S.D. (2023). Oncolytic herpes simplex viruses for the treatment of glioma and targeting glioblastoma stem-like cells. Front. Cell. Infect. Microbiol. *13*, 1206111. https://doi.org/10.3389/fcimb.2023.1206111.

23. Maruyama, Y., Sakurai, A., Noda, S., Fujiwara, Y., Okura, N., Takagi, T., Asano, J., and Honda, F. (2023). Regulatory Issues: PMDA - Review of Sakigake Designation Products: Oncolytic Virus Therapy with Delytact Injection (Teserpaturev) for Malignant Glioma. Oncologist *28*, 664–670. https://doi.org/10.1093/oncolo/oyad041.

24. Kroonen, J., Nassen, J., Boulanger, Y.G., Provenzano, F., Capraro, V., Bours, V., Martin, D., Deprez, M., Robe, P., and Rogister, B. (2011). Human glioblastoma-initiating cells invade specifically the subventricular zones and olfactory bulbs of mice after striatal injection. Int. J. Cancer *129*, 574–585. https://doi.org/10.1002/ijc.25709.

25. Wakimoto, H., Kesari, S., Farrell, C.J., Curry, W.T., Zaupa, C., Aghi, M., Kuroda, T., Stemmer-Rachamimov, A., Shah, K., Liu, T.C., et al. (2009). Human glioblastoma-derived cancer stem cells: Establishment of invasive glioma models and treatment with oncolytic herpes simplex virus vectors. Cancer Res. *69*, 3472–3481. https://doi.org/10.1158/0008-5472.CAN-08-3886.

26. Iannello, A., Debbeche, O., El Arabi, R., Samarani, S., Hamel, D., Rozenberg, F., Heveker, N., and Ahmad, A. (2011). Herpes simplex virus type 1-induced FasL expression in human monocytic cells and its implications for cell death, viral replication, and immune evasion. Viral Immunol. *24*, 11–26. https://doi.org/10.1089/vim.2010.0083.

27. Busillo, J.M., and Benovic, J.L. (2007). Regulation of CXCR4 signaling. Biochim. Biophys. Acta *1768*, 952–963. https://doi.org/10.1016/j.bbamem.2006.11.002.

28. Jackson, M., Hassiotou, F., and Nowak, A. (2015). Glioblastoma stem-like cells: at the root of tumor recurrence and a therapeutic target. Carcinogenesis *36*, 177–185. https://doi.org/10.1093/carcin/bgu243.

29. Shaheen, S., Ahmed, M., Lorenzi, F., and Nateri, A.S. (2016). Spheroid-Formation (Colonosphere) Assay for in Vitro Assessment and Expansion of Stem Cells in Colon Cancer. Stem Cell Rev. Rep. *12*, 492–499. https://doi.org/10.1007/s12015-016-9664-6.

30. Volovetz, J., Berezovsky, A.D., Alban, T., Chen, Y., Lauko, A., Aranjuez, G.F., Burtscher, A., Shibuya, K., Silver, D.J., Peterson, J., et al. (2020). Identifying conserved molecular targets required for cell migration of glioblastoma cancer stem cells. Cell Death Dis. *11*, 152. https://doi.org/10.1038/s41419-020-2342-2.

31. Lombard, A., Isci, D., Reuter, G., Di Valentin, E., Hego, A., Martin, D., Rogister, B., and Neirinckx, V. (2024). Development of an intraventricular adeno-associated virus-based labeling strategy for glioblastoma cells nested in the subventricular zone. Neurooncol. Adv. *6*, vdae161. https://doi.org/10.1093/noajnl/vdae161.

32. Lombard, A., Digregorio, M., Delcamp, C., Rogister, B., Piette, C., and Coppieters, N. (2020). The Subventricular Zone, a Hideout for Adult and Pediatric High-Grade Glioma Stem Cells. Front. Oncol. *10*, 614930. https://doi.org/10.3389/fonc.2020.614930.

33. Würth, R., Bajetto, A., Harrison, J.K., Barbieri, F., and Florio, T. (2014). CXCL12 modulation of CXCR4 and CXCR7 activity in human glioblastoma stem-like cells and regulation of the tumor microenvironment. Front. Cell. Neurosci. *8*, 144. https://doi.org/10.3389/fncel.2014.00144.

34. Ongprakobkul, N., Ishida, Y., Hatano-Sato, K., Li, K., Petdachai, S., Usumi-Fujita, R., Hosomichi, J., Mahatumarat, K., and Ono, T. (2022). Effects of local vs systemic administration of CXCR4 inhibitor AMD3100 on orthodontic tooth movement in rats. Am. J. Orthod. Dentofacial Orthop. *162*, 182–192. https://doi.org/10.1016/j.ajodo.2021.03.018.

35. Xiong, Y., Sun, M., Yang, Q., Zhang, W., Song, A., Tan, Y., Mao, J., Liu, G., and Xue, P. (2025). Nanoparticle-based drug delivery systems to modulate tumor immune response for glioblastoma treatment. Acta Biomater. *194*, 38–57. https://doi.org/10.1016/j.actbio.2025.01.050.

36. Gregory, J.V., Kadiyala, P., Doherty, R., Cadena, M., Habeel, S., Ruoslahti, E., Lowenstein, P.R., Castro, M.G., and Lahann, J. (2020). Systemic brain tumor delivery of synthetic protein nanoparticles for glioblastoma therapy. Nat. Commun. *11*, 5687. https://doi.org/10.1038/s41467-020-19225-7.

37. Wei, R., Li, J., Lin, W., Pang, X., Yang, H., Lai, S., Wei, X., Jiang, X., Yuan, Y., and Yang, R. (2024). Nanoparticle-mediated blockade of CXCL12/CXCR4 signaling enhances glioblastoma immunotherapy: Monitoring early responses with MRI radiomics. Acta Biomater. *177*, 414–430. https://doi.org/10.1016/j.actbio.2024.02.007.

38. Gratpain, V., Mwema, A., Labrak, Y., Muccioli, G.G., van Pesch, V., and des Rieux, A. (2021). Extracellular vesicles for the treatment of central nervous system diseases. Adv. Drug Deliv. Rev. *174*, 535–552. https://doi.org/10.1016/j.addr.2021.05.006.

39. Ehtesham, M., Winston, J.A., Kabos, P., and Thompson, R.C. (2006). CXCR4 expression mediates glioma cell invasiveness. Oncogene *25*, 2801–2806. https://doi.org/10.1038/sj.onc.1209302.

40. Hira, V.V.V., Breznik, B., Vittori, M., Loncq de Jong, A., Mlakar, J., Oostra, R.-J., Khurshed, M., Molenaar, R.J., Lah, T., and Van Noorden, C.J.F. (2020). Similarities Between Stem Cell Niches in Glioblastoma and Bone Marrow: Rays of Hope for Novel Treatment Strategies. J. Histochem. Cytochem. *68*, 33–57. https://doi.org/10.1369/0022155419878416.

41. Hira, V.V.V., Van Noorden, C.J.F., and Molenaar, R.J. (2020). CXCR4 antagonists as stem cell mobilizers and therapy sensitizers for acute myeloid leukemia and glioblastoma? Biology *9*, 31. https://doi.org/10.3390/biology9020031.

42. Lemos de Matos, A., Franco, L.S., and McFadden, G. (2020). Oncolytic Viruses and the Immune System: The Dynamic Duo. Mol. Ther. Methods Clin. Dev. *17*, 349–358. https://doi.org/10.1016/j.omtm.2020.01.001.

43. Benencia, F., Courrèges, M.C., Conejo-García, J.R., Mohamed-Hadley, A., Zhang, L., Buckanovich, R.J., Carroll, R., Fraser, N., and Coukos, G. (2005). HSV oncolytic therapy upregulates interferon-inducible chemokines and recruits immune effector cells in ovarian cancer. Mol. Ther. *12*, 789–802. https://doi.org/10.1016/j.ymthe.2005.03.026.

44. Ribas, A., Dummer, R., Puzanov, I., VanderWalde, A., Andtbacka, R.H.I., Michielin, O., Olszanski, A.J., Malvehy, J., Cebon, J., Fernandez, E., et al. (2017). Oncolytic Virotherapy Promotes Intratumoral T Cell Infiltration and Improves Anti-PD-1 Immunotherapy. Cell *170*, 1109–1119.e10. https://doi.org/10.1016/j.cell.2017.08.027.

45. D'Alterio, C., Buoncervello, M., Ieranò, C., Napolitano, M., Portella, L., Rea, G., Barbieri, A., Luciano, A., Scognamiglio, G., Tatangelo, F., et al. (2019). Targeting CXCR4 potentiates anti-PD-1 efficacy modifying the tumor microenvironment and inhibiting neoplastic PD-1. J. Exp. Clin. Cancer Res. *38*, 432. https://doi.org/10.1186/s13046-019-1420-8.

46. Zeng, Y., Li, B., Liang, Y., Reeves, P.M., Qu, X., Ran, C., Liu, Q., Callahan, M.V., Sluder, A.E., Gelfand, J.A., et al. (2019). Dual blockade of CXCL12-CXCR4 and PD-1–PD-L1 pathways prolongs survival of ovarian tumor–bearing mice by prevention of immunosuppression in the tumor microenvironment. FASEB J. *33*, 6596–6608. https://doi.org/10.1096/fj.201802067RR.

47. Wu, A., Maxwell, R., Xia, Y., Cardarelli, P., Oyasu, M., Belcaid, Z., Kim, E., Hung, A., Luksik, A.S., Garzon-Muvdi, T., et al. (2019). Combination anti-CXCR4 and anti-PD-1 immunotherapy provides survival benefit in glioblastoma through immune cell modulation of tumor microenvironment. J. Neuro Oncol. *143*, 241–249. https://doi.org/10.1007/s11060-019-03172-5.

48. Jayasingam, S.D., Citartan, M., Thang, T.H., Mat Zin, A.A., Ang, K.C., and Ch'ng, E.S. (2019). Evaluating the Polarization of Tumor-Associated Macrophages Into M1 and M2 Phenotypes in Human Cancer Tissue: Technicalities and Challenges in Routine Clinical Practice. Front. Oncol. *9*, 1512. https://doi.org/10.3389/fonc.2019.01512.

49. Fortunato, O., Belisario, D.C., Compagno, M., Giovinazzo, F., Bracci, C., Pastorino, U., Horenstein, A., Malavasi, F., Ferracini, R., Scala, S., et al. (2020). CXCR4 Inhibition Counteracts Immunosuppressive Properties of Metastatic NSCLC Stem Cells. Front. Immunol. *11*, 02168. https://doi.org/10.3389/fimmu.2020.02168.

50. Todo, T., Martuza, R.L., Rabkin, S.D., and Johnson, P.A. (2001). Oncolytic herpes simplex virus vector with enhanced MHC class I presentation and tumor cell killing. Proc. Natl. Acad. Sci. USA *98*, 6396–6401. https://doi.org/10.1073/pnas.101136398.

51. Tischer, B.K., Kaufer, B.B., Sommer, M., Wussow, F., Arvin, A.M., and Osterrieder, N. (2007). A self-excisable infectious bacterial artificial chromosome clone of varicella-zoster virus allows analysis of the essential tegument protein encoded by ORF9. J. Virol. *81*, 13200–13208. https://doi.org/10.1128/JVI.01148-07.

52. Goins, W.F., Huang, S., Hall, B., Marzulli, M., Cohen, J.B., and Glorioso, J.C. (2020). Engineering HSV-1 Vectors for Gene Therapy. Methods Mol. Biol. *2060*, 73–90. https://doi.org/10.1007/978-1-4939-9814-2_4.

53. Marconi, P., and Manservigi, R. (2014). Herpes simplex virus growth, preparation, and assay. Methods Mol. Biol. *1144*, 19–29. https://doi.org/10.1007/978-1-4939-0428-0_2.

54. Percie du Sert, N., Hurst, V., Ahluwalia, A., Alam, S., Avey, M.T., Baker, M., Browne, W.J., Clark, A., Cuthill, I.C., Dirnagl, U., et al. (2020). The ARRIVE guidelines 2.0: Updated guidelines for reporting animal research. PLoS Biol. *18*, e3000410. https://doi.org/10.1371/journal.pbio.3000410.

OMTON, Volume *33*

Supplemental information

An oncolytic herpesvirus expressing a CXCR4 antagonist interferes with glioblastoma cells' stemness features and migration

Paolo D'arrigo, Maxime Dubois, Judit Sanchez Gil, Cédric Lassence, Alexandre Hego, Benoit Brouwers, Arnaud Lombard, Bernard Rogister, Virginie Neirinckx, Marielle Lebrun, and Catherine Sadzot-Delvaux

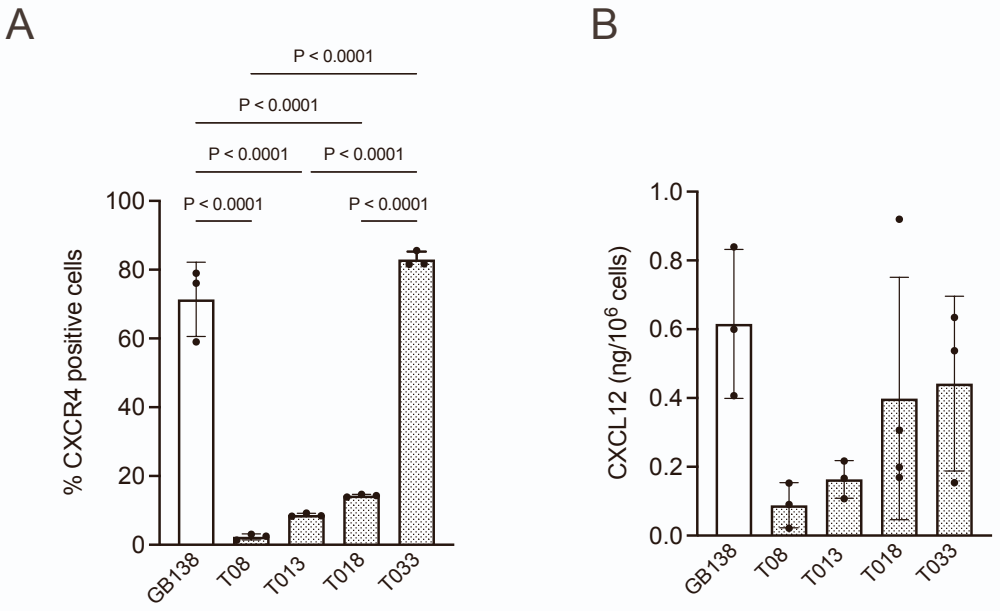

Figure S1. CXCR4 and CXCL12 expression by patient-derived GSCs.
CXCR4 **(A)** and CXCL12 **(B)** expression were evaluated on patient-derived GSCs cultured for 7 days either as monolayers (GB138) or as tumorspheres (T08, 013, 018 and 033). For CXCR4 analysis, cells were dissociated and the percentage of $CXCR4^+$ cells was evaluated by flow cytometry **(A).**
In parallel, the cell culture supernatant was harvested for CXCL12 quantification by ELISA **(B)**.
Bars represent the mean (SD) of 3 independent experiments. Statistical significance was determined by ordinary one-way ANOVA with Tukey's multiple comparisons test, with a single pooled variance.

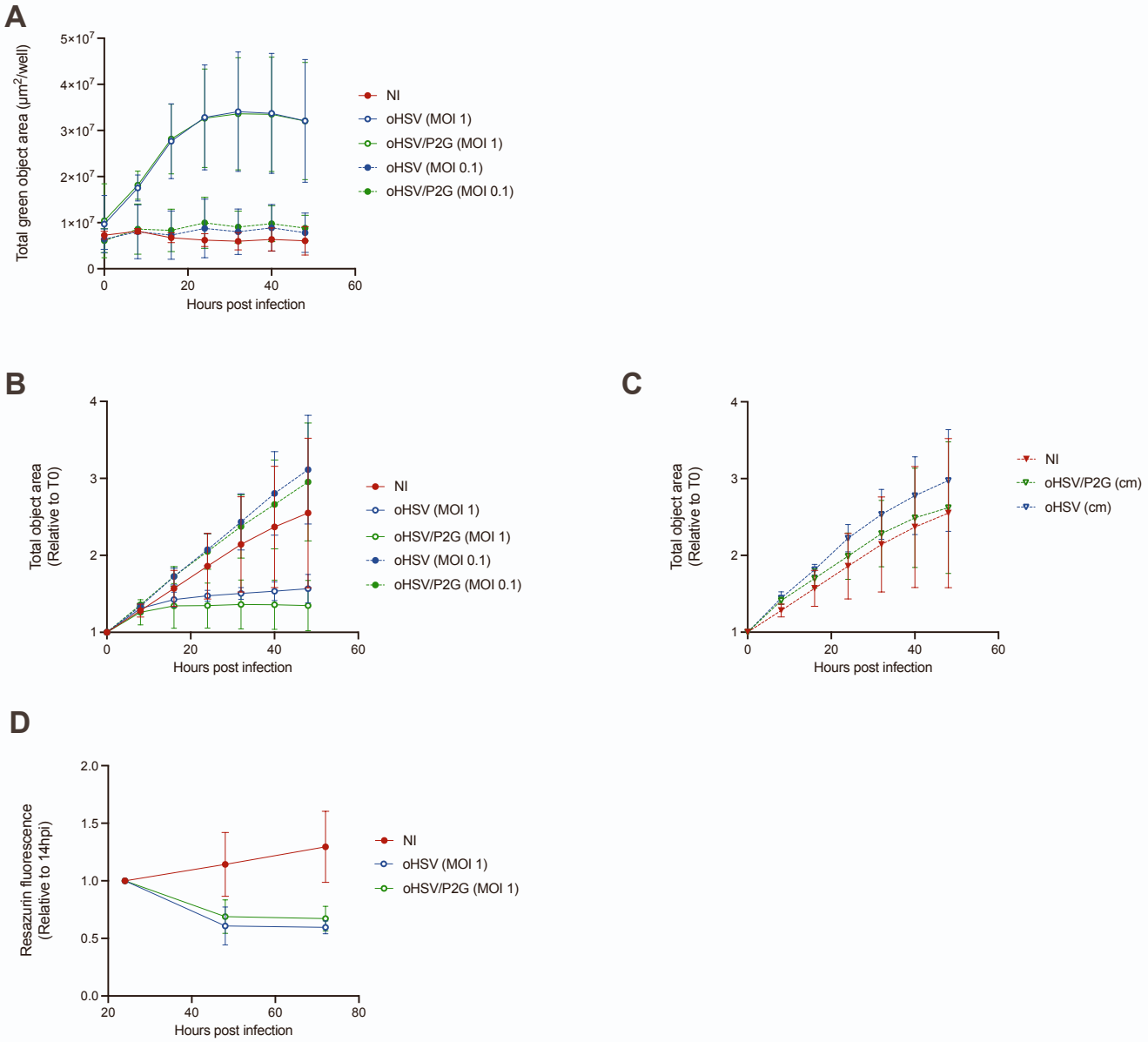

Figure S2. P2G-HA expression does not influence viral replication, cells proliferation or cell-death

Human GB138 primary cells were infected with oHSV or oHSV/P2G at MOI 0.1 or 1.

(A) The capacity of both viruses to replicate in GB138 cells was followed over a 48h period using Incucyte® S3 Live-Cell Analysis System recording eGFP expression. Total green object area (µm^2/well) was used to account for the spread of the infection.

(B and C) The capacity of GB138 cells to proliferate upon oHSV or oHSV/P2G infection **(B)** or cultured in presence of conditioned media **(C)** was followed over a 48h period using Incucyte® S3 Live-Cell Analysis System. Total object area (µm^2/well) was measured on phase contrast pictures and expressed relative to T0 considered as 1.

(D) GB138 Cell-death upon oHSV or oHSV/P2G infection was measured over a 72h period by resazurine assay and expressed as relative to fluorescence at 24hpi considered as 1.

Bars represent the mean (SD) of 3 independent experiments. Statistical significance was determined by Two-way ANOVA. No statistical differences between oHSV and oHSV/P2G were observed in any of the assays.

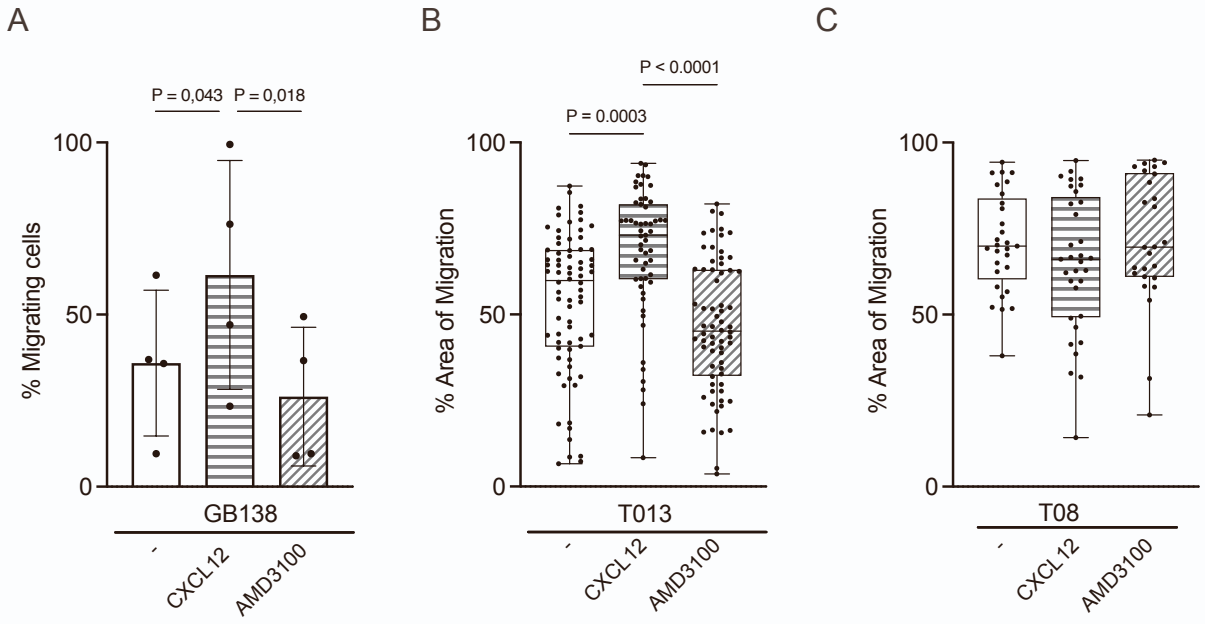

Figure S3: GSC migration is a CXCR4-dependent process.
(A): Dissociated GB138 cells were cultured in two-compartments chambers in normal media or in media supplemented with purified CXCL12 (20 pM) or AMD3100 (40 nM).
The number of cells migrating through the transwell membrane was quantified by manual counting. Bars represents the mean (SD) of 4 independent experiments. Statistical significance was determined by paired t-Test.

(B and C): T013 ($CXCR4^{medium}$) or T08 ($CXCR4^{low}$) tumorspheres were cultured in normal media or in media supplemented with CXCL12 (20 pM) or AMD3100 (40 nM).
The spheres areas were measured at 1 hpi and 24 hpi and the percentage of migration was expressed as follows:

$$\frac{\text{Total area at 24h - Area at 1h}}{\text{Total area at 24h}}$$

Each dot represents one sphere measured in 5 (B) or 3 (C) independent experiments while box plots represent the distribution of all measures, with whiskers representing the minimum and maximum values. Statistical significance was determined by Kruskal-Wallis test after Shapiro-Wilk normality test.

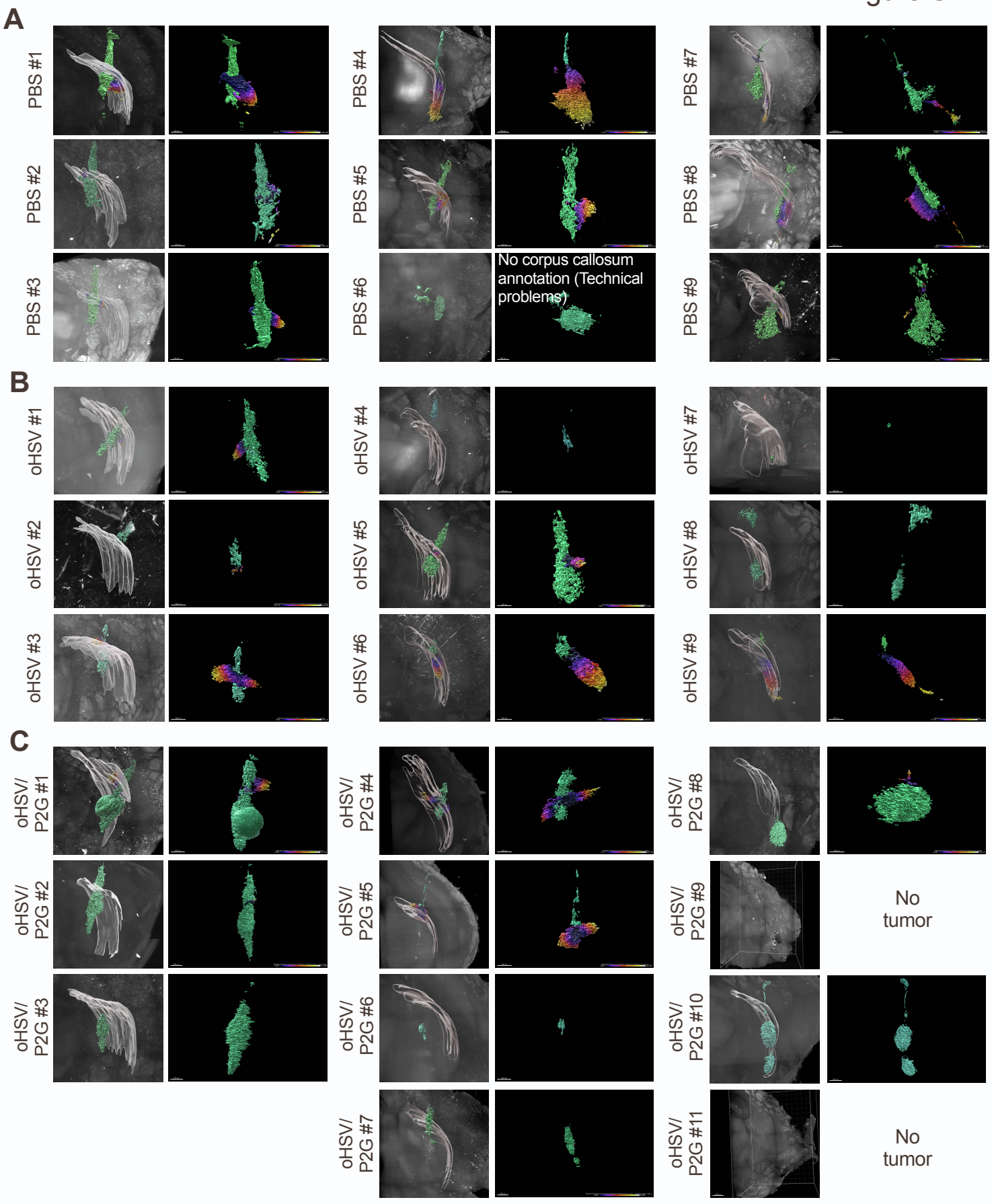

Figure S4 : *In vivo* short-term experiment

Imaris 3D-reconstructions of the tumor mass (green) as well as cells migrating (statistically fire-colored according to their distance to the central tumor mass) through the *corpus callosum* (grey, in the left panels) in all the brains from PBS- (A), oHSV- (B) and oHSV/P2G- (C)treated mice analyzed with light-sheet microscopy. Bar represents 500 µm.

Mice # 1 to 3 on one side and 4 to 9 (or 11 for oHSV/P2G) on the other side have been injected at the same time and correspond to two independent data sets that were pooled for analysis. Quantifications are given in Figures 5C to G.

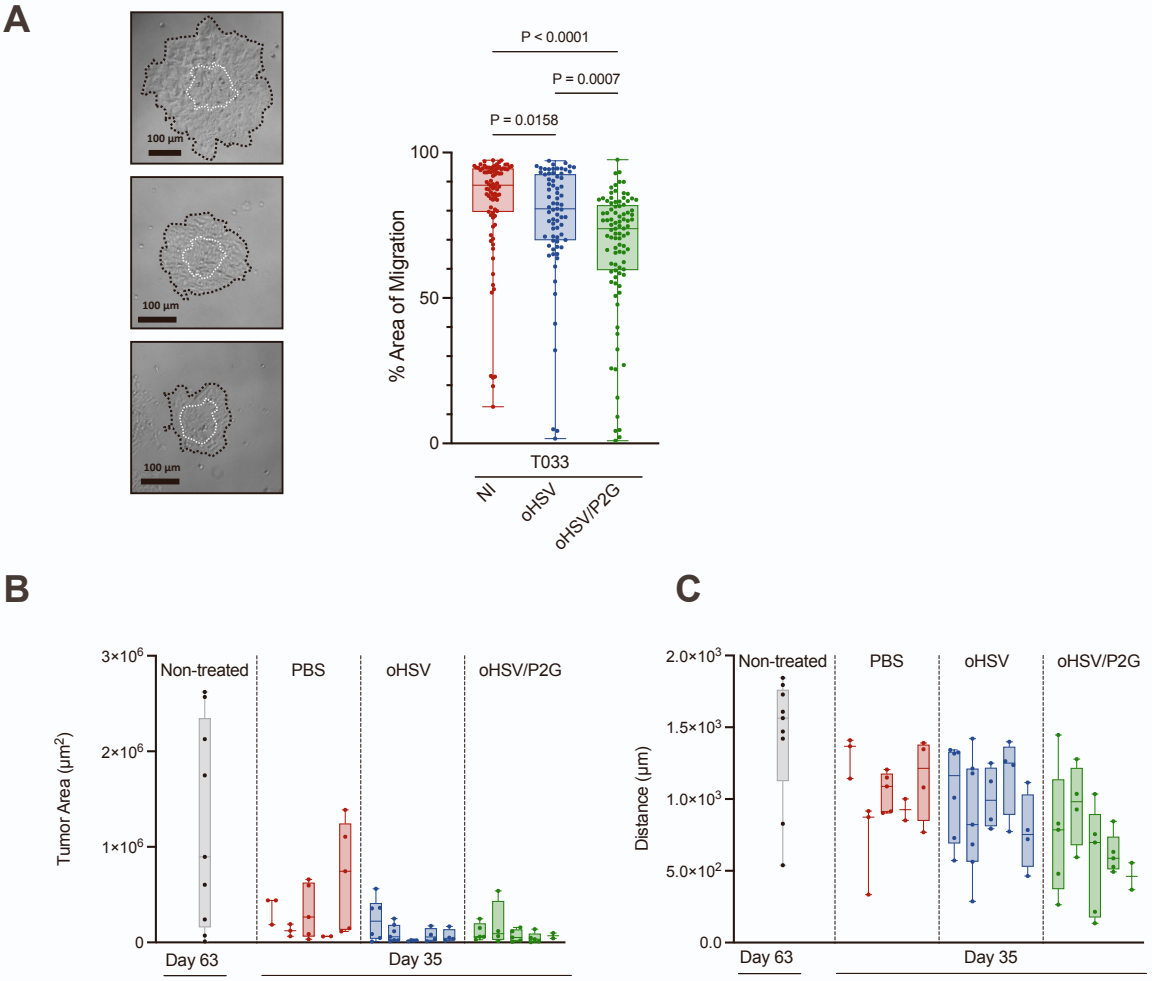

Figure S5: GSC migration is inhibited by oHSV/P2G both in vitro and in vivo.

(A): Sprouting assay onT033(CXCR4^{high}). GSCs cultured as tumorspheres were either non-infected or infected with oHSV or oHSV/P2G. Representative pictures are shown in the left panel. The spheres areas were measured at 1 hpi (hours post-infection, white dotted lines) and 24 hpi (dark dotted line) and the percentage of migration was expressed as follows (right panels):

$$\frac{\text{Total area at 24h - Area at 1h}}{\text{Area at 24h}}$$

Box plots represent the repartition of the values of each dataset, each dot representing one sphere. Area of migration has been measured in 3 independent experiments. Whiskers represent the maximum and minimum values. Statistical significance was determined by Kruskal-Wallis test after the Shapiro-Wilk normality test.

(B): Tumor area estimated on brain sections as the cumulative area of dsRED^{+} tumor cell detected in QuPath using a machine learning–based pixel classifier. Each box plots represent the repartition of the values for one mouse, each dot representing the quantification on one brain slice. Whiskers represent the maximum and minimum values. Statistical significance of Day 35 data was determined by Kruskal-Wallis test after Shapiro-Wilk normality test.

(C): Tumor cells spread estimated by the mean distances between the centroïds of annotated grid elements. Each box plots represent the repartition of the values for one mouse, each dot representing the quantification on one brain slice. Whiskers represent the maximum and minimum values. Statistical significance of Day 35 data was determined by Kruskal-Wallis test after Shapiro-Wilk normality test.

oHSV/P2G disrupts glioblastoma microenvironment. (*preliminary results*)

Oncolytic HSV-1 armed with CXCL12-antagonist "P2G" to disrupt pro-tumoral microenvironment in glioblastoma

DUBOIS, Maxime[1], DUMEZ Sacha[1], LASSENCE Cédric[1], MACHIELS Bénédicte[2,3], LAVERGNE Arnaud[4], BROUWERS Benoit[5], NEIRINCKX Virginie[5], ROGISTER Bernard[5,6], LEBRUN Marielle[1,7], SADZOT-DELVAUX Catherine[1,7]

[1] Laboratory of Virology and Immunology, GIGA-Immunobiology, University of Liège, 4000 Liège, Belgium

[2] Department of Infectious and Parasitic Diseases, Faculty of Veterinary Medicine – FARAH, University of Liège, Liège, Belgium.

[3] Walloon Excellence in Life Sciences and Biotechnology (WELBIO) Department, WEL Research Institute, Wavre, Belgium.

[4] GIGA- Genomics Core Facility, GIGA, University of Liège, 4000 Liège, Belgium

[5] Laboratory of Nervous system Disorders and Therapy, GIGA-Neurosciences, University of Liège, Belgium

[6] Neurology Department, University Hospital, 4000 Liège, Belgium

[7] Equal contributions as last co-authors

Summary

The following introductory section does not add substantial new information beyond the global introduction. It focuses on the "cold" immunogenic profile of glioblastoma, the role of the CXCR4 pathway, and immunotherapeutic strategies, including virotherapy, to promote a cold-to-hot tumour transition. The subsequent results section compares oHSV and oHSV/P2G in immunocompetent models (GL261N4 and 005-GSCs). Based mainly on GL261N4 data, including single-cell RNA sequencing, flow cytometry, and immunofluorescence, it characterises the abundance and nature of leucocyte populations. The result section addresses the transcriptional profiles of tumour-associated macrophages, microglia, and $CD4^+$ and $CD8^+$ T cells. Finally, it compares survival in both murine glioblastoma models. The discussion addresses technical limitations, alternative CXCR4 inhibition trials and elaborates on published immunogenic profiles to propose hypotheses for the differential survival effects of oHSV and oHSV/P2G.

These results remain preliminary and require in-depth analysis of the single-cell RNA sequencing. They also require further validation of tumour size reduction, P2G expression *in vivo*, $CD4^+/CD8^+$ ratios, and investigation in alternative murine glioblastoma models.

ABSTRACT

Background

Glioblastoma is the most common and aggressive primary brain tumour, characterized by hypervascularization, invasiveness, recurrence, glioblastoma stem-like cells (GSCs), and a profoundly immunosuppressive “cold” tumour microenvironment (TME) driving therapeutic resistance. The CXCR4/CXCL12 axis is associated with poor prognosis and contributes to these features. Oncolytic herpes simplex virus type 1 (oHSV) induces immunogenic cell death (ICD) and can partially convert “cold” tumours into “hot” tumours, but its efficacy remains limited in poorly immunogenic settings. We engineered an oHSV expressing the CXCL12 antagonist P2G (oHSV/P2G) to induce ICD within an activated TME and enhance anti-tumour immunity.

Methods

Immunocompetent syngeneic orthotopic mouse models were established by intracranial engraftment of 1×10^5 GL261N4 cells (or 005-GSCs in two experiments) into the right striatum of C57BL/6NRj mice under stereotactic coordinates control. Mice received intratumoral injections of PBS, oHSV, or oHSV/P2G (1×10^6 pfu in 2 µL) at 7- and 14-days post-engraftment (d.p.e.) and were sacrificed at 21 d.p.e., except for survival analyses. Immune profiling was performed using flow cytometry, immunofluorescence, single-cell RNA sequencing with pseudobulk and Ingenuity Pathway analyses, and bulk RNA sequencing.

Results

oHSV/P2G reduced tumour size at 21 d.p.e. compared with PBS- and oHSV-treated mice. In the immunogenic GL261N4 model, both viruses improved survival, although oHSV/P2G induced more pronounced immune remodelling. Treatment increased the recruitment of lymphocytes (T and B cells), resulting in a myeloid-to-lymphoid shift. oHSV/P2G enhanced Th1 and effector-like T cell programs, increased the cytotoxic-to-regulatory T cell ratio (CTLs/Tregs), and limited CTL exhaustion and immune checkpoint expression. Tumour-associated macrophages and microglia (TAMs) were reprogrammed toward an activated, pro-inflammatory, antigen-presenting phenotype, with suppression of anti-inflammatory pathways, including alternative (M2-like) activation, CXCR4, STAT3, and TGFβ signalling. In the poorly immunogenic 005-GSC model, oHSV/P2G significantly prolonged survival compared with both PBS and oHSV, correlating with upregulation of immune-related genes.

Conclusions

oHSV/P2G enhances antitumour immunity by reshaping the TME from a myeloid-dominated, immunologically “cold” state to a lymphoid-enriched, “hot” phenotype through TAM reprogramming as well as recruitment and activation of lymphocytes. Notably, oHSV/P2G significantly improved survival compared with oHSV, particularly in poorly immunogenic glioblastoma models characterized by low lymphocyte abundance and a predominance of APCs with limited antigen-presenting and co-stimulatory capacity.

INTRODUCTION

Glioblastoma (GBM) is the most frequent and aggressive primary brain tumour, with a median overall survival of approximately 15 months.[1,2] Standard treatment consists of maximal surgical resection followed by radiotherapy and temozolomide (TMZ) chemotherapy.[2] Poor prognosis results from treatment failure due to limited surgical feasibility, limited blood–brain barrier permeability, tumour heterogeneity, and intrinsic resistance driven by glioblastoma stem-like cells (GSCs), ultimately leading to recurrence.[3–5] The tumour microenvironment (TME) plays a central role in GBM progression through hypoxic, perivascular, and invasive niches and profound immunosuppression.[4–6] Accordingly, GBM is an immunologically “cold” tumour, characterised by anti-inflammatory factors and the accumulation of immunosuppressive cells, including regulatory T cells (Tregs), myeloid-derived suppressor cells (MDSCs), and predominantly tumour-associated macrophages and microglia (TAMs).[7–9]

The CXCR4/CXCL12 axis is associated with poor prognosis in several cancers, including GBM. CXCR4 is highly expressed by endothelial cells, stem cells, and immunosuppressive populations, while CXCL12 is upregulated in GBM niches, promoting tumour vascularisation, GSC stemness, radioresistance and invasiveness, and TME immunosuppression.[10–13] This pathway also drives bidirectional migration, including GSC invasion of the subventricular zone (SVZ) and migration of oncogenic neural stem cells (NSCs) from the SVZ to the resection cavity, contributing to resection evasion and recurrence, respectively.[14–16] Inhibitors of the CXCR4/CXCL12 axis, including AMD3100 (Plerixafor), HMGB1-BoxA, and CXCL12-P2G, disrupt these processes and enhance antitumour immunity by promoting pro-inflammatory TAM polarisation, limiting Treg and MDSC recruitment, increasing phagocytosis via CD47 downregulation, and shifting the pro- to anti-inflammatory cytokine balance.[13,17–19]

Novel immunotherapeutic approaches aim to restore immune surveillance by inducing a cold-to-hot tumour transition, primarily through immune checkpoint inhibition and cytotoxic T cell activation.[9,20] However, checkpoint blockade has shown limited efficacy in GBM and other immunologically cold tumours.[8,21,22] Oncolytic virotherapy represents a

safe and potent strategy able to induce the cold-to-hot tumour transition and has been approved for the treatment of GBM, melanoma, and head and neck cancers in several countries.[8,9,20,23,24] The oncolytic herpes simplex virus type 1 (HSV-1) teserpaturev (Delytact®, Δ34.5Δ47Δ6-oHSV) was approved in 2021 in Japan for residual and recurrent GBM.[25] Oncolytic HSV-1 injected intratumorally, selectively replicates in tumour cells, and induces immunogenic cell death and local inflammation.[24,26,27] While teserpaturev relies primarily on this mechanism, current oncolytic viruses are increasingly engineered to deliver transgenes targeting tumour and immune pathways.[13,24,28–30] Transgenes can target a wide variety of biological features and include pro-inflammatory cytokines (IL12/15/18, CSF2), suicide genes (HSV-TK, CYP2B1), pro-apoptotic molecules (TRAIL), anti-angiogenic factors (PF4), tumour suppressors (PTEN), tumour-associated antigens (EphA2), extracellular matrix modulators (MMP9), and inhibitors of immune checkpoints (PD1) or oncogenic pathways (VEGFα).[13,28,29,31–35]

We engineered an oncolytic HSV expressing the CXCL12 antagonist P2G (oHSV/P2G) to target multiple glioblastoma features simultaneously, unlike most of the examples above. A previous study from our laboratory had already demonstrated its effects on GSC stemness and migration.[13] Here, we investigate in two immunocompetent orthotopic syngeneic C57BL/6NRj mouse models (GL261N4 and 005-GSCs), the effects of oHSV/P2G on the tumour immune microenvironment, focusing on immune cell recruitment and distribution, as well as polarisation and activation profiles of TAMs, B cells, and T cells.

RESULTS

oHSV/P2G impairs tumour growth *in vivo*

The ability of oHSV/P2G to interfere with tumour growth was evaluated in a syngeneic orthotopic, C57BL/6NRj mouse model. GL261N4 (1×10^5 cells) were engrafted in the right striatum under stereotactic coordinates control. Mice received intratumor injections of oHSV or oHSV/P2G (1×10^6 pfu, 2 µL) or PBS on days 7 and 14 post-engraftment and were sacrificed on day 21 (Fig. 1A)[I].

At endpoint, tumours were delineated on serial haematoxylin-stained cryosections to measure tumour volume (Fig. 1B). Mean tumour volumes of oHSV and oHSV/P2G-treated

[I] **Figure 1: oHSV/P2G impairs tumour growth *in vivo***
(A) Experimental settings of the orthotopic syngeneic model. **(B)** Representative pictures of haematoxylin-stained serial brain cryosections from mice sacrificed 21 days post-engraftment (d.p.e.), with $1x10^5$ GL261N4 tumour cells, delineated in red using QuPath. **(C)** Tumour volume in μm^3. **(D)** Tumour volume relative to PBS mean.
Each dot represents value of one mouse treated with PBS (n=8), oHSV (n=9) or oHSV/P2G (n=7). Boxes indicate the distribution of values, with whiskers denoting the minimum and maximum. Statistical significance was evaluated by ordinary one-way ANOVA with Tukey's multiple comparison test.

Figure 1

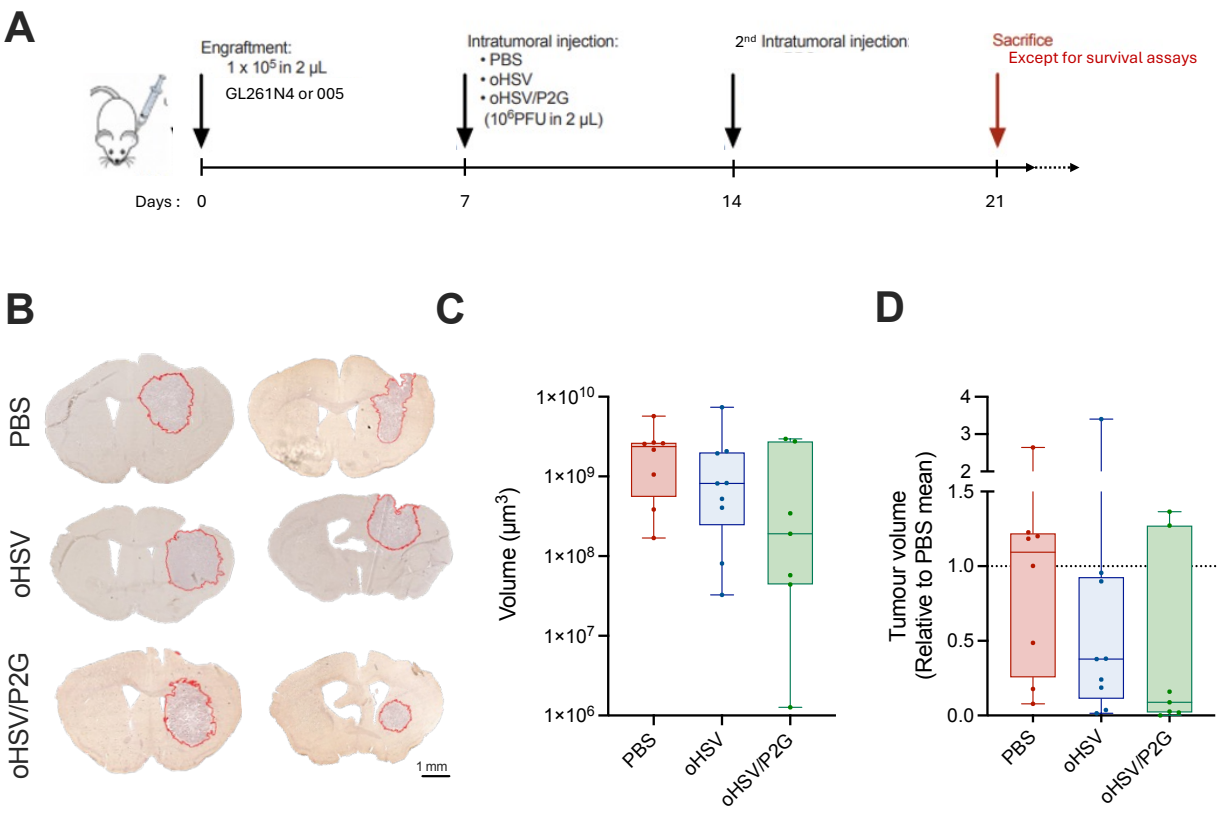
A
Engraftment:
1 x 10^5 in 2 µL
GL261N4 or 005
Intratumoral injection:
• PBS
• oHSV
• oHSV/P2G
(10^6PFU in 2 µL)
2nd Intratumoral injection
Sacrifice
Except for survival assays
Days : 0
7
14
21
B
PBS
oHSV
oHSV/P2G
1 mm
C
Volume (µm3)
1×10^10
1×10^9
1×10^8
1×10^7
1×10^6
PBS
oHSV
oHSV/P2G
D
Tumour volume
(Relative to PBS mean)
4
3
2
1.5
1.0
0.5
0.0
PBS
oHSV
oHSV/P2G

mice had decreased to 72% and 42%, respectively, compared to PBS group, though these differences were not statistically significant. (Fig. 1C, D)

oHSV/P2G promotes immune cell infiltration and alters their distribution

The immune landscape of mice brain hemispheres harbouring GL261N4 tumours was characterized in the same experimental setting. On the day of euthanasia, brains from PBS, oHSV or oHSV/P2G treated mice were harvested and leucocytes were analysed either by flow cytometry or single-cell RNA sequencing (scRNAseq). Leucocytes from a non-engrafted mouse were harvested in parallel as control. Importantly, the following results represent a snapshot of the immune microenvironment 21 days post-engraftment. At this stage, the primary adaptive response may already be partially exhausted (14 days post-initial exposure), while the secondary response may still be developing (7 days post-second exposure). In the absence of time-course data, results and hypotheses regarding the recruitment and activation of immune cells should not be overinterpreted.

As expected, flow cytometric analysis of leucocytes ($CD45^+$ cells) from a non-engrafted brain revealed that the immune compartment was predominantly composed of microglia ($CD45^{medium}$, 96%), with only a minor fraction of $CD45^{high}$ infiltrating leucocytes (4%) (Fig. 2A[II], S1A). By contrast, tumour-bearing PBS-treated mice displayed a substantial infiltration of $CD45^{high}$ leucocytes, representing an average of 35% of the immune population. Notably, infection with either oHSV or oHSV/P2G further increased $CD45^{high}$ leucocytes infiltration to 68% and 63%, respectively. While the absolute number of microglia was not affected by treatment (Fig. S1A), their relative abundance among leucocytes decreased following virotherapy (Fig. 2A).

To further characterise the immune populations recruited upon treatment, we next performed scRNAseq on immune cells isolated from PBS-, oHSV-, and oHSV/P2G-treated brains. Consistent with the flow cytometry data, viral infection resulted in an important recruitment of leucocytes, whose number doubled compared to PBS (Fig. 2B). Cells were

[II] **Figure 2: oHSV/P2G promotes immune cell infiltration and alters their distribution**
(A) Percentage of $CD45^{high}$ infiltrating leucocytes and $CD45^{medium}$ resident microglia isolated 21 d.p.e. from PBS- (n=7), oHSV- (n=7) or oHSV/P2G- (n=6) treated GL261N4 tumour bearing mice brains and analysed by flow cytometry. The brain from a non-engrafted mice was analysed as a control. **(B)** Number of leucocytes recovered from three pooled PBS-, oHSV- or oHSV/P2G-treated mice (n=4 in each group) 21 d.p.e. of $1x10^5$ GL261N4, and analysed by single-cell RNA sequencing (ScRNAseq). **(C)** UMAP representation of the clustering of leucocytes. Leucocyte populations were identified based on cluster-specific differentially expressed marker genes. **(D)** Percentage of each leucocyte populations. **E, F:** Percentage of grouped lymphoid or myeloid populations **(E)** and myeloid-to-lymphoid cells ratio **(F)**.
Each dot represents cells isolated from one mouse **(A)** or pooled from 3 mice **(B-F)**. Boxes indicate the distribution of values, with whiskers denoting the minimum and maximum. Statistical significance was evaluated by either ordinary one-way **(B, F)** or two-way **(A, D, E)** ANOVA with Tukey's multiple comparison test. *p<0.05, ***p<0.001.

Figure 2

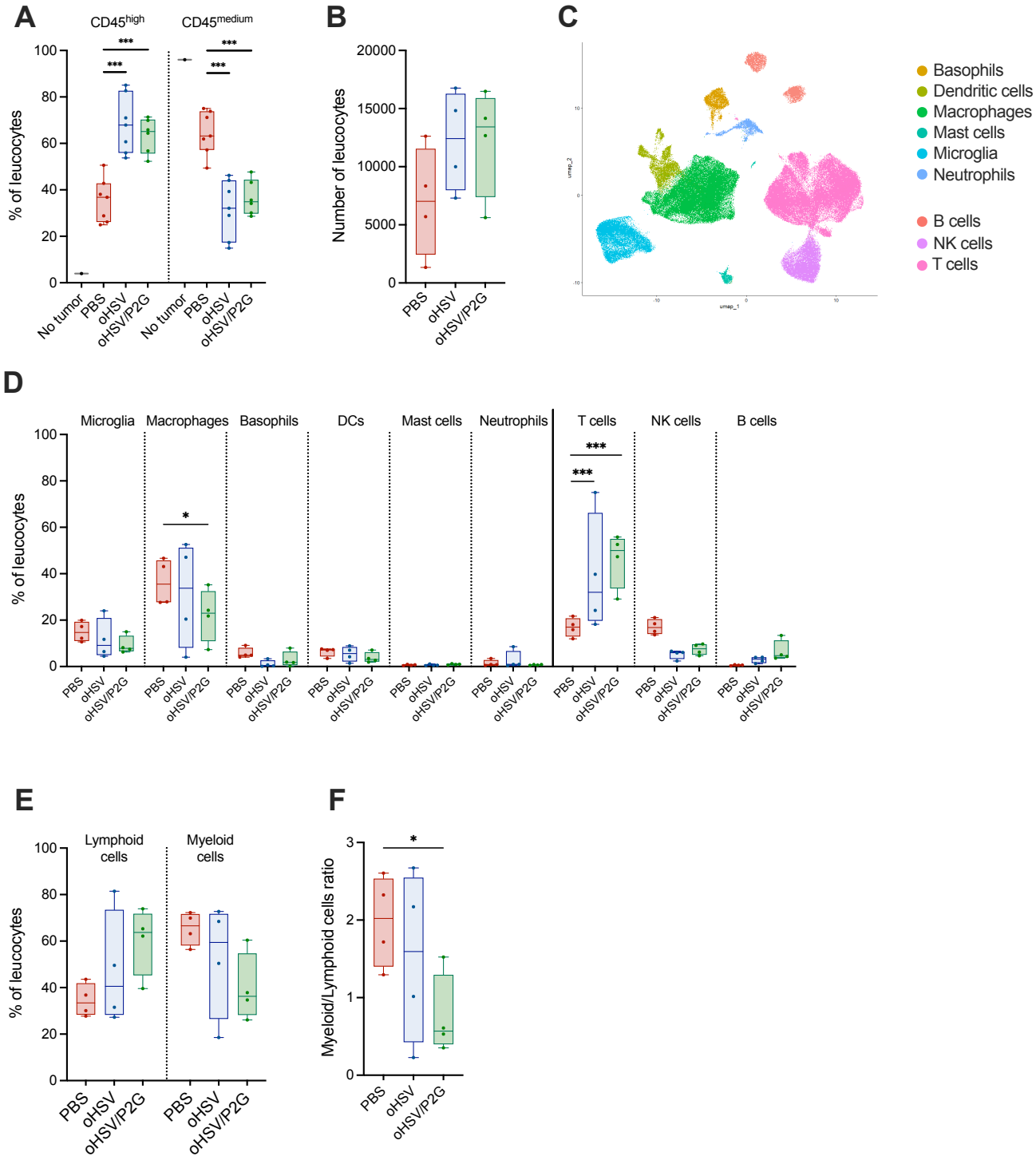
A
CD45high
CD45medium
% of leucocytes
No tumor
PBS
oHSV
oHSV/P2G
B
Number of leucocytes
C
Basophils
Dendritic cells
Macrophages
Mast cells
Microglia
Neutrophils
B cells
NK cells
T cells
D
Microglia
Macrophages
Basophils
DCs
Mast cells
Neutrophils
T cells
NK cells
B cells
E
Lymphoid cells
Myeloid cells
F
Myeloid/Lymphoid cells ratio

clustered based on transcriptomic similarity and visualised using UMAP. Clusters were annotated using top 50 differentially expressed canonical marker genes (upregulated, detected in at least 25% of cells, and with a minimum log fold change of 0.25), listed in the appendix. Top 50 differentially expressed genes distinguishing leucocyte populations, shown in Fig. 2C, D, and S1B, are listed in Appendix 2, enabling functional annotation.

In PBS-treated mice, the immune compartment was dominated by myeloid populations, primarily macrophages (36%) and microglia (15%), with smaller contributions from basophils (6%), dendritic cells (6%), neutrophils (1%) and mast cells (0.65%). Lymphoid populations consisted mainly of T and NK cells (17% each), while B cells represented the rarest leucocyte population (0.57%) (Fig. 2D). Upon viral infection, T cell numbers increased approximately fivefold (Fig. S1B), with their proportion among leucocytes rising significantly to 39% and 46% in oHSV- and oHSV/P2G-treated tumours, respectively (Fig. 2D). B cells expanded following oHSV/P2G treatment. Their absolute numbers increased significantly 15.2 and 8.3-fold compared to PBS and oHSV, respectively (Fig. S1B) and B cells population reached 7% of leucocytes compared to 3% in oHSV-treated tumours (Fig 2D). These results were confirmed by flow cytometry, which showed a significant increase in T cells with both viruses, whereas B cells expanded significantly only in response to oHSV/P2G (Fig. S1C, D). The number of other immune populations was not affected by infection (Fig. S1B), resulting in a relative decrease in their proportion among total leucocytes, which was significant for macrophages in oHSV/P2G-treated tumours compared to PBS. (Fig. 2D). Importantly, the myeloid-to-lymphoid cell ratio decreased significantly from 1.98 (64%/36%) and 1.5 (53%/47%) in PBS- and oHSV-treated tumours, respectively, to 0.75 (40%/60%) with oHSV/P2G (Fig. 2E-F, S1E-F).

Together, these findings demonstrate that intratumor administration of oncolytic herpesviruses induces a significant recruitment of T and B cells, particularly following oHSV/P2G treatment, leading to a myeloid-to-lymphoid transition.

oHSV/P2G modulates lymphoid subpopulations

scRNAseq clustering revealed two subpopulations of B cells: naïve B cells and plasmocytes (Fig. 3A)[III]. Top 50 differentially expressed genes distinguishing these two B cell subpopulations are listed in Appendix 3, enabling functional annotation, and visualised as a z-score heatmap in Fig. S2A. In PBS-treated mice, approximately 70% of B cells were naïve, while infection with both oHSV and oHSV/P2G resulted in a more balanced distribution between naïve and active B cells (Fig. 3B).

T cells were subdivided into four subpopulations: *Cd4*$^+$ T cells (26-43%, depending on treatment), *Cd8*$^+$ T cells (51-55%), *Foxp3*$^+$ regulatory T cells (Tregs, 4-14%) and *γδ Rorc*$^+$ T cells (2-5%) (Fig. 3A, C). Top 50 differentially expressed genes distinguishing these T cell subpopulations are listed in Appendix 3, enabling functional annotation, and visualised as a z-score heatmap in Fig. S2B. While the percentage of *Cd8*+ T cells remained stable across all conditions, *Cd4*$^+$ T cells increased significantly following oHSV treatment compared to PBS, and following oHSV/P2G treatment compared to both PBS and oHSV (Fig. 3C). Consequently, the relative abundance of *γδ Rorc*$^+$ T cells and Tregs decreased, the latter significantly with both viruses compared to PBS (Fig. 3C).

Surprisingly, flow cytometry analysis revealed a predominance of CD4$^+$ (~60%) over CD8$^+$ (~40%) T cells but no treatment-dependent effect on their proportions (Fig. S2C). However, the significative decrease in Tregs (CD25^{high}IL7R^{low}CD4$^+$ T cells) frequency upon viral infection was confirmed (Fig. S2D).

Immunofluorescence staining was performed on brain cryosections, and images were manually annotated to delineate the tumour, as well as the left (LH) and right (RH) hemispheres (Fig. 3D). T cells subpopulations (CD8$^+$, CD4$^+$, FOXP3$^+$) were quantified in LH, RH, tumour and the right hemisphere peritumoral stroma (RH-T). Spatial information on T cell localisation, critical for antitumour activity, was collected, and cell abundance was expressed as a percentage of total cells within each region of interest. Across

[III] **Figure 3: oHSV/P2G modulates lymphoid subpopulations**
(A) UMAP representation of the clustering of leucocytes highlighting B and T cells subpopulations identified based on subcluster-specific differentially expressed marker genes. **(B)** Percentage of both B cells subpopulations: naïve and plasmocyte. **(C)** Percentage of the four T cells subpopulations: *Cd4*$^+$*, Cd8*$^+$*, Foxp3*$^+$ and γδ *Rorc*$^+$. **(D)** Representative picture of DAPI-stained serial brain cryosections from mice sacrificed 21 d.p.e. of 1x10^5 GL261N4 (n=5 in each group). Regions of interest (stroma, tumour, and right or left hemisphere (RH, LH)) were delineated to allow quantification of immunofluorescence staining within specific areas. **(E)** Representative picture of immunodetection of CD4$^+$, CD8$^+$ and FOXP3$^+$ cells. Images were acquired with an epifluorescence slide scanner (upper panels), before modelling and quantification using QuPath (lower panels). **(F)** Percentage of T cells (CD4$^+$ and CD8$^+$) among total cells in the right or left hemisphere. **G-I:** Percentage of CD4$^+$ **(G)**, CD8$^+$ **(H)**, or FOXP3$^+$ **(I)** T cells among total cells within the left or right hemispheres, quantified by immunofluorescence staining on DAPI-stained serial brain cryosections from mice sacrificed 21 d.p.e. of 1x10^5 GL261N4 (n=5 in each group). **(J)** CD8$^+$-to-FOXP3$^+$ T cells ratio.
Each dot represents cells from one mouse **(F-J)** or pooled from 3 mice **(B, C)**. Boxes indicate the distribution of values, with whiskers denoting the minimum and maximum. Statistical significance was evaluated by either ordinary one-way **(F-J)** or two-way **(B, C)** ANOVA with Tukey's multiple comparison test. *p<0.05, **p< 0.01, ***p<0.001, ****p<0.0001.

Figure 3

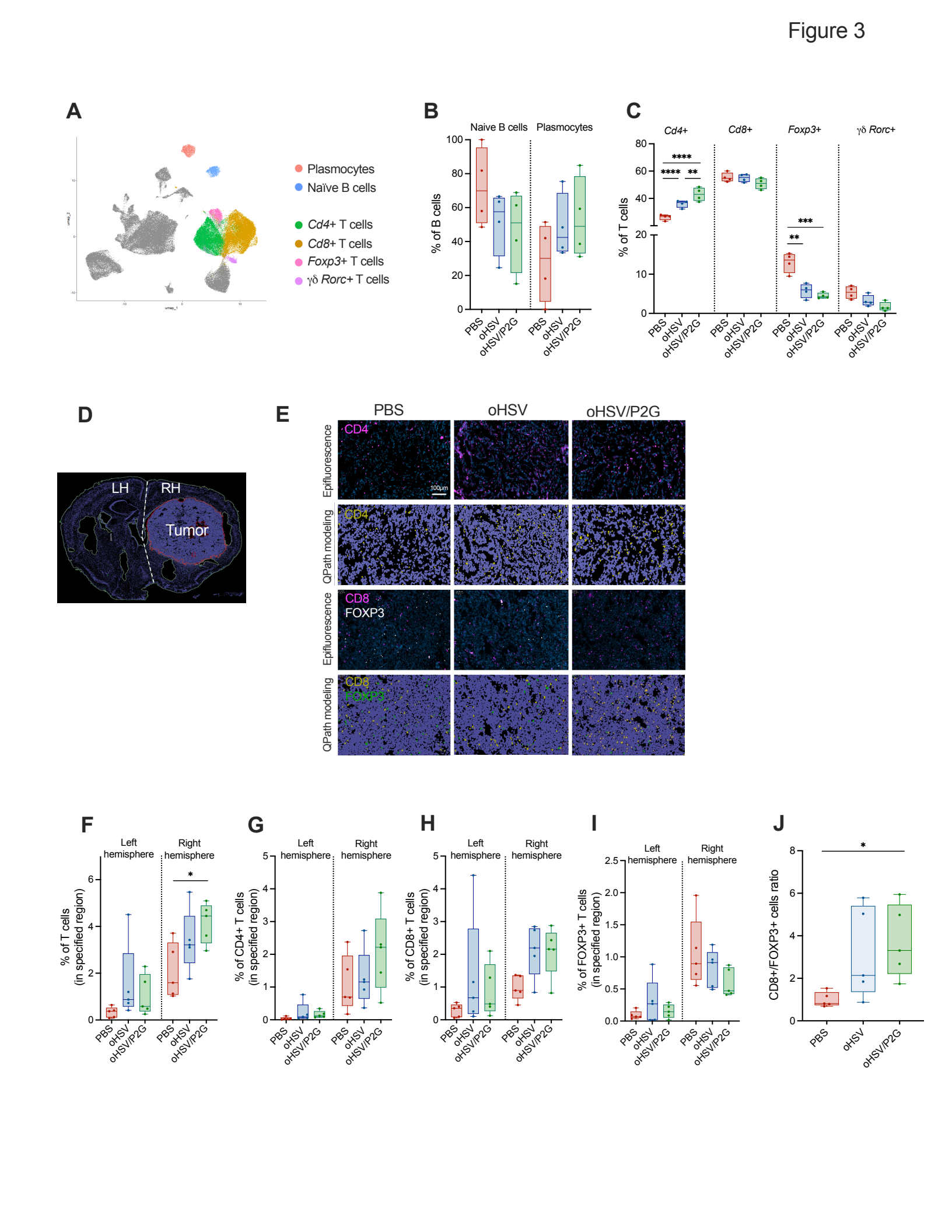
A
Plasmocytes
Naïve B cells
Cd4+ T cells
Cd8+ T cells
Foxp3+ T cells
γδ Rorc+ T cells
B
Naive B cells
Plasmocytes
% of B cells
PBS
oHSV
oHSV/P2G
C
Cd4+
Cd8+
Foxp3+
γδ Rorc+
% of T cells
D
LH
RH
Tumor
E
PBS
oHSV
oHSV/P2G
Epifluorescence
QPath modeling
CD4
CD8
FOXP3
100μm
F
Left hemisphere
Right hemisphere
% of T cells (in specified region)
G
% of CD4+ T cells (in specified region)
H
% of CD8+ T cells (in specified region)
I
% of FOXP3+ T cells (in specified region)
J
CD8+/FOXP3+ cells ratio

conditions, T cells were predominantly enriched in the RH, where the tumour has developed, compared to the LH (Fig 3E-I). Moreover, within the RH, all T cells subpopulations were more abundant in the tumour relative to the peritumoral stroma (Fig. S2E-G). Enrichment of total T cells (CD8+ and CD4+) in the RH increased following infection with both viruses but reached statistical significance only in oHSV/P2G-treated mice (Fig. 3F). Independently, $CD8^+$ and $CD4^+$ cells increase under viral conditions, while $FOXP3^+$ cells decrease, but with important inter-mouse variability (Fig 3G-I). Interestingly, $CD8^+$-to-$FOXP3^+$ ratio, used as a surrogate for cytotoxic-to-regulatory T cell balance, increased with both viruses but significantly only with oHSV/P2G (Fig. 3J).

These findings indicate that the enhanced B cell infiltration observed with oHSV compared to PBS as well as oHSV/P2G, compared to PBS and oHSV, was associated with a shift from naïve B cells toward plasmocytes following infection with both viruses. In parallel, T cell expansion favoured *Cd4*$^+$ and *Cd8*$^+$ subsets, with a relative reduction in *Foxp3*$^+$ T cells. Importantly, immunofluorescence analyses demonstrated that these T cells were predominantly localised within and surrounding the tumour, and that only oHSV/P2G significantly triggered both T cell infiltration and a decrease in the $CD8^+$-to-$FOXP3^+$ ratio in the right hemisphere.

oHSV/P2G modulates myeloid subpopulations

Clustering analysis of macrophages and microglia revealed a higher degree of phenotypic similarity and potential plasticity between subtypes, making it difficult to (clearly) define distinct subpopulations. (Fig. 4A)[IV]. Nevertheless, the top 50 differentially expressed genes distinguishing these subpopulations are listed in Appendix 4, enabling functional annotation, and are visualised as a z-score heatmap in Fig. S3A, B. Consequently, microglia could be classified into three subclusters: pro-inflammatory, anti-inflammatory, and stress-response microglia (Fig. 4A, S3A). Macrophages were subdivided into five subpopulations: monocytes, pro-inflammatory, anti-inflammatory, lipid-associated, and antigen-presenting macrophages (Fig. 4A, S3B).

In microglia, the proportion of stress-response subcluster remained stable across treatments, representing 11%–14% of the microglial population whatever the treatment (Fig. 4B). By contrast, the balance between pro- and anti-inflammatory subclusters was markedly modified by oHSV/P2G. The pro-/anti-inflammatory ratio was below 1 in the

[IV] **Figure 4: oHSV/P2G modulates myeloid subpopulations**
(A) UMAP representation of the clustering of leucocytes highlighting microglia and macrophages subpopulations identified based on subcluster-specific differentially expressed marker genes. **(B)** Percentage of three microglia subpopulations: pro-inflammatory, anti-inflammatory and stress-response. **(C)** Pro-to-anti-inflammatory microglia ratio. **(D)** Percentage of five macrophages subpopulations: monocytes, pro-inflammatory, anti-inflammatory, lipid-associated and antigen-presenting. **(E)** Pro-to-anti-inflammatory macrophages ratio.
Each dot represents cells pooled from 3 mice. Boxes indicate the distribution of values, with whiskers denoting the minimum and maximum. Statistical significance was evaluated by either ordinary one-way **(C, E)** or two-way **(B, D)** ANOVA with Tukey's multiple comparison test. *p<0.05, ***p<0.001.

A

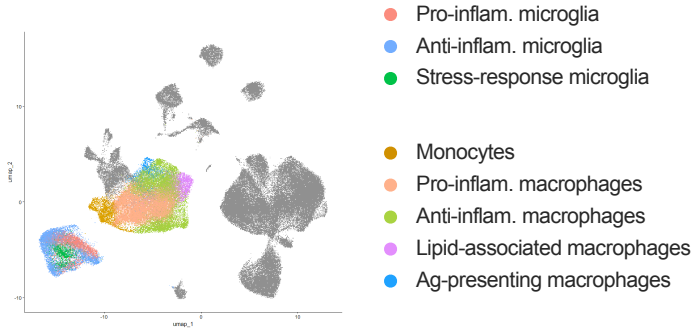
Pro-inflam. microglia
Anti-inflam. microglia
Stress-response microglia
Monocytes
Pro-inflam. macrophages
Anti-inflam. macrophages
Lipid-associated macrophages
Ag-presenting macrophages

B

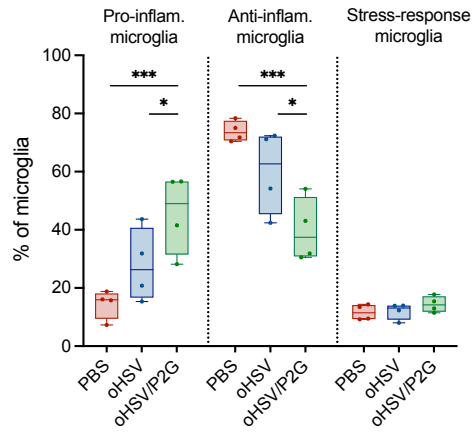
Pro-inflam. microglia
Anti-inflam. microglia
Stress-response microglia
% of microglia
***
*
PBS
oHSV
oHSV/P2G

C

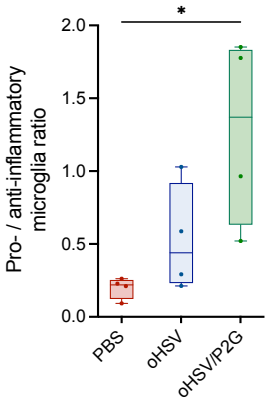
Pro- / anti-inflammatory microglia ratio
*
PBS
oHSV
oHSV/P2G

D

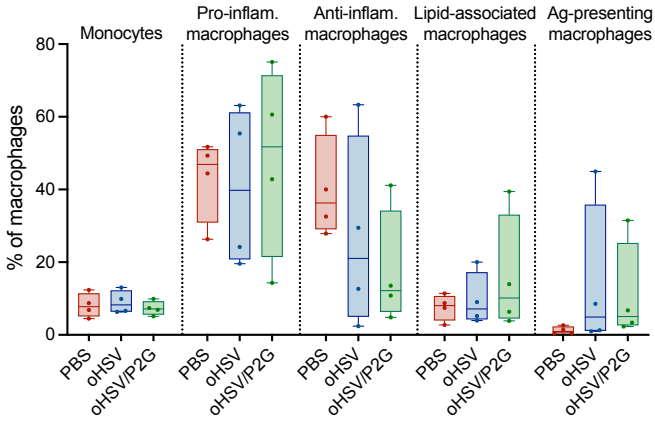
Monocytes
Pro-inflam. macrophages
Anti-inflam. macrophages
Lipid-associated macrophages
Ag-presenting macrophages
% of macrophages
PBS
oHSV
oHSV/P2G

E

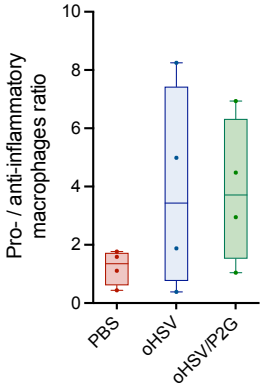
Pro- / anti-inflammatory macrophages ratio
PBS
oHSV
oHSV/P2G

PBS- (0.19, 17%/74%) and oHSV-treated mice (0.53, 28%/60) reflecting an anti-inflammatory predominance but shifted significantly toward a pro-inflammatory profile following oHSV/P2G treatment (1.28, 46%/40%) (Fig. 4B, C).

Within macrophage clusters, monocytes represented a stable fraction (7%–9%) (Fig. 4D). Pro-inflammatory macrophages were the most abundant and remained unchanged across treatments (41%-48%). Conversely, the anti-inflammatory subcluster (40%), initially almost as abundant as the pro-inflammatory one (43%) in PBS-treated mice, decreased progressively to 27% with oHSV and 16% with oHSV/P2G. Meanwhile, the smaller lipid-associated and antigen-presenting subclusters, initially minor (8% and 1% in PBS-treated mice), expanded with viral infection, reaching respectively 10% and 14% with oHSV and 16% and 11% with oHSV/P2G. The pro-/anti-inflammatory ratio was just above 1 in the PBS- (1.22, 43%/40%) shifted toward a pro-inflammatory profile upon virus injection (3.87 and 3.85 respectively) (Fig. 4E). These changes, however, did not reach statistical significance due to high inter-sample variability.

These results indicate that, although treatments did not alter the overall abundance of microglia or macrophages in tumour-bearing mice, oHSV/P2G promoted a shift from anti-inflammatory to pro-inflammatory phenotype. This suggests that oHSV/P2G primarily influences the functional state of myeloid cells rather than their recruitment or expansion.

oHSV/P2G activates *Cd4*$^+$ and *Cd8*$^+$ T cells

To assess activation and exhaustion states, *Cd4*$^+$ and *Cd8*$^+$ T cells were both further subdivided into subclusters. By grouping transcriptionally similar subclusters, two main profiles emerged, defining exhausted (E-T) and non-exhausted (NE-T) T cell subpopulations (Fig 5A, B)[V]. The top 50 differentially expressed genes distinguishing these groups are listed in Appendix 3, enabling functional annotation, and are visualised as a z-score heatmap in Fig. S4A, B.

In PBS-treated tumours, E-T cells represented over 70% of both *Cd4*$^+$ and *Cd8*$^+$ T cells (Fig. 5C, D), and their numbers only modestly variated upon oHSV and oHSV/P2G infection (Fig. S4C, D). By contrast, NE-T cells expanded dramatically with infection by

[V] **Figure 5: oHSV/P2G activates *Cd4*$^+$ and *Cd8*$^+$ T cells**
A, B: UMAP representation of the clustering of *Cd4*$^+$ **(A)** or *Cd8*$^+$ **(B)** T cells, highlighting exhausted (E-T cells) and none-exhausted (NE-T cells) subpopulations identified based on subcluster-specific differentially expressed marker genes. **C, D:** Percentage of both *Cd4*$^+$ **(C)** or *Cd8*$^+$ **(D)** T cells subpopulations. **E, F:** Pseudobulk analysis of *Cd4*$^+$ **(E)** or *Cd8*$^+$ **(F)** NE-T cells showing representative marker genes visualised as heatmaps of z-score from mean normalised expression values. Genes are grouped into several functional gene sets.
Each dot represents cells pooled from 3 mice. Boxes indicate the distribution of values, with whiskers denoting the minimum and maximum. Statistical significance was evaluated by two-way ANOVA with Tukey's multiple comparison test. *p<0.05, **p< 0.01, ***p<0.001, ****p<0.0001.

Figure 5

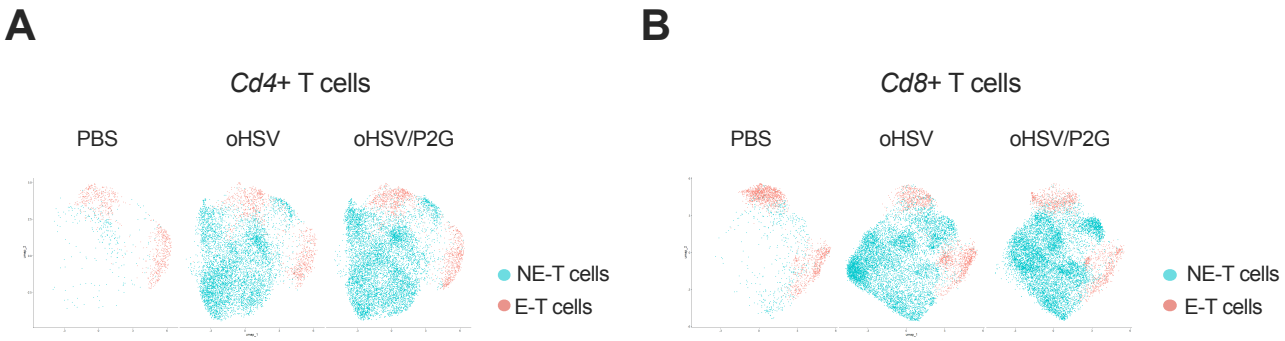
A
Cd4+ T cells
PBS
oHSV
oHSV/P2G
NE-T cells
E-T cells
B
Cd8+ T cells
PBS
oHSV
oHSV/P2G
NE-T cells
E-T cells

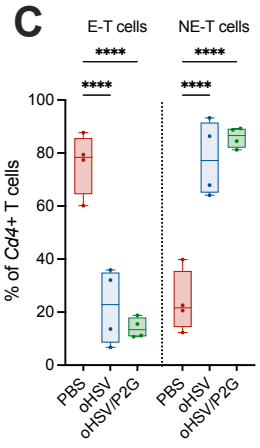
C
E-T cells
NE-T cells
****
****
****
****
% of Cd4+ T cells
100
80
60
40
20
0
PBS
oHSV
oHSV/P2G
PBS
oHSV
oHSV/P2G

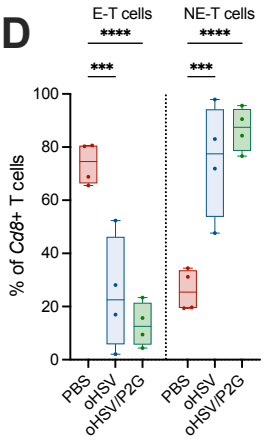
D
E-T cells
NE-T cells
****
****
***
***
% of Cd8+ T cells
100
80
60
40
20
0
PBS
oHSV
oHSV/P2G
PBS
oHSV
oHSV/P2G

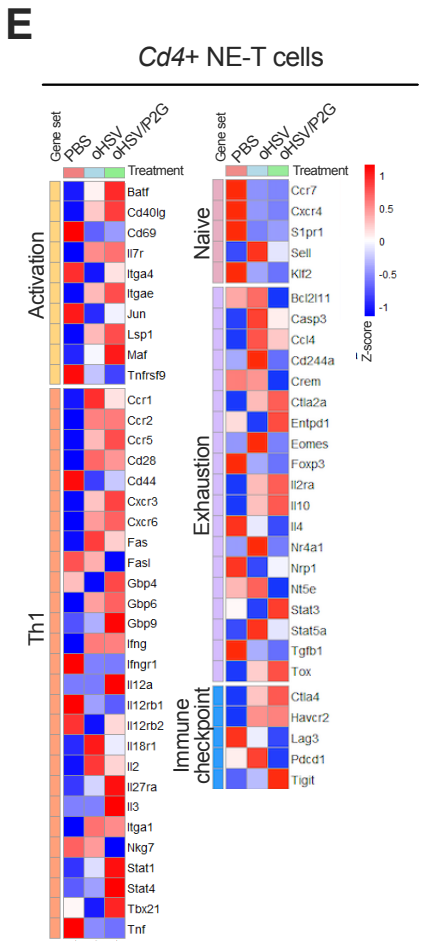
E
Cd4+ NE-T cells
Gene set
PBS
oHSV
oHSV/P2G
Treatment
Activation
Batf
Cd40lg
Cd69
Il7r
Itga4
Itgae
Jun
Lsp1
Maf
Tnfrsf9
Th1
Ccr1
Ccr2
Ccr5
Cd28
Cd44
Cxcr3
Cxcr6
Fas
Fasl
Gbp4
Gbp6
Gbp9
Ifng
Ifngr1
Il12a
Il12rb1
Il12rb2
Il18r1
Il2
Il27ra
Il3
Itga1
Nkg7
Stat1
Stat4
Tbx21
Tnf
Naive
Ccr7
Cxcr4
S1pr1
Sell
Klf2
Exhaustion
Bcl2l11
Casp3
Ccl4
Cd244a
Crem
Ctla2a
Entpd1
Eomes
Foxp3
Il2ra
Il10
Il4
Nr4a1
Nrp1
Nt5e
Stat3
Stat5a
Tgfb1
Tox
Immune checkpoint
Ctla4
Havcr2
Lag3
Pdcd1
Tigit
Z-score
1
0.5
0
-0.5
-1

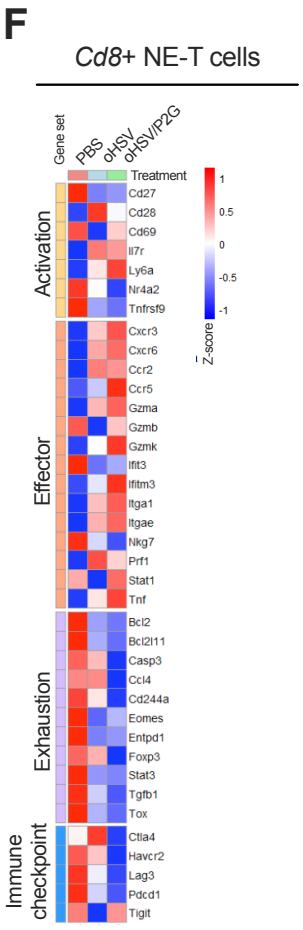
F
Cd8+ NE-T cells
Gene set
PBS
oHSV
oHSV/P2G
Treatment
Activation
Cd27
Cd28
Cd69
Il7r
Ly6a
Nr4a2
Tnfrsf9
Effector
Cxcr3
Cxcr6
Ccr2
Ccr5
Gzma
Gzmb
Gzmk
Ifit3
Ifitm3
Itga1
Itgae
Nkg7
Prf1
Stat1
Tnf
Exhaustion
Bcl2
Bcl2l11
Casp3
Ccl4
Cd244a
Eomes
Entpd1
Foxp3
Stat3
Tgfb1
Tox
Immune checkpoint
Ctla4
Havcr2
Lag3
Pdcd1
Tigit
Z-score
1
0.5
0
-0.5
-1

approximately 25-fold for *Cd4*$^+$ T cells and 16-fold for *Cd8*$^+$ T cells (Fig. S4C, D), representing consequently around 80% of T cells in both subsets (Fig. 5C, D).

The aim of the treatment is to prevent exhaustion in newly recruited cells rather than reverse the profile of already exhausted T cells. Therefore, pseudobulk gene expression analysis was performed to characterise NE-T cells across treatments and visualise results as z-score heatmaps. In *Cd4*$^+$ NE-T cells, activation- and Th1-associated genes were markedly upregulated with both viruses. Conversely, genes characteristic of naïve phenotype were downregulated upon infection. In addition, exhaustion and immune checkpoint markers exhibited a mixed expression pattern, complicating interpretation (Fig. 5E). For example, in oHSV/P2G-treated samples, z-scores of key anti-inflammatory genes such as *Foxp3, Il4, Eomes*, and *Tgfb1* were low, whereas *Il10* and other genes exhibited high z-scores. Similarly, immune checkpoint markers showed positive z-scores for *Ctla4, Havcr2*, and *Tigit*, and negative z-scores for *Lag3* and *Pdcd1* (Fig. 5E). In *Cd8*$^+$ NE-T cells, oHSV/P2G induced strong effector-like gene expression compared to PBS and globally downregulated exhaustion-related genes and immune checkpoints, except *Tigit*. oHSV exhibited a similar trend, albeit with an overall attenuated effect. (Fig. 5F).

Flow cytometry confirmed activation of NE-T cells at the protein level upon infection, with IL7R and LY6A significantly increased in both CD4$^+$ and CD8$^+$ T cells. In contrast, PDCD1 was significantly reduced, while LY6C was increased only in CD8$^+$ T cells. No differences were observed between the two viruses (Fig. S4E).

Overall, these results indicate that infection recruits T cells with a phenotype distinct from naïve and exhausted T cells present during tumour development. Recruited NE-T cells, which become predominant at the tumour site, display an active, effector-like profile. Both viruses similarly increased Th1-like gene expression and decreased naïve signatures in CD4$^+$ T cells. In CD8$^+$ T cells, oHSV/P2G was associated with a greater increase in effector gene expression and a more pronounced reduction of exhaustion-related gene and immune checkpoint expression compared with PBS and oHSV. Collectively, these findings suggest that P2G may enhance oHSV-induced T cell activation and contribute to a reduction of exhaustion within the tumour microenvironment.

oHSV/P2G polarizes TAMs toward a pro-inflammatory phenotype

As one aim of the treatment is to promote the plasticity of macrophages and microglia towards pro-inflammatory subpopulations, pseudobulk gene expression analysis was performed on the entire populations rather than subpopulations to assess treatment-induced transcriptional changes.

oHSV/P2G clearly upregulated genes associated with antigen presentation (MHC-I/II) and activation in both macrophages and microglia compared with PBS. These effects were

more pronounced than with oHSV in at least one of the two populations. Phagocytosis and pro-inflammatory genes were similarly upregulated by both viruses. By contrast, anti-inflammatory genes were downregulated exclusively by oHSV/P2G in macrophages, relative to both PBS and oHSV. Expression of immune checkpoints did not consistently variate, some of them increasing while others decreased upon treatment (Fig. 6A, B)[VI].

Ingenuity Pathway Analysis (IPA, Qiagen) was performed on macrophages to identify significantly modulated canonical pathways associated with macrophage activation and polarization, with each virus compared to PBS (Fig. 6C). Surprisingly, IFNγ signalling and MHC class 2 antigen presentation pathways were predicted to be significantly downregulated by both viruses. Conversely, MHC class 1 antigen presentation and classical macrophage activation (M1-like) were upregulated upon infection, whereas PD1/PDL1 signalling was inhibited. Notably, alternative macrophage activation (M2-like), CXCR4, STAT3, and TGFβ signalling pathways were activated by oHSV but strongly inhibited by oHSV/P2G (Fig. 6C).

Flow cytometry confirmed microglial activation at the protein level, showing significant upregulation of CD80 and ADGRE1 with both viruses, and of ITGAX and MHC-2 specifically following oHSV/P2G treatment (Fig. 6D).

In vitro, human monocyte-derived macrophages (hMDMs) were treated for 48h with conditioned media from GB138 human glioblastoma cells cultured for 72h and either uninfected (mNI) or infected with oHSV (moHSV) or oHSV/P2G (moHSV/P2G). Bulk RNA sequencing of hMDMs showed variable modulation of individual genes across MHC-1, pro- and anti-inflammatory, and immune checkpoints categories. In contrast, both virus-conditioned media similarly increased most MHC-2 and activation-related genes, while unexpectedly reducing most phagocytosis-related genes (Fig. S5A).

Overall, oHSV/P2G enhanced oHSV-induced upregulation of genes involved in antigen presentation, activation, phagocytosis, and pro-inflammatory responses in macrophages and microglia. Importantly, oHSV/P2G was the only treatment associated with a reduction of the anti-inflammatory macrophage program characteristic of the glioblastoma microenvironment. IPA further confirmed the concurrent promotion of pro-inflammatory

---

[VI] **Figure 6: oHSV/P2G polarizes TAMs toward a pro-inflammatory phenotype**
A, B: Pseudobulk analysis of macrophages **(A)** or microglia **(B)** showing representative marker genes visualised as heatmaps of z-score from mean normalised expression values. Genes are grouped into several functional gene sets. **(C)** Gene ontology pathways significantly altered in macrophages, identified via QIAGEN Ingenuity Pathway Analysis visualised as heatmaps of z-score. **(D)** Median fluorescence intensity (MFI) of representative markers expression by microglia following flow cytometry analysis (PBS: n=9, oHSV: n=9, oHSV/P2G: n=10).
Each dot represents cells from one mouse. Boxes indicate the distribution of values, with whiskers denoting the minimum and maximum. Statistical significance was evaluated by ordinary one-way ANOVA with Tukey's multiple comparison test. *p<0.05, **p< 0.01, ***p<0.001, ****p<0.0001.

Figure 6

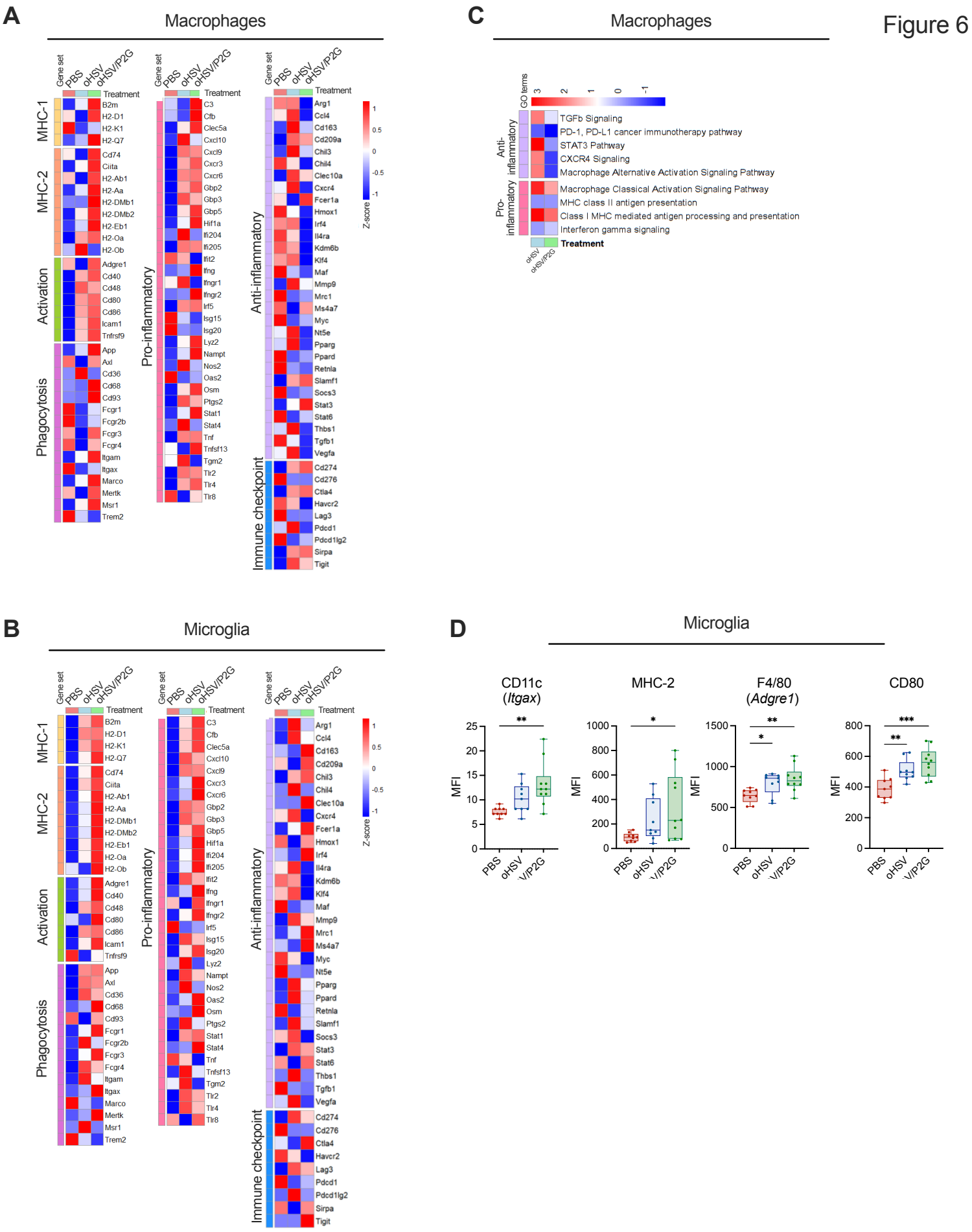
A
Macrophages
Gene set
PBS
oHSV
oHSV/P2G
Treatment
MHC-1
B2m
H2-D1
H2-K1
H2-Q7
MHC-2
Cd74
Ciita
H2-Ab1
H2-Aa
H2-DMb1
H2-DMb2
H2-Eb1
H2-Oa
H2-Ob
Activation
Adgre1
Cd40
Cd48
Cd80
Cd86
Icam1
Tnfrsf9
Phagocytosis
App
Axl
Cd36
Cd68
Cd93
Fcgr1
Fcgr2b
Fcgr3
Fcgr4
Itgam
Itgax
Marco
Mertk
Msr1
Trem2
Pro-inflammatory
C3
Cfb
Clec5a
Cxcl10
Cxcl9
Cxcr3
Cxcr6
Gbp2
Gbp3
Gbp5
Hif1a
Ifi204
Ifi205
Ifit2
Ifng
Ifngr1
Ifngr2
Irf5
Isg15
Isg20
Lyz2
Nampt
Nos2
Oas2
Osm
Ptgs2
Stat1
Stat4
Tnf
Tnfsf13
Tgm2
Tlr2
Tlr4
Tlr8
Anti-inflammatory
Arg1
Ccl4
Cd163
Cd209a
Chil3
Chil4
Clec10a
Cxcr4
Fcer1a
Hmox1
Irf4
Il4ra
Kdm6b
Klf4
Maf
Mmp9
Mrc1
Ms4a7
Myc
Nt5e
Pparg
Ppard
Retnla
Slamf1
Socs3
Stat3
Stat6
Thbs1
Tgfb1
Vegfa
Immune checkpoint
Cd274
Cd276
Ctla4
Havcr2
Lag3
Pdcd1
Pdcd1lg2
Sirpa
Tigit
Z-score
1
0.5
0
-0.5
-1
C
Macrophages
GO terms
3
2
1
0
-1
Anti-inflammatory
TGFb Signaling
PD-1, PD-L1 cancer immunotherapy pathway
STAT3 Pathway
CXCR4 Signaling
Macrophage Alternative Activation Signaling Pathway
Pro-inflammatory
Macrophage Classical Activation Signaling Pathway
MHC class II antigen presentation
Class I MHC mediated antigen processing and presentation
Interferon gamma signaling
Treatment
oHSV
oHSV/P2G
B
Microglia
D
Microglia
CD11c (Itgax)
MHC-2
F4/80 (Adgre1)
CD80
MFI
PBS
oHSV
V/P2G

signalling and inhibition of anti-inflammatory pathways by oHSV/P2G. *In vitro* studies employing hMDMs have thus far yielded somewhat disappointing and variable results.

oHSV/P2G improved survival and immune activation, particularly in a poorly immunogenic model

Finally, survival was evaluated in mice engrafted intracerebrally with 1×10^5 GL261N4 cells and treated with oHSV or oHSV/P2G (1×10^6 pfu) on days 7 and 14 post-engraftment (n=14, 15, 12 for PBS, oHSV, and oHSV/P2G, respectively). Both viral treatments significantly extended survival, with some mice surviving beyond 60 days (2 for both oHSV and oHSV/P2G), whereas all PBS-treated had to be sacrificed by day 31. No significant difference was observed between the viruses, with median survival of 27, 30, and 29 days for PBS, oHSV, and oHSV/P2G, respectively (Fig. 7A)[VII].

Another murine glioblastoma model, 005-GSCs, recently described as less immunogenic and thus less responsive to oncolytic virotherapy[36,37], exhibits a higher correlation with patient glioblastoma (Spearman's R) than GL261N4[36,38]. Using the same protocol as for GL261N4 tumours (n=10 per treatment), oHSV injection showed no effect on survival compared to PBS-treated mice. By contrast, oHSV/P2G significantly prolonged survival compared to PBS, with a median survival of 40 days versus 33 days for both PBS and oHSV. All PBS-treated mice were sacrificed by day 43, whereas one oHSV/P2G-treated mouse survived beyond 80 days (Fig. 7B). These results confirm the survival benefit of oHSV/P2G and suggest its superior efficacy compared to oHSV, particularly in a less immunogenic glioblastoma model that better reflects the immunosuppressive landscape of human glioblastomas.

Immune cells were further analysed in the 005-GSCs model by bulk RNA sequencing of brain right hemisphere from mice sacrificed 21 days post-engraftment. Gene categories previously defined from scRNAseq experiment were used to characterise the tumour microenvironment. Genes appearing in multiple sets were analysed only once to avoid redundancy. oHSV/P2G markedly affected immune cell–related markers, upregulating genes associated with myeloid cells antigen presentation, activation, phagocytosis, and pro-inflammatory pathways, as well as genes linked to activated, effector and Th1-like T cells, B cell surface molecules, and immunoglobulin production. By contrast, the anti-inflammatory myeloid program and T cells exhaustion-related genes exhibited mixed

[VII] **Figure 7: oHSV/P2G improved survival and immune activation, particularly in a poorly immunogenic model**

A, B: Kaplan-Meier analysis of survival after treatment settings described in Figure 1A in GL261N4 model with PBS- (n=14), oHSV- (n=15), oHSV/P2G (n=12) -treated mice **(A)** or 005-GSCs model (n=10 in each group) **(B)**.

C-E: Bulk RNA sequencing analysis of leucocytes, recovered from PBS- (n=4), oHSV- (n=4) or oHSV/P2G- (n=5) treated mice 21 d.p.e. of $1x10^5$ 005-GSCs. Representative marker genes were visualised as heatmaps of z-score from mean normalised expression values. Genes are grouped into several functional gene sets related to myeloid **(C)**, T **(D)**, and B **(E)** cells.

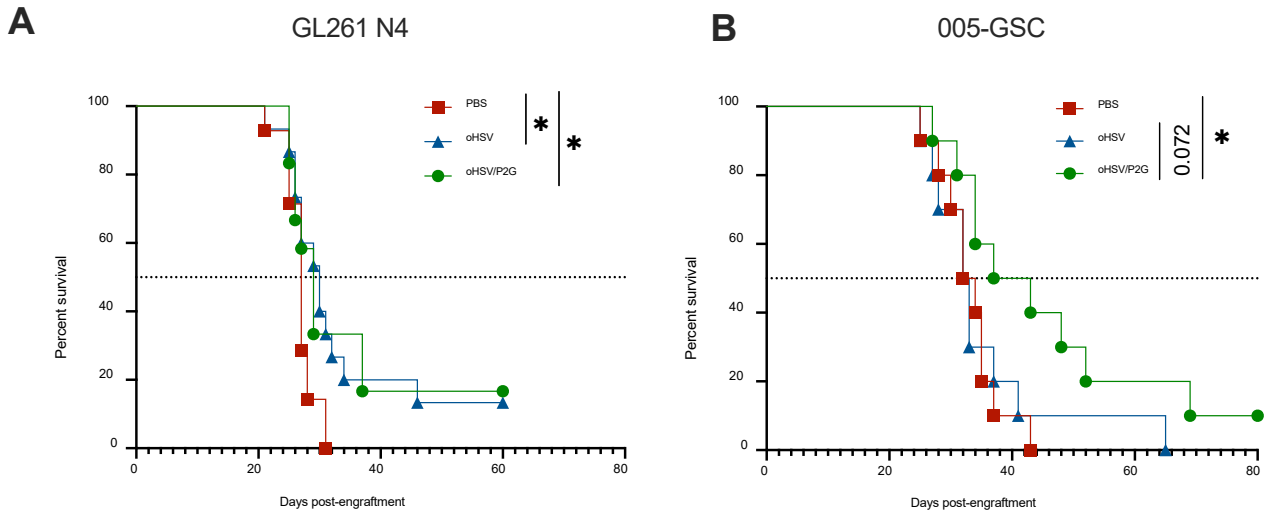
A
GL261 N4
PBS
oHSV
oHSV/P2G
*
*
Percent survival
Days post-engraftment
B
005-GSC
PBS
oHSV
oHSV/P2G
0.072
*
Percent survival
Days post-engraftment

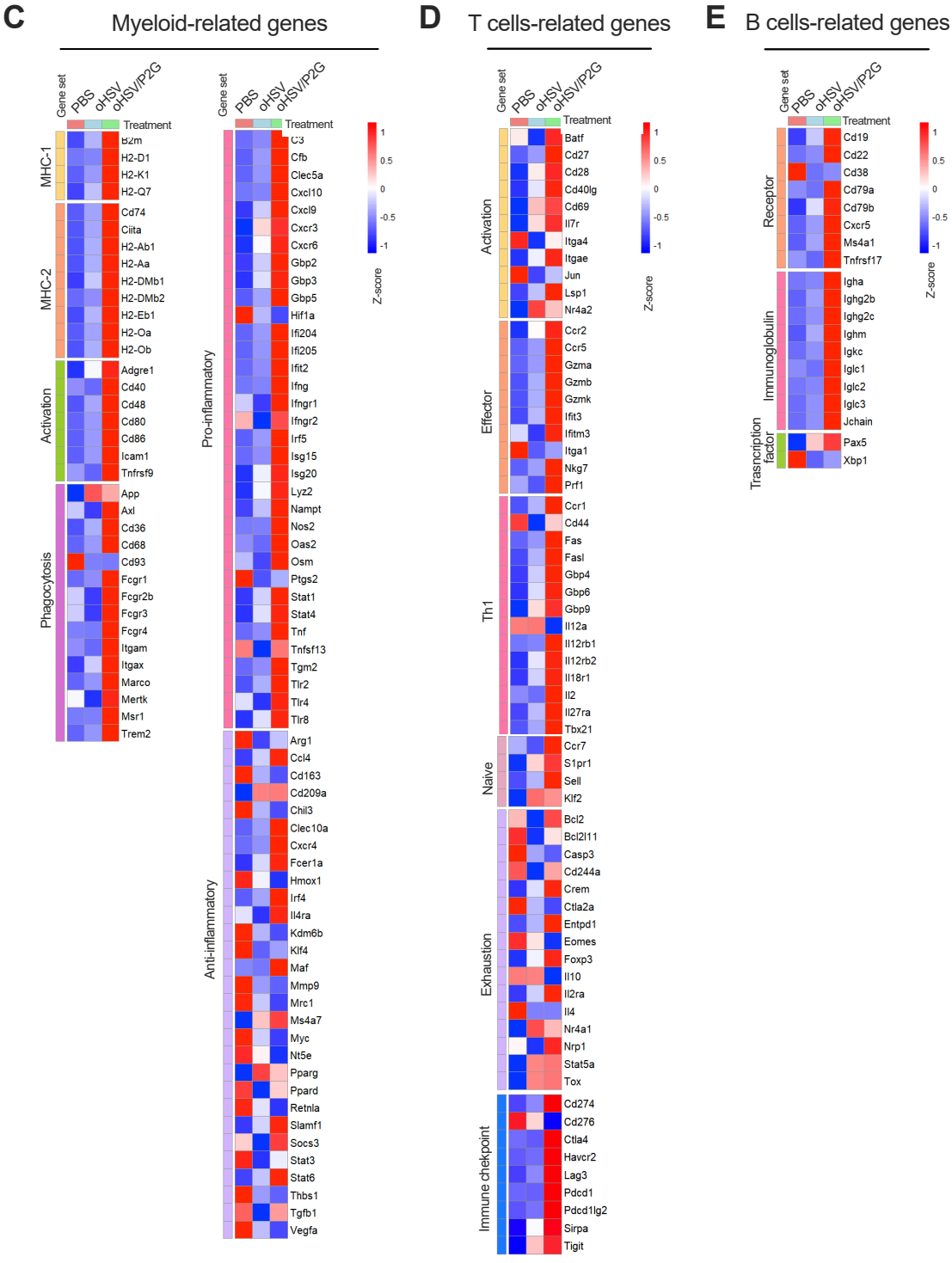
C
Myeloid-related genes
Gene set
PBS
oHSV
oHSV/P2G
Treatment
MHC-1
MHC-2
Activation
Phagocytosis
Pro-inflammatory
Anti-inflammatory
Z-score
D
T cells-related genes
Activation
Effector
Th1
Naive
Exhaustion
Immune chekpoint
E
B cells-related genes
Receptor
Immunoglobulin
Trasnciption factor

patterns across all conditions. Surprisingly, markers of naïve T cells and immune checkpoints were highly upregulated by oHSV/P2G (Fig. 7C–E).

These results indicate distinct immune responses to infection between the GL261N4 and 005-GSCs models, reflecting differences in immune activation and the pathways involved. Importantly, the upregulation of pro-inflammatory genes by oHSV/P2G correlates with the observed survival benefit in the 005-GSCs model. Nevertheless, the ambiguous profile of anti-inflammatory or exhaustion genes, and the concurrent increase in immune checkpoint–related genes following oHSV/P2G treatment, warrants further investigation.

DISCUSSION

Glioblastoma is the most frequent and aggressive primary brain tumour and remains associated with poor prognosis due to intrinsic therapeutic resistance and recurrence. [1,2] Glioblastoma stem-like cells (GSCs) play a central role in treatment failure and actively contribute to the establishment of an immunologically "cold" tumour microenvironment (TME).[4,5,39] Tumour-associated macrophages and microglia (TAMs), the dominant immune populations in glioblastoma, exhibit limited phagocytic and antigen-presenting capacities and secrete anti-inflammatory cytokines, thereby sustaining immunosuppression.[40–42] The recruitment of lymphocyte is restricted by the blood–brain barrier and characterised by low Th1 activity, an unfavourable cytotoxic-to-regulatory T cell (CTL/Treg) ratio, profound T cell exhaustion with elevated immune checkpoint (IC) expression, and scarce, largely naïve B cells.[7–9] Consequently, glioblastoma is resistant to current immunotherapies, including immune checkpoint inhibitors (ICIs) targeting PD-1/PD-L1 or CTLA4.[8,21,22]

The CXCR4/CXCL12 signalling axis is a key driver of glioblastoma progression, invasiveness, angiogenesis, recurrence, immune evasion, and is associated with poor clinical outcome.[11,12,16] CXCR4 is upregulated on endothelial cells, GSCs, and immunosuppressive immune populations such as Tregs, TAMs, and myeloid-derived suppressor cells (MDSCs), all contributing to the "cold" TME.[8] CXCL12, produced primarily by endothelial cells and GSCs, promotes recruitment of suppressive immune cells, downregulation of MHC expression of antigen-presenting cells (APCs), polarization of TAMs toward an anti-inflammatory phenotype, and secretion of pro-tumoral cytokines and growth factors, including VEGFα and TGFβ, through activation of PI3K/AKT, MEK/MAPK, and JAK/STAT3 pathways.[11,43]

Preclinical studies have demonstrated the potential of CXCR4 inhibition in glioblastoma, including impaired invasiveness, intratumoral vasculature, radioresistance, and promotion of pro-inflammatory polarisation of TAMs. In contrast, despite strong preclinical rationale, plerixafor (AMD3100) has only progressed to Phase I trials in newly diagnosed or recurrent glioblastoma. These studies have not demonstrated a survival

benefit in combination with standard treatments or bevacizumab. Notably, CXCR4 inhibition has been associated with increased IFN-γ expression and subsequent upregulation of ICs, which may contribute to therapeutic resistance.[44,45] Similarly, immune checkpoint inhibitors showed encouraging preclinical results but disappointing clinical outcomes. Their limited efficacy in glioblastoma is likely due to the scarcity and transient activation of CTLs, which lack support from functional APCs and are rapidly exhausted by immunosuppressive TAMs and soluble mediators. Therefore, combination strategies are now under investigation. In preclinical models, these approaches enhance anti-tumour immune responses by promoting a pro-inflammatory TAM phenotype, increasing $CD4^+/CD8^+$ ratios while reducing $Treg/CD8^+$ ratios, and improving immune memory.[10,14,46–48] Similar benefits could be expected from combining CXCR4 inhibition with virotherapy.

In this context, we engineered an oncolytic herpes simplex virus type 1 expressing the CXCL12 antagonist P2G (oHSV/P2G). Oncolytic viruses are administered via intratumoral injection, thereby bypassing the blood–brain barrier and enabling localized expression of P2G. Oncolytic viruses elicit potent inflammatory responses by infecting tumour cells and inducing immunogenic cell death, thereby releasing tumour- and virus-derived antigens, PAMPs, DAMPs, and pro-inflammatory cytokines that drive the recruitment of lymphocytes.[8,9,20,23,24] P2G expression is expected to synergize with virotherapy by limiting recruitment of immunosuppressive cells, reprogramming TAMs and helper T cells toward anti-tumoral phenotypes and reducing anti-inflammatory mediator production.[11,19] Together, these effects enhance antigen processing and presentation, leading to more efficient priming and activation of newly recruited functional CTLs that are less prone to exhaustion.

Despite advances in humanized mouse models, organoids, scaffolds and microfluidic platforms, immunocompetent orthotopic syngeneic mouse models remain the most robust systems to study glioblastoma in an intact 3D brain environment, including physiological extracellular matrix, vascularisation, and a lifelong functional immune compartment.[49–52] However, species-specific differences between murine and human immune and central nervous systems can affect tumour biology and therapeutic responses. A major challenge remains the availability of murine glioblastoma models that faithfully recapitulate human disease. Several chemically induced (GL261N4, CT2A) and genetically engineered (005-GSCs, Mut3, NF53, mGB2) models have been developed, each displaying distinct immune and histological features.[36,38,39] In this study, we employed the GL261N4 and 005-GSCs models, which show a strong correlation with human glioblastoma immune profiles, despite their high tumour mutation burden and immune-related gene expression.[38] The 005-GSCs model is considered less immunogenic than GL261N4, due to resistance to T cell–targeted therapies, like ICIs, downregulation of MHC and co-stimulatory molecules on APCs, and low infiltration of reactive or exhausted CTLs.[36] Notably, the 005-GSCs model also displays elevated NK cell

abundance, poor vascularisation, and intermediate invasiveness, that may influence therapeutic response.[39] Given glioblastoma pronounced inter- and intratumoral heterogeneity, the use of multiple complementary models remains essential.[4,5]

In the GL261N4 model, we observed a reduction in mean tumour volume at 21 days post-engraftment, with a more pronounced effect for oHSV/P2G compared with oHSV, although these differences did not reach statistical significance. Previous studies from our lab using immunodeficient xenograft models, engrafted with $1x10^5$ GB138 or T033 human glioblastoma cells, reported significant but similar tumour regression upon oHSV and oHSV/P2G injected at the same dose (1×10^6 pfu in 2 µL), albeit with a different injection schedule due to slower tumour growth.[13] Notably, *in vitro*, all glioblastoma cells are efficiently killed by the virus, even at low doses, and P2G has no direct effect on tumour cell proliferation. The high variability and lack of significant effect on tumour volume in the GL261N4 model are major concerns. This raises the possibility that the observed results reflect chance rather than a true effect of oHSV/P2G. The experiment should therefore be repeated with careful attention to statistical power. A larger number of mice should be included to account for deaths during the three successive surgeries, and the protocol should be optimised to minimise such losses. The model may also need to be revised to ensure detectable differences between conditions, including adjustments to cell number at engraftment, treatment timing and frequency, and the glioblastoma cell line used. The absence of a survival benefit with oHSV/P2G compared to oHSV, discussed below, is consistent with the lack of difference in tumour size. Nevertheless, for scientific interest, potential explanations for the differential impact of oHSV/P2G in the GL261N4 model compared with immunodeficient models will be explored.

oHSV/P2G's impact on the tumour volume observed in the immunocompetent GL261N4 model could be driven by enhanced anti-tumour adaptive immunity. The absence of significant tumour shrinkage *in vivo* may reflect the rapid growth of GL261N4 tumours, which could limit the impact of tumour cell killing, or alternatively, accelerated viral clearance following extensive tumour cell death, as suggested *in silico*.[53] Finally, even though tumour cell killing reduces the tumour burden, the apparent tumour area may increase due to inflammation, oedema, and immune cell infiltration following infection. As a result, tumour shrinkage may be partially masked when measuring manually delineated areas on haematoxylin-stained sections. Nevertheless, in survival assays, both oHSV and oHSV/P2G significantly increased overall survival suggesting partial tumour clearance. We could not exclude the possibility that the reduction in tumour volume measured 7 days after the second treatment may become more pronounced at later time points due to delayed immune-mediated effects.

oHSV/P2G induced substantial remodelling of the immune microenvironment in the GL261N4 model. TAMs were polarized toward an activated, antigen-presenting, and more

pro-inflammatory phenotype, with shifts in the relative abundance of M1- and M2-like subpopulations. Ingenuity pathway analysis revealed inhibition of crucial anti-inflammatory pathways compared to both PBS and oHSV such as CXCR4, STAT3, TGFβ, and alternative activation signalling. Despite not directly targeting T cells, which don't particularly express CXCR4 except for Tregs, oHSV/P2G promoted activation, Th1- and effector-like polarisation, and reduced exhaustion of $CD4^+$ and $CD8^+$ T cells. Finally, oHSV/P2G promoted plasmocyte phenotype among B cells. Furthermore, oHSV/P2G increased intratumor lymphocytes recruitment, resulting in a higher CTL/Treg ratio and a myeloid-to-lymphoid shift. This immune remodelling can be associated with a cold-to-hot tumour transition, as TAMs are the key drivers of the immunosuppressive microenvironment, primarily by inhibiting lymphocytes recruitment and activation and promoting T cell exhaustion, in part through Tregs functions.[8,40,42] Whether the recruited lymphocytes are predominantly specific of virus, infected cells or tumour cells antigens should be determined.

Surprisingly, the CD4/CD8 ratio varies depending on the technique used, with single-cell RNA sequencing suggesting a predominance of $CD8^+$ T cells, while flow cytometry indicates a majority of $CD4^+$ T cells. Immunofluorescence remains relatively equal and too variable to draw firm conclusions. It is difficult to determine which subset is more beneficial for therapeutic outcomes, despite CTLs being the classically described mediators of anti-tumour immunity. This question could be further explored using CD4- or CD8-deficient systems. Notably, single-cell RNA sequencing is less biased, as it does not rely on predefined markers or gating strategies and provides comprehensive transcriptional profiles. Conversely, immunostaining approaches often face technical limitations, including trade-offs between sensitivity and background signal. Altogether, these discrepancies highlight the need for complementary methodologies and further validation. Notably, CD4/CD8 ratio may vary across different tumour models.

Survival analyses in the GL261N4 and 005-GSCs models revealed distinct outcomes. While in GL261N4, both oHSV and oHSV/P2G significantly extended survival, with some mice exhibiting long-term survival suggesting partial tumour clearance, in the 005-GSCs model, only oHSV/P2G significantly improved survival, although one long-term survivor was observed following oHSV treatment. Bulk RNA sequencing in the 005-GSCs model revealed modest immune activation with oHSV, whereas oHSV/P2G induced robust upregulation of nearly all investigated immune-related pathways, except myeloid anti-inflammatory and T cells exhaustion-related genes. This clearly contrasts with GL261N4 tumours, where oHSV itself induced a pronounced immune response relative to PBS. In this model, immune profiles elicited by both viruses were closer, although more antitumoral upon oHSV/P2G injection.

These differences likely reflect the distinct immunogenic landscapes of the two models.[36,38,39] GL261N4 tumours are more immunogenic, allowing oHSV to trigger

substantial immune activation, which oHSV/P2G further enhances on multiple levels. The lack of overall survival differences between the two viruses could thus be attributed to GL261N4 tumour aggressiveness or rapid viral clearance, as discussed above. In contrast, in the poorly immunogenic 005-GSCs model, which is resistant to conventional immunotherapies, CXCR4 blockade is able to overcome immunosuppression and fully exploit virotherapy-induced immunogenic cell death. Precisely, we could speculate that, in the GL261N4 model, oHSV can recruit and activate many CTLs in a tumour microenvironment with relatively low abundance of immunosuppressive APCs, whereas 005-GSCs tumours benefit from oHSV/P2G in a microenvironment with low CTLs numbers and numerous APCs lacking MHC and co-stimulatory molecules.[36,38,39] High NK cell abundance in the 005-GSCs model, with their potential antiviral activity, may further limit the efficacy of oncolytic virotherapy.[54]

Expression of some immune checkpoints increased following treatment in the GL261N4 model compared to PBS. However, in the 005-GSCs model, most ICs were significantly upregulated by oHSV/P2G compared with both PBS and oHSV. Importantly, these analyses cannot be directly compared, ICs expression in the 005-GSCs model was assessed across the entire $CD45^+$ cells population using bulk RNA sequencing, whereas in the GL261N4 model it was evaluated within specific immune populations using pseudobulk analysis of single-cell RNA sequencing data. In this context, the increased ICs expression observed in the 005-GSCs model may primarily reflect an increased proportion of lymphocytes, which are initially scarce in this model.[36,38,39] However, we cannot conclude in the absence of time-course data on the recruitment and activation of the different immune populations. Besides, it might result from the physiological upregulation of exhaustion markers following T cell activation, further supporting the superior immunomodulatory effect of oHSV/P2G over oHSV. Although this resulted into improved survival, upregulation of ICs highlights a potential limitation and provides a strong rationale for combination strategies with ICIs. Overall, the distinct immunogenic profiles of the two models likely explain the observed differences in survival and immune-related gene expression. Nevertheless, future studies incorporating single-cell RNA sequencing and flow cytometry will be essential to more precisely delineate treatment-induced immune dynamics.

In conclusion, we developed an oncolytic HSV-1 expressing the CXCL12 antagonist P2G that retains potent tumour-selective replication and efficient tumour cell killing, while simultaneously reducing the stemness and migratory capacity of GSCs. In addition, we demonstrate that oHSV/P2G enhances anti-tumour immunity by reshaping the tumour microenvironment from a myeloid-dominated, immunologically “cold” to a lymphoid-enriched, “hot” tumour, through reprogramming of TAMs as well as recruitment and activation of lymphocytes. Notably, oHSV/P2G significantly improved survival compared with unarmed oHSV, particularly in poorly immunogenic glioblastoma models characterised by low abundance of lymphocytes and a predominance of APCs with

limited antigen-presenting and co-stimulatory capacity. Future studies should focus on comprehensive immune profiling across diverse and recurrent glioblastoma models to address tumour heterogeneity and improve patient selection. Priority should be given to evaluating additional immune populations, including NK cells, DCs, and neutrophils, as well as exploring combination strategies such as ICIs and investigating T- and B-cell antigen specificity. Alternatively, oHSV/P2G could be involved in preventing recurrence and tumour angiogenesis which are also partly mediated by CXCR4/CXCL12 pathways.

MATERIALS & METHODS

Cell lines

VERO cells (ATCC, CCL-81), patient-derived human glioblastoma GB138 cells[15], and chemically induced murine glioblastoma GL261N4 cells transduced with human Nectin[55] were maintained in Dulbecco's Modified Eagle Medium, high glucose (DMEM HG; Biowest) supplemented with 10% foetal bovine serum (FBS; Gibco). Spontaneous murine glioblastoma 005-GSCs cells transduced with GFP[37] were cultured as tumorospheres in stem cell medium DMEM/F-12 (Gibco) supplemented with 2% B27 without vitamin A (Gibco), 1% Penicillin Streptomycin (P/S; Gibco), 1 µg/mL heparin (Carl Roth), and 20 ng/mL each EGF and βFGF (BioLegend).

Construction of recombinant oHSVs

Recombinant viruses were engineered using the fHsvQuik-1 bacterial artificial chromosome (BAC) containing an attenuated HSV-1 (strain F; Δγ34.5, ΔUL39, GFP^+; kind gift from A. Chiocca, University of Pittsburgh, USA). Additional ICP47 deletion was performed as described by Todo T et al., 2001[56]. Recombinants were generated using the two-step Red recombination "en passant" technique[57]. A human CXCL12 mutant sequence (second amino acid substitution: Pro → Gly) flanked by the IL-2 signal peptide (5') and an HA tag (3'), under the control of the EF1α promoter, was inserted immediately downstream of the eGFP gene[13] VERO cells were transfected with this construct using JETPEI (Polyplus). Virus stocks were produced as previously described[58], ultracentrifuged (SW28 swinging-bucket rotor, Beckman Coulter; 17,000 rpm), resuspended in PBS (Cytiva) containing 10% glycerol, and stored at −80 °C. Viral titer was determined in VERO cells by plaque assay[59].

Virus and conditioned media production

GB138 cells were grown in DMEM HG 10% FBS. At 80% confluence, the medium was replaced with DMEM/F-12, and cells were either not infected (mNI) or infected at MOI of 1 with oHSV (mOHSV) or oHSV/P2G (mOHSV/P2G). After 72h, supernatants were collected, centrifuged (260 × g, 5 min), and filtered through a 0.1 µm membrane (Pall Corporation).

Bulk RNA sequencing of human monocytes-derived-macrophages (hMDMs)

Fresh human PBMCs were obtained from healthy donors (Red Cross, Belgium) after informed consent. All procedures were approved by the Ethics Committee of the University of Liège. $CD14^+$ monocytes were isolated using the EasySep Human CD14 Positive Selection Kit II (StemCell Technologies). Cells were cultured in RPMI (VWR) supplemented with 20% FBS and 100 ng/mL M-CSF (Miltenyi Biotec) for 5 days, then polarized in conditioned medium supplemented 100 ng/mL M-CSF for 48h. Total RNA was extracted using the NucleoSpin RNA kit (Macherey-Nagel).

Bulk RNA sequencing of polyadenylated mRNA was performed by the GIGA-Genomics platform using Illumina high throughput sequencer (Illumina mRNA stranded ligation Kit; Novaseq Sequencing V1.5). Data was analysed with DESeq2 in collaboration with the GIGA-Bioinformatics platform.

In vivo experiments

All animal procedures were approved by the Animal Ethical Committee of the University of Liège, in accordance with the Belgian Ministry of Agriculture and the European Commission Laboratory Animal Care and Use Regulation. Six-week-old female C57BL/6NRj mice (JANVIER) were housed in sterilized, filter-topped cages under controlled temperature (22°C) and a 12h light/dark cycle. After one week of acclimatization, 1×10^5 GL261N4 or 005-GSCs cells in 2 µL PBS were injected into the right striatum (0.5 mm anterior and 2 mm lateral to bregma, depth 2.5 mm) under isoflurane anaesthesia (1–3%; Isoflutek®, Alivira Laboratoire Karizoo). On Day 7 and 14 post-engraftment, PBS (control) or oncolytic viruses (oHSV or oHSV/P2G; 106 PFU in 2µl PBS) were injected into the tumour using the same stereotactic coordinates. Mice were monitored daily for weight and behaviour, with weight recorded weekly or more frequently as needed. On day 21, mice were euthanized by intraperitoneal injection of Euthasol VET (140 mg/kg; Kela Veterinaria) unless enrolled in survival studies (for GL261N4: n=14, 15, 12 for PBS, oHSV, and oHSV/P2G, respectively; for 005-GSCs: n=10 per treatment), in which case cervical dislocation was performed upon onset of neurological symptoms.

ARRIVE 2.0[60] reporting guideline was used to assure the adequate management of animals. G*Power analysis (F-tests; ANOVA fixed effects, one-way; effect size f = 0.5, α = 0.05, power = 0.85) suggested 14 mice per group across three experimental groups. This number was reduced due to technical and cost constraints, particularly when using immunodeficient mice, consistent with similar studies in the field.

Haematoxylin staining and Immunofluorescence

Following euthanasia, mice were perfused intracardially with saline followed by 4% paraformaldehyde (PFA; Carl Roth) in PBS. Brains were incubated in 30% sucrose (Fisher Chemical; 48h, 4°C) and embedded in Neg-50™ (Epredia; -80°C). Serial coronal sections (14 µm) were collected on adhesion slides (SuperFrost Plus™, Epredia) using a CryoStar™ NX70 cryostat (Epredia). On a single SuperFrost® (Thermo Scientific) adhesive slide, two consecutive brain sections are separated by 420 µm (=14 µm x 30 sections) of tissue thickness, with the 29 intermediate sections distributed across 29 other slides.

Tumour area was assessed on haematoxylin-stained (HIGHDEF®, Enzo Life Sciences) brain sections by manual outlining using QuPath, based on samples from two independent experiments analysed together (Exp1 : n=5 per treatment, but one oHSV/P2G-treated mice was statistically identified as an outlier; Exp 2 : n=4 for oHSV, n=3 for PBS and oHSV/P2G). On each slide, whole tumour volume was calculated by summing the volumes between consecutive sections, using the truncated cone volume formula:

$$V=\text{height}\times\pi 3\times(R12+R22+R1\times R2)$$

where height is the distance between two consecutive slices (420µm), and R1 and R2 are their radii, determined by treating their areas (µm2) as circles using the formula: $R=SQRT(Area/\pi)$.

For immunofluorescence (n=5 per treatment), sections were treated for antigen retrieval (Tris–EDTA buffer, pH 9), permeabilization with 0.1% Triton X-100 (VWR) in PBS, and autofluorescence quenching with TrueBlack® Lipofuscin Quencher (Biotium). Slides were then blocked (10% FBS in PBS), incubated with primary antibodies overnight at 4°C, and with secondary antibodies for 1h at room temperature. Nuclei were counterstained with Hoechst (Sigma-Aldrich). Images were acquired using Zeiss Axio Scan 7 slide scanner and analysed using machine learning in QuPath for brain stroma and tumour segmentation, as well as StarDist and QuPath for lymphocyte identification ($CD8^+$, $CD4^+$, $FOXP3^+$).

Bulk RNA sequencing of tumour-bearing mice brain

Following euthanasia, 005-GSCs-engrafted mice were perfused intracardially with saline. Brains were divided into right and left hemispheres, placed in sterile 2 mL screwcap microtubes (Sarstedt), and stored at −80 °C. For RNA extraction, 100 mg solid glass beads (E&R Chemicals) and 1 mL TRIzol® reagent (Invitrogen) were added to tubes containing the right hemisphere, and samples were homogenized using the BeadBug™ Microtube Homogenizer (Sigma-Aldrich; 4000 rpm, 10s, three cycles). RNA was then extracted according to the TRIzol® reagent manufacturer's protocol.

Bulk RNA sequencing was performed as described hereabove (n=4 for PBS- and oHSV- and n=5 for oHSV/P2G-treated mice).

Immune cell isolation

Following euthanasia and intracardiac perfusion with saline, brains were collected in RPMI medium (VWR) on ice. Tissues were digested with collagenase D (2 mg/mL; Roche) and DNase I (10 ng/µL; Roche) at 37 °C for 30 min, then passed through 70 µm cell strainers (Fisherbrand™) and centrifuged. Pellets were resuspended in 90% Percoll (Cytiva) and subjected to density gradient centrifugation with layers of 90%, 60%, 40% Percoll, and PBS (500 × g, 15 min, acc 3, dec off). Myelin was removed, and cells were collected from the 40%-60% interface, washed with PBS, and centrifuged to remove residual Percoll.

Flow cytometry

For samples requiring intracellular staining, stimulation and accumulation were performed for 4h at 37°C after immune cell isolation in RPMI (10% FBS, 1% P/S) supplemented with 50 µM β-mercaptoethanol (Carl Roth), 2 µM brefeldin A (BioLegend), 2 µM monensin (BioLegend), 1 µg/mL CD3 (BioLegend), and 0.5 µg/mL CD28 (BioLegend). For all samples, Zombie NIR or Aqua (BioLegend; 1:1000, 100 µL, 20 min, RT) was added to isolated cells. Cells were washed with 1 mL FACS buffer (FB; 3% FBS in PBS) and transferred to 1.5 mL tubes. Fc receptors were blocked using CD16/32 antibody (BioLegend; 0.5 µg/mL, 15 min) prior to surface marker staining in FB (30 min, 4 °C) and fixation in PFA (20 min, RT). For intracellular staining only, cells were permeabilized with 0.1% saponin (Thermo Scientific; 20 min), washed, and incubated with intracellular antibodies in FB containing 0.1% saponin (30 min, 4 °C). Cells were washed again before acquisition on an ID7000™ Spectral Analyzer (Sony) and analysis using FlowJo v10.4 (BD).

Two independent experiments were conducted using different markers and fluorophore panels (one panel in the first experiment and two separate panels in the second, as shown in Table 1). For overlapping markers, data from a single representative experiment are presented. For the first experiment, n=9 for PBS and oHSV and n=10 for oHSV/P2G. For the second experiment, n = 1 for naïve control, n = 7 for tumour-bearing PBS- and oHSV-treated, and n = 6 for oHSV/P2G-treated mice.

A representative example of the gating strategy is presented in Appendix 1, after supplementary figures.

Single-cell RNA sequencing

Following immune cell isolation (n=4 per treatment, each sample corresponding to a pool of three mice), cells were processed using the Chromium Next GEM Single Cell Fixed RNA Sample Preparation Kit (10x Genomics; 16 reactions; PN-1000414) and sequenced on a Novaseq Sequencing V1.5 (Illumina) in collaboration with the GIGA-Genomics platform. Data processing and sample multiplexing were performed by the GIGA-Bioinformatics

platform. Downstream analysis was conducted using RStudio with the Seurat package. Cells were filtered using standard thresholds (300–7,500 genes; <2% mitochondrial content; genes expressed in ≥3 cells). Data were log-normalized (scale factor 10,000), and 2,000 highly variable genes were selected. PCA was performed, and significant components were determined using JackStraw and ElbowPlot analyses. Clustering was conducted using an SNN graph, and visualization was performed using UMAP. Cell-type annotation was performed based on cluster-specific differentially expressed marker genes identified by the FindAllMarkers function in Seurat. Pseudobulk analysis was performed using AggregateExpression function and visualised as z-score heatmaps for representative markers using AverageExpression (when needed) and pheatmap functions. Gene ontology analysis was performed using QIAGEN Ingenuity Pathway Analysis. The analysis was based on $\log_2$ fold changes in gene expression for oHSV and oHSV/P2G, each compared to PBS, calculated from raw counts using DESeq2.

In Appendices 2-4, after supplementary figures, the top 50 differentially expressed marker genes of each cluster are presented. They were identified with the command *FindAllMarkers(object, only.pos = TRUE, min.pct = 0.25, logfc.threshold = 0.25)*. This selects genes that are upregulated in each cluster, expressed in at least 25% of cells, and exhibiting a minimum log fold change of 0.25.

Statistical analysis

All statistical analyses were performed using GraphPad Prism 10. Data are presented as mean ± SD or as box plots, with whiskers indicating minimum and maximum values. For independent measures within a graph, one-way ANOVAs were conducted separately for each group. For interdependent percentages of the same parent, two-way ANOVAs were applied across all groups. In heatmaps, gene categories comprising multiple genes were analysed as single homogeneous groups using one-way ANOVAs. When comparing only two conditions, comparisons were performed using unpaired t-tests. Statistical significance was indicated as * for $p < 0.05$, ** for $p < 0.01$, *** for $p < 0.001$.

DATA AVAILABILITY STATEMENT

All original data shown in the figures and supplemental figures are available upon reasonable request.

ACKNOWLEDGMENTS

MD is a Research Fellow of the FNRS-Belgium. This work was supported by grants from the National Fund for Scientific Research (FNRS, Télévie); the Special Funds of the University of Liège; the Leon Fredericq Foundation, Liège,Belgium. The authors would like

712 to thank all the members of the GIGA Imaging, Flow Cytometry, and Genomics platforms,
713 and animal facilities for valuable technical support.

714 AUTHORS CONTRIBUTIONS

715 Design of the study and of the experiments: MD, ML and CSD. In vitro experiments: MD. In
716 vivo experiments: MD and SD with the help of CL and BB. Manuscript writing: MD and
717 CSD. Scientific discussions during the project: MD, BM, VN, ML and CSD. All authors
718 critically reviewed and edited the manuscript. Financing acquisition: CSD. ML and CSD
719 contributed equally as last authors. All authors approved the final manuscript.

720 DECLARATION OF INTERESTS STATEMENT

721 The authors declare no competing interests.

722 KEYWORDS

723 Glioblastoma, Virotherapy, Immunotherapy, oncolytic herpesvirus, CXCL12/CXCR4,
724 CXCR4 antagonist

725 REFERENCES

726 1. Louis, D.N., Perry, A., Wesseling, P., Brat, D.J., Cree, I.A., Figarella-Branger, D.,
727 Hawkins, C., Ng, H.K., Pfister, S.M., Reifenberger, G., et al. (2021). The 2021 WHO
728 Classification of Tumors of the Central Nervous System: a summary. Neuro-Oncol. *23*,
729 1231–1251. https://doi.org/10.1093/neuonc/noab106.

730 2. Stupp, R., Mason, W.P., Bent, M.J. van den, Weller, M., Fisher, B., Taphoorn, M.J.B.,
731 Belanger, K., Brandes, A.A., Marosi, C., Bogdahn, U., et al. (2005). Radiotherapy plus
732 Concomitant and Adjuvant Temozolomide for Glioblastoma. N. Engl. J. Med. *352*, 987–
733 996. https://doi.org/10.1056/NEJMoa043330.

734 3. Sim, H.-W., Morgan, E.R., and Mason, W.P. (2018). Contemporary management of
735 high-grade gliomas. CNS Oncol. *7*, 51–65. https://doi.org/10.2217/cns-2017-0026.

736 4. Goenka, A., Tiek, D., Song, X., Huang, T., Hu, B., and Cheng, S.-Y. (2021). The Many
737 Facets of Therapy Resistance and Tumor Recurrence in Glioblastoma. Cells *10*, 484.
738 https://doi.org/10.3390/cells10030484.

739 5. Prager, B.C., Bhargava, S., Mahadev, V., Hubert, C.G., and Rich, J.N. (2020).
740 Glioblastoma Stem Cells: Driving Resiliency through Chaos. Trends Cancer *6*, 223–235.
741 https://doi.org/10.1016/j.trecan.2020.01.009.

6. Lombard, A., Digregorio, M., Delcamp, C., Rogister, B., Piette, C., and Coppieters, N. (2021). The Subventricular Zone, a Hideout for Adult and Pediatric High-Grade Glioma Stem Cells. Front. Oncol. *10*, 614930. https://doi.org/10.3389/fonc.2020.614930.

7. Sharma, P., Aaroe, A., Liang, J., and Puduvalli, V.K. (2023). Tumor microenvironment in glioblastoma: Current and emerging concepts. Neuro-Oncol. Adv. *5*, vdad009. https://doi.org/10.1093/noajnl/vdad009.

8. Tripathy, D.K., Panda, L.P., Biswal, S., and Barhwal, K. (2024). Insights into the glioblastoma tumor microenvironment: current and emerging therapeutic approaches. Front. Pharmacol. *15*. https://doi.org/10.3389/fphar.2024.1355242.

9. Liu, Y., Zhou, F., Ali, H., Lathia, J.D., and Chen, P. (2024). Immunotherapy for glioblastoma: current state, challenges, and future perspectives. Cell. Mol. Immunol. *21*, 1354–1375. https://doi.org/10.1038/s41423-024-01226-x.

10. Goffart, N., Lombard, A., Lallemand, F., Kroonen, J., Nassen, J., Di Valentin, E., Berendsen, S., Dedobbeleer, M., Willems, E., Robe, P., et al. (2017). CXCL12 mediates glioblastoma resistance to radiotherapy in the subventricular zone. Neuro-Oncol. *19*, 66–77. https://doi.org/10.1093/neuonc/now136.

11. Cai, X., Chen, R., Ma, K., Wang, F., Zhou, Y., Wang, Y., and Jiang, T. (2020). Identification of the CXCL12–CXCR4/CXCR7 axis as a potential therapeutic target for immunomodulating macrophage polarization and foreign body response to implanted biomaterials. Appl. Mater. Today *18*, 100454. https://doi.org/10.1016/j.apmt.2019.100454.

12. Shi, Y., Riese, D.J., and Shen, J. (2020). The Role of the CXCL12/CXCR4/CXCR7 Chemokine Axis in Cancer. Front. Pharmacol. *11*. https://doi.org/10.3389/fphar.2020.574667.

13. Paolo, D., Maxime, D., Judit, S.G., Cédric, L., Alexandre, H., Benoit, B., Arnaud, L., Bernard, R., Virginie, N., Marielle, L., et al. (2025). An oncolytic herpesvirus expressing a CXCR4 antagonist interferes with glioblastoma cells' stemness features and migration. Mol. Ther. Oncol. *33*, 201083. https://doi.org/10.1016/j.omton.2025.201083.

14. Goffart, N., Kroonen, J., Di Valentin, E., Dedobbeleer, M., Denne, A., Martinive, P., and Rogister, B. (2015). Adult mouse subventricular zones stimulate glioblastoma stem cells specific invasion through CXCL12/CXCR4 signaling. Neuro-Oncol. *17*, 81–94. https://doi.org/10.1093/neuonc/nou144.

15. Kroonen, J., Nassen, J., Boulanger, Y.-G., Provenzano, F., Capraro, V., Bours, V., Martin, D., Deprez, M., Robe, P., and Rogister, B. (2011). Human glioblastoma-initiating cells invade specifically the subventricular zones and olfactory bulbs of mice after striatal injection. Int. J. Cancer *129*. https://doi.org/10.1002/ijc.25709.

16. Li, X., Kim, H.J., Yoo, J., Lee, Y., Nam, C.H., Park, J., Lee, S.-T., Kim, T.M., Choi, S.H., Won, J.-K., et al. (2025). Distant origin of glioblastoma recurrence: neural stem cells in the subventricular zone serve as a source of tumor reconstruction after primary resection. Mol. Cancer *24*, 64. https://doi.org/10.1186/s12943-025-02273-2.

17. Crump, M.P., Gong, J.H., Loetscher, P., Rajarathnam, K., Amara, A., Arenzana-Seisdedos, F., Virelizier, J.L., Baggiolini, M., Sykes, B.D., and Clark-Lewis, I. (1997). Solution structure and basis for functional activity of stromal cell-derived factor-1; dissociation of CXCR4 activation from binding and inhibition of HIV-1. EMBO J. *16*, 6996–7007. https://doi.org/10.1093/emboj/16.23.6996.

18. Mezzapelle, R., De Marchis, F., Passera, C., Leo, M., Brambilla, F., Colombo, F., Casalgrandi, M., Preti, A., Zambrano, S., Castellani, P., et al. (2021). CXCR4 engagement triggers CD47 internalization and antitumor immunization in a mouse model of mesothelioma. EMBO Mol. Med. *13*, e12344. https://doi.org/10.15252/emmm.202012344.

19. DiPersio, J.F., Micallef, I.N., Stiff, P.J., Bolwell, B.J., Maziarz, R.T., Jacobsen, E., Nademanee, A., McCarty, J., Bridger, G., and Calandra, G. (2009). Phase III Prospective Randomized Double-Blind Placebo-Controlled Trial of Plerixafor Plus Granulocyte Colony-Stimulating Factor Compared With Placebo Plus Granulocyte Colony-Stimulating Factor for Autologous Stem-Cell Mobilization and Transplantation for Patients With Non-Hodgkin's Lymphoma. J. Clin. Oncol. *27*, 4767–4773. https://doi.org/10.1200/JCO.2008.20.7209.

20. Medikonda, R., Dunn, G., Rahman, M., Fecci, P., and Lim, M. (2021). A review of glioblastoma immunotherapy. J. Neurooncol. *151*, 41–53. https://doi.org/10.1007/s11060-020-03448-1.

21. Lee, A.H., Sun, L., Mochizuki, A.Y., Reynoso, J.G., Orpilla, J., Chow, F., Kienzler, J.C., Everson, R.G., Nathanson, D.A., Bensinger, S.J., et al. (2021). Neoadjuvant PD-1 blockade induces T cell and cDC1 activation but fails to overcome the immunosuppressive tumor associated macrophages in recurrent glioblastoma. Nat. Commun. *12*, 6938. https://doi.org/10.1038/s41467-021-26940-2.

22. Long, G.V., Shklovskaya, E., Satgunaseelan, L., Mao, Y., da Silva, I.P., Perry, K.A., Diefenbach, R.J., Gide, T.N., Shivalingam, B., Buckland, M.E., et al. (2025). Neoadjuvant triplet immune checkpoint blockade in newly diagnosed glioblastoma. Nat. Med. *31*, 1557–1566. https://doi.org/10.1038/s41591-025-03512-1.

23. Laureano, R.S., Vanmeerbeek, I., Sprooten, J., Govaerts, J., Naulaerts, S., and Garg, A.D. (2024). The cell stress and immunity cycle in cancer: Toward next generation of cancer immunotherapy. Immunol. Rev. *321*, 71–93. https://doi.org/10.1111/imr.13287.

24. Sanchez Gil, J. (2022). Design and characterization of a CXCR4-retargeted and sTRAILarmed oncolytic HSV-1 to attack Glioblastoma stem-like cells (GSCs).

25. Todo, T., Ito, H., Ino, Y., Ohtsu, H., Ota, Y., Shibahara, J., and Tanaka, M. (2022). Intratumoral oncolytic herpes virus G47Δ for residual or recurrent glioblastoma: a phase 2 trial. Nat. Med. *28*, 1630–1639. https://doi.org/10.1038/s41591-022-01897-x.

26. Aldrak, N., Alsaab, S., Algethami, A., Bhere, D., Wakimoto, H., Shah, K., Alomary, M.N., and Zaidan, N. (2021). Oncolytic Herpes Simplex Virus-Based Therapies for Cancer. Cells *10*, 1541. https://doi.org/10.3390/cells10061541.

27. Shen, Y., and Nemunaitis, J. (2006). Herpes simplex virus 1 (HSV-1) for cancer treatment. Cancer Gene Ther. *13*, 975–992. https://doi.org/10.1038/sj.cgt.7700946.

28. Chiocca, E.A., Nakashima, H., Kasai, K., Fernandez, S.A., and Oglesbee, M. (2020). Preclinical Toxicology of rQNestin34.5v.2: An Oncolytic Herpes Virus with Transcriptional Regulation of the ICP34.5 Neurovirulence Gene. Mol. Ther. Methods Clin. Dev. *17*, 871–893. https://doi.org/10.1016/j.omtm.2020.03.028.

29. Ghonime, M.G., Saini, U., Kelly, M.C., Roth, J.C., Wang, P.-Y., Chen, C.-Y., Miller, K., Hernandez-Aguirre, I., Kim, Y., Mo, X., et al. (2021). Eliciting an immune-mediated antitumor response through oncolytic herpes simplex virus-based shared antigen expression in tumors resistant to viroimmunotherapy. J. Immunother. Cancer *9*. https://doi.org/10.1136/jitc-2021-002939.

30. Sanchez Gil, J., Dubois, M., Neirinckx, V., Lombard, A., Coppieters, N., D'Arrigo, P., Isci, D., Aldenhoff, T., Brouwers, B., Lassence, C., et al. (2022). Nanobody-based retargeting of an oncolytic herpesvirus for eliminating CXCR4+ GBM cells: A proof of principle. Mol. Ther. Oncolytics *26*, 35–48. https://doi.org/10.1016/j.omto.2022.06.002.

31. Ding, J., Murad, Y.M., Sun, Y., Lee, I.-F., Samudio, I., Liu, X., Jia, W.W.-G., and Zhao, R. (2022). Pre-Existing HSV-1 Immunity Enhances Anticancer Efficacy of a Novel Immune-Stimulating Oncolytic Virus. Viruses *14*, 2327. https://doi.org/10.3390/v14112327.

32. Liu, T.-C., Zhang, T., Fukuhara, H., Kuroda, T., Todo, T., Martuza, R.L., Rabkin, S.D., and Kurtz, A. (2006). Oncolytic HSV Armed with Platelet Factor 4, an Antiangiogenic Agent, Shows Enhanced Efficacy. Mol. Ther. *14*, 789–797. https://doi.org/10.1016/j.ymthe.2006.07.011.

33. Noh, M.H., Kang, J.M., Miller, A.A., Nguyen, G., Huang, M., Shim, J.S., Bueso-Perez, A.J., Murphy, S.A., Rivera-Caraballo, K.A., Otani, Y., et al. (2024). Targeting IGF2 to reprogram the tumor microenvironment for enhanced viro-immunotherapy. Neuro-Oncol. *26*, 1602–1616. https://doi.org/10.1093/neuonc/noae105.

34. Sette, P., Amankulor, N., Li, A., Marzulli, M., Leronni, D., Zhang, M., Goins, W.F., Kaur, B., Bolyard, C., Cripe, T.P., et al. (2019). GBM-Targeted oHSV Armed with Matrix

Metalloproteinase 9 Enhances Anti-tumor Activity and Animal Survival. Mol. Ther. Oncolytics *15*, 214–222. https://doi.org/10.1016/j.omto.2019.10.005.

35. Zhang, W., Fulci, G., Wakimoto, H., Cheema, T.A., Buhrman, J.S., Jeyaretna, D.S., Stemmer Rachamimov, A.O., Rabkin, S.D., and Martuza, R.L. (2013). Combination of Oncolytic Herpes Simplex Viruses Armed with Angiostatin and IL-12 Enhances Antitumor Efficacy in Human Glioblastoma Models. Neoplasia N. Y. N *15*, 591–599. https://doi.org/10.1593/neo.13158.

36. Wouters, R., Bevers, S., Riva, M., De Smet, F., and Coosemans, A. (2020). Immunocompetent Mouse Models in the Search for Effective Immunotherapy in Glioblastoma. Cancers *13*, 19. https://doi.org/10.3390/cancers13010019.

37. Marumoto, T., Tashiro, A., Friedmann-Morvinski, D., Scadeng, M., Soda, Y., Gage, F.H., and Verma, I.M. (2009). Development of a novel mouse glioma model using lentiviral vectors. Nat. Med. *15*, 110–116. https://doi.org/10.1038/nm.1863.

38. Khalsa, J.K., Cheng, N., Keegan, J., Chaudry, A., Driver, J., Bi, W.L., Lederer, J., and Shah, K. (2020). Immune phenotyping of diverse syngeneic murine brain tumors identifies immunologically distinct types. Nat. Commun. *11*, 3912. https://doi.org/10.1038/s41467-020-17704-5.

39. Kardani, K., Ghouse, S.M., Din Abdul Jabbar, M.A., Rajasubramanian, N., Sanchez Gil, J., Stemmer-Rachamimov, A., Soda, Y., Martuza, R.L., Hara, T., Wakimoto, H., et al. (2025). Immunocompetent murine glioblastoma stem-like cell models exhibiting distinct phenotypes. Neuro-Oncol. Adv. *7*, vdae215. https://doi.org/10.1093/noajnl/vdae215.

40. López-Gil, J.C., Martin-Hijano, L., Hermann, P.C., and Sainz, B. (2021). The CXCL12 Crossroads in Cancer Stem Cells and Their Niche. Cancers *13*, 469. https://doi.org/10.3390/cancers13030469.

41. Wu, B., Zhang, B., Li, B., Wu, H., and Jiang, M. (2024). Cold and hot tumors: from molecular mechanisms to targeted therapy. Signal Transduct. Target. Ther. *9*, 274. https://doi.org/10.1038/s41392-024-01979-x.

42. Galon, J., and Bruni, D. (2019). Approaches to treat immune hot, altered and cold tumours with combination immunotherapies. Nat. Rev. Drug Discov. *18*, 197–218. https://doi.org/10.1038/s41573-018-0007-y.

43. Mezzapelle, R., Leo, M., Caprioglio, F., Colley, L.S., Lamarca, A., Sabatino, L., Colantuoni, V., Crippa, M.P., and Bianchi, M.E. (2022). CXCR4/CXCL12 Activities in the Tumor Microenvironment and Implications for Tumor Immunotherapy. Cancers *14*, 2314. https://doi.org/10.3390/cancers14092314.

44. Cao, T., Gu, Y., Yagmurlu, B., Yerraballa, H., Bertrand, S., Naya, L., Miller, K., Iv, M., Soltys, S., Patel, C., et al. (2024). A phase II study of plerixafor combined with whole brain

886 radiation therapy (WBRT) for patients with newly diagnosed glioblastoma. J. Clin. Oncol.
887 *42*, 2075–2075. https://doi.org/10.1200/JCO.2024.42.16_suppl.2075.

888 45. Wen, P.Y. (2017). Phase I Study of Plerixafor (AMD3100) and Bevacizumab for
889 Recurrent High-Grade Glioma (clinicaltrials.gov).

890 46. Mercurio, L., Ajmone-Cat, M.A., Cecchetti, S., Ricci, A., Bozzuto, G., Molinari, A.,
891 Manni, I., Pollo, B., Scala, S., Carpinelli, G., et al. (2016). Targeting CXCR4 by a selective
892 peptide antagonist modulates tumor microenvironment and microglia reactivity in a
893 human glioblastoma model. J. Exp. Clin. Cancer Res. CR *35*, 55.
894 https://doi.org/10.1186/s13046-016-0326-y.

895 47. Wu, A., Maxwell, R., Xia, Y., Cardarelli, P., Oyasu, M., Belcaid, Z., Kim, E., Hung, A.,
896 Luksik, A.S., Garzon-Muvdi, T., et al. (2019). Combination anti-CXCR4 and anti-PD-1
897 immunotherapy provides survival benefit in glioblastoma through immune cell
898 modulation of tumor microenvironment. J. Neurooncol. *143*, 241–249.
899 https://doi.org/10.1007/s11060-019-03172-5.

900 48. Wei, R., Li, J., Lin, W., Pang, X., Yang, H., Lai, S., Wei, X., Jiang, X., Yuan, Y., and Yang,
901 R. (2024). Nanoparticle-mediated blockade of CXCL12/CXCR4 signaling enhances
902 glioblastoma immunotherapy: Monitoring early responses with MRI radiomics. Acta
903 Biomater. *177*, 414–430. https://doi.org/10.1016/j.actbio.2024.02.007.

904 49. Liguori, G.L. (2025). Glioblastoma Models for Preclinical Assays: A Strengths,
905 Weaknesses and Purpose Overview. Preprint at Preprints,
906 https://doi.org/10.20944/preprints202508.1705.v1
907 https://doi.org/10.20944/preprints202508.1705.v1.

908 50. Yadav, N., and Purow, B.W. (2024). Understanding Current Experimental Models of
909 Glioblastoma-Brain Microenvironment Interactions. J. Neurooncol. *166*, 213–229.
910 https://doi.org/10.1007/s11060-023-04536-8.

911 51. Jin, F., Jin-Lee, H.J., and Johnson, A.J. (2021). Mouse Models of Experimental
912 Glioblastoma. In Gliomas, W. Debinski, ed. (Exon Publications).

913 52. Boccellato, C., and Rehm, M. (2022). Glioblastoma, from disease understanding
914 towards optimal cell-based in vitro models. Cell. Oncol. Dordr. *45*, 527–541.
915 https://doi.org/10.1007/s13402-022-00684-7.

916 53. Bhatt, D.K., Janzen, T., Daemen, T., and Weissing, F.J. (2022). Modelling the spatial
917 dynamics of oncolytic virotherapy in the presence of virus-resistant tumour cells. PLOS
918 Comput. Biol. *18*, e1010076. https://doi.org/10.1371/journal.pcbi.1010076.

919 54. Alvarez-Breckenridge, C.A., Yu, J., Price, R., Wojton, J., Pradarelli, J., Mao, H., Wei,
920 M., Wang, Y., He, S., Hardcastle, J., et al. (2012). NK cells impede glioblastoma virotherapy

via NKp30 and NKp46 natural cytotoxicity receptors. Nat. Med. *18*, 1827–1834. https://doi.org/10.1038/nm.3013.

55. Szatmári, T., Lumniczky, K., Désaknai, S., Trajcevski, S., Hídvégi, E.J., Hamada, H., and Sáfrány, G. (2006). Detailed characterization of the mouse glioma 261 tumor model for experimental glioblastoma therapy. Cancer Sci. *97*, 546–553. https://doi.org/10.1111/j.1349-7006.2006.00208.x.

56. Todo, T., Martuza, R.L., Rabkin, S.D., and Johnson, P.A. (2001). Oncolytic herpes simplex virus vector with enhanced MHC class I presentation and tumor cell killing. Proc. Natl. Acad. Sci. U. S. A. *98*, 6396–6401. https://doi.org/10.1073/pnas.101136398.

57. Tischer, B.K., Kaufer, B.B., Sommer, M., Wussow, F., Arvin, A.M., and Osterrieder, N. (2007). A Self-Excisable Infectious Bacterial Artificial Chromosome Clone of Varicella-Zoster Virus Allows Analysis of the Essential Tegument Protein Encoded by ORF9. J. Virol. *81*, 13200–13208. https://doi.org/10.1128/jvi.01148-07.

58. Goins, W.F., Huang, S., Hall, B., Marzulli, M., Cohen, J.B., and Glorioso, J.C. (2020). Engineering HSV-1 Vectors for Gene Therapy. In Herpes Simplex Virus : Methods and Protocols, R. J. Diefenbach and C. Fraefel, eds. (Springer), pp. 73–90. https://doi.org/10.1007/978-1-4939-9814-2_4.

59. Marconi, P., and Manservigi, R. (2014). Herpes Simplex Virus Growth, Preparation, and Assay. In Herpes Simplex Virus: Methods and Protocols, R. J. Diefenbach and C. Fraefel, eds. (Springer), pp. 19–29. https://doi.org/10.1007/978-1-4939-0428-0_2.

60. Sert, N.P. du, Hurst, V., Ahluwalia, A., Alam, S., Avey, M.T., Baker, M., Browne, W.J., Clark, A., Cuthill, I.C., Dirnagl, U., et al. (2020). The ARRIVE guidelines 2.0: Updated guidelines for reporting animal research. PLOS Biol. *18*, e3000410. https://doi.org/10.1371/journal.pbio.3000410.

SUPPLEMENTARY FIGURE LEGENDS

Figure S1: oHSV/P2G promotes immune cell infiltration and alters their distribution

(A) Numbers of $CD45^{high}$ infiltrating leucocytes and $CD45^{medium}$ resident microglia isolated 21 days post-engraftment (d.p.e.) from PBS- (n=7), oHSV- (n=7) or oHSV/P2G- (n=6) treated GL261N4 tumour-bearing mice brains and analysed by flow cytometry. The brain from a non-engrafted mice was analysed as a control.

(B) Number of leucocytes recovered from three pooled PBS-, oHSV- or oHSV/P2G-treated mice (n=4 in each group) 21 d.p.e. of $1x10^5$ GL261N4, and analysed by single-cell RNA sequencing (ScRNAseq). Leucocytes are divided into several populations identified

based on cluster-specific differentially expressed marker genes, represented as a UMAP in Figure 2.

C, D: Number of T cells **(C)** and B cells **(D)** analysed by flow cytometry.

(E) UMAPs representation of the clustering of leucocytes, grouped by treatment, highlighting myeloid and lymphoid populations identified based on subcluster-specific differentially expressed marker genes.

(F) Numbers of grouped lymphoid or myeloid populations.

Each dot represents cells isolated from one mouse **(A, C, D)** or pooled from 3 mice **(B, F)**. Boxes indicate the distribution of values, with whiskers denoting the minimum and maximum. Statistical significance was evaluated by ordinary one-way ANOVA with Tukey's multiple comparison test. *p<0.05, **p< 0.01, ***p<0.001.

Figure S2: oHSV/P2G modulates lymphoid subpopulations

A, B: Pseudobulk analysis of B cells **(A)** and T cells **(B)** grouped into subpopulations, showing representative marker genes visualised as heatmaps of z-score from mean normalised expression values. Genes are grouped into several functional gene sets.

C, D: Percentage of $CD4^+$ and $CD8^+$ T cells **(C)** or of $CD25^{high}IL7R^{low}$ (regulatory) $CD4^+$ T cells **(D)** isolated 21 d.p.e. from PBS- (n=9), oHSV- (n=9) or oHSV/P2G- (n=10) treated GL261N4 tumour-bearing mice brains and analysed by flow cytometry.

E-G: Percentage of $CD4^+$ **(E)**, $CD8^+$ **(F)**, or $FOXP3^+$ **(G)** T cells among total cells within the right hemisphere stroma (RH-T) or tumour.

Each dot represents cells from one mouse**.** Boxes indicate the distribution of values, with whiskers denoting the minimum and maximum. Statistical significance was evaluated by ordinary one-way ANOVA with Tukey's multiple comparison test. ****p<0.0001.

Figure S3: oHSV/P2G modulates myeloid subpopulations

A, B: Pseudobulk analysis of microglia **(A)** and macrophages **(B)** grouped into subpopulations, showing representative marker genes visualised as heatmaps of z-score from mean normalised expression values. Genes are grouped into several functional gene sets.

Figure S4: oHSV/P2G activates *Cd4*$^+$ and *Cd8*$^+$ T cells

A, B: Pseudobulk analysis of *Cd4*$^+$ **(A)** and *Cd8*$^+$ **(B)** T cells grouped into subpopulations (exhausted and non-exhausted T cells, T-/NE-T cells respectively), showing representative marker genes visualised as heatmaps of z-score from mean normalised expression values. Genes are grouped into several functional gene sets.

C, D: Number of both *Cd4*$^+$ **(C)** or *Cd8*$^+$ **(D)** T cells subpopulations.

(E) Median fluorescence intensity (MFI) of representative markers expression by $CD4^+$ and $CD8^+$ T cells following flow cytometry analysis (PBS: n=9, oHSV: n=9, oHSV/P2G: n=10).

Each dot represents cells from one mouse **(E)** or pooled from 3 mice **(C, D)**. Boxes indicate the distribution of values, with whiskers denoting the minimum and maximum. Statistical significance was evaluated by ordinary one-way ANOVA with Tukey's multiple comparison test. *p<0.05, **p< 0.01, ***p<0.001, ****p<0.0001.

Figure S5: oHSV/P2G polarizes TAMs toward a pro-inflammatory phenotype

(A) Bulk RNA sequencing analysis of human monocyte-derived-macrophages (hMDMs), recovered from fresh healthy donor's blood, treated for 48h with conditioned media from GB138 human glioblastoma cells cultured for 72h, either uninfected (mNI) or infected with oHSV (moHSV) or oHSV/P2G (moSHV/P2G) (n=3 in each group). Representative marker genes were visualised as heatmaps of z-score from mean normalised expression values. Genes are grouped into several functional gene sets.

Figure S1

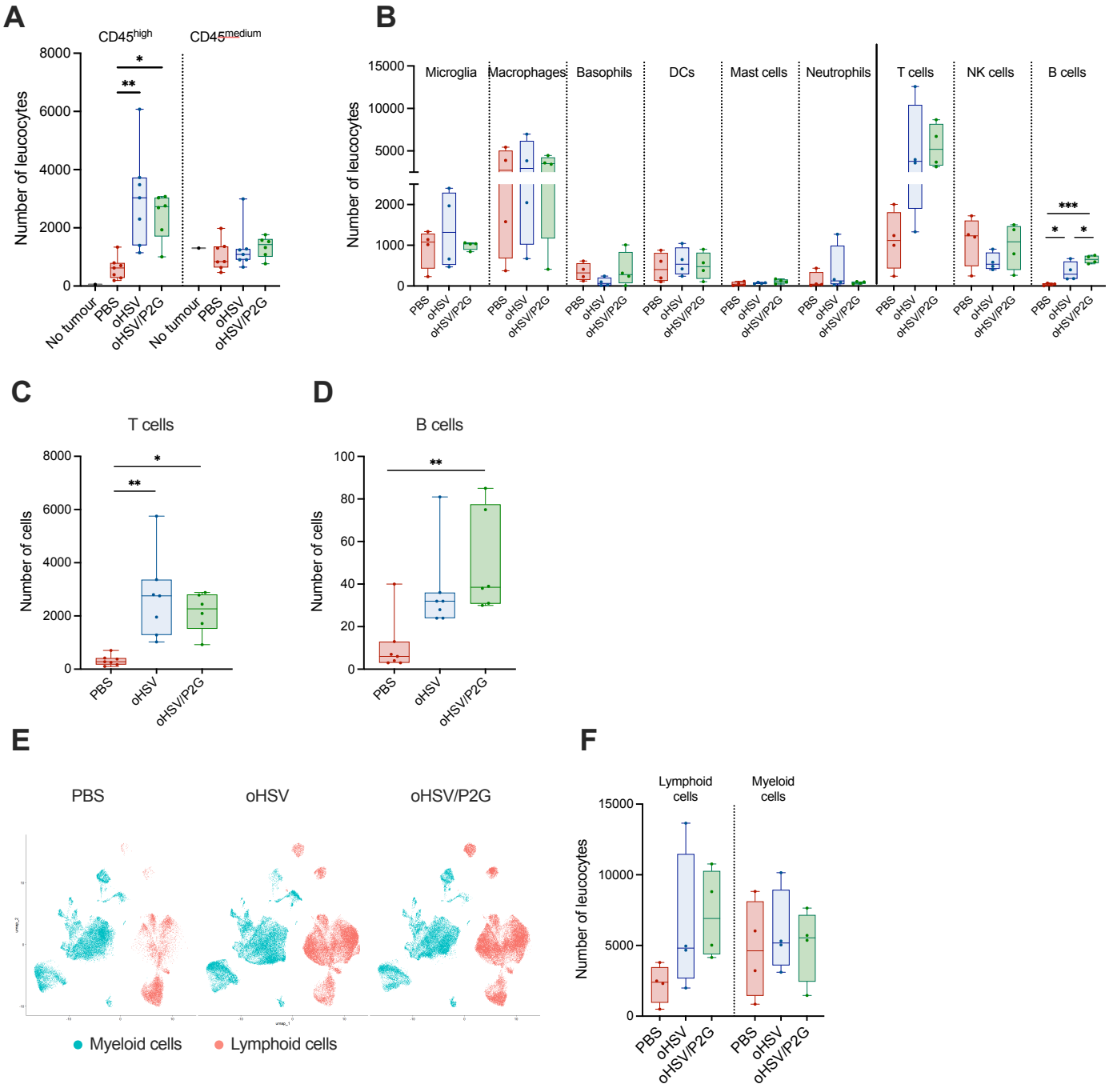
A
CD45high
CD45medium
Number of leucocytes
No tumour
PBS
oHSV
oHSV/P2G
B
Microglia
Macrophages
Basophils
DCs
Mast cells
Neutrophils
T cells
NK cells
B cells
C
T cells
Number of cells
D
B cells
E
PBS
oHSV
oHSV/P2G
Myeloid cells
Lymphoid cells
F
Lymphoid cells
Myeloid cells

Figure S2

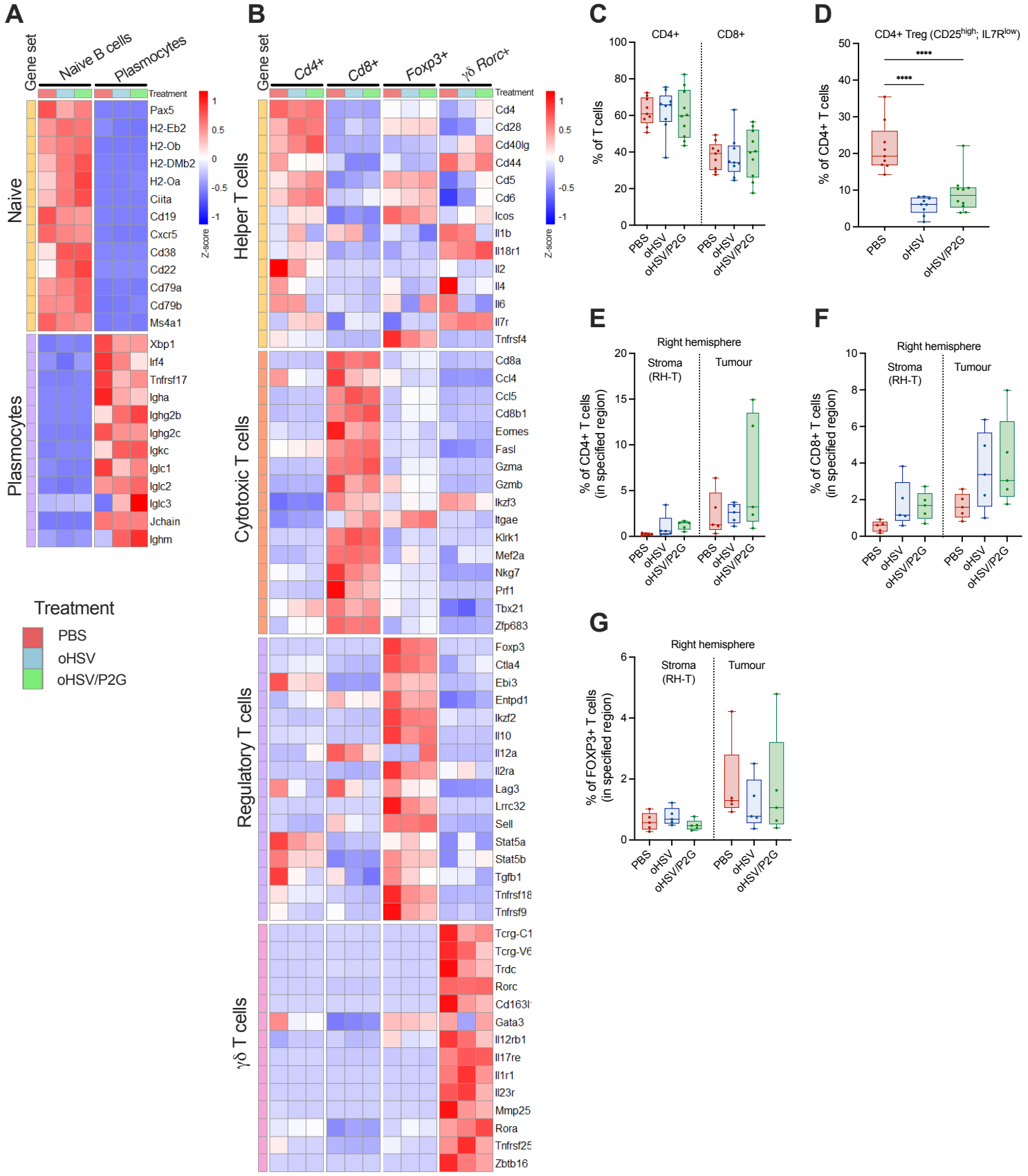
A
Gene set
Naive B cells
Plasmocytes
Treatment
Naive
Plasmocytes
Pax5
H2-Eb2
H2-Ob
H2-DMb2
H2-Oa
Ciita
Cd19
Cxcr5
Cd38
Cd22
Cd79a
Cd79b
Ms4a1
Xbp1
Irf4
Tnfrsf17
Igha
Ighg2b
Ighg2c
Igkc
Iglc1
Iglc2
Iglc3
Jchain
Ighm
Z-score
1
0.5
0
-0.5
-1
Treatment
PBS
oHSV
oHSV/P2G
B
Gene set
Cd4+
Cd8+
Foxp3+
γδ Rorc+
Treatment
Helper T cells
Cytotoxic T cells
Regulatory T cells
γδ T cells
Cd4
Cd28
Cd40lg
Cd44
Cd5
Cd6
Icos
Il1b
Il18r1
Il2
Il4
Il6
Il7r
Tnfrsf4
Cd8a
Ccl4
Ccl5
Cd8b1
Eomes
Fasl
Gzma
Gzmb
Ikzf3
Itgae
Klrk1
Mef2a
Nkg7
Prf1
Tbx21
Zfp683
Foxp3
Ctla4
Ebi3
Entpd1
Ikzf2
Il10
Il12a
Il2ra
Lag3
Lrrc32
Sell
Stat5a
Stat5b
Tgfb1
Tnfrsf18
Tnfrsf9
Tcrg-C1
Tcrg-V6
Trdc
Rorc
Cd163l
Gata3
Il12rb1
Il17re
Il1r1
Il23r
Mmp25
Rora
Tnfrsf25
Zbtb16
Z-score
1
0.5
0
-0.5
-1
C
CD4+
CD8+
% of T cells
PBS
oHSV
oHSV/P2G
D
CD4+ Treg (CD25high; IL7Rlow)
% of CD4+ T cells
****
****
PBS
oHSV
oHSV/P2G
E
Right hemisphere
Stroma (RH-T)
Tumour
% of CD4+ T cells (in specified region)
PBS
oHSV
oHSV/P2G
F
Right hemisphere
Stroma (RH-T)
Tumour
% of CD8+ T cells (in specified region)
PBS
oHSV
oHSV/P2G
G
Right hemisphere
Stroma (RH-T)
Tumour
% of FOXP3+ T cells (in specified region)
PBS
oHSV
oHSV/P2G

Figure S3

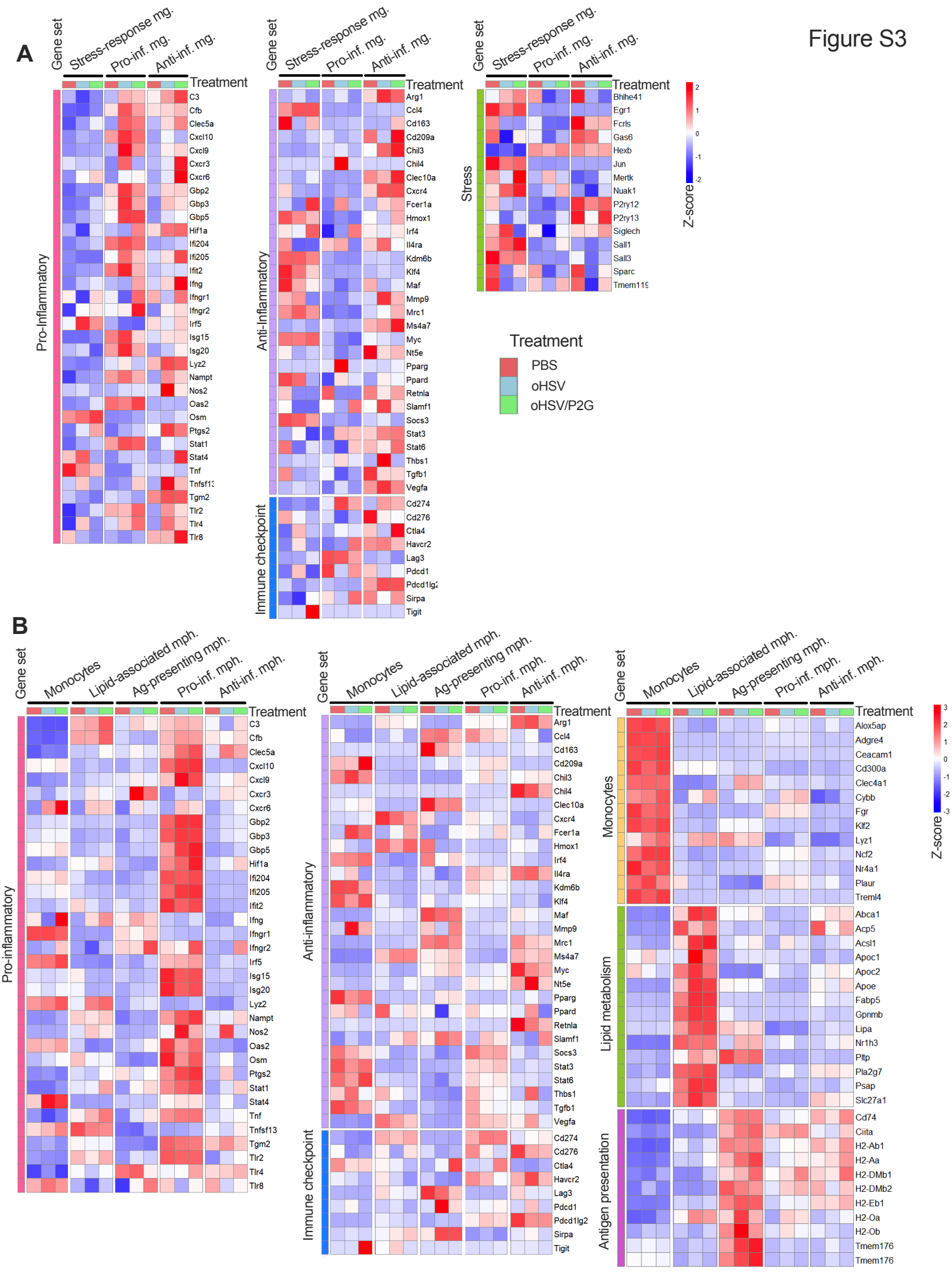
A
Gene set
Stress-response mg.
Pro-inf. mg.
Anti-inf. mg.
Treatment
Pro-Inflammatory
C3
Cfb
Clec5a
Cxcl10
Cxcl9
Cxcr3
Cxcr6
Gbp2
Gbp3
Gbp5
Hif1a
Ifi204
Ifi205
Ifit2
Ifng
Ifngr1
Ifngr2
Irf5
Isg15
Isg20
Lyz2
Nampt
Nos2
Oas2
Osm
Ptgs2
Stat1
Stat4
Tnf
Tgm2
Tlr2
Tlr4
Tlr8
Anti-Inflammatory
Arg1
Ccl4
Cd163
Cd209a
Chil3
Chil4
Clec10a
Cxcr4
Fcer1a
Hmox1
Irf4
Il4ra
Kdm6b
Klf4
Maf
Mmp9
Mrc1
Ms4a7
Myc
Nt5e
Pparg
Ppard
Retnla
Slamf1
Socs3
Stat3
Stat6
Thbs1
Tgfb1
Vegfa
Immune checkpoint
Cd274
Cd276
Ctla4
Havcr2
Lag3
Pdcd1
Pdcd1lg2
Sirpa
Tigit
Stress
Bhlhe41
Egr1
Fcrls
Gas6
Hexb
Jun
Mertk
Nuak1
P2ry12
P2ry13
Siglech
Sall1
Sall3
Sparc
Tmem119
Z-score
2
1
0
-1
-2
Treatment
PBS
oHSV
oHSV/P2G
B
Gene set
Monocytes
Lipid-associated mph.
Ag-presenting mph.
Pro-inf. mph.
Anti-inf. mph.
Treatment
Pro-inflammatory
C3
Cfb
Clec5a
Cxcl10
Cxcl9
Cxcr3
Cxcr6
Gbp2
Gbp3
Gbp5
Hif1a
Ifi204
Ifi205
Ifit2
Ifng
Ifngr1
Ifngr2
Irf5
Isg15
Isg20
Lyz2
Nampt
Nos2
Oas2
Osm
Ptgs2
Stat1
Stat4
Tnf
Tnfsf13
Tgm2
Tlr2
Tlr4
Tlr8
Anti-inflammatory
Arg1
Ccl4
Cd163
Cd209a
Chil3
Chil4
Clec10a
Cxcr4
Fcer1a
Hmox1
Irf4
Il4ra
Kdm6b
Klf4
Maf
Mmp9
Mrc1
Ms4a7
Myc
Nt5e
Pparg
Ppard
Retnla
Slamf1
Socs3
Stat3
Stat6
Thbs1
Tgfb1
Vegfa
Immune checkpoint
Cd274
Cd276
Ctla4
Havcr2
Lag3
Pdcd1
Pdcd1lg2
Sirpa
Tigit
Monocytes
Alox5ap
Adgre4
Ceacam1
Cd300a
Clec4a1
Cybb
Fgr
Klf2
Lyz1
Ncf2
Nr4a1
Plaur
Treml4
Lipid metabolism
Abca1
Acp5
Acsl1
Apoc1
Apoc2
Apoe
Fabp5
Gpnmb
Lipa
Nr1h3
Pltp
Pla2g7
Psap
Slc27a1
Antigen presentation
Cd74
Ciita
H2-Ab1
H2-Aa
H2-DMb1
H2-DMb2
H2-Eb1
H2-Oa
H2-Ob
Tmem176
Tmem176
Z-score
3
2
1
0
-1
-2
-3

Figure S4

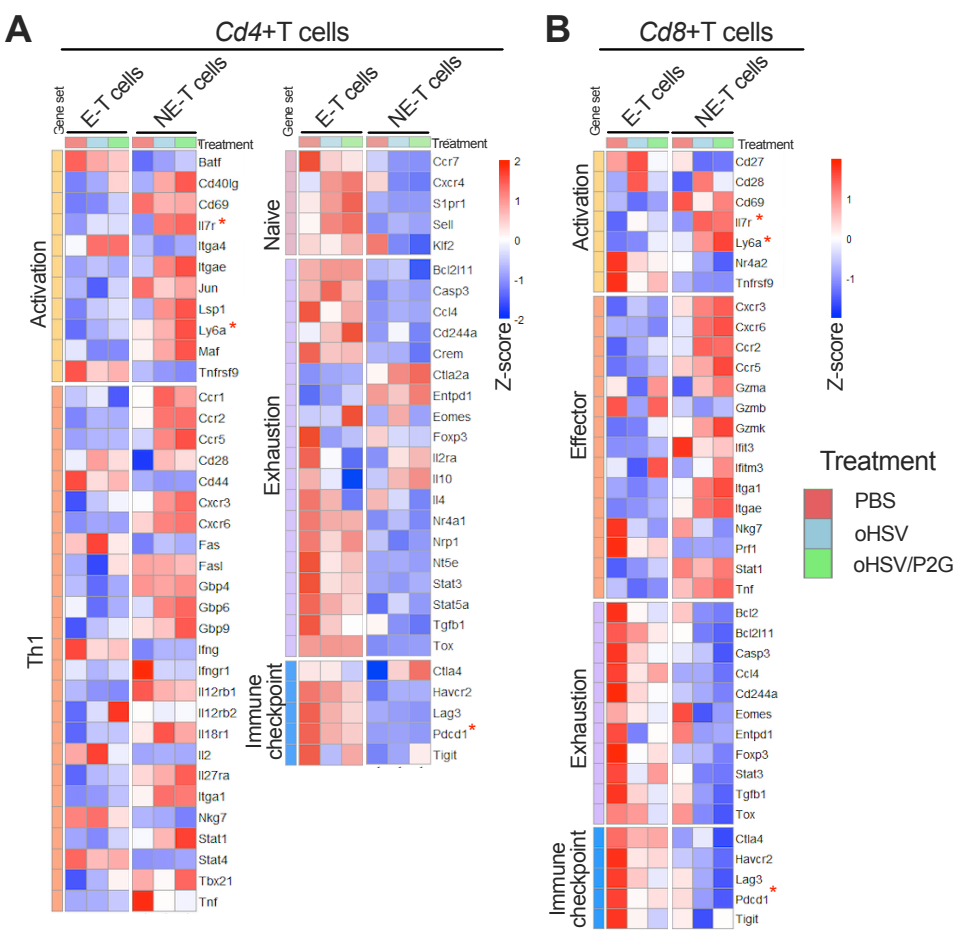
A
Cd4+T cells
E-T cells
NE-T cells
Gene set
Treatment
Activation
Batf
Cd40lg
Cd69
Il7r *
Itga4
Itgae
Jun
Lsp1
Ly6a *
Maf
Tnfrsf9
Th1
Ccr1
Ccr2
Ccr5
Cd28
Cd44
Cxcr3
Cxcr6
Fas
Fasl
Gbp4
Gbp6
Gbp9
Ifng
Ifngr1
Il12rb1
Il12rb2
Il18r1
Il2
Il27ra
Itga1
Nkg7
Stat1
Stat4
Tbx21
Tnf
Naive
Ccr7
Cxcr4
S1pr1
Sell
Klf2
Exhaustion
Bcl2l11
Casp3
Ccl4
Cd244a
Crem
Ctla2a
Entpd1
Eomes
Foxp3
Il2ra
Il10
Il4
Nr4a1
Nrp1
Nt5e
Stat3
Stat5a
Tgfb1
Tox
Immune checkpoint
Ctla4
Havcr2
Lag3
Pdcd1 *
Tigit
Z-score
2
1
0
-1
-2
B
Cd8+T cells
E-T cells
NE-T cells
Gene set
Treatment
Activation
Cd27
Cd28
Cd69
Il7r *
Ly6a *
Nr4a2
Tnfrsf9
Effector
Cxcr3
Cxcr6
Ccr2
Ccr5
Gzma
Gzmb
Gzmk
Ifit3
Ifitm3
Itga1
Itgae
Nkg7
Prf1
Stat1
Tnf
Exhaustion
Bcl2
Bcl2l11
Casp3
Ccl4
Cd244a
Eomes
Entpd1
Foxp3
Stat3
Tgfb1
Tox
Immune checkpoint
Ctla4
Havcr2
Lag3
Pdcd1 *
Tigit
Z-score
1
0
-1
Treatment
PBS
oHSV
oHSV/P2G

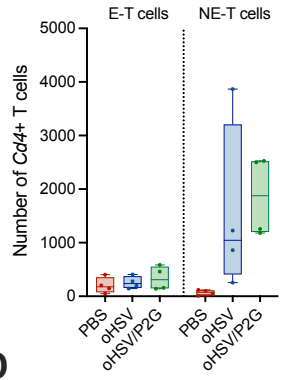
C
E-T cells
NE-T cells
Number of Cd4+ T cells
5000
4000
3000
2000
1000
0
PBS
oHSV
oHSV/P2G

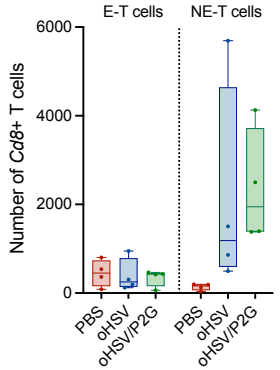
D
E-T cells
NE-T cells
Number of Cd8+ T cells
6000
4000
2000
0
PBS
oHSV
oHSV/P2G

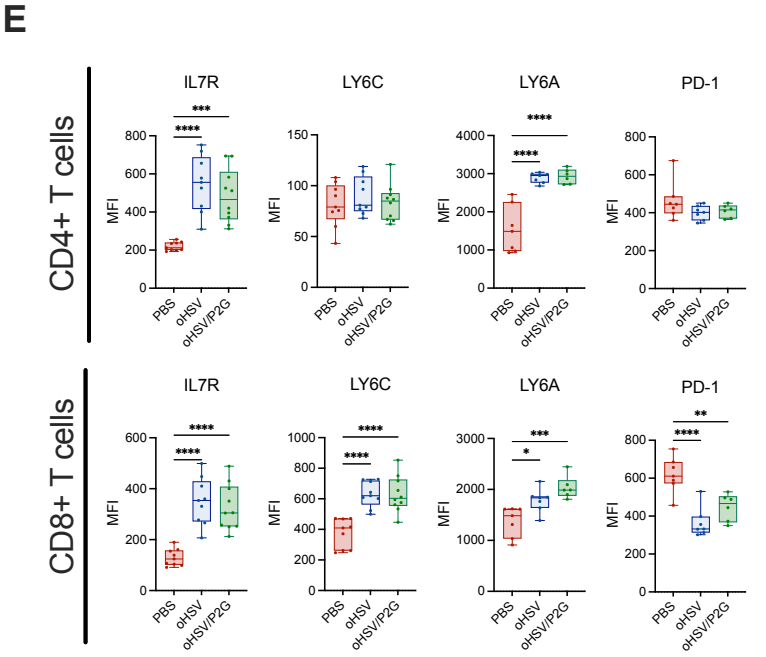
E
CD4+ T cells
CD8+ T cells
IL7R
LY6C
LY6A
PD-1
MFI
PBS
oHSV
oHSV/P2G

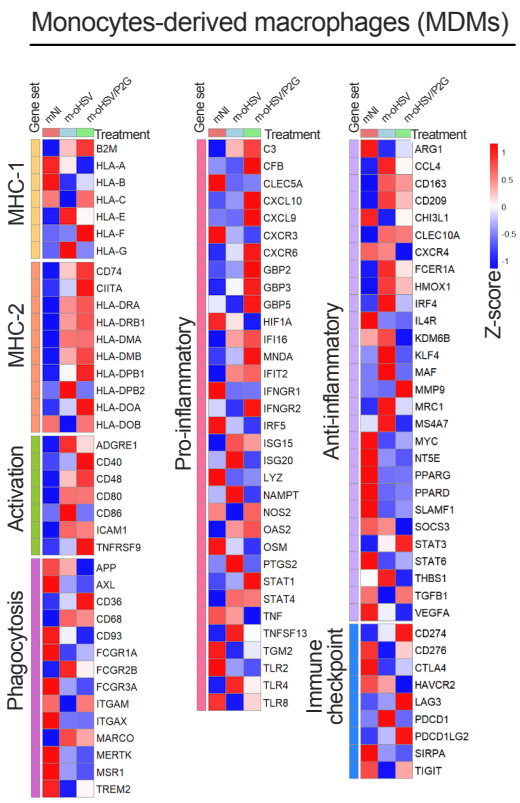
Monocytes-derived macrophages (MDMs)
Gene set
mNI
m-oHSV
m-oHSV/P2G
Treatment
MHC-1
B2M
HLA-A
HLA-B
HLA-C
HLA-E
HLA-F
HLA-G
MHC-2
CD74
CIITA
HLA-DRA
HLA-DRB1
HLA-DMA
HLA-DMB
HLA-DPB1
HLA-DPB2
HLA-DOA
HLA-DOB
Activation
ADGRE1
CD40
CD48
CD80
CD86
ICAM1
TNFRSF9
Phagocytosis
APP
AXL
CD36
CD68
CD93
FCGR1A
FCGR2B
FCGR3A
ITGAM
ITGAX
MARCO
MERTK
MSR1
TREM2
Pro-inflammatory
C3
CFB
CLEC5A
CXCL10
CXCL9
CXCR3
CXCR6
GBP2
GBP3
GBP5
HIF1A
IFI16
MNDA
IFIT2
IFNGR1
IFNGR2
IRF5
ISG15
ISG20
LYZ
NAMPT
NOS2
OAS2
OSM
PTGS2
STAT1
STAT4
TNF
TNFSF13
TGM2
TLR2
TLR4
TLR8
Anti-inflammatory
ARG1
CCL4
CD163
CD209
CHI3L1
CLEC10A
CXCR4
FCER1A
HMOX1
IRF4
IL4R
KDM6B
KLF4
MAF
MMP9
MRC1
MS4A7
MYC
NT5E
PPARG
PPARD
SLAMF1
SOCS3
STAT3
STAT6
THBS1
TGFB1
VEGFA
Immune checkpoint
CD274
CD276
CTLA4
HAVCR2
LAG3
PDCD1
PDCD1LG2
SIRPA
TIGIT
Z-score
1
0.5
0
-0.5
-1

APPENDIX

Appendix 1

Gating strategy of flow cytometry analysis.

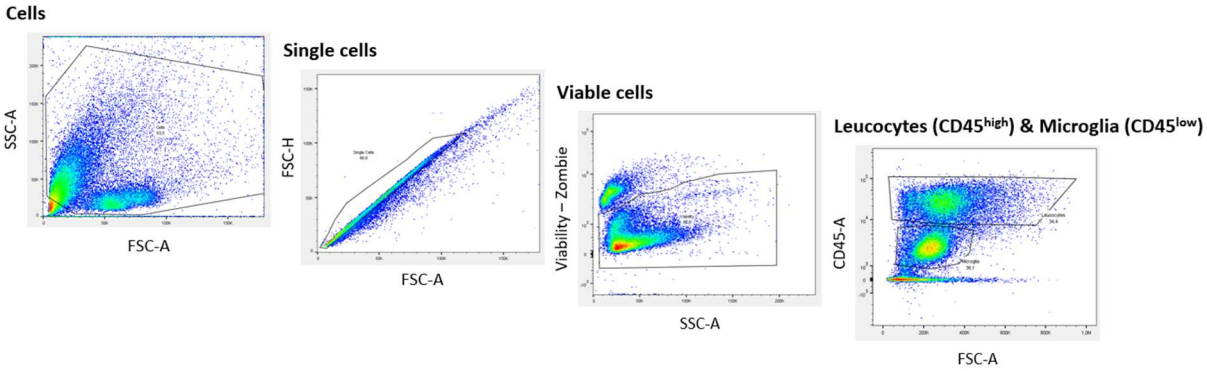

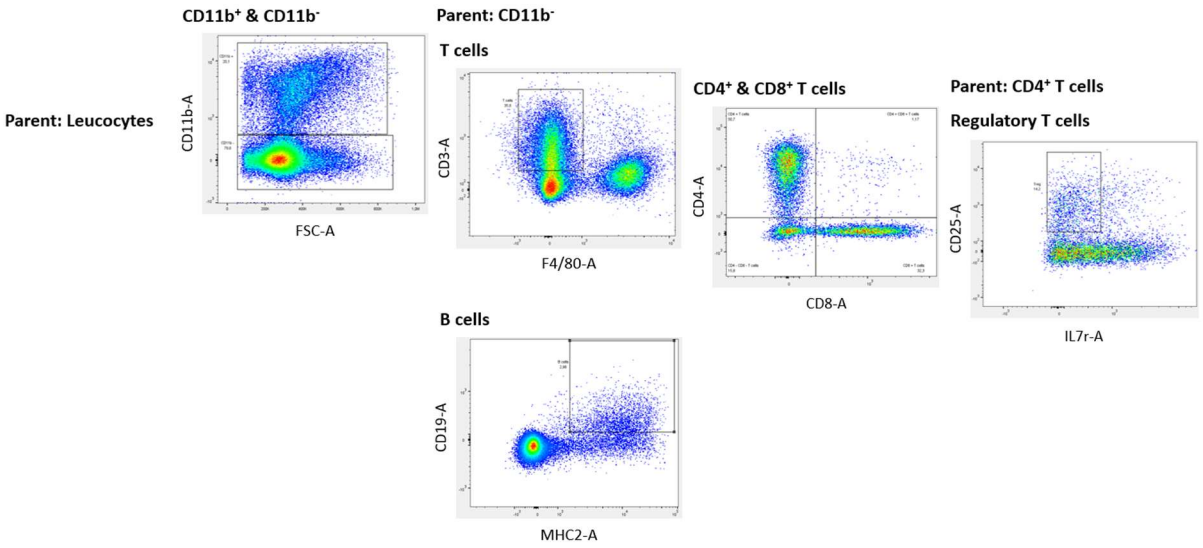

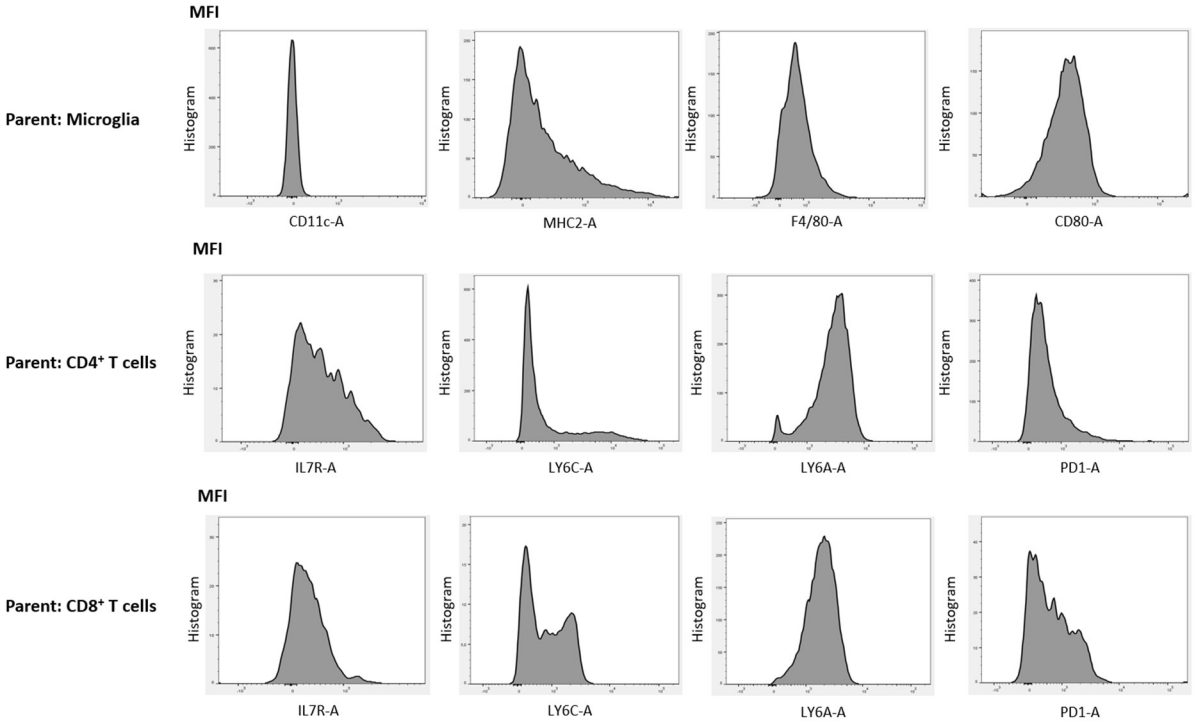
MFI
Parent: Microglia
Histogram
CD11c-A
MHC2-A
F4/80-A
CD80-A
MFI
Parent: CD4+ T cells
IL7R-A
LY6C-A
LY6A-A
PD1-A
MFI
Parent: CD8+ T cells
IL7R-A
LY6C-A
LY6A-A
PD1-A

1011

Appendix 2

Differentially expressed marker genes of leucocytes populations.

	Macrophages	Microglia	Dendritic cells	Basophils	Mastocytes	Neutrophils	B cells	T cells	NK cells
1	Slc7a2	Slc2a5	Flt3	Grm6	Mcpt4	Il1f9	Pax5	Trac	Klra4
2	F13a1	Csmd3	Zfp366	Lama5	Mcpt1	S100a8	Fcmr	Cd3e	Klra8
3	F10	Lrrc3	Cd209a	Il4	Mcpt2	S100a9	Cd79a	Themis	Ncr1
4	Msr1	Ecscr	Clec9a	Mcpt8	Tpsg1	Wfdc21	Ms4a1	Cd6	Klrb1c
5	Fn1	Sall1	Il4i1	Il6	Tpsb2	Lcn2	Cd19	Cd8a	Adamts14
6	Ms4a7	Sparc	Kmo	Cd200r3	Nphs2	Asprv1	Fcer2a	Cxcr6	Klri2
7	Apoc2	Sall3	Zbtb46	Fam110c	Tpsab1	G0s2	Ebf1	Cd5	Klrb1f
8	Ly6i	Slco2b1	Clec10a	Cyp11a1	Tmem233	Retnlg	Iglc2	Bcl11b	Eomes
9	Tgfbi	Crybb1	Nectin1	Car8	Mrgpra9	Lrg1	Vpreb3	Cd3d	Clnk
10	Klra2	Gal3st4	Net1	Myo1d	Tph1	Mmp9	Iglc1	Cd3g	Txk
11	Cfb	Mlxipl	Mmp25	Gata2	Adamts5	Cxcl2	Ighg2b	Cd8b1	Klrb1b
12	Myof	Capn3	Cbfa2t3	Ptger3	Cpa3	Rdh12	Ighg2c	B4galnt4	Klre1
13	Ms4a4a	Nav3	Rnd3	Hgf	Gp1ba	Il1r2	Igkc	Cd4	Xcl1
14	Mmp19	Ctsf	Kynu	Hdc	Otop1	Hcar2	Pou2af1	Gzmk	Car2
15	Sirpb1c	Ptprm	Tbc1d8	P2ry1	Hs6st2	Ankrd33b	Jchain	Pdcd1	Gpc1
16	Arg1	Ppp1r9a	Ccnd1	Ms4a2	Slc45a3	Cxcr2	Iglc3	Icos	Arl4d
17	Fam20c	Pmp22	Pkib	Aqp9	Rprm	Trem1	Mzb1	Ctla4	Spry2
18	Fcrlb	Agmo	Wdfy4	Fgfr1	Thsd4	Trem3	Dennd5b	Trbc2	Emid1
19	Siglec1	P2ry12	Slc30a4	Itga2b	Cma1	Arg2	Eaf2	Camk4	Itga2
20	Lyz1	Col27a1	Rnase6	Ccl6	Cobl	Acod1	Ighd	Thy1	Samd3
21	Clec4a1	Sgce	Htr7	Slc6a9	Arhgap20	Clec4d	Scd1	Cd28	Styk1
22	C3	Serpine2	Syngr2	Kcnj2	Ddc	Clec4e	Chst3	Celsr1	Serpinb9
23	Flt1	Plxdc2	Grk3	Rab44	Slc30a2	Gadd45a	Derl3	Lat	Pde2a
24	Lyz2	Ltc4s	Fcgrt	Slc24a3	Rab38	Il1b	Oosp1	Zfp683	Atp1b1
25	Mgst1	Tpbgl	Olfm1	Ccl9	Muc13	Padi4	Bhlha15	Ubash3a	Prf1
26	Sash1	Tgfa	Nav1	Tgm1	Gnaz	Csf3r	H2-Eb2	Il2ra	Sh2d1b1
27	Pla2g7	Fcrls	Batf3	Alox5	Fcer1a	Pi16	Cd79b	Slamf1	Cd7
28	Chil3	Slc1a3	H2-DMb2	Id1	Nrip3	Cd24a	Fkbp11	Gstp3	Gzma
29	Mmp14	Rapgef5	Napsa	Cxcr2	Itga7	Ptgs2	Fcrla	Itgae	Trdc
30	Mrc1	Phyhd1	Kit	Ccl3	Kit	Ets2	Cacna1h	Fam169b	Il2rb
31	Dram1	Tmem119	Ciita	Bcar3	Rab27b	Gadd45b	Bank1	Sntb1	Gem
32	Clec4n	Slc46a1	Ccdc88a	Mboat1	Creb3l1	Plaur	Tnfrsf13c	Il7r	Bcl2
33	Spon1	Siglech	Shtn1	Adgrg3	Scin	Pram1	Ighm	Rora	Pear1
34	Dab2	Scamp5	Arhgef40	Osm	Rbp1	Slfn4	Ly6d	Gpr68	Sulf2
35	Thbs1	Tspan7	Ifi205	Il1rl1	Il1rl1	Cd300ld	Cd22	Cxcr3	Klrk1
36	Creb5	Cadm1	Marcksl1	Asb2	Homer2	Dgat2	Tnfrsf13b	Cd96	Ctla2b
37	Ms4a6d	Tanc2	Pmaip1	Nfe2	Ahnak2	Dusp1	Ccr6	Il27ra	Gas7
38	Tmem51	Whrn	Cd83	Cdh1	Tmem158	Trim30b	Pycr1	Gprin3	Cd244a
39	Bst1	Cd81	Rogdi	Csf1	Gna14	Csrnp1	Slpi	Cd2	Vps37b
40	Mefv	Hexb	Pdcd1lg2	Slc41a3	Gata1	Jdp2	Spib	Ltb	Gramd4
41	Gpr141	Cd34	Ccdc102a	Fcer1a	Serpinb1a	Hp	H2-Ob	Grap2	Dapk2
42	Cybb	Nuak1	H2-Oa	Slc7a5	Ms4a2	Ccrl2	Fcrl1	Lck	Il12rb2
43	Tgm2	P2ry13	Cd40	Ifitm1	Arhgap6	Cpeb2	Cxcr5	Itga1	Sh2d2a
44	Krt80	Gas6	Etv3	Chst15	Alox5	Ppp1r3b	Cd55	Hid1	Ugcg
45	Sdc4	Bhlhe41	Tcf4	Egr1	Lpar1	Mxd1	Blk	Zap70	Klrd1
46	Arhgef10l	Hpgd	Fdps	Ccl4	Papss2	Nlrp3	Siglecg	Inpp4b	Rras2
47	Vegfa	Cfh	Plbd1	Lilrb4a	Enah	Smox	Prg2	Adam19	Arsb
48	Anpep	Gpr34	Cyb561a3	Cd200r1	Itga2b	Fpr2	H2-DMb2	Cd226	Sell
49	Ms4a6c	Inka1	Pltp	Itga2	Prnp	Pglyrp1	Sdc1	Cd247	Rbpms
50	Clec4a3	Atp8a2	Myadm	Syne1	Il13	Cebpd	Bcl11a	Ms4a4b	Bcl2l11

Appendix 3

Differentially expressed marker genes of lymphocytes subpopulations.

	B cells		T cells				*Cd4*$^+$ T cells		*Cd8*$^+$ T cells	
	Naive	**Plasmocyte**	***Cd4*$^+$**	***Cd8*$^+$**	***Foxp3*$^+$**	**γδ *Rorc*$^+$**	**Exhausted**	**Non-exhausted**	**Exhausted**	**Non-exhausted**
1	Ighd	Fut1	Cd40lg	Cd8b1	Foxp3	Blk	Tnfrsf9	Ccr5	Klf2	Itgae
2	Ccr6	Izumo1	Cd4	Cd8a	Lrrc32	Cd163l1	Rgs16	Ccr2	Fcer1g	Qpct
3	Fcer2a	Slpi	Podnl1	Ccl5	Itgb8	Il23r	Spry1	Itga1	Tnfrsf9	Cdh1
4	B3gnt5	Bhlha15	Ccr8	Gzmk	Neb	Tcrg-V6	S1pr1	Glrx	Rgs16	Gzmk
5	H2-Oa	Ighg2c	Slamf1	Gzma	Ncmap	Il1r1	Dusp4	Hid1	Txk	Ifit1bl1
6	Pax5	Jchain	Tmem154	Prf1	Il10	Zbtb16	Lag3	Fgl2	Irf8	Ccr2
7	Cd22	Prg2	Maf	Adgrg5	Ikzf2	Rorc	Klf2	Cxcr6	Bcl2l11	Tent5a
8	Bcl11a	Igha	St8sia1	Slamf7	Klrg1	Mmp25	Ptprs	Il12rb1	Ccl3	St3gal6
9	H2-DMb2	Fads3	Zbtb7b	Klrk1	Ecm1	Trdc	Tcf7	B4galnt4	Kbtbd11	Itga1
10	Serpinb1a	Ighg2b	Plk3	Gzmb	Tnfrsf9	Il17re	Eea1	Id2	Lag3	Ighg2b
11	Cxcr5	Derl3	Gna15	Itgae	Izumo1r	Tmem176a	Plek	Ctla2a	Vps37b	Cd86
12	Cnn3	Pycr1	Cd5	Klrd1	Tnfrsf4	Tcrg-C1	Slamf6	AA467197	Plek	Rgs10
13	Spib	Tnfrsf17	Furin	Cdh1	Arl5a	Tmem176b	Ptms	Sema4a	Bcl2	Igkc
14	Fcmr	Hid1	Icos	Klrc1	Il2ra	Ltb4r1	Twsg1	Ifitm3	Pdcd1	Plac8
15	Ciita	Eef1akmt3	Hif1a	Tm6sf1	Ikzf4	Serpinb1a	Pdcd1	Podnl1	Cd74	Cxcr3
16	Lrrk2	Chac1	Cd28	Atp8b4	Snx9	Ramp1	Vps37b	Isg20	Fosl2	Il7r
17	Bach2	Slc6a9	Il18r1	Mctp2	Ighm	Aqp3	Tiam1	Plac8	Lat2	Hid1
18	Sell	Eaf2	Hspa1a	Jaml	Sh3rf1	Nr1d1	St6gal1	Ctsw	Tex2	Ifit3
19	Ccr7	Fads2	Selenop	Itga1	Gpr55	sept-08	Bcl2l11	Sytl2	H2-Ab1	Ttc39c
20	Cnr2	Asns	Nxpe3	Dapk2	Bmyc	Igf1r	Ifng	Rasgrp1	Styk1	Isg20
21	Cd72	Igkc	Rora	Nkg7	Sell	Olfr60	Kdm2b	Tmem154	Satb1	Slfn1
22	Zfp318	Alpl	Tnfrsf4	Ifitm10	Dusp4	Plxnd1	Rnf19a	Kctd12	Emb	Ly6a
23	Hhex	Pon3	Hspa1b	Pik3ap1	Tnfrsf18	Lmo4	Fosl2	Furin	Galnt6	H2-Q7
24	Ms4a4c	Tent5c	Ttc39c	Nod1	Timp2	Ckb	Nrp1	F2r	Socs1	Slfn8
25	Srpk3	Atf5	Faah	Zfp683	Asb2	Smox	Crem	Dnajc15	Rilpl2	Txnip
26	Samd9l	Sdc1	Arap2	Cd38	Tspan32	Tnfrsf25	Ybx3	Cmtm7	Cebpb	Cxcr6
27	Egr3	Nuggc	Cd44	Padi2	Maf	Abhd15	Rel	Pglyrp2	Mxd1	Sumo2
28	S1pr1	Gpr160	Orai1	Cst7	Ctla4	Tmem64	Nt5e	Ttc39c	Nab2	Lpar6
29	Rasgef1b	Xbp1	Ifitm3	Gem	Lamc1	Arrb1	Nkg7	Selenop	Crem	Ms4a4b
30	Btla	Tmem176a	Junb	Mef2a	Samsn1	St6galnac3	Cxcr4	Lpar6	Cd244a	Fyco1
31	Fam43a	Iglc1	Cd6	Chsy1	Iigp1	Mgat5	Rilpl2	Crot	Ptms	Bicral
32	Treml2	Creb3l2	Gpr183	Ctsw	Dusp1	Selenop	Tnfrsf4	Igtp	Anxa2	Themis
33	Sbk1	Fkbp11	Kctd12	Plac8	Itgb3	Cpd	Anxa2	Themis	Pgam1	Trip4
34	H2-Ob	Cpeb3	B4galnt4	Ugcg	Crem	Dgat1	Dusp6	Il27ra	Havcr2	Itgb7
35	Blk	Selenom	Il18rap	B4galt5	Wls	Prrt1	Ptpn11	Coro2a	Jund	Slfn2
36	Haao	Plpp5	Ifitm2	Abi3	Slc16a3	Rarg	Nr4a1	Ms4a4b	Lyz2	Fam78a
37	Id3	Gpm6a	Casp1	Fasl	Psen2	Plin3	Tspan13	Adam19	Slc2a1	Ctla2a
38	Sorl1	Rapgef3	Satb1	Fgl2	Pim1	Tnfsf14	Tagap	Ctsd	Tpm4	Hipk1
39	March1	Creld2	H1f0	Usp18	Twsg1	Itgb3	Trps1	Txnip	Dusp5	Tab2
40	Cd40	Fndc3b	Bhlhe40	Ikzf3	Nt5e	Crmp1	Tex2	Il7r	Ccl4	Cd226
41	Evl	Vegfa	Hnrnpll	Ccl4	Odc1	Emb	Rnf125	Ifit1bl1	Cd44	Hcst
42	Icosl	Prdm1	Rab11fip1	Gimap7	Tnfrsf1b	Gabbr1	Cd74	Ly6a	Ldha	Igtp
43	Rcsd1	Sec24d	Cd84	Armc7	Mmd	Gclc	Farp1	St8sia1	Nt5e	S100a10
44	Snn	Sdf2l1	Irf2bp2	Cd86	Matk	Sema4b	Tpm4	S100a10	Sik1	Phf11b
45	Tlr1	Tmem176b	Gpr132	Dennd4a	Nfil3	Furin	Itga4	Fkbp3	Rexo2	B2m
46	Ephx1	Rgcc	Btg2	Klk8	Sema4b	Ern1	Orai1	Epsti1	Tgfb1	Glrx
47	Lrmp	Prdx4	Jak2	S100a6	Cd200r1	Pi4k2a	Emb	Cd52	Rin3	Id2
48	Cd83	Cacna1h	Dusp1	Ctsd	Cd27	Ero1l	P2ry10	Sephs2	Ifng	Mxd4
49	Slc28a2	Epcam	Rabgap1l	Havcr2	Itgav	Rora	Samsn1	Arl4c	Prf1	Smpdl3a
50	Arhgef18	Slamf9	Hivep2	Ptp4a3	Socs2	Ly6g5b	Ptger2	Ly6e	Zfp36	Itgax

Appendix 4

Differentially expressed marker genes of macrophages and microglia subpopulations.

	Macorphages					Microglia		
	Pro-inflammatory	**Anti-inflammatory**	**Antigen-presenting**	**Lipid-associated**	**Monocytes**	**Pro-inflammatory**	**Anti-inflammatory**	**Stress-response**
1	Cxcl10	Arg1	Tmem176a	Gpnmb	Ace	H2-Aa	Gpr165	Egr1
2	Ifi205	Slc7a2	Mrc1	Saa3	Treml4	H2-Eb1	Fcrls	Fos
3	Cxcl9	Fcrlb	Mgl2	Stra6l	Adgre4	Cd74	Tgfbi	Jun
4	Ly6i	Mrc1	Tmem176b	Apoe	Ceacam1	Oas2	Tuba1a	Egr2
5	Gpr141	Ms4a7	Pltp	Fabp5	Ldlrad3	H2-Ab1	Stab1	Klf2
6	Batf2	Spp1	Igfbp4	Ms4a7	Thbd	Itgax	Jam2	Fosb
7	Flt1	Fn1	Clec12a	Nr1h3	Arhgef37	Ifi204	Gabbr1	Ier2
8	Il1rn	Thbs1	H2-Aa	Mmp2	Ifitm6	H2-Oa	Tgm2	Nr4a1
9	Cfb	Adamtsl4	H2-Eb1	Plxna1	Krt80	Gbp5	Idh2	Hspa1b
10	Slfn4	Dpep2	Lyz1	Gpr162	F13a1	Ifitm3	Csmd3	Hspa1a
11	Ifi211	Ecm1	Clec4a2	Slc6a8	Tppp3	H2-Q7	Comtd1	Atf3
12	Cnn3	Dab2	Slamf9	Fam20c	Pi16	C4b	C5ar1	Dusp1
13	Phf11d	Fam20c	Adgre1	Pltp	Cd177	Ly6a	Ecscr	Dnajb1
14	Klra2	Gatm	Ms4a7	Fblim1	Hp	Slfn5	Man2a2	Hsp90aa1
15	Dram1	Vegfa	Cyp27a1	Adgb	Scarb1	Rnf213	Ltc4s	Zfp36
16	Tfec	Sash1	Stard8	Apoc2	Cd300a	Fgl2	Camk2n1	Btg2
17	Ms4a4c	Rai14	Clec10a	Plxnd1	Stom	Stat1	Cryl1	Jund
18	Fpr2	Fblim1	Tspan33	Vat1	Lyz1	Rtp4	Ifitm10	Nfkbid
19	Ifi204	Apoc2	Clec4a1	Fnip2	Cd300lb	Ifi209	Tm6sf1	Ccl4
20	Gbp2	Ms4a4a	Stab1	Hebp1	Lyz2	Ccl12	Slc2a5	Junb
21	Mefv	Mmp19	Shtn1	Sash1	Atp1a3	Gbp2	P2ry12	Ccl3
22	F10	Sh3pxd2b	Cd93	Gas2l3	Gsr	Nlrc5	Fscn1	Ppp1r15a
23	Ms4a6d	Zmynd15	H2-Ab1	Cd93	Clec4a1	Igtp	Pmp22	Nfkbiz
24	Cd40	Myof	Cd74	Il18bp	Grk5	Parp14	Rtn1	Dnaja1
25	Ifit2	Pdcd1lg2	Selenop	Pla2g7	Arhgef10l	Axl	Syngr1	Ier5
26	Ifi207	Tgfbi	Clec4a3	Lyz1	Aldh2	Sp100	Rin3	Rgs1
27	Oasl1	Cd14	Tlr8	Nrp2	Nfe2	Ccl5	Sox4	Nfkbia
28	C3	Clec4n	Lifr	Cpq	Grk3	Stat2	Tbkbp1	Cd83
29	Msr1	C3ar1	Prxl2b	Fzd7	Mgst1	Slamf8	Zfp703	Tsc22d3
30	Slamf8	Msr1	Apoe	Spp1	Chil3	Zbp1	Sec11c	Per1
31	Tgm2	Siglec1	Siglece	Acsl1	Gda	Il2rg	Cd164	Ubc
32	Smpdl3b	Apoe	Dock1	Lyz2	Clec4a3	Irf7	Bcl9l	Klf6
33	Pstpip2	Hmox1	H2-DMb1	Gpr157	Mefv	Oasl2	Abtb1	Hspa8
34	Nod2	Mmp14	Fcgrt	Tnfsf13	Cd300ld	Oas1a	Sem1	Ccrl2
35	Mlkl	Spon1	Nrp1	Syngr1	Napsa	B2m	Arap3	Rhob
36	Sirpb1c	Plin2	Myo5a	Fmn1	Fgr	Cst7	Cnpy3	Tsc22d2
37	Tgfbi	Pla2g7	Itsn1	Ctsb	Camkk2	Gbp9	Chsy1	Kdm6b
38	Tarm1	Mafb	Rab7b	Pdgfa	Idh1	Xaf1	Gpr183	Tnfaip3
39	Tnfaip2	Sdc4	Axl	Sgk1	Rasgrp4	Lgals3bp	Ptprs	Il1a
40	Pira2	Cxcl16	Siglec1	C1ra	Gngt2	Dhx58	Arhgef40	Ier3
41	Alpk1	C5ar1	Hacd4	Mgst1	Rras	H2-D1	Tspan4	Socs3
42	Creb5	Fcgr2b	Stard9	Ninj1	Rassf4	Fcgr4	Frmd8	Rasgef1b
43	Il18	Ccl12	C1qa	Lhfpl2	Fam49a	Irgm1	Iffo1	Cited2
44	Clec5a	B3gnt8	Pdlim4	Psap	Gpr141	Herc6	Gpr34	Plk3
45	Sdc4	F10	Cybb	Zfp704	Tpd52	Ly9	Srsf1	Zfand5
46	Calhm6	Fth1	Ehd4	Abca1	Fgd4	Eif2ak2	Cables1	Hmox1
47	Ass1	F13a1	Lyz2	Hmox1	Klf4	Isg15	Golm1	Hist1h1e
48	Gda	Fcgr4	Prcp	Slc27a1	Tmem51	Parp9	Ykt6	Tagap
49	Tlr2	Acvrl1	Dse	Acp5	Pdlim1	Bst2	Ctdsp1	Ifrd1
50	Ms4a6c	Anpep	Cd300c2	Cd63	Rap1gap2	Siglecf	Maf	Zc3h12a

oHSV/P2G disrupts glioblastoma angiogenesis. *(preliminary results*)

Preliminary results:

Oncolytic HSV-1 armed with CXCL12-antagonist "P2G" to disrupt to disrupt angiogenesis, by interfering with tumour and immune cell–mediated pro-angiogenic signalling

DUBOIS, Maxime[1], LASSENCE Cédric[1], LEBRUN Marielle[1,2], SADZOT-DELVAUX Catherine[1, 2]

[1] Laboratory of Virology and Immunology, GIGA-Immunobiology, University of Liège, 4000 Liège, Belgium

[2] Equal contributions as last co-authors

Summary

The following introductory section addresses the capacity of oHSVs to induce angiogenesis, which is not covered in the global introduction. It also compiles dispersed information to summarise the development and impact of hypervascularisation in glioblastoma. It also highlights the limited clinical benefit of current single-target anti-angiogenic strategies (bevacizumab). Conversely, CXCR4 inhibition combined with virotherapy would simultaneously target many glioblastoma features. The aim of the subsequent results section is to provide insights into the potential pro-angiogenic adverse effects of oHSV treatment, whether mediated by the immune response or not, and to explore the possible advantages of oHSV/P2G. This work is only discussed in the global discussion within the broader context of the thesis.

The following results are preliminary, and most experiments should be repeated to improve statistical power. They are nevertheless included because:

- Potential inhibition of angiogenesis is crucial to the characterisation of oHSV/P2G.
- These effects are relevant to glioblastoma hypervascularisation and the historically limited efficacy of anti-angiogenic single-target strategies (bevacizumab, plerixafor).
- Pro-angiogenic effects of virotherapy remain underexplored yet clinically relevant.
- Potential immune-mediated angiogenesis is especially pertinent in the context of glioblastoma immunotherapy.

Overall, these findings provide a useful basis for generating new insights and hypotheses.

INTRODUCTION

Glioblastoma is the most frequent and aggressive primary brain tumour, with a median overall survival of approximately 15 months.[1,2] Standard treatment consists of maximal surgical resection followed by radiotherapy and temozolomide (TMZ) chemotherapy.[2] Poor prognosis results from treatment failure, driven by limited surgical accessibility, restricted drug delivery across the blood–brain barrier, tumour heterogeneity, immunosuppressive microenvironment, glioblastoma stem-like cells (GSCs), and pronounced hypervascularisation, ultimately leading to recurrence.[3–5] Hypervascularisation plays a key role in glioblastoma growth, aggressiveness and therapeutic resistance by increasing the supply of oxygen, nutrients, and growth factors, and promoting the formation of perivascular niches that maintain GSCs' stemness, migration, and resistance features.[6–8]

The aberrant vascular network in glioblastoma is induced by pro-angiogenic secreted factors, including growth factors (EGF, FGF, TGFβ, VEGFα) and cytokines (IL10/17, CXCL12) produced by tumour cells and non-neoplastic cells such as cancer-associated fibroblasts, endothelial cells (ECs), astrocytes and neurons.[9–14] Hypoxic niches, frequent in glioblastoma, also contribute to hypervascularisation via HIF1α stabilisation, inducing VEGFα expression, which triggers VEGFR-mediated EC proliferation and migration, leading to microvascular proliferation and perivascular niche formation, another hallmark of glioblastoma.[4–7,15–17] Finally, pro-angiogenic tumour-associated macrophages and microglia (TAMs), driven by HIF1α, secrete MMPs, VEGFα, CXCL12, TGFβ, and IL1β/6/23. These cytokines contribute to helper and γδ T cells polarisation towards a Th17-like phenotype (driven by RORγ, HIF1α, and STAT3), promoting angiogenesis via VEGFα expression and further pro-angiogenic TAMs polarisation through IL17/21/23 release.[18–20]

Despite its importance, targeting angiogenesis alone has shown limited efficacy in glioblastoma, including VEGFα inhibition with bevacizumab as well as CXCR4 inhibition via plerixafor (AMD3100).[21–23] Contrasting with strong preclinical glioblastoma data, plerixafor (AMD3100) has only reached Phase I trials, combined with standard treatments or bevacizumab, for newly diagnosed or recurrent glioblastoma. These treatments aimed at reducing tumour perfusion and growth. They showed safety and biological activity but no survival or tumour control benefit.[24,25] Tumours have seemingly the ability to adapt to anti-angiogenic treatments by reorganising around residual hypoxic and invasive niches.[5,26] Moreover, angiogenesis inhibition may impair immune infiltration and increase hypoxia, paradoxically reducing immunotherapy efficacy while promoting HIF1α-mediated pro-angiogenic signalling. However, combined multi-targeted strategies integrating anti-angiogenic properties may increase tumour susceptibility by reducing

access to oxygen and nutrients, and limiting rescue and maintenance of GSCs by perivascular niches.

The CXCR4/CXCL12 axis is linked to angiogenesis, invasiveness, GSCs maintenance, immunosuppression, recurrence, and poor prognosis.[27–30] CXCR4 is expressed by ECs, stem cells, and immunosuppressive populations, while CXCL12 is enriched in glioblastoma niches, promoting vascularisation, stemness, radioresistance, invasion, and immune suppression. In perivascular niches or following surgical resection, ECs and pericytes secrete CXCL12, recruiting $CXCR4^+$ GSCs (vascular co-option) and enhancing their stemness and resistance features. In turn, GSCs secrete VEGFα and may acquire pericyte- or endothelial-like phenotypes (vascular mimicry), supporting vessel stability, blood–brain barrier integrity, and neovascularisation.[5,6,26] Inhibitors such as AMD3100 (plerixafor), HMGB1-BoxA, and CXCL12-P2G disrupt this pathway.[30–33]

Oncolytic virotherapy is a promising immunotherapeutic approach leading to selective replication of genetically engineered viruses in tumour cells, immunogenic cell death, and stimulation of anti-tumour immunity. These viruses can additionally deliver transgenes targeting tumour and immune pathways.[30,34–37] Several oncolytic viruses have been approved for glioblastoma and other cancers.[34,38–41] Notably, the oncolytic HSV1 (oHSV) teserpaturev (Delytact®, Δ34.5Δ47Δ6) was approved in Japan in 2021 for residual or recurrent glioblastoma.[42] However, HSV1 infection may promote angiogenesis via, for instance, *CCN1* upregulation and *TSP1/2* downregulation in immunodeficient mouse models. Comparative analyses of HSV1 and oHSVs indicate that the Δ34.5Δ6 deletions do not significantly alter the pro-angiogenic properties of HSV1, whereas the Δ47 deletion appears to attenuate them, although the mechanisms responsible for this effect and the impact of the immune response remain to be elucidated.[43,44] Considering the relation between hypervascularisation and aggressiveness as well as the importance of tumour immune microenvironment in angiogenesis, it seems crucial to characterise the impact of oncolytic virotherapy on tumour vasculature in immunocompetent models.

We engineered an oncolytic HSV1 expressing CXCL12-P2G (oHSV/P2G). Previous studies showed, upon treatment, reduced GSCs stemness and migration[30], enhanced tumour-infiltrating lymphocyte recruitment and activation, and TAMs polarisation towards a pro-inflammatory phenotype. Given the expected opposite effects of CXCR4/CXCL12 inhibition and oncolytic virotherapy, assessing the impact of oHSV and oHSV/P2G on angiogenesis is of particular interest.

Here, we present preliminary results evaluating the effects of oHSV/P2G, *in vivo*, on tumour vasculature ($CD31^+$ immunofluorescence) as well as pro-angiogenic immune polarisation (single-cell RNA sequencing). Both experiments were performed in immunocompetent orthotopic syngeneic C57BL/6NRj mice engrafted with GL261N4 cells, treated with PBS, oHSV, or oHSV/P2G at days 7 and 14 post-engraftment, and sacrificed 21 d.p.e. *In vitro*, conditioned media from infected or uninfected glioblastoma

cells (72 h) were applied to human umbilical vein endothelial cells (HUVECs) for tube formation assays, as well as to monocyte-derived macrophages and HMC3 microglia for bulk RNA sequencing and RT-qPCR analyses, respectively.

The results are preliminary but point towards assay-dependent effects of oHSV compared to control, whereas oHSV/P2G tends to reduce angiogenesis compared to both oHSV and control. Moreover, immune response seems to be involved in these observations.

PRELIMINARY RESULTS

Inhibition of CXCR4 pathway by virotherapy impairs tubulogenesis *in vitro*

Human umbilical vein endothelial cells (HUVECs) were pre-treated for 24h with various conditioned media before being seeded on polymerized Matrigel in EGM2 culture medium for a tube formation assay. After 6h incubation at 37°C, the number of branch points was quantified relative to controls. Other parameters, such as total tube length and mesh area, were also considered but were not prioritised in the present analysis. Future experiments will consider adding these readouts to consolidate the conclusions.

First, the involvement of the CXCR4 pathway in tubulogenesis was confirmed by assessing the effects of AMD3100, a well-established FDA-approved CXCR4 antagonist, and CXCL12, CXCR4 main ligand. HUVECs pre-cultured in EGM2 medium exhibited robust tube formation and served as the positive control. Stimulation of CXCR4 signalling with CXCL12 treatment did not enhance tubulogenesis beyond control levels. Conversely, CXCR4 inhibition with AMD3100 significantly reduced the number of branch points compared to both control and CXCL12-treated samples. Combined treatment with AMD3100 and CXCL12 partially restored tube formation relative to AMD3100 alone, without reaching the control or CXCL12-treated cells levels (Fig. 1A)[I].

The impact of glioblastoma-derived factors was then assessed using conditioned media from GB138 cells cultured for 72h in uncomplemented DMEM/F12 (mNI). Treatment of

[I] **Figure 1: Inhibition of CXCR4 pathway by virotherapy impair tubulogenesis *in vitro***
A–D: HUVECs were pre-treated for 24 h with conditioned media, harvested, and seeded onto polymerized Matrigel. Tube formation was quantified by counting branch points using ImageJ and normalized to the condition with the highest number of branch points. **(A)** Role of CXCR4/CXCL12 pathway: EGM2 compared to EGM2 supplemented with CXCL12, AMD3100, or both. **(B)** Role of human glioblastoma GB138-secreted factors: EGM2 compared to fresh DMEM/F12 and GB138 conditioned media (DMEM/F12; 72 h; mNI). **(C)** Representative brightfield images from Figure 1B. **(D)** Role of glioblastoma infection: mNI compared to conditioned media from GB138 infected for 72h with oHSV (moHSV) or oHSV/P2G (moHSV/P2G). **(E)** GB138 cells used for conditioned media production were analysed for angiogenic gene expression by RT-qPCR, normalised to PBS control (NI).
Each dot represents the mean of five images from independent wells **(A–D)** or one flask of cells per conditioned media batch **(E)**. Bars indicate mean ± SD. Statistical significance was determined by one-way ANOVA with Tukey's multiple-comparison test. *p<0.05, **p< 0.01, ***p<0.001, ****p<0.0001.

Figure 1

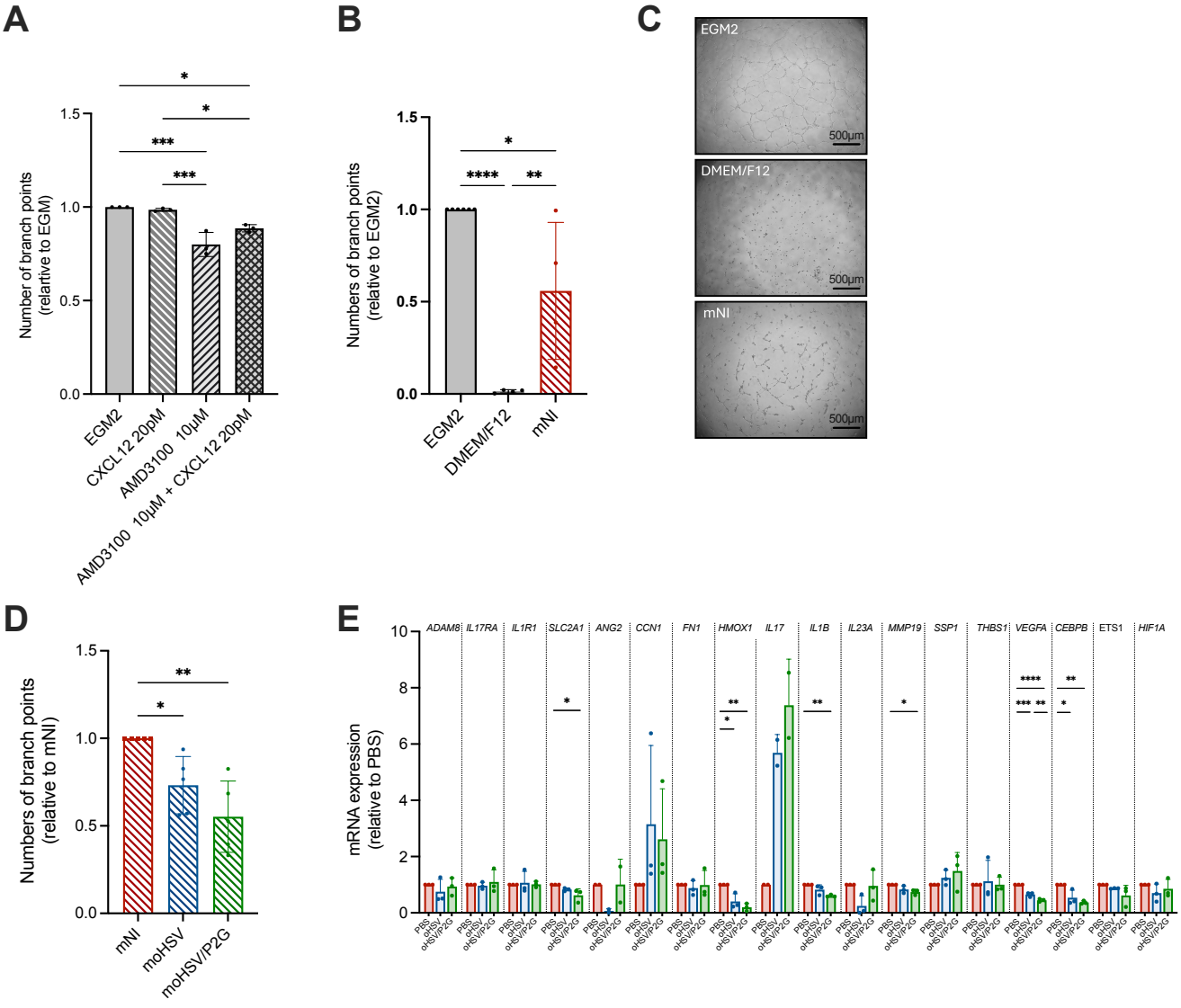
A
B
C
D
E
Number of branch points (relartive to EGM)
EGM2
CXCL12 20pM
AMD3100 10µM
AMD3100 10µM + CXCL12 20pM
Numbers of branch points (relative to EGM2)
DMEM/F12
mNI
500µm
Numbers of branch points (relative to mNI)
moHSV
moHSV/P2G
mRNA expression (relative to PBS)
ADAM8
IL17RA
IL1R1
SLC2A1
ANG2
CCN1
FN1
HMOX1
IL17
IL1B
IL23A
MMP19
SSP1
THBS1
VEGFA
CEBPB
ETS1
HIF1A

HUVECs for 24h with mNI markedly increased tube formation compared to fresh DMEM/F12, which was almost unable to support tube formation (Fig. 1B, C).

Finally, HUVECs treated with conditioned media from GB138 cells infected with oHSV (moHSV) showed some reduction in tube formation relative to mNI. Treatment with moHSV/P2G showed a trend of decrease compared to moHSV, but the experiment should be repeated before drawing any conclusion on this aspect (Fig. 1D).

These findings confirm the pro-angiogenic activity of the glioblastoma microenvironment, known to be partly driven by CXCR4-dependent signalling, and suggest that this activity can be attenuated through virotherapy or CXCR4 inihibtion (AMD3100). However, the synergistic effects of the combination therapy with oHSV/P2G remain to be demonstrated.

oHSV/P2G-conditioned media inhibits pro-angiogenic genes expression in human glioblastoma cells *in vitro*

To investigate the molecular basis of the anti-angiogenic effects observed with conditioned media, the expression of several angiogenic genes was analysed by RT-qPCR, in GB138 cells, infected or not with oHSV or oHSV/P2G. Although *CCN1*, previously linked to oHSV-mediated angiogenesis[44], as well as *IL17* were significantly upregulated by both oHSV and oHSV/P2G, *HMOX1, CEBPB, SLC2A1, MMP19* and *IL1β* were significantly downregulated, with SLC2A1, MMP19 and IL1β downregulation significant only upon oHSV/P2G infection. Importantly, *VEGFα*, a key angiogenic factor present in EGM2 media, was significantly reduced by both viruses, with a further significant decrease upon oHSV/P2G infection relative to oHSV infection (Fig. 1E).

These preliminary data suggest potentially controversial roles of infection in tumour angiogenesis, characterized by both upregulated and downregulated genes. However, CXCR4 inhibition seems to induce downregulation of some genes compared to oHSV.

oHSV/P2G disrupts tumour angiogenesis *in vivo*

The anti-angiogenic effect of oHSV/P2G was evaluated in a syngeneic orthotopic, C57BL/6NRj mouse model. GL261N4 (1×10^5 cells) were engrafted in the right striatum under stereotactic coordinates control. Mice received intratumor injections of each virus (1×10^6 pfu, 2 µL) or PBS on days 7 and 14 post-engraftment and were sacrificed on day 21 (Fig. 2A)[II].

Immunofluorescence staining of $CD31^+$ cells was performed on brain cryosections to evaluate tumour vascularization. Tumour regions were manually delineated and average area covered by each $CD31^+$ vessels was quantified with QuPath in both tumour and stroma independently. In PBS-treated mice, average $CD31^+$ vessel area was 10-fold higher in tumours than in stroma. While oHSV surprisingly increased average vessel area within the tumour without reaching significance (p=0.66), oHSV/P2G significantly reduced it compared to oHSV (Fig. 2B, C).

These results suggest an antagonistic effect between oHSV and oHSV/P2G on tumour angiogenesis, resulting in significant inhibition of tumour vasculature in oHSV/P2G-treated mice compared to oHSV-treated mice. PBS-treated tumours display an intermediate phenotype.

[II] **Figure 2: oHSV/P2G disrupts tumour angiogenesis *in vivo***
(A) Experimental settings of the orthotopic syngeneic model. **(B)** Average area of CD31+ staining (µm2) quantified by QuPath machine-learning analysis within tumour and brain stroma. **(C)** Representative picture of serial brain cryosections from mice sacrificed 21 d.p.e. of $1x10^5$ GL261N4 following treatment with PBS (n=4), oHSV (n=4), or oHSV/P2G (n=5). Epifluorescence acquisition of DAPI staining allow delineation of tumour and stroma (red line) (upper panel), and CD31 immunofluorescence identifies vessels (middle panel). QuPath modelling of $CD31^+$ vasculature within tumour (yellow) and stroma (magenta) (lower panel).
Each dot represents the mean $CD31^+$ area of several serial brain cryosections of one mouse. Boxes indicate the distribution of values, with whiskers denoting the minimum and maximum. Statistical significance was determined by one-way ANOVA with Tukey's multiple-comparison test. *p<0.05.

Figure 2

A

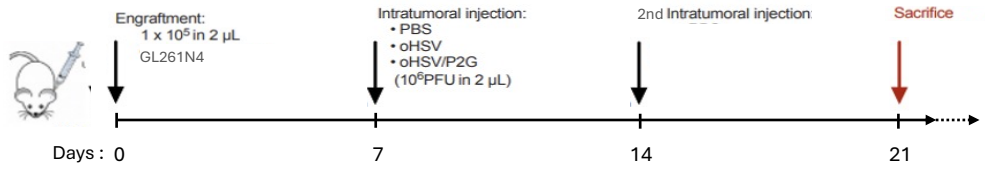
Engraftment:
1 x 10^5 in 2 µL
GL261N4
Intratumoral injection:
• PBS
• oHSV
• oHSV/P2G
(10^6PFU in 2 µL)
2nd Intratumoral injection
Sacrifice
Days : 0
7
14
21

B

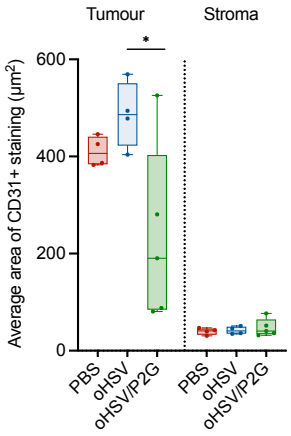
Tumour
Stroma
*
Average area of CD31+ staining (µm²)
600
400
200
0
PBS
oHSV
oHSV/P2G
PBS
oHSV
oHSV/P2G

C

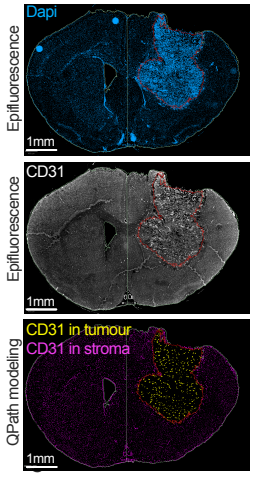
Epifluorescence
Dapi
1mm
Epifluorescence
CD31
1mm
QPath modeling
CD31 in tumour
CD31 in stroma
1mm

oHSV/P2G inhibits pro-angiogenic phenotype in immune cells

The effect of oHSV/P2G on pro-angiogenic polarisation of immune cells was evaluated in the same syngeneic GL261N4 model using single-cell RNA sequencing on leucocytes isolated from PBS-, oHSV- or oHSV/P2G- treated mice's brains.

Pseudobulk gene expression analysis of representative angiogenic markers was performed on major immune populations and visualized as z-score heatmaps. Angiogenic gene expression was globally downregulated in macrophages treated with oHSV/P2G compared to PBS and oHSV. Interestingly, oHSV increased many angiogenic gene expression in macrophages compared to PBS-treated mice (Fig. 3A)[III]. In microglia, these effects is less clearly observed (Fig. 3B). In T cells, most angiogenic gene expression is also reduced by oHSV/P2G compared to both PBS and oHSV (Fig. 3C).

Cells were clustered based on transcriptomic similarity and visualised using UMAP. Clusters were annotated using the top 50 differentially expressed canonical marker genes (upregulated, detected in at least 25% of cells, and with a minimum log fold change of 0.25), listed in Appendix 1. Clustering of macrophages identified three major subpopulations: pro-inflammatory (M1-like), anti-inflammatory (M2-like), and a combined anti-inflammatory/pro-angiogenic phenotype (Fig. 3D). Phenotypic assignments were validated using Seurat's AddModuleScore function to compute scores for each profile based on gene sets from the MSigDB Mouse collections (Fig. 3E, S1).

These results highlight the potential contribution of the immune system to the pro-angiogenic tumour microenvironment. They also support the hypothesis that oHSV/P2G could counteract this effect by inhibiting pro-angiogenic pathways in both myeloid and lymphoid immune cells.

oHSV/P2G inhibits angiogenesis resulting from the synergy between tumour and immune cells *in vitro*

In vitro, human monocyte-derived macrophages (hMDMs) were treated for 48h with PBS, oHSV or oHSV/P2G conditioned media. Bulk RNA sequencing showed that pro-

[III] **Figure 3: oHSV/P2G inhibits pro-angiogenic phenotype in immune cells**
A-C: Leucocytes recovered from three pooled PBS-, oHSV- or oHSV/P2G-treated mice (n=4 in each group) 21 d.p.e. of $1x10^5$ GL261N4, and analysed by single-cell RNA sequencing (ScRNAseq). Leucocytes are divided into several populations identified based on cluster-specific differentially expressed marker genes. Pseudobulk analysis of macrophages **(A)**, microglia **(B)**, and T cells **(C)** showing representative angiogenic genes visualised as heatmaps of z-score from mean normalised expression values. Genes are grouped into several functional gene sets. **(D)** UMAP representation of the clustering of macrophages highlighting subpopulations identified based on subcluster-specific differentially expressed marker genes. **(E)** UMAP representation of the clustering of macrophages, grouped by treatment, highlighting expression scores for gene sets related to pro-inflammatory, anti-inflammatory and pro-angiogenic phenotypes (Expression scores were computed using Seurat's AddModuleScore function on gene sets derived from MSigDB Mouse collections).

Figure 3

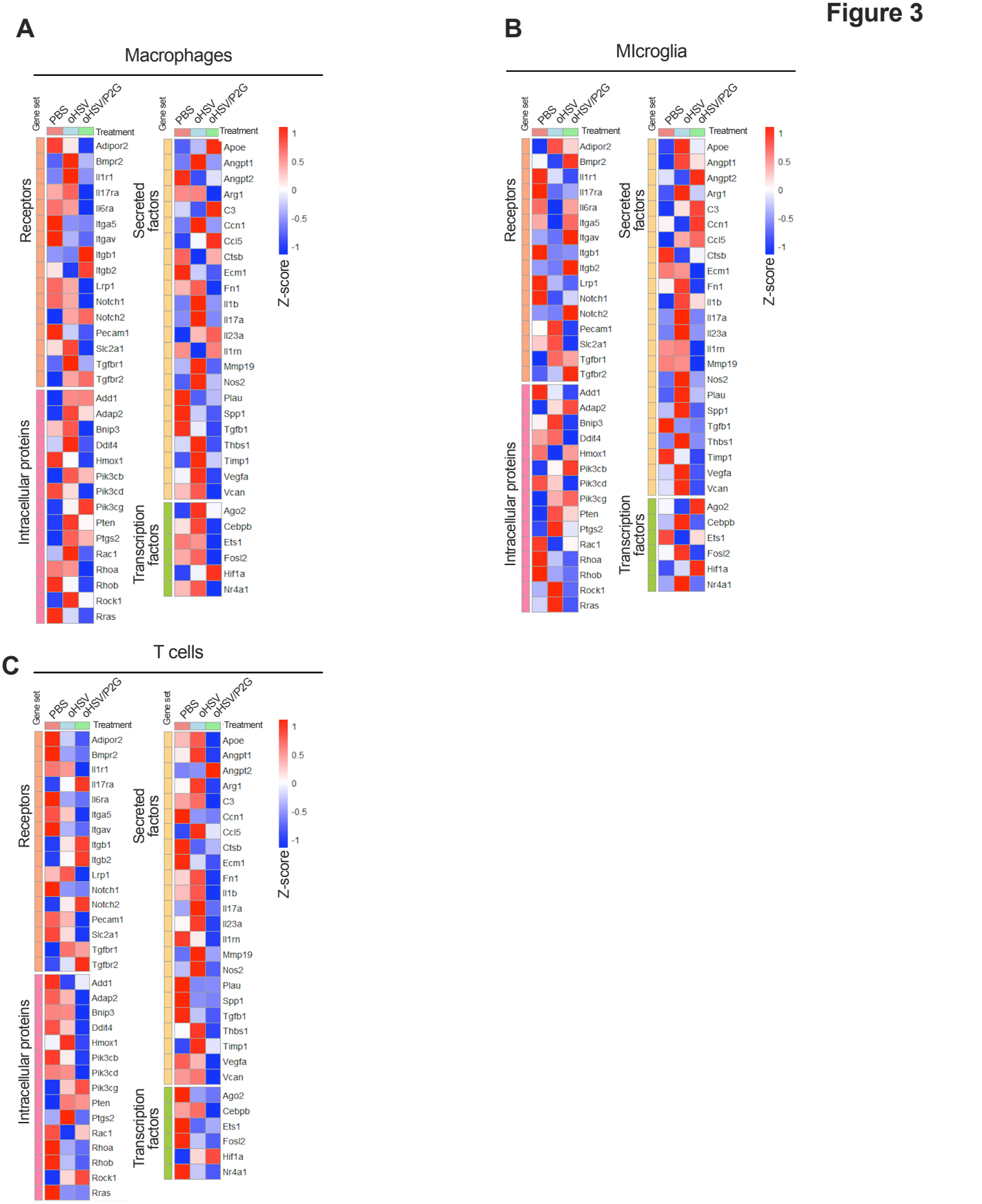
A
Macrophages
B
MIcroglia
C
T cells
Gene set
PBS
oHSV
oHSV/P2G
Treatment
Receptors
Secreted factors
Intracellular proteins
Transcription factors
Adipor2
Bmpr2
Il1r1
Il17ra
Il6ra
Itga5
Itgav
Itgb1
Itgb2
Lrp1
Notch1
Notch2
Pecam1
Slc2a1
Tgfbr1
Tgfbr2
Add1
Adap2
Bnip3
Ddit4
Hmox1
Pik3cb
Pik3cd
Pik3cg
Pten
Ptgs2
Rac1
Rhoa
Rhob
Rock1
Rras
Apoe
Angpt1
Angpt2
Arg1
C3
Ccn1
Ccl5
Ctsb
Ecm1
Fn1
Il1b
Il17a
Il23a
Il1rn
Mmp19
Nos2
Plau
Spp1
Tgfb1
Thbs1
Timp1
Vegfa
Vcan
Ago2
Cebpb
Ets1
Fosl2
Hif1a
Nr4a1
Z-score
1
0.5
0
-0.5
-1
D
Pro-inflammatory marcophages
Anti-inflammatory marcophages
Pro-angiogenic marcophages
umap_1
umap_2
E
Pro-inflammatory
M1-like gene set
Anti-inflammatory
M2-like gene set
Pro-angiogenic
gene set

angiogenic genes were downregulated by both moHSV or moHSV/P2G, this downregulation being more drastic with moHSV/P2G. (Fig. 4A)[IV].

In parallel, HMC3 microglial cells were treated similarly, and the expression of the angiogenesis-related genes previously analysed in GB138 cells was quantified by RT-qPCR. Only *ADAM8* was significantly downregulated by both oHSV and oHSV/P2G, while *IL23A* was significantly reduced only by oHSV/P2G. Expression of the other genes showed high variability, precluding meaningful interpretation (Fig. 4B).

Tube formation assays were then performed using conditioned media from GB138 cells (mNI GB138), HMC3 cells (mNI HMC3), or from a HMC3-GB138 coculture 2/3-1/3 (mNI Coculture), infected or not with oHSV (moHSV Coculture) or oHSV/P2G (moHSV/P2G Coculture). Interestingly, branch points formation was higher in the HMC3-GB138 coculture compared to mNI GB138, which itself was significantly higher than mNI HMC3. Conditioned media from oHSV- or oHSV/P2G-treated GB138 and HMC3 coculture showed a trend toward reduced branch points compared to mNI Coculture, though these differences did not reach statistical significance ($p = 0.068$) (Fig. 4C).

These results suggest that HMC3 cells alone play a relatively minor role in tumour angiogenesis *in vitro*. However, coculture experiments indicate a potential synergistic effect between HMC3 and GB138 cells. In this coculture conditions, P2G tends to impair angiogenesis. These results remain preliminary and should be repeated. Future tube formation assays should include MDMs, as their pro-angiogenic transcriptional profile appears more strongly affected by oHSV/P2G than that of HMC3 cells, in accordance with the transcriptional profile differences observed *in vivo* between macrophages and microglia.

[IV] **Figure 4: oHSV/P2G inhibits pro-angiogenic phenotype in immune cells *in vitro***
(A) Bulk RNA sequencing analysis of human monocyte-derived-macrophages (MDMs), recovered from fresh healthy donor's blood, treated for 48h with conditioned media from GB138 human glioblastoma cells cultured for 72h, either uninfected (mNI) or infected with oHSV (moHSV) or oHSV/P2G (moHSV/P2G) (n=3 in each group). Representative angiogenic genes were visualised as heatmaps of z-score from mean normalised expression values. Genes are grouped into several functional gene sets but analysed altogether. **(B)** HMC3 human microglia cells were treated for 48h with mNI, moHSV, or moHSV/P2G (n=3 in each group) were analysed for angiogenic gene expression by RT-qPCR, normalised to mNI control. **(C)** HUVECs were pre-treated for 24 h with conditioned media, harvested, and seeded onto polymerized Matrigel. Tube formation was quantified by counting branch points using ImageJ and normalized to the condition with the highest number of branch points. Role of microglia and glioblastoma crosstalk: conditioned media from 72h coculture composed of 2/3 HMC3 and 1/3 GB138 (mNI Coculture) was compared to mNI (GB138), conditioned media from HMC3 culture (mNI HMC3), and coculture media infected for 72h with oHSV (moHSV Coculture) or oHSV/P2G (moHSV/P2G Coculture).
Each dot represents one flask of cells treated with a single batch of conditioned media **(B)**, or the mean of five images from independent wells **(C)**. Bars indicate mean ± SD. Statistical significance was determined by one-way ANOVA with Tukey's multiple-comparison test. *p<0.05, **p< 0.01, ****p<0.0001.

Figure 4

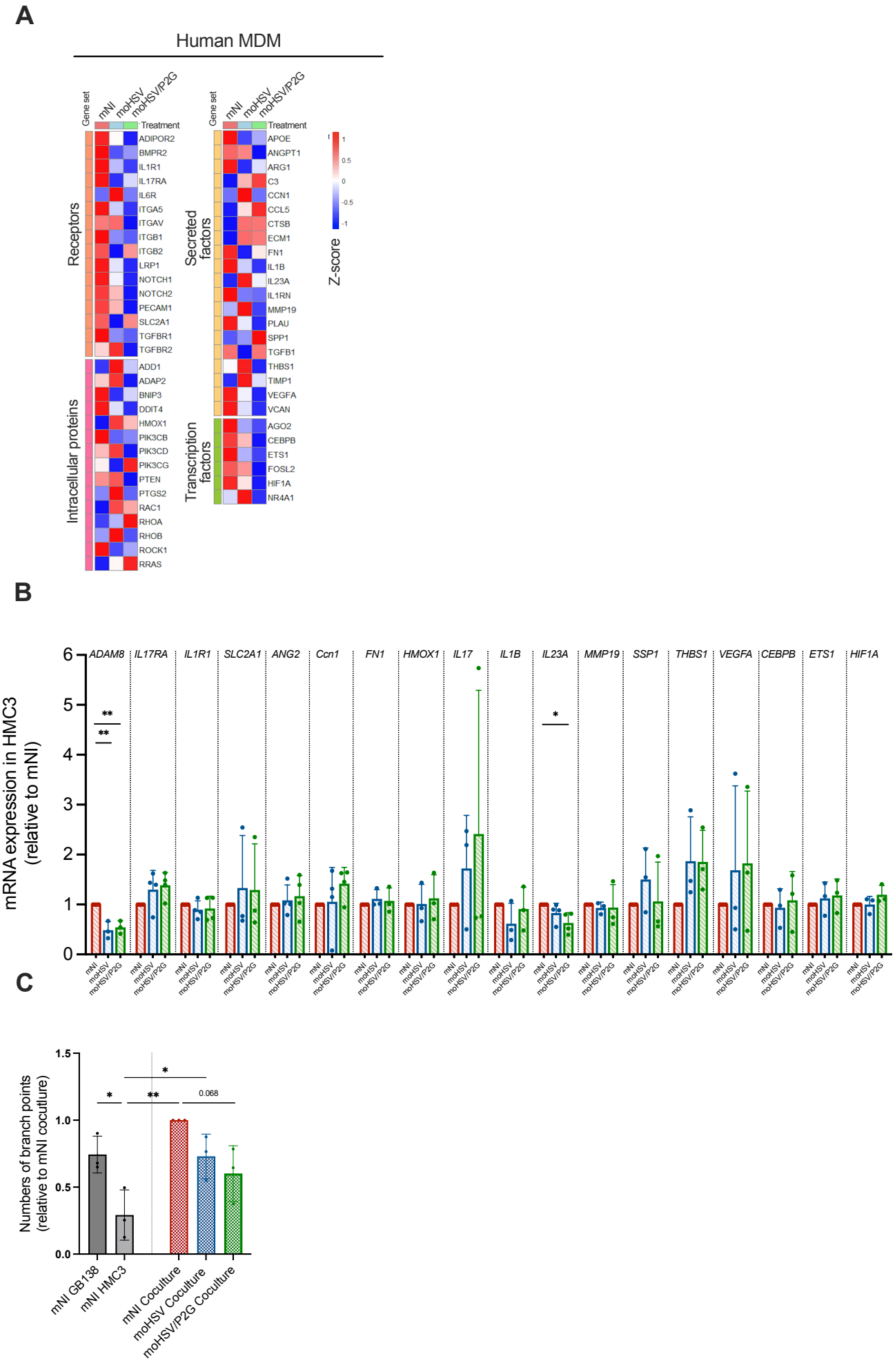
A
Human MDM
Gene set
mNI
moHSV
moHSV/P2G
Treatment
Receptors
ADIPOR2
BMPR2
IL1R1
IL17RA
IL6R
ITGA5
ITGAV
ITGB1
ITGB2
LRP1
NOTCH1
NOTCH2
PECAM1
SLC2A1
TGFBR1
TGFBR2
Intracellular proteins
ADD1
ADAP2
BNIP3
DDIT4
HMOX1
PIK3CB
PIK3CD
PIK3CG
PTEN
PTGS2
RAC1
RHOA
RHOB
ROCK1
RRAS
Secreted factors
APOE
ANGPT1
ARG1
C3
CCN1
CCL5
CTSB
ECM1
FN1
IL1B
IL23A
IL1RN
MMP19
PLAU
SPP1
TGFB1
THBS1
TIMP1
VEGFA
VCAN
Transcription factors
AGO2
CEBPB
ETS1
FOSL2
HIF1A
NR4A1
Z-score
1
0.5
0
-0.5
-1
B
mRNA expression in HMC3
(relative to mNI)
ADAM8
IL17RA
IL1R1
SLC2A1
ANG2
Ccn1
FN1
HMOX1
IL17
IL1B
IL23A
MMP19
SSP1
THBS1
VEGFA
CEBPB
ETS1
HIF1A
C
Numbers of branch points
(relative to mNI cocutlure)
0.068
mNI GB138
mNI HMC3
mNI Coculture
moHSV Coculture
moHSV/P2G Coculture

Conclusion

Overall, the *in vitro* and *in vivo* preliminary results helped us construct the following hypothesis. Glioblastoma tumour cells and immune cells establish a pro-angiogenic tumour microenvironment, which is controversially affected by oHSV and could potentially be effectively disrupted by oHSV/P2G infection. Given their preliminary nature, these results are not sufficient for an independent discussion. However, they will be addressed in the "global discussion" within the broader context of the thesis, in a section dedicated to the impact of oHSV/P2G on angiogenesis.

MATERIAL and METHODS

Cell lines

VERO cells (ATCC, CCL-81), human microglial clone 3 cells (HMC3, ATCC, CRL-3304), patient-derived human glioblastoma GB138 cells[45], and chemically induced murine glioblastoma GL261N4 cells transduced with human Nectin[46] were maintained in Dulbecco's Modified Eagle Medium, high glucose (DMEM HG; Biowest), supplemented with 10% foetal bovine serum (FBS; Gibco).

Human umbilical vein endothelial cells (HUVECs; Lonza) were cultured in EGM2 media consisting of EBM-2 medium (Lonza) supplemented with 10% FBS, hydrocortisone, human fibroblast growth factor (hFGF), vascular endothelial growth factor (VEGF), R3–insulin-like growth factor-1 (R3-IGF-1), ascorbic acid, and human epidermal growth factor (hEGF), according to the manufacturer's instructions. Culture flasks and plates for HUVECs were pre-coated with 0.2% gelatine solution (Sigma) diluted in PBS.

Construction of recombinant oHSVs.

Recombinant viruses were engineered using the fHsvQuik-1 bacterial artificial chromosome (BAC) containing an attenuated HSV-1 (strain F; Δγ34.5, ΔUL39, GFP^+; kind gift from A. Chiocca, University of Pittsburgh, USA). Additional ICP47 deletion was performed as described by Todo T *et al.*, 2001[47]. Recombinants were generated using the two-step Red recombination "en passant" technique[48]. A human CXCL12 mutant sequence (second amino acid substitution: Pro → Gly) flanked by the IL-2 signal peptide (5') and an HA tag (3'), under the control of the EF1α promoter, was inserted immediately downstream of the eGFP gene[49] VERO cells were transfected with this construct using JETPEI (Polyplus). Virus stocks were produced as previously described[50], ultracentrifuged (SW28 swinging-bucket rotor, Beckman Coulter; 17,000 rpm), resuspended in PBS (Cytiva) containing 10% glycerol, and stored at −80 °C. Viral titer was determined in VERO cells by plaque assay[51].

Virus and conditioned media production

GB138 or HMC3 cells, or coculture composed of 2/3 HMC3 and 1/3 GB138, were grown in DMEM HG 10% FBS. At 80% confluence, the medium was replaced with DMEM/F-12, and cells were either not infected (mNI) or infected at MOI of 1 with oHSV (mOHSV) or oHSV/P2G (mOHSV/P2G). After 72h, supernatants were collected, centrifuged (260 × g, 5 min), and filtered through a 0.1 µm membrane (Pall Corporation).

Tube Formation Assay

HUVECs were treated for 24 hours with the different conditioned media. Subsequently, pre-treated HUVECs were tripsinised to be seeded into sterile 96-well plate (8,000 cells/well, 100 µL culture media) precoated with 35 µL of polymerized Matrigel (Corning). The plate was then incubated (37°C, 6h) to allow for the formation of tubular structures. Images were acquired (Olympus microscope, 4× objective), and tube formation was quantified by counting the number of branch points using ImageJ software. The number of branch points was then normalised to the condition with the highest number of branch points, set to 1.

RT-qPCR

GB138 human glioblastoma and HMC3 microglial cells were cultured in DMEM HG (10% FBS, 1% P/S). GB138 cells were treated under conditions used to generate mNI, mOHSV, and mOHSV/P2G conditioned media. By contrast, HMC3 cells were treated for 48h with mNI, mOHSV, or mOHSV/P2G.

Total RNA was extracted using the NucleoSpin RNA kit (Macherey-Nagel). 1 µg of RNA was reverse transcribed using RevertAid H Minus First Strand cDNA Synthesis Kit (Thermo Scientific) with random primers. Human TBP was used as housekeeping gene. qPCR reactions were prepared with 10 ng cDNA (4 µL), Takyon No ROX SYBR MasterMix (5 µL; Eurogentec), and primers (0.5 µL, 4 µM each). Amplification was performed on a Roche LightCycler480 (Roche; 95 °C, 3 min; 45 cycles of 95 °C, 3 s and 60 °C, 25 s).

Bulk RNA sequencing of monocytes-derived-macrophages

Fresh human PBMCs were obtained from healthy donors (Red Cross, Belgium) after informed consent. All procedures were approved by the Ethics Committee of the University of Liège. $CD14^+$ monocytes were isolated using the EasySep Human CD14 Positive Selection Kit II (StemCell Technologies). Cells were cultured in RPMI (VWR) supplemented with 20% FBS and 100 ng/mL M-CSF (Miltenyi Biotec) for 5 days, then polarized in conditioned medium supplemented 100 ng/mL M-CSF for 48h. Total RNA was extracted using the NucleoSpin RNA kit (Macherey-Nagel).

Bulk RNA sequencing of polyadenylated mRNA was performed by the GIGA-Genomics platform using Illumina high throughput sequencer (Illumina mRNA stranded ligation Kit;

Novaseq Sequencing V1.5). Data was analysed with DESeq2 in collaboration with the GIGA-Bioinformatics platform.

In vivo experiments

All animal procedures were approved by the Animal Ethical Committee of the University of Liège, in accordance with the Belgian Ministry of Agriculture and the European Commission Laboratory Animal Care and Use Regulation. Six-week-old female C57BL/6NRj mice (JANVIER) were housed in sterilized, filter-topped cages under controlled temperature (22°C) and a 12h light/dark cycle. After one week of acclimatization, 1×10^5 GL261N4 cells in 2 µL PBS were injected into the right striatum (0.5 mm anterior and 2 mm lateral to bregma, depth 2.5 mm) under isoflurane anaesthesia (1–3%; Isoflutek®, Alivira Laboratoire Karizoo). On Day 7 and 14 post-engraftment, PBS (control) or oncolytic viruses (oHSV or oHSV/P2G; 10^6 PFU in 2µl PBS) were injected into the tumour using the same stereotactic coordinates. Mice were monitored daily for weight and behaviour, with weight recorded weekly or more frequently as needed. On day 21, mice were euthanized by intraperitoneal injection of Euthasol VET (140 mg/kg; Kela Veterinaria).

ARRIVE 2.0[52] reporting guideline was used to assure the adequate management of animals.

Immunofluorescence

Following euthanasia, mice were perfused intracardially with saline followed by 4% paraformaldehyde (PFA; Carl Roth) in PBS. Brains were incubated in 30% sucrose (Fisher Chemical; 48h, 4°C) and embedded in Neg-50™ (Epredia; -80°C). Serial coronal sections (14 µm) were collected on adhesion slides (SuperFrost Plus™, Epredia) using a CryoStar™ NX70 cryostat (Epredia). For immunofluorescence (n=4 for PBS and oHSV, n=5 for oHSV/P2G), sections were treated for antigen retrieval (Tris–EDTA buffer, pH 9), permeabilization with 0.1% Triton X-100 (VWR) in PBS, and autofluorescence quenching with TrueBlack® Lipofuscin Quencher (Biotium). Slides were then blocked (10% FBS in PBS), incubated with primary antibodies overnight at 4°C, and with secondary antibodies for 1h at room temperature. Nuclei were counterstained with Hoechst (Sigma-Aldrich). Image analysis was performed using machine learning in QuPath for brain stroma, tumour, and vessel segmentation ($CD31^+$).

Immune cells isolation

Following euthanasia and intracardiac perfusion with saline, brains were collected in RPMI medium (VWR) on ice. Tissues were digested with collagenase D (2 mg/mL; Roche) and DNase I (10 ng/µL; Roche) at 37°C for 30 min, then passed through 70 µm cell strainers (Fisherbrand™) and centrifuged. Pellets were resuspended in 90% Percoll (Cytiva) and subjected to density gradient centrifugation with layers of 90%, 60%, 40%

Percoll, and PBS (500 × g, 15 min, acc 3, dec off). Myelin was removed, and cells were collected from the 40%-60% interface, washed with PBS, and centrifuged to remove residual Percoll.

Single-cell RNA sequencing

Following immune cell isolation (n=4 per treatment, each sample corresponding to a pool of three mice), cells were processed using the Chromium Next GEM Single Cell Fixed RNA Sample Preparation Kit (10x Genomics; 16 reactions; PN-1000414) and sequenced on a Novaseq Sequencing V1.5 (Illumina) in collaboration with the GIGA-Genomics platform. Data processing and sample multiplexing were performed by the GIGA-Bioinformatics platform. Downstream analysis was conducted using RStudio with the Seurat package. Cells were filtered using standard thresholds (300–7,500 genes; <2% mitochondrial content; genes expressed in ≥3 cells). Data were log-normalized (scale factor 10,000), and 2,000 highly variable genes were selected. PCA was performed, and significant components were determined using JackStraw and ElbowPlot analyses. Clustering was conducted using an SNN graph, and visualization was performed using UMAP. Cell-type annotation was performed based on cluster-specific differentially expressed marker genes identified by the FindAllMarkers function in Seurat. Phenotypic assignments were also validated using Seurat's AddModuleScore function to compute scores for each profile based on gene sets from the MSigDB Mouse collections, accessible via the GSEA website. Pseudobulk analysis was performed using AggregateExpression function and visualised as z-score heatmaps for representative markers using AverageExpression (when needed) and pheatmap functions.

In Appendix 1, after supplementary figures, the top 50 differentially expressed marker genes of each cluster are presented. They were identified with the command *FindAllMarkers(object, only.pos = TRUE, min.pct = 0.25, logfc.threshold = 0.25)*. This selects genes that are upregulated in each cluster, expressed in at least 25% of cells, and exhibiting a minimum log fold change of 0.25.

Statistical analysis

All statistical analyses were performed using GraphPad Prism 10. Data are presented as box plots, with whiskers indicating minimum and maximum values. For independent measures within a graph, one-way ANOVAs were conducted separately for each group. In heatmaps, all angiogenic genes were analysed as a single homogeneous group using one-way ANOVAs (Table 2, 3). Statistical significance was indicated as * for $p < 0.05$, ** for $p < 0.01$, *** for $p < 0.001$.

REFERENCES

1. Louis, D.N., Perry, A., Wesseling, P., Brat, D.J., Cree, I.A., Figarella-Branger, D., Hawkins, C., Ng, H.K., Pfister, S.M., Reifenberger, G., et al. (2021). The 2021 WHO Classification of Tumors of the Central Nervous System: a summary. Neuro-Oncol. *23*, 1231–1251. https://doi.org/10.1093/neuonc/noab106.

2. Stupp, R., Mason, W.P., Bent, M.J. van den, Weller, M., Fisher, B., Taphoorn, M.J.B., Belanger, K., Brandes, A.A., Marosi, C., Bogdahn, U., et al. (2005). Radiotherapy plus Concomitant and Adjuvant Temozolomide for Glioblastoma. N. Engl. J. Med. *352*, 987–996. https://doi.org/10.1056/NEJMoa043330.

3. Sim, H.-W., Morgan, E.R., and Mason, W.P. (2018). Contemporary management of high-grade gliomas. CNS Oncol. *7*, 51–65. https://doi.org/10.2217/cns-2017-0026.

4. Goenka, A., Tiek, D., Song, X., Huang, T., Hu, B., and Cheng, S.-Y. (2021). The Many Facets of Therapy Resistance and Tumor Recurrence in Glioblastoma. Cells *10*, 484. https://doi.org/10.3390/cells10030484.

5. Prager, B.C., Bhargava, S., Mahadev, V., Hubert, C.G., and Rich, J.N. (2020). Glioblastoma Stem Cells: Driving Resiliency through Chaos. Trends Cancer *6*, 223–235. https://doi.org/10.1016/j.trecan.2020.01.009.

6. Goffart, N., Kroonen, J., and Rogister, B. (2013). Glioblastoma-Initiating Cells: Relationship with Neural Stem Cells and the Micro-Environment. Cancers *5*, 1049–1071. https://doi.org/10.3390/cancers5031049.

7. Biserova, K., Jakovlevs, A., Uljanovs, R., and Strumfa, I. (2021). Cancer Stem Cells: Significance in Origin, Pathogenesis and Treatment of Glioblastoma. Cells *10*, 621. https://doi.org/10.3390/cells10030621.

8. Tang, J., Karbhari, N., and Campian, J.L. (2025). Therapeutic Targets in Glioblastoma: Molecular Pathways, Emerging Strategies, and Future Directions. Cells *14*, 494. https://doi.org/10.3390/cells14070494.

9. López-Gil, J.C., Martin-Hijano, L., Hermann, P.C., and Sainz, B. (2021). The CXCL12 Crossroads in Cancer Stem Cells and Their Niche. Cancers *13*, 469. https://doi.org/10.3390/cancers13030469.

10. Ahmedna, T., Khela, H., Weber-Levine, C., Azad, T.D., Jackson, C.M., Gabrielson, K., Bettegowda, C., and Rincon-Torroella, J. (2023). The Role of γδ T-Lymphocytes in Glioblastoma: Current Trends and Future Directions. Cancers *15*, 5784. https://doi.org/10.3390/cancers15245784.

11. McLean, H., Drill, M., Sequeira, R., Jayakrishnan, P.C., Jeffree, R.L., Hunn, M., O'Brien, T.J., Hamilton, J., and Monif, M. (2025). Harnessing the innate immune system for

glioblastoma therapeutics. J. Neuroimmunol. *407*, 578713. https://doi.org/10.1016/j.jneuroim.2025.578713.

12. Palanivelu, L., Liu, C.-H., and Lin, L.-T. (2023). Immunogenic cell death: The cornerstone of oncolytic viro-immunotherapy. Front. Immunol. *13*, 1038226. https://doi.org/10.3389/fimmu.2022.1038226.

13. Sharma, P., Aaroe, A., Liang, J., and Puduvalli, V.K. (2023). Tumor microenvironment in glioblastoma: Current and emerging concepts. Neuro-Oncol. Adv. *5*, vdad009. https://doi.org/10.1093/noajnl/vdad009.

14. Wu, B., Zhang, B., Li, B., Wu, H., and Jiang, M. (2024). Cold and hot tumors: from molecular mechanisms to targeted therapy. Signal Transduct. Target. Ther. *9*, 274. https://doi.org/10.1038/s41392-024-01979-x.

15. Hu, Q., Zhu, Y., Mei, J., Liu, Y., and Zhou, G. (2025). Extracellular matrix dynamics in tumor immunoregulation: from tumor microenvironment to immunotherapy. J. Hematol. Oncol.J Hematol Oncol *18*, 65. https://doi.org/10.1186/s13045-025-01717-y.

16. Dapash, M., Hou, D., Castro, B., Lee-Chang, C., and Lesniak, M.S. (2021). The Interplay between Glioblastoma and Its Microenvironment. Cells *10*, 2257. https://doi.org/10.3390/cells10092257.

17. Henke, E., Nandigama, R., and Ergün, S. (2020). Extracellular Matrix in the Tumor Microenvironment and Its Impact on Cancer Therapy. Front. Mol. Biosci. *6*. https://doi.org/10.3389/fmolb.2019.00160.

18. Ma, R.-Y., Black, A., and Qian, B.-Z. (2022). Macrophage diversity in cancer revisited in the era of single-cell omics. Trends Immunol. *43*, 546–563. https://doi.org/10.1016/j.it.2022.04.008.

19. Łaszczych, D., Czernicka, A., Gostomczyk, K., Szylberg, Ł., and Borowczak, J. (2024). The role of IL-17 in the pathogenesis and treatment of glioblastoma—an update on the state of the art and future perspectives. Med. Oncol. Northwood Lond. Engl. *41*, 187. https://doi.org/10.1007/s12032-024-02434-1.

20. Choi, H., Kim, T.-G., Jeun, S.-S., and Ahn, S. (2023). Human gamma-delta (γδ) T cell therapy for glioblastoma: A novel alternative to overcome challenges of adoptive immune cell therapy. Cancer Lett. *571*, 216335. https://doi.org/10.1016/j.canlet.2023.216335.

21. Cohen, M.H., Shen, Y.L., Keegan, P., and Pazdur, R. (2009). FDA drug approval summary: bevacizumab (Avastin) as treatment of recurrent glioblastoma multiforme. The Oncologist *14*, 1131–1138. https://doi.org/10.1634/theoncologist.2009-0121.

22. Reardon, D.A., Brandes, A.A., Omuro, A., Mulholland, P., Lim, M., Wick, A., Baehring, J., Ahluwalia, M.S., Roth, P., Bähr, O., et al. (2020). Effect of Nivolumab vs Bevacizumab in Patients With Recurrent Glioblastoma: The CheckMate 143 Phase 3

Randomized Clinical Trial. JAMA Oncol. *6*, 1003–1010. https://doi.org/10.1001/jamaoncol.2020.1024.

23. Vredenburgh, J.J., Desjardins, A., Herndon, J.E., II, Dowell, J.M., Reardon, D.A., Quinn, J.A., Rich, J.N., Sathornsumetee, S., Gururangan, S., Wagner, M., et al. (2007). Phase II Trial of Bevacizumab and Irinotecan in Recurrent Malignant Glioma. Clin. Cancer Res. *13*, 1253–1259. https://doi.org/10.1158/1078-0432.CCR-06-2309.

24. Cao, T., Gu, Y., Yagmurlu, B., Yerraballa, H., Bertrand, S., Naya, L., Miller, K., Iv, M., Soltys, S., Patel, C., et al. (2024). A phase II study of plerixafor combined with whole brain radiation therapy (WBRT) for patients with newly diagnosed glioblastoma. J. Clin. Oncol. *42*, 2075–2075. https://doi.org/10.1200/JCO.2024.42.16_suppl.2075.

25. Wen, P.Y. (2017). Phase I Study of Plerixafor (AMD3100) and Bevacizumab for Recurrent High-Grade Glioma (clinicaltrials.gov).

26. Gimple, R.C., Bhargava, S., Dixit, D., and Rich, J.N. (2019). Glioblastoma stem cells: lessons from the tumor hierarchy in a lethal cancer. Genes Dev. *33*, 591–609. https://doi.org/10.1101/gad.324301.119.

27. Goffart, N., Lombard, A., Lallemand, F., Kroonen, J., Nassen, J., Di Valentin, E., Berendsen, S., Dedobbeleer, M., Willems, E., Robe, P., et al. (2017). CXCL12 mediates glioblastoma resistance to radiotherapy in the subventricular zone. Neuro-Oncol. *19*, 66–77. https://doi.org/10.1093/neuonc/now136.

28. Cai, X., Chen, R., Ma, K., Wang, F., Zhou, Y., Wang, Y., and Jiang, T. (2020). Identification of the CXCL12–CXCR4/CXCR7 axis as a potential therapeutic target for immunomodulating macrophage polarization and foreign body response to implanted biomaterials. Appl. Mater. Today *18*, 100454. https://doi.org/10.1016/j.apmt.2019.100454.

29. Shi, Y., Riese, D.J., and Shen, J. (2020). The Role of the CXCL12/CXCR4/CXCR7 Chemokine Axis in Cancer. Front. Pharmacol. *11*. https://doi.org/10.3389/fphar.2020.574667.

30. Paolo, D., Maxime, D., Judit, S.G., Cédric, L., Alexandre, H., Benoit, B., Arnaud, L., Bernard, R., Virginie, N., Marielle, L., et al. (2025). An oncolytic herpesvirus expressing a CXCR4 antagonist interferes with glioblastoma cells' stemness features and migration. Mol. Ther. Oncol. *33*, 201083. https://doi.org/10.1016/j.omton.2025.201083.

31. Crump, M.P., Gong, J.H., Loetscher, P., Rajarathnam, K., Amara, A., Arenzana-Seisdedos, F., Virelizier, J.L., Baggiolini, M., Sykes, B.D., and Clark-Lewis, I. (1997). Solution structure and basis for functional activity of stromal cell-derived factor-1; dissociation of CXCR4 activation from binding and inhibition of HIV-1. EMBO J. *16*, 6996–7007. https://doi.org/10.1093/emboj/16.23.6996.

445 32. Tirone, M., Tran, N.L., Ceriotti, C., Gorzanelli, A., Canepari, M., Bottinelli, R.,
446 Raucci, A., Di Maggio, S., Santiago, C., Mellado, M., et al. (2018). High mobility group box
447 1 orchestrates tissue regeneration via CXCR4. J. Exp. Med. *215*, 303–318.
448 https://doi.org/10.1084/jem.20160217.

449 33. Li, J.-K., Yu, L., Shen, Y., Zhou, L.-S., Wang, Y.-C., and Zhang, J.-H. (2008). Inhibition
450 of CXCR4 activity with AMD3100 decreases invasion of human colorectal cancer cells in
451 vitro. World J. Gastroenterol. WJG *14*, 2308–2313. https://doi.org/10.3748/wjg.14.2308.

452 34. Sanchez Gil, J. (2022). Design and characterization of a CXCR4-retargeted and
453 sTRAILarmed oncolytic HSV-1 to attack Glioblastoma stem-like cells (GSCs).

454 35. Chiocca, E.A., Nakashima, H., Kasai, K., Fernandez, S.A., and Oglesbee, M. (2020).
455 Preclinical Toxicology of rQNestin34.5v.2: An Oncolytic Herpes Virus with Transcriptional
456 Regulation of the ICP34.5 Neurovirulence Gene. Mol. Ther. Methods Clin. Dev. *17*, 871–
457 893. https://doi.org/10.1016/j.omtm.2020.03.028.

458 36. Ghonime, M.G., Saini, U., Kelly, M.C., Roth, J.C., Wang, P.-Y., Chen, C.-Y., Miller, K.,
459 Hernandez-Aguirre, I., Kim, Y., Mo, X., et al. (2021). Eliciting an immune-mediated
460 antitumor response through oncolytic herpes simplex virus-based shared antigen
461 expression in tumors resistant to viroimmunotherapy. J. Immunother. Cancer *9*.
462 https://doi.org/10.1136/jitc-2021-002939.

463 37. Sanchez Gil, J., Dubois, M., Neirinckx, V., Lombard, A., Coppieters, N., D'Arrigo, P.,
464 Isci, D., Aldenhoff, T., Brouwers, B., Lassence, C., et al. (2022). Nanobody-based
465 retargeting of an oncolytic herpesvirus for eliminating CXCR4+ GBM cells: A proof of
466 principle. Mol. Ther. Oncolytics *26*, 35–48. https://doi.org/10.1016/j.omto.2022.06.002.

467 38. Tripathy, D.K., Panda, L.P., Biswal, S., and Barhwal, K. (2024). Insights into the
468 glioblastoma tumor microenvironment: current and emerging therapeutic approaches.
469 Front. Pharmacol. *15*. https://doi.org/10.3389/fphar.2024.1355242.

470 39. Liu, Y., Zhou, F., Ali, H., Lathia, J.D., and Chen, P. (2024). Immunotherapy for
471 glioblastoma: current state, challenges, and future perspectives. Cell. Mol. Immunol. *21*,
472 1354–1375. https://doi.org/10.1038/s41423-024-01226-x.

473 40. Medikonda, R., Dunn, G., Rahman, M., Fecci, P., and Lim, M. (2021). A review of
474 glioblastoma immunotherapy. J. Neurooncol. *151*, 41–53.
475 https://doi.org/10.1007/s11060-020-03448-1.

476 41. Laureano, R.S., Vanmeerbeek, I., Sprooten, J., Govaerts, J., Naulaerts, S., and
477 Garg, A.D. (2024). The cell stress and immunity cycle in cancer: Toward next generation of
478 cancer immunotherapy. Immunol. Rev. *321*, 71–93. https://doi.org/10.1111/imr.13287.

42. Todo, T., Ito, H., Ino, Y., Ohtsu, H., Ota, Y., Shibahara, J., and Tanaka, M. (2022). Intratumoral oncolytic herpes virus G47Δ for residual or recurrent glioblastoma: a phase 2 trial. Nat. Med. *28*, 1630–1639. https://doi.org/10.1038/s41591-022-01897-x.

43. Aghi, M., Rabkin, S.D., and Martuza, R.L. (2007). Angiogenic Response Caused by Oncolytic Herpes Simplex Virus–Induced Reduced Thrombospondin Expression Can Be Prevented by Specific Viral Mutations or by Administering a Thrombospondin-Derived Peptide. Cancer Res. *67*, 440–444. https://doi.org/10.1158/0008-5472.CAN-06-3145.

44. Kurozumi, K., Hardcastle, J., Thakur, R., Shroll, J., Nowicki, M., Otsuki, A., Chiocca, E.A., and Kaur, B. (2008). Oncolytic HSV-1 Infection of Tumors Induces Angiogenesis and Upregulates CYR61. Mol. Ther. J. Am. Soc. Gene Ther. *16*, 1382–1391. https://doi.org/10.1038/mt.2008.112.

45. Kroonen, J., Nassen, J., Boulanger, Y.-G., Provenzano, F., Capraro, V., Bours, V., Martin, D., Deprez, M., Robe, P., and Rogister, B. (2011). Human glioblastoma-initiating cells invade specifically the subventricular zones and olfactory bulbs of mice after striatal injection. Int. J. Cancer *129*. https://doi.org/10.1002/ijc.25709.

46. Szatmári, T., Lumniczky, K., Désaknai, S., Trajcevski, S., Hídvégi, E.J., Hamada, H., and Sáfrány, G. (2006). Detailed characterization of the mouse glioma 261 tumor model for experimental glioblastoma therapy. Cancer Sci. *97*, 546–553. https://doi.org/10.1111/j.1349-7006.2006.00208.x.

47. Todo, T., Martuza, R.L., Rabkin, S.D., and Johnson, P.A. (2001). Oncolytic herpes simplex virus vector with enhanced MHC class I presentation and tumor cell killing. Proc. Natl. Acad. Sci. U. S. A. *98*, 6396–6401. https://doi.org/10.1073/pnas.101136398.

48. Tischer, B.K., Kaufer, B.B., Sommer, M., Wussow, F., Arvin, A.M., and Osterrieder, N. (2007). A Self-Excisable Infectious Bacterial Artificial Chromosome Clone of Varicella-Zoster Virus Allows Analysis of the Essential Tegument Protein Encoded by ORF9. J. Virol. *81*, 13200–13208. https://doi.org/10.1128/jvi.01148-07.

49. Paolo, D., Maxime, D., Judit, S.G., Cédric, L., Benoit, B., Arnaud, L., Bernard, R., Virginie, N., Marielle, L., and Catherine, S.-D. (2025). An oncolytic herpesvirus expressing a CXCR4 antagonist interferes with Glioblastoma cells stemness features and migration. Preprint at bioRxiv, https://doi.org/10.1101/2025.05.21.655102 https://doi.org/10.1101/2025.05.21.655102.

50. Goins, W.F., Huang, S., Hall, B., Marzulli, M., Cohen, J.B., and Glorioso, J.C. (2020). Engineering HSV-1 Vectors for Gene Therapy. In Herpes Simplex Virus : Methods and Protocols, R. J. Diefenbach and C. Fraefel, eds. (Springer), pp. 73–90. https://doi.org/10.1007/978-1-4939-9814-2_4.

514 51. Marconi, P., and Manservigi, R. (2014). Herpes Simplex Virus Growth, Preparation,
515 and Assay. In Herpes Simplex Virus: Methods and Protocols, R. J. Diefenbach and C.
516 Fraefel, eds. (Springer), pp. 19–29. https://doi.org/10.1007/978-1-4939-0428-0_2.

517 52. Sert, N.P. du, Hurst, V., Ahluwalia, A., Alam, S., Avey, M.T., Baker, M., Browne, W.J.,
518 Clark, A., Cuthill, I.C., Dirnagl, U., et al. (2020). The ARRIVE guidelines 2.0: Updated
519 guidelines for reporting animal research. PLOS Biol. *18*, e3000410.
520 https://doi.org/10.1371/journal.pbio.3000410.

521 SUPPLEMENTARY FIGURE LEGENDS

522 Figure S1: oHSV polarise macrophages towards an anti-
523 inflammatory and pro-angiogenic phenotype

524 List of genes adapted from MSigDB Mouse collections related to pro-inflammatory (M1-
525 like), anti-inflammatory (M2-like) and pro-angiogenic macrophages. Genes were filtered
526 for mean normalised expression values of more than 0.25, before computing expression
527 scores via Seurat's AddModuleScore function.

Figure S1

Category	MSigDB Mouse collections Genes	Filtered Genes
Pro-inflammation	Aim2, Adgre1, App, Axl, B2m, C3, Ccl1, Cfb, Cd36, Cd38, Cd40, Cd48, Cd68, Cd74, Cd80, Cd86, Calhm6, Clec4e, Clec5a, Cxcl10, Cxcl9, Cxcr3, Cxcr6, Gbp2, Gbp3, Gbp4, Gbp5, H2-Ab1, H2-Aa, H2-D1, H2-DMb1, H2-DMb2, H2-Eb1, H2-K1, H2-Oa, H2-Ob, Fcgr1, Fcgr2b, Fcgr3, Fcgr4, Hif1a, Icam1, Ido1, Ifi204, Ifi205, Ifit2, Ifit3, Ifitm1, Ifng, Ifngr1, Ifngr2, Irf1, Irf5, Isg15, Isg20, Il1b, Il12a, Il18, Il3ra, Il31ra, Il6, Inhba, Jak3, Limk2, Lyz2, Marco, Mertk, Msr1, Ncf1, Nampt, Nos2, Oas2, Osm, Sod2, Socs1, Stat1, Stat4, Tap1, Tap2, Tgm2, Tnf, Tnfsf13, Tnfrsf9, Tlr2, Tlr4, Tlr8, Ubd, Vamp5, Zbp1	Aim2, Adgre1, App, Axl, B2m, C3, Cfb, Cd38, Cd40, Cd48, Cd68, Cd74, Cd80, Cd86, Calhm6, Clec4e, Clec5a, Cxcl10, Cxcl9, Gbp2, Gbp3, Gbp4, Gbp5, H2-Ab1, H2-Aa, H2-D1, H2-DMb1, H2-Eb1, H2-K1, Fcgr1, Fcgr2b, Fcgr3, Fcgr4, Hif1a, Icam1, Ifi204, Ifi205, Ifit2, Ifit3, Ifitm1, Ifngr1, Ifngr2, Irf1, Irf5, Isg15, Isg20, Il1b, Il18, Il3ra, Jak3, Lyz2, Mertk, Msr1, Ncf1, Nampt, Nos2, Oas2, Osm, Sod2, Socs1, Stat1, Tap1, Tap2, Tgm2, Tnfsf13, Tlr2, Tlr4, Zbp1
Anti-Inflammation	Adam12, Akap5, Alox15, Arg1, Ccl17, Ccl4, Cd163, Cd163l1, Cd209a, Cd274, Cd276, Cd93, Chil3, Chil4, Clec10a, Clec5a, Ctla4, Cyp27b1, Ehf, Fabp4, Fbln5, Fcer1a, Fn1, Guca1a, Havcr2, Hmox1, Homer2, Il10, Il4ra, Irf4, Kdm6b, Klf4, Lag3, Maf, Map1a, Mcemp1, Mertk, Mmp12, Mmp14, Mmp2, Mmp9, Mt1, Mt2, Mrc1, Ms4a7, Myc, Nt5e, Pdcd1, Pdcd1lg2, Pparg, Ppard, Ramp1, Retnla, Sirpa, Slc16a10, Slamf1, Socs1, Socs3, Spon2, Stat1, Stat3, Stat6, Tgfb1, Tgfb2, Tgfb3, Thbd, Thbs1, Tgm2, Tigit, Tnc, Vegfa, Vcan	Arg1, Ccl4, Cd274, Cd93, Chil3, Clec5a, Fn1, Havcr2, Hmox1, Il4ra, Kdm6b, Klf4, Maf, Mertk, Mmp14, Mt1, Mrc1, Ms4a7, Myc, Pdcd1lg2, Sirpa, Socs1, Socs3, Stat1, Stat3, Stat6, Tgfb1, Thbs1, Tgm2, Vegfa
Angiogenesis	Abcc8, Abcc9, Abi3bp, Abl1, Abl2, Acacb, Acadm, Acan, Ace, Ackr3, Actc1, Actg1, Actn2, Acvr1, Acvr1b, Acvr2b, Acvrl1, Adam10, Adam12, Adam15, Adam19, Adam8, Adamts1, Adamts5, Adamts6, Adamts9, Adap2, Add1, Adgra2, Adgrb1, Adgrb2, Adgrb3, Adgrf4, Adgrf5, Adgrg1, Adgrg6, Adipor2, Adm, Adm2, Adra1a, Adra1b, Adra2b, Adrb1, Adrb2, Adtrp, Aggf1, Ago1, Ago2, Agt, Agtr1a, Agtr1b, Agtr2, Ahr, Aimp1, Akap13, Akap6, Akt1, Akt3, Aldh1a2, Alox5, Alpk3, Amhr2, Amot, Amotl1, Amotl2, Ang, Ang2, Ang4, Ang5, Ang6, Angpt1, Angpt2, Angpt4, Angptl3, Angptl4, Angptl6, Angptl7, Ank2, Ankrd1, Ankrd17, Anks6, Anp32b, Anpep, Antxr1, Anxa1, Anxa2, Anxa3, Ap1b1, Ap2b1, Apc, Apela, Apln, Aplnr, Apob, Apoe, Apold1, Aqp1, Arg1, Arhgap22, Arhgap24, Arhgef15, Arid1a, Arid2, Arl13b, Arrb2, Asb2, Asb4, Asxl1, Asxl2, Atf2, Atf7, Atg5, Atg7, Atm, Atp2b4, Atp7a, AW551984, Axin2, B4galt1, B9d1, Bak1, Bax, Bbs7, Bcas3, Becn1, Bicc1, Bmp10, Bmp2, Bmp4, Bmp5, Bmp7, Bmper, Bmpr1a, Bmpr2, Brca1, Brpf1, Bsg, Btg1, Bves, C1galt1, C2cd3, C3, C3ar1, C5ar1, C6, Cacna1c, Cacybp, Calcrl, Cald1, Camk2d, Camp, Card10, Casp3, Casp7, Casp8, Cav1, Cav3, Cavin4, Cby1, Cc2d2a, Ccbe1, Ccdc103, Ccdc134, Ccdc39, Ccdc40, Ccl11, Ccl12, Ccl2, Ccl24, Ccl5, Ccm2, Ccm2l, Ccn1, Ccn2, Ccn3, Ccn4, Ccn6, Ccnd2, Ccr2, Ccr3, Cd160, Cd24a, Cd34, Cd38, Cd40, Cd47, Cd59a, Cdc42, Cdh13, Cdh2, Cdh5, Cdk1, Cdkn1a, Cdkn1b, Cdx2, Cdx4, Ceacam1, Cela1, Cemip2, Cep290, Cer1, Cfc1, Cfd, Cfh, Cflar, Chd7, Chm, Chrd, Cib1, Cited1, Cited2, Cldn5, Clec14a, Clic4, Cluap1, Cma1, Cnmd, Cntrl, Col11a1, Col14a1, Col18a1, Col1a1, Col1a2, Col27a1, Col2a1, Col3a1, Col4a1, Col4a2, Col4a3, Col5a1, Col6a1, Col8a1, Col8a2, Comp, Comt, Cpe, Cplane1, Crb2, Creb1, Creb3l1, Crhr2, Cspg4, Csrp3, Ctcf, Ctdp1, Cth, Ctnnb1, Ctsh, Cul7, Cx3cl1, Cxadr, Cxcl10, Cxcl12, Cxcl17, Cxcr2, Cxcr3, Cxcr4, Cybb, Cyp1b1, Cysltr1, Cysltr2, Dab2ip, Dag1, Dand5, Daw1, Dchs1, Dcn, Dctn5, Ddah1, Ddit3, Ddit4, Ddx39b, Dhcr7, Dhrs3, Dhx36, Dicer1, Dipk2a, Dkk1, Dlc1, Dll1, Dll4, Dlx3, Dnaaf1, Dnaaf3, Dnaaf4, Dnah11, Dnah5, Dnm2, Dnmt1, Drc1, Dsg2, Dsp, Dusp6, Dvl1, Dvl2, Dvl3, Dyrk1a, Dysf, Dzip1, E2f2, E2f7, E2f8, Ece1, Ecm1, Ecscr, Edn1, Edn2, Ednra, Efemp2, Efna1, Efna3, Efnb2, Egf, Egfl7, Egfr, Egln1, Egln3, Egr1, Egr2, Egr3, Eif2ak3, Elk3, Eln, Emc10, Emilin1, Emilin2, Emp2, Eng, Enpep, Enpp1, Eomes, Ep300, Epas1, Epgn, Epha1, Epha2, Epha3, Epha5, Ephb1, Ephb2, Ephb3, Ephb4, Epn1, Epn2, Epo, Epor, Erap1, Erbb2, Erbb3, Erbb4, Ereg, Errfi1, Esm1, Esx1, Ets1, Etv2, Ext1, Eya1, F3, Fadd, Fap, Fasl, Fat4, Fbln5, Fbn1, Fbxw7, Fbxw8, Fdps, Fgf1, Fgf10, Fgf15, Fgf18, Fgf2, Fgf20, Fgf3, Fgf6, Fgf8, Fgf9, Fgfbp1, Fgfr1, Fgfr2, Fgfrl1, Fhl2, Fhod3, Fkbp10, Fkbp1a, Fkbpl, Fkrp, Flna, Flrt2, Flrt3, Flt1, Flt4, Flvcr1, Flvcr2, Fmnl3, Fn1, Folr1, Fosl1, Fosl2, Foxc1, Foxc2, Foxf1, Foxh1, Foxj1, Foxj2, Foxl1, Foxm1, Foxn1, Foxo1, Foxo4, Foxp1, Foxp4, Foxs1, Frem2, Frs2, Fut1, Fuz, Fzd1, Fzd2, Fzd4, Fzd5, Fzd7, Fzd8, G6pd2, G6pdx, Gaa, Gab1, Gadd45a, Gata2, Gata3, Gata4, Gata5, Gata6, Gatad2a, Gbx2, Gdf2, Ggnbp2, Ghsr, Gja1, Gja4, Gja5, Gja6, Gjc1, Gla, Gli1, Gli2, Gli3, Glmn, Glul, Gna11, Gna13, Gnaq, Gng5, Gpc3, Gper1, Gpld1, Gpr15, Gpr4, Gpx1, Greb1l, Grem1, Grhl2, Grk2, Grn, Gsk3a, Gsk3b, Gtf2i, Gys1, Hamp, Hamp2, Hand1, Hand2, Has2, Hbegf, Hc, Hdac2, Hdac3, Hdac5, Hdac7, Hdac9, Hectd1, Heg1, Hes1, Hexim1, Hey1, Hey2, Heyl, Hgf, Hgs, Hhex, Hhip, Hif1a, Hif3a, Hipk2, Hk2, Hmga2, Hmgb1, Hmox1, Hnrnpu, Hopx, Hoxa1, Hoxa13, Hoxa5, Hpgd, Hpse, Hrg, Hs6st1, Hspb1, Hspb6, Hspb7, Hspg2, Htatip2, Htr2b, Hyal1, Id1, Id2, Id3, Ier3, Ifng, Ift122, Ift140, Ift172, Ift20, Ift52, Ift57, Ift74, Ift88, Igf1, Igf2, Ihh, Il10, Il12a, Il12b, Il17a, Il17f, Il18, Il1a, Il1b, Il23a, Il6ra, Ilk, Immp2l, Inhba, Insr, Invs, Irx3, Irx4, Isl1, Ism1, Itga2b, Itga4, Itga5, Itga7, Itgav, Itgax, Itgb1, Itgb1bp1, Itgb2, Itgb2l, Itgb3, Itgb8, Jag1, Jak1, Jam3, Jarid2, Jcad, Jmjd6, Jmjd8, Jph2, Jun, Junb, Jup, Kat2a, Kat6a, Kcnj1, Kcnj11, Kcnj8, Kcnq1, Kctd10, Kdm2a, Kdm6a, Kdm6b, Kdr, Kif3a, Kif7, Kit, Klf2, Klf4, Klf5, Klk1b1, Krit1, Lama1, Lama4, Large1, Lbx1, Ldb3, Ldlr, Lef1, Lefty1, Lemd2, Lemd3, Lep, Lepr, Lgals3, Lgals8, Lif, Lipa, Llgl2, Lmna, Lmo4, Lox, Loxl2, Lrg1, Lrp1, Lrp2, Lrp5, Lrp6, Lrrc10, Lrrc27, Ltbp1, Luzp1, Ly6e, Lyl1, Maml1, Map2k1, Map2k2, Map2k4, Map2k5, Map3k3, Map3k7, Mapk1, Mapk11, Mapk14, Mapk3, Mapk7, Matr3, Mb, Mcam, Mdk, Mdm2, Mdm4, Mecom, Mecp2, Med1, Med12, Mef2a, Mef2b, Mef2c, Megf8, Meis1, Meox2, Mesp1, Mesp2, Met, Mfge8, Mia3, Mib1, Minar1, Minar2, Mixl1, Mks1, Mmp13, Mmp19, Mmp2, Mmp21, Mmp9, Mnat1, Mosmo, Mospd3, Mrtfb, Msx1, Msx2, Mtdh, Mterf4, Mthfd1, Mtor, Mybpc3, Mydgf, Myh10, Myh11, Myh6, Myh7, Myh9, Myl2, Myl3, Myl7, Mylk, Mylk2, Mylk3, Myo18b, Myo1e, Myocd, Myod1, Naa15, Naca, Naglu, Nat8f5, Naxe, Ncam1, Nckap1, Ncl, Ncoa6, Ncor2, Ndnf, Ndp, Ndrg4, Ndst1, Ndufs6, Ndufv2, Neb, Nebl, Nedd4, Nek8, Nf1, Nfatc1, Nfatc2, Nfatc3, Nfatc4, Nfe2, Nfe2l2, Nfix, Ngfr, Ngp, Ninj1, Nipbl, Nkx2-5, Nkx2-6, Nkx3-1, Nodal, Nog, Nos2, Notch1, Notch2, Notch3, Noto, Nox1, Nox4, Nphp3, Nppb, Nppc, Npr2, Npr3, Nprl3, Npy1r, Npy2r, Npy5r, Nr2e1, Nr2f2, Nr3c1, Nr4a1, Nrap, Nrarp, Nras, Nrg1, Nrp1, Nrp2, Nrxn1, Nsd2, Nsdhl, Ntrk1, Ntrk2, Ntrk3, Nus1, Nxn, Optc, Osr1, Otulin, Ovol2, Pak1, Pak4, Pank2, Parp2, Parva, Pax3, Pax6, Pax8, Paxip1, Pbrm1, Pcdha9, Pcnt, Pcsk5, Pdcd10, Pdcd4, Pdcd6, Pdcl3, Pde2a, Pde3b, Pdgfa, Pdgfb, Pdgfd, Pdgfra, Pdgfrb, Pdlim1, Pdlim2, Pdlim3, Pdlim4, Pdlim5, Pdlim7, Pdpn, Pds5a, Pecam1, Pgf, Pgk1, Pi16, Pik3c2a, Pik3ca, Pik3cb, Pik3cd, Pik3cg, Pik3r2, Pik3r3, Pik3r6, Pim1, Pin1, Pin1rt1, Pitx2, Pkd1, Pkd1l1, Pkd2, Pkm, Pknox1, Pkp2, Plau, Plcd1, Plcd3, Plcg1, Plec, Plg, Plk2, Pln, Plpp3, Plxna4, Plxnd1, Pml, Pnpla6, Pofut1, Poglut1, Popdc2, Popdc3, Pou4f1, Pou4f2, Ppara, Pparg, Ppp1r13l, Ppp1r15a, Ppp1r16b, Ppp3cb, Ppp3r1, Prcp, Prdm1, Prickle1, Prickle4, Prkar1a, Prkca, Prkcb, Prkd1, Prkd2, Prkdc, Prkx, Prl7d1, Prmt1, Prok1, Prok2, Prokr1, Prop1, Prox1, Prrx1, Prrx2, Psen1, Psg22, Pskh1, Ptcd2, Ptch1, Pten, Ptger4, Ptgis, Ptgs2, Ptk2, Ptk2b, Ptk7, Ptn, Ptpn11, Ptpn14, Ptprb, Ptprj, Ptprm, Pxdn, Pxn, Rac1, Ramp1, Ramp2, Rap1a, Rapgef1, Rapgef2, Rapgef3, Rara, Rarb, Rasa1, Rasip1, Rb1, Rb1cc1, Rbm10, Rbm15, Rbm20, Rbm24, Rbp4, Rbpj, Reck, Rela, Rest, Rgcc, Rgs2, Rgs4, Rhoa, Rhob, Rhoj, Ric8a, Rin2, Ripply3, Rnf207, Rnf213, Rnh1, Robo1, Robo2, Robo4, Rock1, Rock2, Rom1, Rora, Rpgrip1l, Rras, Rspo3, Rtl1, Rtn4, Runx1, Rxra, Rxrb, Ryr1, Ryr2, S100a1, S1pr1, Sall1, Sall4, Sash1, Sav1, Scg2, Scn11a, Scn5a, Scx, Sec24b, Sema3c, Sema3e, Sema4a, Sema5a, Sema6a, Senp2, Serpinb7, Serpine1, Serpinf1, Serpinf2, Setd2, Sfrp2, Sgcb, Sgcd, Sgcg, Sgcz, Sgpl1, Sh2b3, Sh3pxd2b, Shb, Shc1, Shh, Shox2, Sik1, Sin3b, Sirt1, Sirt6, Six1, Slc12a2, Slc1a1, Slc22a5, Slc25a4, Slc2a1, Slc2a10, Slc31a1, Slc39a12, Slc4a7, Slc8a1, Slc9a1, Slit2, Slit3, Slitrk5, Smad1, Smad2, Smad3, Smad4, Smad5, Smad6, Smad7, Smarca2, Smarca4, Smarcd3, Smg9, Smo, Smoc2, Smyd1, Smyd4, Snai1, Snai2, Snx17, Socs3, Sod2, Sorbs2, Sos1, Sox11, Sox17, Sox18, Sox4, Sox6, Sox9, Sp1, Sp100, Sp2, Sparc, Speg, Sphk1, Sphk2, Spi1, Spint1, Spp1, Spred1, Spry1, Spry2, Srf, Srpk2, Srpx2, Stab1, Stard13, Stat1, Stat3, Stil, Stim1, Stk11, Stk3, Stk4, Stra6, Sufu, Sulf1, Svep1, Syde1, Syk, Synb, Synj2bp, Synpo2l, Sypl2, Tab1, Tab2, Tafa5, Tal1, Tbc1d32, Tbx1, Tbx18, Tbx19, Tbx2, Tbx20, Tbx3, Tbx4, Tbx5, Tbx6, Tbxa2r, Tcap, Tcf21, Tcf4, Tcf7l2, Tead1, Tead2, Tek, Tenm4, Tert, Tfap2a, Tfap2b, Tgfa, Tgfb1, Tgfb2, Tgfb3, Tgfbr1, Tgfbr2, Tgfbr3, Tgm2, Th, Thbs1, Thbs2, Thsd7a, Thy1, Tie1, Tiparp, Tjp1, Tlr3, Tmed2, Tmem100, Tmem204, Tmem215, Tmem231, Tmem65, Tmem67, Tmem94, Tnf, Tnfaip2, Tnfrsf12a, Tnfrsf1a, Tnfrsf1b, Tnfsf12, Tnfsf4, Tnmd, Tnn, Tnnc1, Tnni1, Tnni3, Tnnt2, Tomm70a, Tpm1, Traf3ip1, Traf3ip2, Trip10, Trip11, Trp53, Trp53bp2, Trp73, Tsc1, Tsc2, Tspan12, Tspan18, Ttn, Twist1, Txnrd2, Ube4b, Ubp1, Ucp2, Unc5b, Uts2, Uts2r, Uty, Vangl2, Vash1, Vash2, Vav2, Vav3, Vcam1, Vcan, Vegfa, Vegfb, Vegfc, Vegfd, Vezf1, Vgll4, Vhl, Vps4b, Vstm4, Wars2, Wasf2, Wdpcp, Wdr11, Wdr83, Wif1, Wnk1, Wnt11, Wnt16, Wnt2, Wnt3a, Wnt4, Wnt5a, Wnt7a, Wnt7b, Wt1, Xbp1, Xdh, Xirp1, Xirp2, Yap1, Ywhaz, Yy1, Zbtb14, Zc3h12a, Zdhhc16, Zfand5, Zfp354c, Zfp418, Zfp950, Zfpm1, Zfpm2, Zic3, Zmiz1, Zmpste24	Abl1, Actg1, Acvr1b, Acvrl1, Adam10, Adam15, Adam8, Adap2, Add1, Adipor2, Ago2, Akap13, Akt1, Akt3, Ankrd17, Anxa2, Anxa3, Ap1b1, Ap2b1, Apoe, Arg1, Arid1a, Arid2, Arrb2, Atg7, Atp7a, B4galt1, Bak1, Bax, Becn1, Bmpr2, Brpf1, Bsg, Btg1, C3, C3ar1, C5ar1, Camk2d, Casp7, Casp8, Ccl5, Ccr2, Cd24a, Cd38, Cd40, Cd47, Cdc42, Cdkn1a, Cdkn1b, Cflar, Chd7, Cited2, Clic4, Comt, Creb1, Ctnnb1, Ctsh, Cxcr4, Cybb, Ddit4, Dhrs3, Dnm2, Dnmt1, Dusp6, Ecm1, Egln1, Egln3, Egr1, Egr2, Elk3, Emc10, Emilin2, Ep300, Epn1, Ext1, Fadd, Fkbp1a, Fkrp, Flna, Fmnl3, Fn1, Fosl2, Fzd7, G6pdx, Gaa, Gab1, Gatad2a, Gla, Glul, Gna13, Gnaq, Gpx1, Grk2, Grn, Gsk3a, Gsk3b, Gys1, Hdac5, Hectd1, Hgs, Hhex, Hif1a, Hipk2, Hk2, , Hmox1, Hnrnpu, Hopx, Hpse, Id2, Ier3, Il1a, Il1b, Il6ra, Ilk, Inhba, Itga4, Itga5, Itgav, Itgb1, Itgb2, Jak1, Jarid2, Jun, Junb, Kat6a, Kctd10, Kdm2a, Kdm6b, Klf2, Klf4, Ldlr, Lemd2, Lgals3, Lgals8, Lipa, Lmna, Lmo4, Lrg1, Lrp1, Ly6e, Lyl1, Maml1, Map2k1, Map2k2, Map3k3, Mapk1, Mapk14, Mapk3, Mdm2, Mef2a, Mia3, Mib1, Mmp19, Mtdh, Mydgf, Myh9, Myo1e, Naca, Naglu, Ncor2, Ndst1, Nfatc1, Nfe2l2, Nfix, Ninj1, Nos2, Notch1, Notch2, Nr3c1, Nr4a1, Nras, Nrg1, Nsd2, Nus1, Otulin, Pank2, Pdcd10, Pdcd6, Pdcl3, Pde3b, Pdlim7, Pdpn, Pds5a, Pecam1, Pgk1, Pik3cb, Pik3cd, Pik3cg, Pik3r6, Pim1, Pkm, Plau, Plec, Pml, Ppp1r15a, Ppp3cb, Prdm1, Prkar1a, Psen1, Pten, Ptgs2, Ptk2b, Ptpn11, Ptprj, Pxn, Rac1, Rap1a, Rapgef2, Rara, Rb1, Rbpj, Rela, Rest, Rgcc, Rgs2, Rhoa, Rhob, Ric8a, Rnf213, Rnh1, Rock1, Rras, Rtn4, Runx1, Rxra, Rxrb, Sash1, Sav1, Sec24b, Sema4a, Sgpl1, Sh2b3, Sh3pxd2b, Shb, Shc1, Sik1, Sin3b, Slc2a1, Slc8a1, Slc9a1, Smad4, Smarca4, Smg9, Snx17, Socs3, Sod2, Sp100, Sphk2, Spi1, Spint1, Spp1, Spred1, Srf, Stab1, Stat1, Stat3, Stk11, Stk3, Syk, Tab2, Tcf4, Tcf7l2, Tgfb1, Tgfbr1, Tgfbr2, Tgm2, Thbs1, Tiparp, Tmed2, Tmem65, Tnfaip2, Tnfrsf1a, Tnfrsf1b, Tnfsf12, Ubp1, Ucp2, Vcan, Vegfa, Vgll4, Vhl, Wasf2, Wnk1, Xbp1, Xdh, Yy1, Zc3h12a, Zfand5, Zmiz1, Zmpste24

APPENDIX

Appendix 1

Differentially expressed marker genes of macrophages subpopulations.

	Macorphages		
	Pro-inflammatory	**Anti-inflammatory**	**Pro-angiogenic**
1	Cxcl10	Mrc1	Thbs1
2	Ifi205	Ccl7	Nos2
3	Cxcl9	Ms4a7	Vegfa
4	Ly6i	Slc7a2	Cd14
5	Gpr141	Pf4	Mmp19
6	Batf2	Gatm	Arg1
7	Flt1	Arg1	Fn1
8	Il1rn	Pdcd1lg2	Adamtsl4
9	Cfb	Fcrlb	Clec4d
10	Slfn4	Zmynd15	Plin2
11	Ifi211	Ccl12	Spp1
12	Cnn3	Dab2	Cacna1d
13	Phf11d	Emilin1	Egln3
14	Klra2	Ecm1	Fcrlb
15	Dram1	Fblim1	F13a1
16	Tfec	Sash1	Ier3
17	Ms4a4c	Dpep2	Hmox1
18	Fpr2	Siglec1	Fam20c
19	Ifi204	Anpep	Hilpda
20	Gbp2	Spon1	Apoc2
21	Mefv	C3ar1	Dpep2
22	F10	Spp1	Ptgfrn
23	Ms4a6d	Cd72	Rai14
24	Cd40	Apoe	Adssl1
25	Ifit2	Cxcl16	Bst1
26	Ifi207	Myof	Ecm1
27	Oasl1	Ms4a4a	Clec4n
28	C3	Itga9	F10
29	Msr1	Sh3pxd2b	Cebpb
30	Slamf8	Hfe	Fos
31	Tgm2	Fam20c	Ptgs2
32	Smpdl3b	Msr1	Lsr
33	Pstpip2	Mmp14	Fth1
34	Nod2	Axl	Arg2
35	Mlkl	Flt1	Abca1
36	Sirpb1c	Hebp1	Dmxl2
37	Tgfbi	Sdc4	Akap7
38	Tarm1	Plau	Hp
39	Tnfaip2	H2-Eb1	Clec4e
40	Pira2	Fcgr2b	Slc2a1
41	Alpk1	Tgfbi	C5ar1
42	Creb5	Fn1	Basp1
43	Il18	B3gnt8	Fam129b
44	Clec5a	Prxl2b	Gys1
45	Sdc4	Acvrl1	Dab2
46	Calhm6	Rab7b	Sh3pxd2b
47	Ass1	Adamtsl4	Pid1
48	Gda	Mafb	Cxcl2
49	Tlr2	H2-Ab1	Cfp
50	Ms4a6c	Fcgr4	Grina

Global Discussion

Glioblastoma is the most frequent and aggressive primary brain cancer. Despite the introduction of the Stupp protocol over 25 years ago, no major therapeutic breakthrough has significantly improved prognosis, with median overall survival remaining approximately 15 months.[1–5] Therapeutic failure results from limited feasibility and repeatability of maximal surgical resection, blood-brain barrier permeability, invasiveness, hypervascularisation, intra- and inter-tumour heterogeneity, tumour plasticity and niches, glioblastoma stem-like cells (GSCs), profound immunosuppression, and systematic recurrence.[2,11,12,18,31,36,53]

1. CXCR4/CXCL12 pathway as a target for multiple biological features

The CXCR4/CXCL12 axis is involved in tumour aggressiveness, resistance and recurrence, resulting in cancer progression and poor prognosis.[63,135–137,145,157] CXCL12 is secreted by endothelial (ECs), stromal, and immunosuppressive immune cells, as well as stem cells or GSCs. CXCR4 is expressed in vascular, immune, and central nervous systems and upregulated in hypoxic, damaged and neoplastic tissues. For instance, CXCR4 is overexpressed by immune suppressive cells such as regulatory T cells (Tregs) and tumour-associated macrophages and microglia (TAMs), as well as stem cells including GSCs.[63,136–143,146,158]

CXCR4/CXCL12 signalling promotes tumour development and survival, sustains GSC stemness and self-renewal, and drives their migration toward tumour niches, including the SVZ.[40,135,157–159] CXCL12 expression in injured brain regions, including the resection cavity further promotes NSC and GSC migration towards them, and differentiation into proliferative OPC-like cells, leading to recurrence.[28,37,41] CXCL12, which is upregulated by hypoxia-induced HIF1α signalling, also promotes angiogenesis through secretion of VEGFα and other pro-angiogenic factors by ECs and GSCs.[135,145] CXCL12 also prevent effective immune response through (1) recruitment of suppressive immune cells, (2) MHC downregulation by tumour and antigen-presenting cells (APCs), and (3) TAMs polarisation towards an anti-inflammatory state.[49,51,59,62,63] Consequently, CXCR4 inhibition using FDA-approved AMD3100, HMGB1-BoxA, or CXCL12-P2G has been shown to reduce radioresistance, angiogenesis, invasion, and tumour growth.[63,133,134,146,156,158,161–167,170,171] Besides, nanoparticle-mediated (iRGD-PEG-PCL) delivery of AMD3100 limits recruitment of suppressive immune cells and reprograms TAMs and helper T cells toward antitumour phenotypes, reducing anti-inflammatory mediator production.[93] All in all, the CXCR4/CXCL12 pathway lies at the core of glioblastoma development, biological features, and recurrence, making it a particularly compelling target. This is especially relevant given that the profound heterogeneity of glioblastoma cell states, together with

the diversity of tumour microenvironmental niches, renders strategies targeting a single biological feature insufficient.

We hypothesised that combining virotherapy with targeted CXCR4 inhibition would provide complementary therapeutic benefits. Intra-tumoral delivery of a viral vector expressing a CXCR4 antagonist enables bypass of the blood–brain barrier, ensures sustained local production, and avoids systemic inhibition. The latter could otherwise cause adverse effects such as impaired tissue repair, vascular dysfunction, and dysregulated inflammation. In parallel, oncolytic virotherapy induces local inflammation by selectively infecting tumour cells and triggering immunogenic cell death. This effect could benefit from CXCR4 pathway inhibition, relieving immunosuppression and directing immune activation toward a more effective anti-tumour response. Importantly, both oncolytic herpes simplex viruses and CXCR4-targeting strategies have independently demonstrated safety and clinical potential in cancer, supporting the feasibility and rationality of this combined approach.

In this context, we engineered and characterised an oncolytic herpes simplex virus type 1 (oHSV) expressing the CXCL12 antagonist P2G (oHSV/P2G). Importantly, insertion of the P2G transgene did not impair viral replication or oncolytic activity and resulted in efficient production and release of CXCL12-P2G (P2G) at levels comparable to endogenous CXCL12, leading to effective disruption of CXCR4 downstream signalling. This validation step was important to confirm that CXCL12-P2G expression and inhibitory function were effectively mediated by oHSV/P2G infection, ensuring that any subsequent differences observed between oHSV and oHSV/P2G could be attributed specifically to CXCR4 pathway inhibition.

In vivo P2G expression was not clearly demonstrated in this thesis. RT-qPCR analyses on whole brains or dissected regions (frontal, middle, occipital) detected gD mRNA in both oHSV and oHSV/P2G groups, and HA-P2G mRNA only in oHSV/P2G-treated mice. However, these analyses were limited by the small sample size, as RT-qPCR was performed mostly on mice that required premature sacrifice across multiple experiments. While somewhat reassuring, they remain inconclusive and were not presented. Indirect evidence also supports P2G activity. oHSV/P2G consistently inhibited tumour cell migration toward the SVZ via the corpus callosum, a CXCR4/CXCL12-dependent process. This effect would be difficult to explain in absence of P2G expression. Immunostaining failed to detect P2G likely reflecting limitations rather than absence of expression. Indeed, specific targeting of P2G is challenging due to its similarity to CXCL12. Although HA tagging was effective *in vitro*, it was unsuccessful in brain sections in our hands. Timing may also be critical, as viral expression may decline after a couple of days, according to the literature. Future studies should incorporate time-course analyses of the glycoprotein D and of P2G expression and complementary approaches such as flow cytometry on whole brain or microdissected tumours. GFP-positive 005-GSCs could

enable discrimination between tumour and healthy cells, while viral markers (gD) could confirm infection. HA-tagged P2G and downstream signalling markers such as phospho-ERK and phospho-AKT should be evaluated.

We demonstrated that oHSV/P2G targets several key features of glioblastoma aggressiveness, particularly those related to GSC stemness, invasiveness, hypervascularization and immune dysregulation. Although we did not explore every mechanistic aspect in depth, the central objective of this thesis was to highlight the broad spectrum of glioblastoma features that are targeted by oHSV/P2G. Resistance and recurrence are also critical aspects which are partially CXCR4 dependent but were not addressed in this thesis. Several recurrence models are available, including GSCs derived from recurrent patient tumours (such as T033), suicide gene–based models (HSVTK-transduced glioblastoma cells sensitive to ganciclovir), and models incorporating resection and chemo-/radio-therapy, which each better recapitulate the aggressiveness, invasiveness, and immune remodelling observed in recurrent glioblastoma.[28,172,173] It would be of high interest to evaluate the impact of CXCR4/CXCL12 blockade in such models, particularly as oncolytic virotherapy is nowadays a second line treatment.

Besides its interaction with CXCR4, CXCL12 can also interact with CXCR7. The involvement of this alternative receptor was not investigated in this thesis. One reason is that CXCR7 is poorly characterised while CXCR4 functions are extensively described. More importantly, CXCR7 appears to be only moderately expressed in the brain and tumour microenvironment, although some expression has been reported in vascular and neoplastic tissues as well as in astrocytes.[153] As an atypical chemokine receptor (ACKR3), CXCR7 that has an approximately 10-fold higher affinity for CXCL12 than CXCR4, was long considered to lack downstream signalling activity and to function primarily as a CXCL12 scavenger. It could thus modulate local CXCL12 availability, enhancing chemokine gradient formation and preventing excessive CXCR4 downregulation under high ligand concentrations. However, it was more recently shown to heterodimerize with CXCR4, leading to βARRESTIN-mediated signalling and inhibition of CXCR4 G protein–dependent pathways. For example, in TAMs, CXCL12 binding to CXCR4 promotes an M2-like phenotype via STAT3, whereas binding to CXCR7 favours an M1-like phenotype through STAT1 activation. Accordingly, AMD3100, an FDA-approved antagonist of CXCR4 might function as an allosteric agonist of CXCR7. [63,137,140,146,150–153,158,167]

In this context, it remains unclear whether CXCL12-P2G would act as an antagonist or potentially an agonist of CXCR7 or CXCR4-CXCR7 heterodimers. In immune populations, we did not observe any evidence suggesting a contribution of CXCR7. However, its function was not specifically examined in glioblastoma cells, astrocytes, endothelial cells, or pericytes, which may represent the principal CXCR7-expressing populations. Future work should therefore assess the affinity of CXCL12-P2G for both CXCR7 and CXCR4, using receptor-transduced cells if necessary. Its affinity for CXCR4 is already

known to be approximately threefold lower than that of wild-type CXCL12. Subsequent analyses should determine whether βARRESTIN recruitment is increased or decreased upon P2G binding to CXCR7. Comprehensive profiling of CXCR7 expression across all cell populations within tumour-bearing mouse brains, in comparison with CXCR4 expression, would further clarify receptors distribution. Such investigations would allow to delineate the respective contributions of CXCR7 and CXCR4 signalling, and integrate this knowledge into the interpretation of oHSV/P2G-mediated effects within the tumour microenvironment.

Notably, similar considerations apply to other receptors that can heterodimerise with CXCR4, as well as to ligands such as HMGB1 that can form heterocomplexes with CXCL12, and potentially with CXCL12-P2G, thereby influencing receptor affinity and potentially downstream signalling.[134,145,154–156]

2. oHSV/P2G disrupts glioblastoma stem-like cells stemness and migration.

Glioblastoma stem-like cells (GSCs) play a central role in therapeutic resistance and recurrence. GSCs constitute a heterogeneous, multipotent, undifferentiated, self-renewing population capable of initiating tumours *in vivo* and regenerating tumour heterogeneity.[20,35,36]

They are intrinsically resistant to therapy-induced cell death through downregulation of apoptotic pathways, upregulation of DNA repair and drug efflux mechanisms, and frequent quiescence, reducing chemo- and radiotherapy efficacy.[12,16,20,23,36,37,39–42] This resistance is further reinforced by pronounced cellular plasticity, enabled by high transcriptional entropy and permissive epigenetic landscapes, and sustained by interactions with neurogenic, perivascular, hypoxic, and invasive niches.[12,20,23,32,36,42–44]

GSCs display strong invasive capacities, allowing escape from surgical resection, with tumour cells detected up to 2 cm from the tumour margin.[2,20,35,36,39,40] They can also migrate through the *corpus callosum* to the subventricular zone (SVZ), definitively evading resection.[37,41,160] This migration is bidirectional, mimicking neural stem cells (NSCs) trafficking via the rostral migratory stream to the olfactory bulb.[41] Similarly to oncogenic NSCs, it is likely that GSCs can migrate from the SVZ to the resection cavity post-surgery, initiating recurrence.[28]

GSCs also promote angiogenesis by secreting VEGFα or adopting $VEGFR^+$ pericyte- or endothelial-like phenotypes under hypoxia via HIF1α signalling.

Finally, they evade immune surveillance by downregulating innate immune sensors (TLRs) and antigen presentation molecules (MHCs), while actively inducing immunosuppression through immune checkpoint (ICs) expression like PDL1 and secretion of anti-inflammatory cytokines, including IL-10, TGFβ, and CXCL12.[16,20,23,35–37]

The impact of CXCR4 inhibition on tumour cells, particularly GSCs, was evaluated *in vitro* using the human glioblastoma cell line GB138 and several patient-derived cell lines (T08, T013, T018, and T033-LRLG). oHSV/P2G significantly reduced the expression of stemness-associated markers, self-renewal capacity, and migratory behaviour of GSCs in a CXCR4-dependent manner. *In vivo*, using an orthotopic immunodeficient athymic nude mouse model, both GB138 and T033-LRLG tumours showed a marked reduction in GSCs migration through the *corpus callosum* toward the SVZ following oHSV/P2G treatment.

While both oHSV and oHSV/P2G significantly reduced total tumour burden compared to controls, oHSV/P2G did not further decrease tumour volume relative to oHSV alone. This was expected, as CXCR4 inhibition did not affect tumour cell proliferation or cytotoxicity *in vitro*. However, histological analyses of T033-LRLG mouse model revealed that oHSV/P2G-treated tumours were markedly less diffuse and infiltrative than those treated with PBS or oHSV.

Collectively, these results demonstrate that oHSV/P2G effectively limits GSCs invasiveness and dissemination within the brain parenchyma. This reduced infiltration could substantially improve the efficacy of surgical resection, while decreased migration of GSCs to neurogenic niches such as the SVZ may limit their resistance to radiotherapy and chemotherapy. Moreover, attenuation of GSCs stemness and self-renewal also suggests a potential increase in sensitivity to standard therapies.

As virotherapy is intended as a second-line treatment, validation should be conducted in clinically relevant recurrence models. These models would permit to explore the potential of oHSV/P2G in preventing tumour recurrence, particularly by disrupting the bidirectional trafficking of GSCs between the tumour and the SVZ. We have already employed the T033-LRLG recurrence-derived model, but we did not seize the opportunity to exploit its potential for conditional labelling of GSCs that migrated to the contralateral SVZ. Briefly, $dsRed^+$ T033 cells reaching this region can be converted to GFP^+ cells via AAV-mediated recombination following intraventricular injection in the contralateral ventricle. These GFP^+ T033 cells can then be tracked during their subsequent migration and clearly distinguished from tumour cells that never trafficked through the contralateral ventricular region.[117,174] Partial surgical resection could be implemented in this model, as surgical injury itself may act as a chemotactic signal, potentially attracting oncogenic NSCs or GSCs back to the resection cavity.[28] Evaluation of oHSV/P2G in this model might thus be very useful.

As an alternative to oHSV/P2G injection, intraventricular AAV-mediated expression of CXCR4 antagonists could provide sustained inhibition of CXCR4 signalling, preventing migration and CXCR4-dependent OPC-like differentiation required for recurrence initiation, while limiting lysis of NSCs and extending transgene expression over time.

However, if recurrent tumours originate from resident oncogenic NSCs, direct targeting and killing of these cells may be necessary. Retargeted oHSV variants engineered to infect $CXCR4^+$ cells via nanobody-modified glycoproteins could selectively eliminate NSCs and GSCs within the SVZ upon intraventricular delivery.[123] In this scenario, replacement with non-oncogenic patient-derived NSCs could be considered, as explored in neurodegenerative disease settings.[175]

3. oHSV/P2G disrupts glioblastoma microenvironment

Alongside GSCs and CXCR4 pathway, the immune-privileged status of the CNS further impairs antitumour immunity, as it is initially principally composed of microglia surrounded by the blood-brain barrier which restricts the recruitment of lymphocytes, resulting in a myeloid-dominant tumour microenvironment (TME) with abundant TAMs. TME is also characterised by scarce and naïve B cells, as well as numerous Tregs relative to cytotoxic T cells (CTLs), which are exhausted and expressing high levels of ICs.[51,53,65–69,76–78,176] Stromal cells, neurons, astrocytes, and cancer-associated fibroblasts contribute to tumour growth and microenvironment through direct stimulation of tumour cells, ECM remodelling, secretion of immunosuppressive mediators, and metabolic dysregulation. In turn, these signals further polarise TAMs toward pro-tumoral phenotypes that promote angiogenesis, invasion, and therapy resistance.[39,45–52]

As a result, glioblastoma is classified as an immunologically “cold” or “altered” tumour, in contrast to “hot” tumours which are characterised by high tumour mutation burden, high neoantigen load, profound inflammation, active innate immunity and robust recruitment of lymphocytes. These include inflammation signals like DAMPs/PAMPs, pro-inflammatory cytokines and actively phagocytic APCs expressing high levels of co-stimulatory molecules and MHCs for antigen-presentation leading to successful priming of T cells with effector-/Th1-like functions allowing tumour clearance.[52,55–57] Consequently, glioblastoma remains largely resistant to immunotherapies, including vaccines, adoptive cell therapies, immune checkpoint inhibitors (ICIs), and virotherapy.[53,91–107,176]

Immunotherapy failure in glioblastoma largely stems from ineffective innate immune activation and restricted lymphocyte infiltration. Indeed, adoptive lymphocytes are rapidly exhausted, vaccines fail due to defective antigen presentation, and ICIs encounter limited quantities of CTLs, which will be rapidly re-exhausted. Consequently, these immunotherapies are often combined with adjuvants to increase inflammation, APCs activity and lymphocytes infiltration.

In contrast, intra-tumoral virotherapy directly induces inflammation by selectively infecting tumour cells, triggering immunogenic cell death and release of tumour and virus antigens, DAMPs, PAMPs, and pro-inflammatory cytokines, leading to the recruitment of lymphocytes.[6,48,50,53,91,95,98,107,176] Virotherapy can also be combined with other

immunotherapies or directly engineered to deliver transgenes encoding peptide-vaccines, ICIs, or adjuvants such as cytokines, chemokines or pathway modulators. Clinical safety and efficacy have led to approval of oncolytic viruses for treatment of melanoma, head and neck cancer as well as for residual and recurrent glioblastoma with oncolytic HSV-1 teserpaturev (Delytact®, Δ34.5Δ47Δ6, Japan).[6,53,91,95,98,107,176–178]

Beyond oHSV/P2G direct effects on tumour cells stemness and invasiveness, combining virotherapy with CXCR4 inhibition was expected to exert synergistic effects on the tumour immune microenvironment. Oncolytic viruses are potent inducers of inflammation, promoting tumour and viral antigen release, innate immune activation, and recruitment of cytotoxic T lymphocytes (CTLs). CXCR4 blockade alleviates multiple immunosuppressive mechanisms, particularly those mediated by myeloid cells, such as TAMs. Together, these effects are expected to promote a cold-to-hot tumour transition by enhancing antigen uptake, processing, and presentation by APCs, in an environment enriched in DAMPs, PAMPs, and pro-inflammatory cytokines. This further facilitates effective priming and persistence of functional CTLs, and limits their exhaustion trough ICs upregulation. This functional interactions between the innate and adaptive immune responses favours tumour clearance.

Importantly, this thesis compares an oHSV vector carrying a GFP transgene under pORF6 control with an oHSV/P2G vector carrying both the same GFP transgene and the CXCL12-P2G transgene under pEF1a control. We show that these additions do not affect viral replication. However, their impact on the immune system was not specifically evaluated. In particular, oHSV/P2G could potentially induce an additional immune response against the P2G protein. That being said, the rationale for combining CXCR4 blockade with virotherapy is precisely the resistance of the glioblastoma microenvironment to such non-specific inflammation. Our results support this hypothesis, showing pro-inflammatory TAM polarisation and reduced Tregs rather than a broad inflammatory response. This pattern is more consistent with CXCR4 inhibition than with a P2G-driven immune response, which would be sufficient to be distinguishable from the response induced by oHSV and its GFP transgene. However, both mechanisms may still occur simultaneously. Consequently, an ideal additional control would be an oHSV vector expressing an irrelevant transgene under the same promoter as P2G.

Although immunocompetent orthotopic syngeneic mouse models remain essential for studying glioblastoma microenvironment within an intact three-dimensional brain, including physiological extracellular matrix, vascularisation, and a fully functional immune compartment, no single model fully recapitulates human disease. The main issues are species-specific differences and the intrinsic properties of engineered murine glioblastoma cell lines. Accordingly, several chemically induced (GL261, CT2A) and genetically engineered (005, Mut3, NF53, mGB2) models have been developed, each

displaying distinct immune and histological features, influencing therapeutic response.[85–90,179,180]

In the literature, both GL261 and 005 models, which have been used in this work, exhibit a strong correlation with patient glioblastoma immune profiles despite high tumour mutation burden and immune-related gene expression. Compared with GL261, the 005 model is considered less immunogenic, characterised by resistance to T cell-targeted immunotherapies, reduced antigen presentation and co-stimulation by APCs, and limited CTL infiltration, alongside increased NK cell abundance, greater invasiveness and reduced vascularisation.[88,180] By contrast, immunologically inert models such as CT2A and Mut3, which show fewer infiltrating immune cells, with suppressive phenotype, surprisingly exhibit lower spearman rank correlation coefficient with human glioblastoma.[179,181] Furthermore, worst prognosis has been reported in tumours infiltrated by a mixture of TAMs, neutrophils and lymphocytes compared with tumours displaying minimal immune infiltrate.[60] This underscores the particularity of the glioblastoma "cold" microenvironment, which does not reflect a static immune deficiency but rather a dynamic, dysfunctional, and actively pro-tumoral immune response.[88,180]

Comprehensive analyses of the TME were performed in an immunocompetent orthotopic syngeneic C57BL6 mouse model, engrafted with GL261N4 murine glioblastoma cells using single-cell RNA sequencing, flow cytometry, and immunofluorescence. These data demonstrated that oHSV/P2G markedly enhanced TAM phagocytic and antigen-presentation activity. This was accompanied by a shift toward a pro-inflammatory phenotype, reflected at both at the transcriptional level and in subpopulation distribution. Ingenuity pathway analysis further revealed inhibition of key anti-inflammatory pathways in macrophages, including CXCR4, STAT3, TGFβ, and alternative activation signalling, relative to both PBS and oHSV treatments. Additionally, oHSV/P2G induced a pronounced myeloid-to-lymphoid transition characterised by robust recruitment of lymphocytes. B cells exhibited enhanced plasmocyte-like activity. Surprisingly, the CD4/CD8 ratio varies depending on the technique used, with single-cell RNA sequencing suggesting a predominance of $CD8^+$ T cells, while flow cytometry indicates a majority of $CD4^+$ T cells. Immunofluorescence remains relatively equal and too variable to draw firm conclusions. Interestingly, both $CD4^+$ and $CD8^+$ T cells exhibit Th1-like and effector-like phenotypes, respectively, with reduced exhaustion signatures. This makes it difficult to determine which subset is more beneficial for therapeutic outcomes, despite CTLs being the classically described mediators of anti-tumour immunity. This question could be further explored using CD4- or CD8-deficient systems. Notably, single-cell RNA sequencing is less biased, as it does not rely on predefined markers or gating strategies and provides comprehensive transcriptional profiles. Conversely, immunostaining approaches often face technical limitations, including trade-offs between sensitivity and background signal. Altogether, these discrepancies highlight the need for complementary methodologies and further validation. Notably, CD4/CD8 ratio may vary across different

tumour models. All in all, these findings suggest a coordinated reprogramming of both innate and adaptive immunity toward an antitumour state. Nevertheless, both oHSV and oHSV/P2G significantly prolonged survival compared to PBS without significant disparity between viruses.

In mice of the same genetic background, but engrafted with 005-GSCs murine glioblastoma cells, bulk RNA sequencing revealed distinct immune dynamics. oHSV alone induced only modest activation of immune-related genes and a reduction of myeloid anti-inflammatory signatures compared to PBS. In contrast, oHSV/P2G strongly upregulated nearly all immune gene categories, except for the same myeloid anti-inflammatory genes, indicating a more robust immune activation. Notably, oHSV/P2G treatment in the 005 model was associated with broad upregulation of ICs. Survival benefit in the 005 model was observed only with oHSV/P2G, as oHSV alone had no effect, except for a single long-term survivor.

These outcomes are certainly surprising but are in line with the distinct immunogenic profiles of the two models, described hereabove. Importantly, 005 bulk RNA sequencing performed on all immune and tumour cells reflects global transcriptional changes upon oHSV/P2G infection in the right hemisphere, whereas GL261 pseudobulk analyses derived from single-cell RNA sequencing capture gene expression within defined subpopulations such as macrophages, *Cd4*$^{+}$ or *Cd8*$^{+}$ T cells. Consequently, these datasets are hardly comparable. For instance, increased expression of ICs in the 005 model may reflect increased abundance of lymphocytes rather than enhanced exhaustion, particularly given the initially low infiltration in this model, and may also result from physiological ICs upregulation following T cell activation. However, we cannot conclude in the absence of time-course data on the recruitment and activation of the different immune populations (discussed below).

Although no survival difference was observed between oHSV and oHSV/P2G in the GL261 model, single-cell analyses support our initial hypothesis: oHSV/P2G enhanced immune response efficacy compared with oHSV across multiple parameters. This effect was not limited, as might be expected, to immunosuppressive CXCR4^{+} immune cells, which primarily consist of myeloid cells of the innate immune response. Indeed, these effects were also extended to adaptive immune populations, including B cells, *Cd4*$^{+}$ helper T cells, and *Cd8*$^{+}$ effector T cells. These findings suggest that CXCR4 blockade suppresses the immunosuppressive programs at the source of the cold microenvironment, thereby unleashing the full potential of the infection-induced anti-tumour immune response through coordinated crosstalk between innate and adaptive immunity.

Accordingly, the significant increase in survival with oHSV in GL261 may reflect the intrinsic responsiveness of this model to virotherapy, as oHSV alone appears sufficient to trigger inflammation, promote the recruitment of lymphocytes, and support effective CTLs effector function in a context of relatively limited immunosuppressive APC activity.

In this setting, the added benefit of CXCR4 inhibition may be attenuated by aggressive tumour proliferation or by rapid tumour cell lysis following viral infection, potentially leading to accelerated viral clearance, as suggested by *in silico* modelling (see below). [182] In contrast, in the 005 model, CXCR4 blockade appears necessary to overcome profound immunosuppression and fully exploit virotherapy-induced immunogenic cell death within a microenvironment characterised by low CTL abundance and numerous APCs lacking MHC and co-stimulatory molecule expression. High NK cell abundance in this model may further limit the efficacy of oHSVs through antiviral activity.[183,184] These interpretations are drawn from combined immune and survival analyses of both models independently. Again, direct comparisons between single-cell and bulk RNA sequencing should be avoided.

Future studies should include comprehensive immune profiling using single-cell RNA sequencing and flow cytometry across a broader range of glioblastoma models to better capture treatment-induced immune dynamics, address tumour heterogeneity, and refine patient stratification.[88,179,180] Importantly, recurrence models should also be prioritised, as the immune landscape of recurrent tumours is thought to differ from that of primary glioblastoma, with increased T cell infiltration, activated TAMs, and reduced immune checkpoint expression following resection due to removal of the immunosuppressive tumour core, although this environment may subsequently reform.[179] Particular attention should be given to underexplored immune populations, including NK cells, dendritic cells, and neutrophils, as well as to the antigen specificity of T and B cell responses.[105,106,185,186] The observed upregulation of ICs further supports the rationale for combination strategies incorporating ICIs. Finally, potential direct effects of CXCL12-P2G on CXCR4-dependent immunosurveillance warrant investigation, in light of parallels with HMGB1-BoxA, which promotes internalisation of CD47-CXCR4 complexes and enhances phagocytosis by removing the “don’t eat me” signal without activating downstream CXCR4 signalling.[63,155,156] Emerging platforms such as humanised mouse models, organoids, and glioblastoma-on-a-chip systems may provide complementary relevant insights.[79–84]

Importantly, the effects of oHSV/P2G on innate and adaptive immune responses were analysed only at 21 days post-engraftment (d.p.e.), 14 days after the first treatment and 7 days after the second. No alternative time points were examined. This timing was constrained by the rapid tumour growth, especially in the GL261 model, as some mice had to be sacrificed soon after 21 d.p.e. Reducing the initial number of engrafted cells ($<1\times10^5$) might modestly extend survival. However, this cell number was originally selected to maximise successful engraftment. Immune response is a temporally regulated process with increasing activation, eventually followed by immune resolution. Moreover, the innate immune response is activated almost immediately upon infection and typically declines within approximately one week, as adaptive immunity reaches its

peak. Upon secondary exposure, both innate and adaptive responses should be more rapid and robust, if adaptive memory cells were previously generated.[187–189]

In our setting, analysing responses 7 days after the second injection may have missed the peak of the second innate response. Moreover, the short interval between treatments may also have limited memory development and subsequent rapid secondary adaptive response. In this scenario, the primary adaptive response could already be partially exhausted (14 days post initial exposure), while the secondary response may still be developing (7 days post second exposure).

All in all, these questions will only be clarified by analysing adaptive immune specificity (TCR and BCR repertoires) and memory development at multiple time points (3, 7, and 14 days) after both the first and second treatments. Besides, tumour rechallenge experiments would help determine whether a protective adaptive response was established. The longer survival in the 005-GSC model compared with GL261 may also allow wider spacing of treatments and better memory development.

Finally, treatment timing is important for combination strategies, as immune checkpoint inhibitors given as neoadjuvant therapy have shown better outcomes than adjuvant use,[53,94–99] which should be considered when combining them with oHSV/P2G.

4. oHSV/P2G disrupts glioblastoma angiogenesis

As CXCR4/CXCL12 axis is a key regulator of angiogenesis, oHSV/P2G is expected to modulate tumour vascularisation, a major driver of glioblastoma aggressiveness and therapy resistance. Hypervascularisation supports tumour growth by increasing the availability of nutrients, oxygen, metabolites, and growth factors, while expanding perivascular niches that sustain GSCs development, maintenance, migration, and resistance to therapy. Glioblastoma aberrant vasculature network is induced by HIF1α-driven hypoxia resulting from rapid tumour expansion. This process is further amplified by GSCs, described earlier, and pro-tumoral immune populations with angiogenic activity. Most notably, pro-angiogenic TAMs subpopulations, driven by HIF1α, produce MMPs, VEGFα, CXCL12, IL1β/6/23 and typically exhibit anti-inflammatory phenotypes (MRC1, TGFβ). In parallel, under the influence of TGFβ and IL1β/6/23, helper T cells and γδ T cells can polarise towards a pro-angiogenic Th17-like phenotype driven by RORγ, HIF1α, and STAT3 activation. These cells secrete IL17, a cytokine with context-dependent roles that can promote inflammation, immune cell recruitment and direct tumour cell killing, but may also sustain chronic inflammation, drive Treg-like features, and promote angiogenesis through IL17/21/23, VEGFα and MMP-mediated ECM remodelling. In turn, IL17 can further induce pro-angiogenic polarisation of TAMs.

Despite this central role, targeting angiogenesis alone, including VEGFα inhibition with bevacizumab, has shown limited efficacy in glioblastoma.[24,25,190] Targeting a single tumour niche (perivascular, hypoxic, or invasive) seems to result in tumour reorganisation around

remaining niches. Moreover, angiogenesis inhibition may impair immune infiltration or exacerbate hypoxia, paradoxically reinforcing pro-angiogenic signalling. Nonetheless, integrating anti-angiogenic strategies into multi-targeted therapeutic approaches may increase tumour susceptibility, limit rescue of resistant cells by perivascular niches, and reduce access to oxygen and nutrients.

Importantly, HSV-1 infection has been reported to promote angiogenesis in glioblastoma models through CCN1 upregulation and TSP1/2 downregulation in immunodeficient mouse models, leading to increased vascularisation. Comparative analyses of HSV1 and oHSVs indicate that the Δ34.5Δ6 deletions do not significantly alter the pro-angiogenic properties of HSV1, whereas the Δ47 deletion appears to attenuate them, although the mechanisms responsible for this effect and the impact of the immune response remain to be elucidated.[191,192] Considering the relation between hypervascularisation and aggressiveness as well as the importance of tumour immune microenvironment in angiogenesis, it seems crucial to thoroughly assess the impact of oHSV/P2G on tumour vasculature, in immunocompetent models. Besides, given the expected opposite effects of CXCR4/CXCL12 inhibition and HSV-1 infection, assessing the impact of oHSV and oHSV/P2G on angiogenesis is of particular interest.

In vitro, conditioned media from infected or uninfected human glioblastoma cell lines (GB138), filtered to remove infectious particles and prevent cell killing, were applied to HUVECs in tube formation assays to isolate the effects of secreted factors. These experiments confirmed the intrinsic pro-angiogenic activity of glioblastoma-conditioned media. Inhibition of the CXCR4/CXCL12 pathway reduced tube formation, as both oHSV/P2G- and AMD3100-supplemented uninfected-conditioned media impaired tubulogenesis. In this setting, oHSV-conditioned media also modestly reduced tube formation. Gene expression analyses revealed mixed regulation of angiogenic factors following infection, with VEGFα being significantly downregulated by oHSV compared to PBS and further reduced by oHSV/P2G compared to oHSV.

In vivo, analysis of the immunocompetent orthotopic syngeneic GL261 model showed increased tumour vascularisation relative to surrounding brain parenchyma. Tumour vasculature was further enhanced following oHSV treatment compared to PBS, whereas oHSV/P2G induced a significant reduction in vascular density relative to oHSV. Single-cell RNA sequencing further indicated that oHSV could be involved in the polarisation of a subset of macrophages toward anti-inflammatory, pro-angiogenic state. Conversely, oHSV/P2G downregulated multiple pro-angiogenic genes compared to both PBS and oHSV, particularly within T cells and macrophages. The latter was supported *ex vivo* by bulk RNA sequencing of human monocyte-derived macrophages (MDMs) treated with conditioned media. However, these effects were less evident in HMC3 microglia analysed by RT-qPCR or in tube formation assays, although co-culture of HMC3 with GB138 cells suggested a modest synergistic pro-angiogenic effect.

Overall, these results support the conclusion that CXCR4/CXCL12 inhibition impairs angiogenesis, whereas the effect of oHSV remains context dependent. Reduced tubulogenesis in oHSV-conditioned media compared with non-infected controls may reflect tumour cell killing in infected GB138 cultures, leading to decreased overall secretion of pro-angiogenic factors. However, residual tumour cells surviving oHSV infection may upregulate pro-angiogenic mediators such as CCN1 and IL17, as observed by RT-qPCR. In the absence of an immune response, the balance between tumour cell killing and pro-angiogenic factor secretion may account for the contradictory effects observed with oHSV.

In the same conditions, given that oHSV/P2G exhibits infectivity and cytotoxicity comparable to oHSVs', its enhanced anti-angiogenic effect underscores the specific contribution of CXCR4 blockade. Notably, CXCR4 inhibition appears to suppress angiogenesis primarily through VEGFα downregulation rather than modulation of CCN1 or IL17 compared to oHSV. Once again, the interplay between these opposing pathways and tumour cell killing likely influences tumour angiogenesis, increasing the complexity of the process.

Importantly, these *in vitro* experiments, as well as previous studies conducted in athymic nude mice, likely underestimated immune-driven angiogenesis in response to infection. The pro-angiogenic effects of IL17 are largely mediated through polarisation of TAMs and T cells toward pro-angiogenic and Th17 phenotypes, promoting VEGFα release. This may partly explain why oHSV Δ47 showed no impact on tumour vascularisation in immunodeficient mice, whereas we observed increased vascularisation in our immunocompetent model. It may also account for the discrepancies observed between our mono-culture *in vitro* experiments (reduced tubulogenesis with oHSV infected glioblastoma-conditioned media) and *in vivo* findings (increased angiogenesis with oHSV infection). Moreover, our *in vitro* glioblastoma/microglia co-culture experiments using conditioned media revealed a modest synergistic pro-angiogenic effect. Nevertheless, oHSV still slightly inhibited tubulogenesis under these conditions. This may reflect limitations of the co-culture model, the relatively limited pro-angiogenic polarisation of microglia compared with macrophages, as suggested by single-cell analyses, or the requirement for additional immune populations, such as T cells.

Here, we discussed the potential reasons for increased glioblastoma angiogenesis following oHSV treatment, but its clinical implications also deserve emphasis. Glioblastoma progression is highly dependent on hypervascularisation, which provides essential nutrients and oxygen for tumour growth. As highlighted in the introduction, microvascular niches also contribute to tumour heterogeneity and support GSCs, thereby promoting resistance to multiple therapies. Given that virotherapy is unlikely to fully eradicate the tumour without potent anti-tumour immune responses, residual cancer cells will thus likely proliferate in a more vascularised and more aggressive

microenvironment. Virotherapy shows highly variable effects in glioblastoma patients. Identifying such ambivalent treatment effects may help anticipate patient outcomes and guide subsequent clinical decisions. For instance, this could support combining oHSV with anti-angiogenic therapy such as bevacizumab, already used as a second-line treatment in glioblastoma. Alternatively, a deeper understanding of oHSV-induced angiogenesis mechanisms could lead to the design of next-generation oHSVs. Finally, the potential induction of angiogenesis by a non-specific immune response further highlights the importance of directing immune activation toward specific pathways, rather than relying on broad pro-inflammatory approaches such as GM-CSF.

Future studies should further characterise tumour vasculature and vessel leakiness by assessing pericyte coverage, as vascular normalisation could reduce hypoxia and limit niche formation. Bulk RNA sequencing across multiple glioblastoma cell lines may help identify conserved angiogenic programs regulated by infection and CXCR4 inhibition. Co-culture experiments should be repeated using human MDMs rather than microglial cell lines, given the stronger angiogenic modulation of macrophages *in vivo*. Finally, given its inherently poor vascularisation, the 005 model may not be suited for studying angiogenesis and alternative models should be prioritised for this aspect.

5. Immune response and virotherapy: paradoxical interplay

5.1. Immunogenic cell death, temozolomide, and HSV-1 prevalence.

The primary aim of oncolytic virotherapy is to selectively kill cancer cells and induce systemic antitumour immunity through immunogenic cell death (ICD), facilitating a cold-to-hot tumour transition and promoting tumour clearance. However, ICD induced by viral infection predominantly consists of apoptosis, a poorly immunogenic form of regulated cell death (RCD) involving caspase-mediated cell shrinkage, chromatin condensation, nuclear fragmentation, and formation of apoptotic bodies that are rapidly phagocytosed, thereby limiting antigen exposure. Strategies to favour alternative RCD pathways, such as pyroptosis or necroptosis, through inflammasome activation or disruption of caspase-8-RIPK1 interactions, respectively, could enhance immunogenicity.[50]

In addition, standard temozolomide (TMZ) chemotherapy in glioblastoma can modulate the immune system, although its effects are controversial. TMZ treatment following oncolytic viruses (OVs) treatment has been reported to enhance virotherapy efficacy, whereas concomitant TMZ with G47Δ-IL12 or anti-PD1 therapy has reduced survival benefits as well as immune recruitment and activation. As TMZ remains standard of care and extends overall survival by a few but precious months, optimizing its dose and scheduling in combination with immunotherapies is critical. Notably, clinical trials suggest that repeated virotherapy even in the absence of concurrent chemotherapy, can sustain long-term survival. This finding raises the question of whether the lack of TMZ is

neutral or may enhance therapeutic efficacy by limiting treatment-induced immunosuppression.[193,194]

Third, the high prevalence of HSV-1 in adults initially raised concerns that pre-existing neutralising antibodies could limit viral infection and therapeutic efficacy. For similar reasons, virotherapy was long considered as a single-dose treatment. However, intra-tumoral virus delivery circumvents systemic antibody neutralisation and, following rapid initial infection, enables viral spread to surrounding tumour cells, including via intercellular transmission pathways. Furthermore, pre-immunisation with HSV-1 has paradoxically enhanced anti-tumour immunity, likely by accelerating recognition and killing of infected tumour cells, thereby increasing tumour-specific antigen (TSA) presentation and subsequent anti-tumour immune response.[118]

5.2. Virotherapy optimisation

In silico modelling provides insight into how to achieve optimal virotherapy efficacy, which depends on both viral properties and the quality of the induced immune response. [182,195]

- Virotherapy requires relatively **low tumour cell death rates** and **efficient viral propagation** to allow total cancer eradication. The presence of resistant tumour subclones, or resistant stromal cells (which should be normal following OVs attenuation), can create barriers to viral dissemination, particularly in multifocal or invasive tumours.
- **Spatial and temporal dynamics** also contribute to virotherapy efficacy including treatment timing, localised versus systemic tumour infection, as well as immunogenic molecules diffusion, consumption, and degradation. For instance, localised ICD can generate inflammation hotspots, recruiting immune cells that eliminate infected and neighbouring tumour cells, creating a spatial barrier that limits further viral spread. This challenge can be mitigated by replacing simple intra-tumoral diffusion with approaches that improve virus spatial and temporal distribution, including enhanced diffusion coefficients (EDC), hydrogel scaffolds in the resection cavity, or intraventricular injections, all of which avoid the systemic toxicity associated with intravenous delivery.
- **Adaptive immune response specificity** is critical for virotherapy efficacy. Even if the two conditions above are met, virus-induced immunogenicity may remain suboptimal in immunologically “cold” tumours, making adaptive immune specificity towards resistant, or at least uninfected, tumour cells essential. In contrast, in “hot” tumours, non-specific (anti-tumour and anti-viral) cytotoxicity may suffice, although excessive inflammation risks recruiting dysfunctional immune populations.

5.3. Reciprocal inhibition between virotherapy and immune response

Early innate immune responses can induce viral clearance and therapy failure. NK cells are particularly potent antiviral cytotoxic lymphocytes, acting within hours of infection. Moreover, NK cells deficiencies are associated with HSV-1-mediated encephalitis. In fact, infection upregulates natural cytotoxicity receptors (NCR) ligands (NKp30, NKp46), leading to recognition by NK cells, IFNγ secretion, and subsequent recruitment of TAMs that produce CXCL9/10/11, further promoting viral clearance.

While initial innate immunity can hinder virotherapy, OVs-mediated reprogramming of the tumour microenvironment can enhance NK cells contributions to anti-tumour immunity by killing uninfected tumour cells and supporting DCs maturation and adaptive immune cell priming.[183,184] However, virotherapy may also paradoxically impair antitumoral immunity through excessive type I cytokine release or viral antigen dominance, resulting in early immune exhaustion, limited development of anti-tumoral response and reducing the effectiveness of combination strategies with ICIs or CAR-T therapies.

Overall, immune response can limit the efficacy of virotherapy unless it is (1) delayed allowing viral spread, (2) stimulated to achieve tumour clearance within an optimal TME, or (3) specifically redirected toward uninfected or preferentially resistant cells. Virotherapy-induced immune response failure can be addressed by (4) exploiting pre-existing antiviral immunity. [118,183,184,194–196]

1. “Trojan horse” delivery employs non-immunogenic carrier cells, such as mesenchymal or adipose-derived stem cells, or nanoparticles to shield the virus from early immune detection. This approach enhances delivery, tumour targeting, combination therapies, and allows intravenous administration, while ensuring scalable production and stability.
2. Enhancement of induced immune response can be achieved by arming viruses with transgenes encoding pro-inflammatory cytokines or inhibitors of anti-inflammatory pathways. This promotes local inflammation and strengthens both innate and adaptive immunity, while immune cells are exposed to virus- and tumour-specific antigens during infection and cell lysis. Extensive inflammation may also generate a bystander killing effect, as activated adaptive immune cells release cytotoxic cytokines and factors which can affect surrounding cells without strict specificity. Additionally, priming the immune system with viral antigens expands antigen-specific memory responses and improves immune cell efficacy.
3. Immune retargeting can occur naturally, as viral antigens may spread to non-infected cells, a potential viral mechanism to evade immune responses directed at the truly infected cells. Infected cell killing can also be modulated by transgenes, for example, by expressing E-cadherin to inhibit NK cells–mediated killing. Infected cells can also be driven to overexpress tumour-specific antigens, promoting clonal expansion of specific anti-tumour lymphocytes or enabling

subsequent targeted therapies, such as antibody-drug conjugates (T-DM1 against HER2). Bispecific engagers can additionally link ligands on immune effectors (macrophages, NK cells) to antigens on tumour cells, inducing specific phagocytosis or cytotoxicity.

4. Leveraging pre-existing antiviral immunity requires innovative approaches. Dual-specific CAR-T cells, engineered to recognize both tumour antigens (via the CAR) and viral antigens (via an engineered TCR), can be exposed *ex vivo* to the oncolytic virus for clonal expansion and enhanced recognition before infusion. Alternatively, pre-existing CMV immunity, common in glioblastoma patients, can be harnessed as CMV infection has been shown to expand CMV-specific T cells and enhance tumour cell killing. Thus, a CMV vector was developed encoding CD3-targeted lentiviral components, preferentially transducing CMV-specific T cells and generating dual-specific CAR-T cells *in situ* within the inflamed TME.

5.4. Conclusion and perspectives

Our approach aligns with strategies aimed at enhancing the induced immune response, focusing on the cold-to-hot tumour transition, through inflammation, active innate immunity, and non-specific (anti-tumour and anti-viral) adaptive cytotoxicity. Inhibition of the CXCR4/CXCL12 pathway, which is associated with immunosuppression, combined with repeated oHSV dosing, can enhance long-term memory and anti-tumour immunity, particularly in the context of pre-existing HSV-1 seropositivity. Achieving this cold-to-hot tumour transition should be considered a fundamental prerequisite, before considering the above complementary strategies (“Trojan horse”, immune retargeting, leveraging pre-existing immunity), or combination with other immunotherapies.

For instance, oHSV/P2G remodels the TME, promoting inflammation, a myeloid-to-lymphoid shift, activation of tumour-associated macrophages and microglia, enhanced *Cd4*$^{+}$ and *Cd8*$^{+}$ T cell effector function, an increased cytotoxic-to-regulatory T cell ratio, and improved survival, especially under low-immunogenic conditions. These findings suggest that our treatment could synergize with ICIs to facilitate tumour clearance by preventing CTL exhaustion post-activation. Moreover, TME reprogramming supports potential combination with CAR-T cell therapy by improving infiltration and delaying premature exhaustion. Dual-specific CAR-T cells, engineered with an anti-oHSV TCR, could further exploit viral antigen dominance.

At a practical level, oHSV/P2G may also benefit from alternative delivery routes to optimise systemic tumour infection and viral spread. Induction of more immunogenic, regulated cell death pathways should also be considered. Importantly, the goal of virotherapy is the development of robust anti-tumour effector and memory immunity, not complete tumour clearance through viral replication and cell lysis. In this context, rapid viral clearance should be viewed as advantageous, limiting toxicity and the risk of encephalitis.

References

1. Louis, D.N., Perry, A., Wesseling, P., Brat, D.J., Cree, I.A., Figarella-Branger, D., Hawkins, C., Ng, H.K., Pfister, S.M., Reifenberger, G., et al. (2021). The 2021 WHO Classification of Tumors of the Central Nervous System: a summary. Neuro-Oncol. *23*, 1231–1251. https://doi.org/10.1093/neuonc/noab106.

2. Wang, L.M., Englander, Z.K., Miller, M.L., and Bruce, J.N. (2023). Malignant Glioma. Adv. Exp. Med. Biol. *1405*, 1–30. https://doi.org/10.1007/978-3-031-23705-8_1.

3. Abedi, A.A., Grunnet, K., Christensen, I.J., Michaelsen, S.R., Muhic, A., Møller, S., Hasselbalch, B., Poulsen, H.S., and Urup, T. (2021). A Prognostic Model for Glioblastoma Patients Treated With Standard Therapy Based on a Prospective Cohort of Consecutive Non-Selected Patients From a Single Institution. Front. Oncol. *11*, 597587. https://doi.org/10.3389/fonc.2021.597587.

4. Ostrom, Q.T., Gittleman, H., Fulop, J., Liu, M., Blanda, R., Kromer, C., Wolinsky, Y., Kruchko, C., and Barnholtz-Sloan, J.S. (2015). CBTRUS Statistical Report: Primary Brain and Central Nervous System Tumors Diagnosed in the United States in 2008-2012. Neuro-Oncol. *17*, iv1–iv62. https://doi.org/10.1093/neuonc/nov189.

5. Stupp, R., Mason, W.P., Bent, M.J. van den, Weller, M., Fisher, B., Taphoorn, M.J.B., Belanger, K., Brandes, A.A., Marosi, C., Bogdahn, U., et al. (2005). Radiotherapy plus Concomitant and Adjuvant Temozolomide for Glioblastoma. N. Engl. J. Med. *352*, 987–996. https://doi.org/10.1056/NEJMoa043330.

6. Sanchez Gil, J. (2022). Design and characterization of a CXCR4-retargeted and sTRAILarmed oncolytic HSV-1 to attack Glioblastoma stem-like cells (GSCs).

7. Sim, H.-W., Morgan, E.R., and Mason, W.P. (2018). Contemporary management of high-grade gliomas. CNS Oncol. *7*, 51–65. https://doi.org/10.2217/cns-2017-0026.

8. Gupta, S., Nawabi, N.L., Emani, S., Medeiros, L., Bernstock, J.D., Duvall, J., Ng, P., Smith, T.R., Wen, P.Y., Reardon, D.A., et al. (2023). An expanded role for surgery in grade 3 1p/19q co-deleted oligodendroglioma. Neuro-Oncol. Adv. *5*, vdad046. https://doi.org/10.1093/noajnl/vdad046.

9. Kapoor, M., and Gupta, V. (2025). Astrocytoma. In StatPearls (StatPearls Publishing).

10. Hasel, P., Cooper, M.L., Marchildon, A.E., Rufen-Blanchette, U., Kim, R.D., Ma, T.C., Groh, A.M.R., Hill, E.J., Lewis, E.M., Januszewski, M., et al. (2025). Defining the molecular identity and morphology of glia limitans superficialis astrocytes in vertebrates. Cell Rep. *44*, 115344. https://doi.org/10.1016/j.celrep.2025.115344.

11. Chang, C., Chavarro, V.S., Gerstl, J.V.E., Blitz, S.E., Spanehl, L., Dubinski, D., Valdes, P.A., Tran, L.N., Gupta, S., Esposito, L., et al. (2024). Recurrent Glioblastoma—Molecular Underpinnings and Evolving Treatment Paradigms. Int. J. Mol. Sci. *25*, 6733. https://doi.org/10.3390/ijms25126733.

12. Goenka, A., Tiek, D., Song, X., Huang, T., Hu, B., and Cheng, S.-Y. (2021). The Many Facets of Therapy Resistance and Tumor Recurrence in Glioblastoma. Cells *10*, 484. https://doi.org/10.3390/cells10030484.

13. Kim, H.J., Park, J.W., and Lee, J.H. (2021). Genetic Architectures and Cell-of-Origin in Glioblastoma. Front. Oncol. *10*, 615400. https://doi.org/10.3389/fonc.2020.615400.

14. Nair, N.U., Schäffer, A.A., Gertz, E.M., Cheng, K., Zerbib, J., Sahu, A.D., Leor, G., Shulman, E.D., Aldape, K.D., Ben-David, U., et al. (2024). Chromosome 7 gain compensates for chromosome 10 loss in glioma. Cancer Res. *84*, 3464–3477. https://doi.org/10.1158/0008-5472.CAN-24-1366.

15. Alcantara Llaguno, S.R., Wang, Z., Sun, D., Chen, J., Xu, J., Kim, E., Hatanpaa, K.J., Raisanen, J.M., Burns, D.K., Johnson, J.E., et al. (2015). Adult Lineage Restricted CNS Progenitors Specify Distinct Glioblastoma Subtypes. Cancer Cell *28*, 429–440. https://doi.org/10.1016/j.ccell.2015.09.007.

16. Goffart, N., Kroonen, J., and Rogister, B. (2013). Glioblastoma-Initiating Cells: Relationship with Neural Stem Cells and the Micro-Environment. Cancers *5*, 1049–1071. https://doi.org/10.3390/cancers5031049.

17. Friedmann-Morvinski, D., and Verma, I.M. (2014). Dedifferentiation and reprogramming: origins of cancer stem cells. EMBO Rep. *15*, 244–253. https://doi.org/10.1002/embr.201338254.

18. Wu, Y., Liu, Y., Huang, Z., Wang, X., Jin, Z., Li, J., Limsakul, P., Zhu, L., Allen, M., Pan, Y., et al. (2021). Control of the activity of CAR-T cells within tumours via focused ultrasound. Nat. Biomed. Eng. *5*, 1336–1347. https://doi.org/10.1038/s41551-021-00779-w.

19. Zhou, Z., Singh, R., and Souweidane, M.M. (2017). Convection-Enhanced Delivery for Diffuse Intrinsic Pontine Glioma Treatment. Curr. Neuropharmacol. *15*, 116–128. https://doi.org/10.2174/1570159X14666160614093615.

20. Gimple, R.C., Bhargava, S., Dixit, D., and Rich, J.N. (2019). Glioblastoma stem cells: lessons from the tumor hierarchy in a lethal cancer. Genes Dev. *33*, 591–609. https://doi.org/10.1101/gad.324301.119.

21. Quinn, J.A., Jiang, S.X., Reardon, D.A., Desjardins, A., Vredenburgh, J.J., Rich, J.N., Gururangan, S., Friedman, A.H., Bigner, D.D., Sampson, J.H., et al. (2009). Phase II Trial of Temozolomide Plus O6-Benzylguanine in Adults With Recurrent, Temozolomide-

Resistant Malignant Glioma. J. Clin. Oncol. *27*, 1262–1267. https://doi.org/10.1200/JCO.2008.18.8417.

22. Liu, Q., Fang, L., and Wu, C. (2022). Alternative Splicing and Isoforms: From Mechanisms to Diseases. Genes *13*, 401. https://doi.org/10.3390/genes13030401.

23. Biserova, K., Jakovlevs, A., Uljanovs, R., and Strumfa, I. (2021). Cancer Stem Cells: Significance in Origin, Pathogenesis and Treatment of Glioblastoma. Cells *10*, 621. https://doi.org/10.3390/cells10030621.

24. Cohen, M.H., Shen, Y.L., Keegan, P., and Pazdur, R. (2009). FDA drug approval summary: bevacizumab (Avastin) as treatment of recurrent glioblastoma multiforme. The Oncologist *14*, 1131–1138. https://doi.org/10.1634/theoncologist.2009-0121.

25. Vredenburgh, J.J., Desjardins, A., Herndon, J.E., II, Dowell, J.M., Reardon, D.A., Quinn, J.A., Rich, J.N., Sathornsumetee, S., Gururangan, S., Wagner, M., et al. (2007). Phase II Trial of Bevacizumab and Irinotecan in Recurrent Malignant Glioma. Clin. Cancer Res. *13*, 1253–1259. https://doi.org/10.1158/1078-0432.CCR-06-2309.

26. Bourmeau, G., Anezo, O., Raymond, J., Ballestín, A., Pichol-Thievend, C., Reveilles, J., Thomas, A., Wang, L., Miranda, M., Moutaux, E., et al. (2025). Proneural–mesenchymal hybrid glioblastoma cells are resistant to therapy and dependent on nuclear import. Neuro-Oncol., noaf160. https://doi.org/10.1093/neuonc/noaf160.

27. Tang, J., Karbhari, N., and Campian, J.L. (2025). Therapeutic Targets in Glioblastoma: Molecular Pathways, Emerging Strategies, and Future Directions. Cells *14*, 494. https://doi.org/10.3390/cells14070494.

28. Li, X., Kim, H.J., Yoo, J., Lee, Y., Nam, C.H., Park, J., Lee, S.-T., Kim, T.M., Choi, S.H., Won, J.-K., et al. (2025). Distant origin of glioblastoma recurrence: neural stem cells in the subventricular zone serve as a source of tumor reconstruction after primary resection. Mol. Cancer *24*, 64. https://doi.org/10.1186/s12943-025-02273-2.

29. Lee, J.-K., Wang, J., Sa, J.K., Ladewig, E., Lee, H.-O., Lee, I.-H., Kang, H.J., Rosenbloom, D.S., Camara, P.G., Liu, Z., et al. (2017). Spatiotemporal genomic architecture informs precision oncology in glioblastoma. Nat. Genet. *49*, 594–599. https://doi.org/10.1038/ng.3806.

30. Verhaak, R.G.W., Hoadley, K.A., Purdom, E., Wang, V., Qi, Y., Wilkerson, M.D., Miller, C.R., Ding, L., Golub, T., Mesirov, J.P., et al. (2010). An integrated genomic analysis identifies clinically relevant subtypes of glioblastoma characterized by abnormalities in PDGFRA, IDH1, EGFR and NF1. Cancer Cell *17*, 98. https://doi.org/10.1016/j.ccr.2009.12.020.

31. Neftel, C., Laffy, J., Filbin, M.G., Hara, T., Shore, M.E., Rahme, G.J., Richman, A.R., Silverbush, D., Shaw, M.L., Hebert, C.M., et al. (2019). An Integrative Model of Cellular

States, Plasticity, and Genetics for Glioblastoma. Cell *178*, 835-849.e21. https://doi.org/10.1016/j.cell.2019.06.024.

32. Stanzani, E., Pedrosa, L., Bourmeau, G., Anezo, O., Noguera-Castells, A., Esteve-Codina, A., Passoni, L., Matteoli, M., de la Iglesia, N., Seano, G., et al. (2021). Dual Role of Integrin Alpha-6 in Glioblastoma: Supporting Stemness in Proneural Stem-Like Cells While Inducing Radioresistance in Mesenchymal Stem-Like Cells. Cancers *13*, 3055. https://doi.org/10.3390/cancers13123055.

33. Jin, X., Kim, L.J.Y., Wu, Q., Wallace, L.C., Prager, B.C., Sanvoranart, T., Gimple, R.C., Wang, X., Mack, S.C., Miller, T.E., et al. (2017). Targeting Glioma Stem Cells through Combined BMI1 and EZH2 Inhibition. Nat. Med. *23*, 1352–1361. https://doi.org/10.1038/nm.4415.

34. Pichol-Thievend, C., Anezo, O., Pettiwala, A.M., Bourmeau, G., Montagne, R., Lyne, A.-M., Guichet, P.-O., Deshors, P., Ballestín, A., Blanchard, B., et al. (2024). VC-resist glioblastoma cell state: vessel co-option as a key driver of chemoradiation resistance. Nat. Commun. *15*, 3602. https://doi.org/10.1038/s41467-024-47985-z.

35. Kardani, K., Sanchez Gil, J., and Rabkin, S.D. (2023). Oncolytic herpes simplex viruses for the treatment of glioma and targeting glioblastoma stem-like cells. Front. Cell. Infect. Microbiol. *13*, 1206111. https://doi.org/10.3389/fcimb.2023.1206111.

36. Prager, B.C., Bhargava, S., Mahadev, V., Hubert, C.G., and Rich, J.N. (2020). Glioblastoma Stem Cells: Driving Resiliency through Chaos. Trends Cancer *6*, 223–235. https://doi.org/10.1016/j.trecan.2020.01.009.

37. Lombard, A., Digregorio, M., Delcamp, C., Rogister, B., Piette, C., and Coppieters, N. (2021). The Subventricular Zone, a Hideout for Adult and Pediatric High-Grade Glioma Stem Cells. Front. Oncol. *10*, 614930. https://doi.org/10.3389/fonc.2020.614930.

38. Bakhshinyan, D., Savage, N., Salim, S.K., Venugopal, C., and Singh, S.K. (2021). The Strange Case of Jekyll and Hyde: Parallels Between Neural Stem Cells and Glioblastoma-Initiating Cells. Front. Oncol. *10*, 603738. https://doi.org/10.3389/fonc.2020.603738.

39. Hu, Q., Zhu, Y., Mei, J., Liu, Y., and Zhou, G. (2025). Extracellular matrix dynamics in tumor immunoregulation: from tumor microenvironment to immunotherapy. J. Hematol. Oncol.J Hematol Oncol *18*, 65. https://doi.org/10.1186/s13045-025-01717-y.

40. López-Gil, J.C., Martin-Hijano, L., Hermann, P.C., and Sainz, B. (2021). The CXCL12 Crossroads in Cancer Stem Cells and Their Niche. Cancers *13*, 469. https://doi.org/10.3390/cancers13030469.

41. Kroonen, J., Nassen, J., Boulanger, Y.-G., Provenzano, F., Capraro, V., Bours, V., Martin, D., Deprez, M., Robe, P., and Rogister, B. (2011). Human glioblastoma-initiating

cells invade specifically the subventricular zones and olfactory bulbs of mice after striatal injection. Int. J. Cancer *129*. https://doi.org/10.1002/ijc.25709.

42. Goffart, N., Lombard, A., Lallemand, F., Kroonen, J., Nassen, J., Di Valentin, E., Berendsen, S., Dedobbeleer, M., Willems, E., Robe, P., et al. (2017). CXCL12 mediates glioblastoma resistance to radiotherapy in the subventricular zone. Neuro-Oncol. *19*, 66–77. https://doi.org/10.1093/neuonc/now136.

43. Liu, G., Yuan, X., Zeng, Z., Tunici, P., Ng, H., Abdulkadir, I.R., Lu, L., Irvin, D., Black, K.L., and Yu, J.S. (2006). Analysis of gene expression and chemoresistance of CD133+ cancer stem cells in glioblastoma. Mol. Cancer *5*, 67. https://doi.org/10.1186/1476-4598-5-67.

44. Vander Heiden, M.G., Cantley, L.C., and Thompson, C.B. (2009). Understanding the Warburg Effect: The Metabolic Requirements of Cell Proliferation. Science *324*, 1029–1033. https://doi.org/10.1126/science.1160809.

45. Dapash, M., Hou, D., Castro, B., Lee-Chang, C., and Lesniak, M.S. (2021). The Interplay between Glioblastoma and Its Microenvironment. Cells *10*, 2257. https://doi.org/10.3390/cells10092257.

46. Henke, E., Nandigama, R., and Ergün, S. (2020). Extracellular Matrix in the Tumor Microenvironment and Its Impact on Cancer Therapy. Front. Mol. Biosci. *6*. https://doi.org/10.3389/fmolb.2019.00160.

47. Ma, D., Liu, S., Lal, B., Wei, S., Wang, S., Zhan, D., Zhang, H., Lee, R.S., Gao, P., Lopez-Bertoni, H., et al. (2019). Extracellular matrix protein tenascin C increases phagocytosis mediated by CD47 loss of function in glioblastoma. Cancer Res. *79*, 2697–2708. https://doi.org/10.1158/0008-5472.CAN-18-3125.

48. Ahmed, A., and Tait, S.W.G. (2020). Targeting immunogenic cell death in cancer. Mol. Oncol. *14*, 2994–3006. https://doi.org/10.1002/1878-0261.12851.

49. McLean, H., Drill, M., Sequeira, R., Jayakrishnan, P.C., Jeffree, R.L., Hunn, M., O'Brien, T.J., Hamilton, J., and Monif, M. (2025). Harnessing the innate immune system for glioblastoma therapeutics. J. Neuroimmunol. *407*, 578713. https://doi.org/10.1016/j.jneuroim.2025.578713.

50. Palanivelu, L., Liu, C.-H., and Lin, L.-T. (2023). Immunogenic cell death: The cornerstone of oncolytic viro-immunotherapy. Front. Immunol. *13*, 1038226. https://doi.org/10.3389/fimmu.2022.1038226.

51. Sharma, P., Aaroe, A., Liang, J., and Puduvalli, V.K. (2023). Tumor microenvironment in glioblastoma: Current and emerging concepts. Neuro-Oncol. Adv. *5*, vdad009. https://doi.org/10.1093/noajnl/vdad009.

52. Wu, B., Zhang, B., Li, B., Wu, H., and Jiang, M. (2024). Cold and hot tumors: from molecular mechanisms to targeted therapy. Signal Transduct. Target. Ther. *9*, 274. https://doi.org/10.1038/s41392-024-01979-x.

53. Tripathy, D.K., Panda, L.P., Biswal, S., and Barhwal, K. (2024). Insights into the glioblastoma tumor microenvironment: current and emerging therapeutic approaches. Front. Pharmacol. *15*. https://doi.org/10.3389/fphar.2024.1355242.

54. Łaszczych, D., Czernicka, A., Gostomczyk, K., Szylberg, Ł., and Borowczak, J. (2024). The role of IL-17 in the pathogenesis and treatment of glioblastoma—an update on the state of the art and future perspectives. Med. Oncol. Northwood Lond. Engl. *41*, 187. https://doi.org/10.1007/s12032-024-02434-1.

55. Clifton, G.T., Rothenberg, M., Ascierto, P.A., Begley, G., Cecchini, M., Eder, J.P., Ghiringhelli, F., Italiano, A., Kochetkova, M., Li, R., et al. (2023). Developing a definition of immune exclusion in cancer: results of a modified Delphi workshop. J. Immunother. Cancer *11*, e006773. https://doi.org/10.1136/jitc-2023-006773.

56. Galon, J., and Bruni, D. (2019). Approaches to treat immune hot, altered and cold tumours with combination immunotherapies. Nat. Rev. Drug Discov. *18*, 197–218. https://doi.org/10.1038/s41573-018-0007-y.

57. Tiwari, A., Oravecz, T., Dillon, L.A., Italiano, A., Audoly, L., Fridman, W.H., and Clifton, G.T. (2023). Towards a consensus definition of immune exclusion in cancer. Front. Immunol. *14*, 1084887. https://doi.org/10.3389/fimmu.2023.1084887.

58. Liu, Y., Zhou, F., Ali, H., Lathia, J.D., and Chen, P. (2024). Immunotherapy for glioblastoma: current state, challenges, and future perspectives. Cell. Mol. Immunol. *21*, 1354–1375. https://doi.org/10.1038/s41423-024-01226-x.

59. Chen, Z., and Hambardzumyan, D. (2018). Immune Microenvironment in Glioblastoma Subtypes. Front. Immunol. *9*, 1004. https://doi.org/10.3389/fimmu.2018.01004.

60. González-Tablas Pimenta, M., Otero, Á., Arandia Guzman, D.A., Pascual-Argente, D., Ruíz Martín, L., Sousa-Casasnovas, P., García-Martin, A., Roa Montes de Oca, J.C., Villaseñor-Ledezma, J., Torres Carretero, L., et al. (2021). Tumor cell and immune cell profiles in primary human glioblastoma: Impact on patient outcome. Brain Pathol. *31*, 365–380. https://doi.org/10.1111/bpa.12927.

61. Perus, L., and Walsh, L. (2019). Microenvironmental Heterogeneity in Brain Malignancies. Front. Immunol. *10*. https://doi.org/10.3389/fimmu.2019.02294.

62. Zhao, W., Zhang, Z., Xie, M., Ding, F., Zheng, X., Sun, S., and Du, J. (2025). Exploring tumor-associated macrophages in glioblastoma: from diversity to therapy. Npj Precis. Oncol. *9*, 126. https://doi.org/10.1038/s41698-025-00920-x.

63. Mezzapelle, R., Leo, M., Caprioglio, F., Colley, L.S., Lamarca, A., Sabatino, L., Colantuoni, V., Crippa, M.P., and Bianchi, M.E. (2022). CXCR4/CXCL12 Activities in the Tumor Microenvironment and Implications for Tumor Immunotherapy. Cancers *14*, 2314. https://doi.org/10.3390/cancers14092314.

64. Ma, R.-Y., Black, A., and Qian, B.-Z. (2022). Macrophage diversity in cancer revisited in the era of single-cell omics. Trends Immunol. *43*, 546–563. https://doi.org/10.1016/j.it.2022.04.008.

65. Habibi, M.A., Nejati, N., Najafi, M.B., Khodadadiyan, A., Dashti, M., Lorestani, P., Karimizadeh, Z., Ahmadpour, M., Kalantari, A., Jokar-Derisi, A., et al. (2025). Enhancing T cell infiltration in glioblastoma: a review article on challenges and therapeutic strategies. Cancer Treat. Res. Commun. *45*, 100999. https://doi.org/10.1016/j.ctarc.2025.100999.

66. Lin, Y., Song, Y., Zhang, Y., Li, X., Kan, L., and Han, S. (2025). New insights on anti-tumor immunity of CD8+ T cells: cancer stem cells, tumor immune microenvironment and immunotherapy. J. Transl. Med. *23*, 341. https://doi.org/10.1186/s12967-025-06291-y.

67. Mauldin, I.S., Jo, J., Wages, N.A., Yogendran, L.V., Mahmutovic, A., Young, S.J., Lopes, M.B., Slingluff, C.L., Erickson, L.D., and Fadul, C.E. (2021). Proliferating CD8+ T Cell Infiltrates Are Associated with Improved Survival in Glioblastoma. Cells *10*, 3378. https://doi.org/10.3390/cells10123378.

68. Noor, L., Upadhyay, A., and Joshi, V. (2024). Role of T Lymphocytes in Glioma Immune Microenvironment: Two Sides of a Coin. Biology *13*, 846. https://doi.org/10.3390/biology13100846.

69. Wang, H., Zhou, H., Xu, J., Lu, Y., Ji, X., Yao, Y., Chao, H., Zhang, J., Zhang, X., Yao, S., et al. (2021). Different T-cell subsets in glioblastoma multiforme and targeted immunotherapy. Cancer Lett. *496*, 134–143. https://doi.org/10.1016/j.canlet.2020.09.028.

70. Andreu-Sanz, D., and Kobold, S. (2023). Role and Potential of Different T Helper Cell Subsets in Adoptive Cell Therapy. Cancers *15*, 1650. https://doi.org/10.3390/cancers15061650.

71. Madkouri, R., Kaderbhai, C.G., Bertaut, A., Truntzer, C., Vincent, J., Aubriot-Lorton, M.H., Farah, W., Limagne, E., Ladoire, S., Boidot, R., et al. (2017). Immune classifications with cytotoxic CD8+ and Th17 infiltrates are predictors of clinical prognosis in glioblastoma. Oncoimmunology *6*, e1321186. https://doi.org/10.1080/2162402X.2017.1321186.

72. Ahmedna, T., Khela, H., Weber-Levine, C., Azad, T.D., Jackson, C.M., Gabrielson, K., Bettegowda, C., and Rincon-Torroella, J. (2023). The Role of γδ T-Lymphocytes in

Glioblastoma: Current Trends and Future Directions. Cancers *15*, 5784. https://doi.org/10.3390/cancers15245784.

73. Choi, H., Kim, T.-G., Jeun, S.-S., and Ahn, S. (2023). Human gamma-delta (γδ) T cell therapy for glioblastoma: A novel alternative to overcome challenges of adoptive immune cell therapy. Cancer Lett. *571*, 216335. https://doi.org/10.1016/j.canlet.2023.216335.

74. Dieli, C., Maugeri, R., Corsale, A.M., Di Simone, M., Avellone, C., Dieli, F., Iacopino, D.G., Brunasso, L., Cannarozzo, A., Costanzo, R., et al. (2025). γδ T Cells in Glioblastoma Multiforme: Novel Roles and Therapeutic Opportunities. Cancers *17*, 2660. https://doi.org/10.3390/cancers17162660.

75. Veglia, F., Sanseviero, E., and Gabrilovich, D.I. (2021). Myeloid-derived suppressor cells in the era of increasing myeloid cell diversity. Nat. Rev. Immunol. *21*, 485–498. https://doi.org/10.1038/s41577-020-00490-y.

76. Candolfi, M., Curtin, J.F., Yagiz, K., Assi, H., Wibowo, M.K., Alzadeh, G.E., Foulad, D., Muhammad, A.G., Salehi, S., Keech, N., et al. (2011). B Cells Are Critical to T-cell-Mediated Antitumor Immunity Induced by a Combined Immune-Stimulatory/Conditionally Cytotoxic Therapy for Glioblastoma. Neoplasia N. Y. N *13*, 947–960. https://doi.org/10.1593/neo.11024.

77. De Domenico, P., Gagliardi, F., Roncelli, F., Snider, S., and Mortini, P. (2025). Tumor-infiltrating and circulating B cells mediate local and systemic immunomodulatory mechanisms in Glioblastoma. J. Neurooncol. *172*, 527–548. https://doi.org/10.1007/s11060-025-04989-z.

78. Gao, J., Gu, D., Yang, K., Zhang, J., Lin, Q., Yuan, W., Zhu, X., Dixit, D., Gimple, R.C., You, H., et al. (2025). Infiltrating plasma cells maintain glioblastoma stem cells through IgG-Tumor binding. Cancer Cell *43*, 122-143.e8. https://doi.org/10.1016/j.ccell.2024.12.006.

79. Boccellato, C., and Rehm, M. (2022). Glioblastoma, from disease understanding towards optimal cell-based in vitro models. Cell. Oncol. Dordr. *45*, 527–541. https://doi.org/10.1007/s13402-022-00684-7.

80. Papaioannou, M.-D., Sangster, K., Sajid, R.S., Djuric, U., and Diamandis, P. (2020). Cerebral organoids: emerging ex vivo humanoid models of glioblastoma. Acta Neuropathol. Commun. *8*, 209. https://doi.org/10.1186/s40478-020-01077-3.

81. Liguori, G.L. (2025). Glioblastoma Models for Preclinical Assays: A Strengths, Weaknesses and Purpose Overview. Preprint at Preprints, https://doi.org/10.20944/preprints202508.1705.v1 https://doi.org/10.20944/preprints202508.1705.v1.

82. Yadav, N., and Purow, B.W. (2024). Understanding Current Experimental Models of Glioblastoma-Brain Microenvironment Interactions. J. Neurooncol. *166*, 213–229. https://doi.org/10.1007/s11060-023-04536-8.

83. Linkous, A., Balamatsias, D., Snuderl, M., Edwards, L., Miyaguchi, K., Milner, T., Reich, B., Cohen-Gould, L., Storaska, A., Nakayama, Y., et al. (2019). Modeling Patient-Derived Glioblastoma with Cerebral Organoids. Cell Rep. *26*, 3203-3211.e5. https://doi.org/10.1016/j.celrep.2019.02.063.

84. Jin, F., Jin-Lee, H.J., and Johnson, A.J. (2021). Mouse Models of Experimental Glioblastoma. In Gliomas, W. Debinski, ed. (Exon Publications).

85. Lenting, K., Verhaak, R., ter Laan, M., Wesseling, P., and Leenders, W. (2017). Glioma: experimental models and reality. Acta Neuropathol. (Berl.) *133*, 263–282. https://doi.org/10.1007/s00401-017-1671-4.

86. Malo, C.S., Khadka, R.H., Ayasoufi, K., Jin, F., AbouChehade, J.E., Hansen, M.J., Iezzi, R., Pavelko, K.D., and Johnson, A.J. (2018). Immunomodulation Mediated by Anti-angiogenic Therapy Improves CD8 T Cell Immunity Against Experimental Glioma. Front. Oncol. *8*, 320. https://doi.org/10.3389/fonc.2018.00320.

87. Tritz, Z.P., Orozco, R.C., Malo, C.S., Ayasoufi, K., Fain, C.E., Khadka, R.H., Goddery, E.N., Yokanovich, L.T., Settell, M.L., Hansen, M.J., et al. (2020). Conditional Silencing of H-2Db Class I Molecule Expression Modulates the Protective and Pathogenic Kinetics of Virus-Antigen-Specific CD8 T Cell Responses during Theiler's Virus Infection. J. Immunol. Baltim. Md 1950 *205*, 1228–1238. https://doi.org/10.4049/jimmunol.2000340.

88. Wouters, R., Bevers, S., Riva, M., De Smet, F., and Coosemans, A. (2020). Immunocompetent Mouse Models in the Search for Effective Immunotherapy in Glioblastoma. Cancers *13*, 19. https://doi.org/10.3390/cancers13010019.

89. Marumoto, T., Tashiro, A., Friedmann-Morvinski, D., Scadeng, M., Soda, Y., Gage, F.H., and Verma, I.M. (2009). Development of a novel mouse glioma model using lentiviral vectors. Nat. Med. *15*, 110–116. https://doi.org/10.1038/nm.1863.

90. Costa, B., Eisemann, T., Strelau, J., Spaan, I., Korshunov, A., Liu, H.-K., Bugert, P., Angel, P., and Peterziel, H. (2019). Intratumoral platelet aggregate formation in a murine preclinical glioma model depends on podoplanin expression on tumor cells. Blood Adv. *3*, 1092–1102. https://doi.org/10.1182/bloodadvances.2018015966.

91. Medikonda, R., Dunn, G., Rahman, M., Fecci, P., and Lim, M. (2021). A review of glioblastoma immunotherapy. J. Neurooncol. *151*, 41–53. https://doi.org/10.1007/s11060-020-03448-1.

92. Alghamri, M.S., Banerjee, K., Mujeeb, A.A., Mauser, A., Taher, A., Thalla, R., McClellan, B.L., Varela, M.L., Stamatovic, S.M., Martinez-Revollar, G., et al. (2022).

Systemic delivery of an adjuvant CXCR4-CXCL12 signaling inhibitor encapsulated in synthetic protein nanoparticles for glioma immunotherapy. ACS Nano *16*, 8729–8750. https://doi.org/10.1021/acsnano.1c07492.

93. Wei, R., Li, J., Lin, W., Pang, X., Yang, H., Lai, S., Wei, X., Jiang, X., Yuan, Y., and Yang, R. (2024). Nanoparticle-mediated blockade of CXCL12/CXCR4 signaling enhances glioblastoma immunotherapy: Monitoring early responses with MRI radiomics. Acta Biomater. *177*, 414–430. https://doi.org/10.1016/j.actbio.2024.02.007.

94. Cloughesy, T.F., Mochizuki, A.Y., Orpilla, J.R., Hugo, W., Lee, A.H., Davidson, T.B., Wang, A.C., Ellingson, B.M., Rytlewski, J.A., Sanders, C.M., et al. (2019). Neoadjuvant anti-PD-1 immunotherapy promotes a survival benefit with intratumoral and systemic immune responses in recurrent glioblastoma. Nat. Med. *25*, 477–486. https://doi.org/10.1038/s41591-018-0337-7.

95. Laureano, R.S., Vanmeerbeek, I., Sprooten, J., Govaerts, J., Naulaerts, S., and Garg, A.D. (2024). The cell stress and immunity cycle in cancer: Toward next generation of cancer immunotherapy. Immunol. Rev. *321*, 71–93. https://doi.org/10.1111/imr.13287.

96. Lee, A.H., Sun, L., Mochizuki, A.Y., Reynoso, J.G., Orpilla, J., Chow, F., Kienzler, J.C., Everson, R.G., Nathanson, D.A., Bensinger, S.J., et al. (2021). Neoadjuvant PD-1 blockade induces T cell and cDC1 activation but fails to overcome the immunosuppressive tumor associated macrophages in recurrent glioblastoma. Nat. Commun. *12*, 6938. https://doi.org/10.1038/s41467-021-26940-2.

97. Long, G.V., Shklovskaya, E., Satgunaseelan, L., Mao, Y., da Silva, I.P., Perry, K.A., Diefenbach, R.J., Gide, T.N., Shivalingam, B., Buckland, M.E., et al. (2025). Neoadjuvant triplet immune checkpoint blockade in newly diagnosed glioblastoma. Nat. Med. *31*, 1557–1566. https://doi.org/10.1038/s41591-025-03512-1.

98. Nabian, N., Ghalehtaki, R., Zeinalizadeh, M., Balaña, C., and Jablonska, P.A. (2024). State of the neoadjuvant therapy for glioblastoma multiforme—Where do we stand? Neuro-Oncol. Adv. *6*, vdae028. https://doi.org/10.1093/noajnl/vdae028.

99. Soh, J., Hamada, A., Fujino, T., and Mitsudomi, T. (2021). Perioperative Therapy for Non-Small Cell Lung Cancer with Immune Checkpoint Inhibitors. Cancers *13*. https://doi.org/10.3390/cancers13164035.

100. Frederico, S.C., Hancock, J.C., Brettschneider, E.E.S., Ratnam, N.M., Gilbert, M.R., and Terabe, M. (2021). Making a Cold Tumor Hot: The Role of Vaccines in the Treatment of Glioblastoma. Front. Oncol. *11*, 672508. https://doi.org/10.3389/fonc.2021.672508.

101. Cobbs, C.S., Harkins, L., Samanta, M., Gillespie, G.Y., Bharara, S., King, P.H., Nabors, L.B., Cobbs, C.G., and Britt, W.J. (2002). Human Cytomegalovirus Infection and Expression in Human Malignant Glioma1. Cancer Res. *62*, 3347–3350.

102. Dziurzynski, K., Chang, S.M., Heimberger, A.B., Kalejta, R.F., McGregor Dallas, S.R., Smit, M., Soroceanu, L., and Cobbs, C.S. (2012). Consensus on the role of human cytomegalovirus in glioblastoma. Neuro-Oncol. *14*, 246–255. https://doi.org/10.1093/neuonc/nor227.

103. Reap, E.A., Suryadevara, C.M., Batich, K.A., Sanchez-Perez, L., Archer, G.E., Schmittling, R.J., Norberg, P.K., Herndon, J.E., Healy, P., Congdon, K.L., et al. (2018). Dendritic cells enhance polyfunctionality of adoptively transferred T cells which target cytomegalovirus in glioblastoma. Cancer Res. *78*, 256–264. https://doi.org/10.1158/0008-5472.CAN-17-0469.

104. Vaz-Salgado, M.A., Villamayor, M., Albarrán, V., Alía, V., Sotoca, P., Chamorro, J., Rosero, D., Barrill, A.M., Martín, M., Fernandez, E., et al. (2023). Recurrent Glioblastoma: A Review of the Treatment Options. Cancers *15*, 4279. https://doi.org/10.3390/cancers15174279.

105. Hou, D., Katz, J.L., and Lee-Chang, C. (2023). Generation of B-cell-based cellular vaccine for cancer in murine models. STAR Protoc. *4*, 102219. https://doi.org/10.1016/j.xpro.2023.102219.

106. Lee-Chang, C., Miska, J., Hou, D., Rashidi, A., Zhang, P., Burga, R.A., Jusué-Torres, I., Xiao, T., Arrieta, V.A., Zhang, D.Y., et al. (2020). Activation of 4-1BBL+ B cells with CD40 agonism and IFNγ elicits potent immunity against glioblastoma. J. Exp. Med. *218*, e20200913. https://doi.org/10.1084/jem.20200913.

107. Perez, O.D., Logg, C.R., Hiraoka, K., Diago, O., Burnett, R., Inagaki, A., Jolson, D., Amundson, K., Buckley, T., Lohse, D., et al. (2012). Design and selection of Toca 511 for clinical use: modified retroviral replicating vector with improved stability and gene expression. Mol. Ther. J. Am. Soc. Gene Ther. *20*, 1689–1698. https://doi.org/10.1038/mt.2012.83.

108. Al-Shammari, A.M., and Piccaluga, P.P. (2023). Editorial: Oncolytic virotherapy. Front. Mol. Biosci. *10*. https://doi.org/10.3389/fmolb.2023.1287885.

109. Davison, A.J., Eberle, R., Ehlers, B., Hayward, G.S., McGeoch, D.J., Minson, A.C., Pellett, P.E., Roizman, B., Studdert, M.J., and Thiry, E. (2009). The Order Herpesvirales. Arch. Virol. *154*, 171–177. https://doi.org/10.1007/s00705-008-0278-4.

110. Denes, C.E., Everett, R.D., and Diefenbach, R.J. (2020). Tour de Herpes: Cycling Through the Life and Biology of HSV-1. In Herpes Simplex Virus : Methods and Protocols, R. J. Diefenbach and C. Fraefel, eds. (Springer), pp. 1–30. https://doi.org/10.1007/978-1-4939-9814-2_1.

111. Jambunathan, N., Clark, C.M., Musarrat, F., Chouljenko, V.N., Rudd, J., and Kousoulas, K.G. (2021). Two Sides to Every Story: Herpes Simplex Type-1 Viral

Glycoproteins gB, gD, gH/gL, gK, and Cellular Receptors Function as Key Players in Membrane Fusion. Viruses *13*, 1849. https://doi.org/10.3390/v13091849.

112. Ahmad, I., and Wilson, D.W. (2020). HSV-1 Cytoplasmic Envelopment and Egress. Int. J. Mol. Sci. *21*, 5969. https://doi.org/10.3390/ijms21175969.

113. Döhner, K., Cornelius, A., Serrero, M.C., and Sodeik, B. (2021). The journey of herpesvirus capsids and genomes to the host cell nucleus. Curr. Opin. Virol. *50*, 147–158. https://doi.org/10.1016/j.coviro.2021.08.005.

114. Aldrak, N., Alsaab, S., Algethami, A., Bhere, D., Wakimoto, H., Shah, K., Alomary, M.N., and Zaidan, N. (2021). Oncolytic Herpes Simplex Virus-Based Therapies for Cancer. Cells *10*, 1541. https://doi.org/10.3390/cells10061541.

115. Shen, Y., and Nemunaitis, J. (2006). Herpes simplex virus 1 (HSV-1) for cancer treatment. Cancer Gene Ther. *13*, 975–992. https://doi.org/10.1038/sj.cgt.7700946.

116. Chiocca, E.A., Nakashima, H., Kasai, K., Fernandez, S.A., and Oglesbee, M. (2020). Preclinical Toxicology of rQNestin34.5v.2: An Oncolytic Herpes Virus with Transcriptional Regulation of the ICP34.5 Neurovirulence Gene. Mol. Ther. Methods Clin. Dev. *17*, 871–893. https://doi.org/10.1016/j.omtm.2020.03.028.

117. Paolo, D., Maxime, D., Judit, S.G., Cédric, L., Alexandre, H., Benoit, B., Arnaud, L., Bernard, R., Virginie, N., Marielle, L., et al. (2025). An oncolytic herpesvirus expressing a CXCR4 antagonist interferes with glioblastoma cells' stemness features and migration. Mol. Ther. Oncol. *33*, 201083. https://doi.org/10.1016/j.omton.2025.201083.

118. Ding, J., Murad, Y.M., Sun, Y., Lee, I.-F., Samudio, I., Liu, X., Jia, W.W.-G., and Zhao, R. (2022). Pre-Existing HSV-1 Immunity Enhances Anticancer Efficacy of a Novel Immune-Stimulating Oncolytic Virus. Viruses *14*, 2327. https://doi.org/10.3390/v14112327.

119. Ghonime, M.G., Saini, U., Kelly, M.C., Roth, J.C., Wang, P.-Y., Chen, C.-Y., Miller, K., Hernandez-Aguirre, I., Kim, Y., Mo, X., et al. (2021). Eliciting an immune-mediated antitumor response through oncolytic herpes simplex virus-based shared antigen expression in tumors resistant to viroimmunotherapy. J. Immunother. Cancer *9*. https://doi.org/10.1136/jitc-2021-002939.

120. Harfouche, M., AlMukdad, S., Alareeki, A., Osman, A.M.M., Gottlieb, S., Rowley, J., Abu-Raddad, L.J., and Looker, K.J. (2024). Estimated global and regional incidence and prevalence of herpes simplex virus infections and genital ulcer disease in 2020: mathematical modelling analyses. Sex. Transm. Infect. *101*, e056307. https://doi.org/10.1136/sextrans-2024-056307.

121. Liu, T.-C., Zhang, T., Fukuhara, H., Kuroda, T., Todo, T., Martuza, R.L., Rabkin, S.D., and Kurtz, A. (2006). Oncolytic HSV Armed with Platelet Factor 4, an Antiangiogenic

Agent, Shows Enhanced Efficacy. Mol. Ther. *14*, 789–797. https://doi.org/10.1016/j.ymthe.2006.07.011.

122. Noh, M.H., Kang, J.M., Miller, A.A., Nguyen, G., Huang, M., Shim, J.S., Bueso-Perez, A.J., Murphy, S.A., Rivera-Caraballo, K.A., Otani, Y., et al. (2024). Targeting IGF2 to reprogram the tumor microenvironment for enhanced viro-immunotherapy. Neuro-Oncol. *26*, 1602–1616. https://doi.org/10.1093/neuonc/noae105.

123. Sanchez Gil, J., Dubois, M., Neirinckx, V., Lombard, A., Coppieters, N., D'Arrigo, P., Isci, D., Aldenhoff, T., Brouwers, B., Lassence, C., et al. (2022). Nanobody-based retargeting of an oncolytic herpesvirus for eliminating CXCR4+ GBM cells: A proof of principle. Mol. Ther. Oncolytics *26*, 35–48. https://doi.org/10.1016/j.omto.2022.06.002.

124. Sette, P., Amankulor, N., Li, A., Marzulli, M., Leronni, D., Zhang, M., Goins, W.F., Kaur, B., Bolyard, C., Cripe, T.P., et al. (2019). GBM-Targeted oHSV Armed with Matrix Metalloproteinase 9 Enhances Anti-tumor Activity and Animal Survival. Mol. Ther. Oncolytics *15*, 214–222. https://doi.org/10.1016/j.omto.2019.10.005.

125. Zhang, W., Fulci, G., Wakimoto, H., Cheema, T.A., Buhrman, J.S., Jeyaretna, D.S., Stemmer Rachamimov, A.O., Rabkin, S.D., and Martuza, R.L. (2013). Combination of Oncolytic Herpes Simplex Viruses Armed with Angiostatin and IL-12 Enhances Antitumor Efficacy in Human Glioblastoma Models. Neoplasia N. Y. N *15*, 591–599. https://doi.org/10.1593/neo.13158.

126. Loetscher, M., Geiser, T., O'Reilly, T., Zwahlen, R., Baggiolini, M., and Moser, B. (1994). Cloning of a human seven-transmembrane domain receptor, LESTR, that is highly expressed in leukocytes. J. Biol. Chem. *269*, 232–237. https://doi.org/10.1016/S0021-9258(17)42339-8.

127. Feng, Y., Broder, C.C., Kennedy, P.E., and Berger, E.A. (1996). HIV-1 entry cofactor: functional cDNA cloning of a seven-transmembrane, G protein-coupled receptor. Science *272*, 872–877. https://doi.org/10.1126/science.272.5263.872.

128. Mason, D., André, P., Bensussan, A., Buckley, C., Civin, C., Clark, E., de Haas, M., Goyert, S., Hadam, M., Hart, D., et al. (2001). CD Antigens 2001: Aims and Results of HLDA Workshops. Stem Cells *19*, 556–562. https://doi.org/10.1634/stemcells.19-6-556.

129. Oberlin, E., Amara, A., Bachelerie, F., Bessia, C., Virelizier, J.L., Arenzana-Seisdedos, F., Schwartz, O., Heard, J.M., Clark-Lewis, I., Legler, D.F., et al. (1996). The CXC chemokine SDF-1 is the ligand for LESTR/fusin and prevents infection by T-cell-line-adapted HIV-1. Nature *382*, 833–835. https://doi.org/10.1038/382833a0.

130. Nagasawa, T., Kikutani, H., and Kishimoto, T. (1994). Molecular cloning and structure of a pre-B-cell growth-stimulating factor. Proc. Natl. Acad. Sci. U. S. A. *91*, 2305–2309. https://doi.org/10.1073/pnas.91.6.2305.

131. Tashiro, K., Tada, H., Heilker, R., Shirozu, M., Nakano, T., and Honjo, T. (1993). Signal sequence trap: a cloning strategy for secreted proteins and type I membrane proteins. Science *261*, 600–603. https://doi.org/10.1126/science.8342023.

132. Ma, Q., Jones, D., Borghesani, P.R., Segal, R.A., Nagasawa, T., Kishimoto, T., Bronson, R.T., and Springer, T.A. (1998). Impaired B-lymphopoiesis, myelopoiesis, and derailed cerebellar neuron migration in CXCR4- and SDF-1-deficient mice. Proc. Natl. Acad. Sci. U. S. A. *95*, 9448–9453. https://doi.org/10.1073/pnas.95.16.9448.

133. Crump, M.P., Gong, J.H., Loetscher, P., Rajarathnam, K., Amara, A., Arenzana-Seisdedos, F., Virelizier, J.L., Baggiolini, M., Sykes, B.D., and Clark-Lewis, I. (1997). Solution structure and basis for functional activity of stromal cell-derived factor-1; dissociation of CXCR4 activation from binding and inhibition of HIV-1. EMBO J. *16*, 6996–7007. https://doi.org/10.1093/emboj/16.23.6996.

134. Mezzapelle, R., De Marchis, F., Passera, C., Leo, M., Brambilla, F., Colombo, F., Casalgrandi, M., Preti, A., Zambrano, S., Castellani, P., et al. (2021). CXCR4 engagement triggers CD47 internalization and antitumor immunization in a mouse model of mesothelioma. EMBO Mol. Med. *13*, e12344. https://doi.org/10.15252/emmm.202012344.

135. Smaldone, G., Di Matteo, F., Castelluccio, R., Napolitano, V., Miranda, M.R., Manfra, M., Campiglia, P., and Vestuto, V. (2025). Targeting the CXCR4/CXCL12 Axis in Cancer Therapy: Analysis of Recent Advances in the Development of Potential Anticancer Agents. Molecules *30*, 1380. https://doi.org/10.3390/molecules30061380.

136. Maksym, R.B., Tarnowski, M., Grymula, K., Tarnowska, J., Wysoczynski, M., Liu, R., Czerny, B., Ratajczak, J., Kucia, M., and Ratajczak, M.Z. (2009). THE ROLE OF STROMAL DERIVED FACTOR-1 – CXCR7 AXIS IN DEVELOPMENT AND CANCER. Eur. J. Pharmacol. *625*, 31–40. https://doi.org/10.1016/j.ejphar.2009.04.071.

137. Würth, R., Bajetto, A., Harrison, J.K., Barbieri, F., and Florio, T. (2014). CXCL12 modulation of CXCR4 and CXCR7 activity in human glioblastoma stem-like cells and regulation of the tumor microenvironment. Front. Cell. Neurosci. *8*, 144. https://doi.org/10.3389/fncel.2014.00144.

138. Zou, Y.-R., Kottmann, A.H., Kuroda, M., Taniuchi, I., and Littman, D.R. (1998). Function of the chemokine receptor CXCR4 in haematopoiesis and in cerebellar development. Nature *393*, 595–599. https://doi.org/10.1038/31269.

139. Nagasawa, T., Hirota, S., Tachibana, K., Takakura, N., Nishikawa, S., Kitamura, Y., Yoshida, N., Kikutani, H., and Kishimoto, T. (1996). Defects of B-cell lymphopoiesis and bone-marrow myelopoiesis in mice lacking the CXC chemokine PBSF/SDF-1. Nature *382*, 635–638. https://doi.org/10.1038/382635a0.

140. Ma, Q., Jones, D., and Springer, T.A. (1999). The Chemokine Receptor CXCR4 Is Required for the Retention of B Lineage and Granulocytic Precursors within the Bone Marrow Microenvironment. Immunity *10*, 463–471. https://doi.org/10.1016/S1074-7613(00)80046-1.

141. Bleul, C.C., Fuhlbrigge, R.C., Casasnovas, J.M., Aiuti, A., and Springer, T.A. (1996). A highly efficacious lymphocyte chemoattractant, stromal cell-derived factor 1 (SDF-1). J. Exp. Med. *184*, 1101–1109. https://doi.org/10.1084/jem.184.3.1101.

142. Aiuti, A., Webb, I.J., Bleul, C., Springer, T., and Gutierrez-Ramos, J.C. (1997). The Chemokine SDF-1 Is a Chemoattractant for Human CD34+ Hematopoietic Progenitor Cells and Provides a New Mechanism to Explain the Mobilization of CD34+ Progenitors to Peripheral Blood. J. Exp. Med. *185*, 111–120. https://doi.org/10.1084/jem.185.1.111.

143. Tachibana, K., Hirota, S., Iizasa, H., Yoshida, H., Kawabata, K., Kataoka, Y., Kitamura, Y., Matsushima, K., Yoshida, N., Nishikawa, S., et al. (1998). The chemokine receptor CXCR4 is essential for vascularization of the gastrointestinal tract. Nature *393*, 591–594. https://doi.org/10.1038/31261.

144. Domanska, U.M., Kruizinga, R.C., Nagengast, W.B., Timmer-Bosscha, H., Huls, G., Vries, E.G.E. de, and Walenkamp, A.M.E. (2013). A review on CXCR4/CXCL12 axis in oncology: No place to hide. Eur. J. Cancer *49*, 219–230. https://doi.org/10.1016/j.ejca.2012.05.005.

145. Bianchi, M.E., and Mezzapelle, R. (2020). The Chemokine Receptor CXCR4 in Cell Proliferation and Tissue Regeneration. Front. Immunol. *11*, 2109. https://doi.org/10.3389/fimmu.2020.02109.

146. Cai, X., Chen, R., Ma, K., Wang, F., Zhou, Y., Wang, Y., and Jiang, T. (2020). Identification of the CXCL12–CXCR4/CXCR7 axis as a potential therapeutic target for immunomodulating macrophage polarization and foreign body response to implanted biomaterials. Appl. Mater. Today *18*, 100454. https://doi.org/10.1016/j.apmt.2019.100454.

147. Cojoc, M., Peitzsch, C., Trautmann, F., Polishchuk, L., Telegeev, G.D., and Dubrovska, A. (2013). Emerging targets in cancer management: role of the CXCL12/CXCR4 axis. OncoTargets Ther. *6*, 1347–1361. https://doi.org/10.2147/OTT.S36109.

148. Décaillot, F.M., Kazmi, M.A., Lin, Y., Ray-Saha, S., Sakmar, T.P., and Sachdev, P. (2011). CXCR7/CXCR4 Heterodimer Constitutively Recruits β-Arrestin to Enhance Cell Migration. J. Biol. Chem. *286*, 32188–32197. https://doi.org/10.1074/jbc.M111.277038.

149. Pozzobon, T., Goldoni, G., Viola, A., and Molon, B. (2016). CXCR4 signaling in health and disease. Immunol. Lett. *177*, 6–15. https://doi.org/10.1016/j.imlet.2016.06.006.

150. Bachelerie, F., Ben-Baruch, A., Burkhardt, A.M., Combadiere, C., Farber, J.M., Graham, G.J., Horuk, R., Sparre-Ulrich, A.H., Locati, M., Luster, A.D., et al. (2014). International Union of Pharmacology. LXXXIX. Update on the Extended Family of Chemokine Receptors and Introducing a New Nomenclature for Atypical Chemokine Receptors. Pharmacol. Rev. *66*, 1–79. https://doi.org/10.1124/pr.113.007724.

151. Balabanian, K., Lagane, B., Infantino, S., Chow, K.Y.C., Harriague, J., Moepps, B., Arenzana-Seisdedos, F., Thelen, M., and Bachelerie, F. (2005). The Chemokine SDF-1/CXCL12 Binds to and Signals through the Orphan Receptor RDC1 in T Lymphocytes*. J. Biol. Chem. *280*, 35760–35766. https://doi.org/10.1074/jbc.M508234200.

152. Burns, J.M., Summers, B.C., Wang, Y., Melikian, A., Berahovich, R., Miao, Z., Penfold, M.E.T., Sunshine, M.J., Littman, D.R., Kuo, C.J., et al. (2006). A novel chemokine receptor for SDF-1 and I-TAC involved in cell survival, cell adhesion, and tumor development. J. Exp. Med. *203*, 2201–2213. https://doi.org/10.1084/jem.20052144.

153. Isci, D. (2024). Multilevel investigation of the atypical chemokine receptor 3 (ACKR3) expression and function in glioblastoma.

154. Chen, R., Kang, R., and Tang, D. (2022). The mechanism of HMGB1 secretion and release. Exp. Mol. Med. *54*, 91–102. https://doi.org/10.1038/s12276-022-00736-w.

155. Tirone, M., Tran, N.L., Ceriotti, C., Gorzanelli, A., Canepari, M., Bottinelli, R., Raucci, A., Di Maggio, S., Santiago, C., Mellado, M., et al. (2018). High mobility group box 1 orchestrates tissue regeneration via CXCR4. J. Exp. Med. *215*, 303–318. https://doi.org/10.1084/jem.20160217.

156. Schiraldi, M., Raucci, A., Muñoz, L.M., Livoti, E., Celona, B., Venereau, E., Apuzzo, T., De Marchis, F., Pedotti, M., Bachi, A., et al. (2012). HMGB1 promotes recruitment of inflammatory cells to damaged tissues by forming a complex with CXCL12 and signaling via CXCR4. J. Exp. Med. *209*, 551–563. https://doi.org/10.1084/jem.20111739.

157. Shi, Y., Riese, D.J., and Shen, J. (2020). The Role of the CXCL12/CXCR4/CXCR7 Chemokine Axis in Cancer. Front. Pharmacol. *11*. https://doi.org/10.3389/fphar.2020.574667.

158. Ma, Z., Zhou, F., Jin, H., and Wu, X. (2024). Crosstalk between CXCL12/CXCR4/ACKR3 and the STAT3 Pathway. Cells *13*, 1027. https://doi.org/10.3390/cells13121027.

159. Lee, C.-C., Lai, J.-H., Hueng, D.-Y., Ma, H.-I., Chung, Y.-C., Sun, Y., Tsai, Y.-J., Wu, W.-B., and Chen, C.-L. (2013). Disrupting the CXCL12/CXCR4 axis disturbs the characteristics of glioblastoma stem-like cells of rat RG2 glioblastoma. Cancer Cell Int. *13*, 85. https://doi.org/10.1186/1475-2867-13-85.

160. Goffart, N., Kroonen, J., Di Valentin, E., Dedobbeleer, M., Denne, A., Martinive, P., and Rogister, B. (2015). Adult mouse subventricular zones stimulate glioblastoma stem cells specific invasion through CXCL12/CXCR4 signaling. Neuro-Oncol. *17*, 81–94. https://doi.org/10.1093/neuonc/nou144.

161. Donzella, G.A., Schols, D., Lin, S.W., Esté, J.A., Nagashima, K.A., Maddon, P.J., Allaway, G.P., Sakmar, T.P., Henson, G., DeClercq, E., et al. (1998). AMD3100, a small molecule inhibitor of HIV-1 entry via the CXCR4 co-receptor. Nat. Med. *4*, 72–77. https://doi.org/10.1038/nm0198-072.

162. D'Alterio, C., Barbieri, A., Portella, L., Palma, G., Polimeno, M., Riccio, A., Ieranò, C., Franco, R., Scognamiglio, G., Bryce, J., et al. (2012). Inhibition of stromal CXCR4 impairs development of lung metastases. Cancer Immunol. Immunother. CII *61*, 1713–1720. https://doi.org/10.1007/s00262-012-1223-7.

163. Rubin, J.B., Kung, A.L., Klein, R.S., Chan, J.A., Sun, Y., Schmidt, K., Kieran, M.W., Luster, A.D., and Segal, R.A. (2003). A small-molecule antagonist of CXCR4 inhibits intracranial growth of primary brain tumors. Proc. Natl. Acad. Sci. U. S. A. *100*, 13513–13518. https://doi.org/10.1073/pnas.2235846100.

164. Li, J.-K., Yu, L., Shen, Y., Zhou, L.-S., Wang, Y.-C., and Zhang, J.-H. (2008). Inhibition of CXCR4 activity with AMD3100 decreases invasion of human colorectal cancer cells in vitro. World J. Gastroenterol. WJG *14*, 2308–2313. https://doi.org/10.3748/wjg.14.2308.

165. Yoon, Y., Liang, Z., Zhang, X., Choe, M., Zhu, A., Cho, H.T., Shin, D.M., Goodman, M.M., Chen, Z. (Georgia), and Shim, H. (2007). CXC Chemokine Receptor-4 Antagonist Blocks Both Growth of Primary Tumor and Metastasis of Head and Neck Cancer in Xenograft Mouse Models. Cancer Res. *67*, 7518–7524. https://doi.org/10.1158/0008-5472.CAN-06-2263.

166. DiPersio, J.F., Micallef, I.N., Stiff, P.J., Bolwell, B.J., Maziarz, R.T., Jacobsen, E., Nademanee, A., McCarty, J., Bridger, G., and Calandra, G. (2009). Phase III Prospective Randomized Double-Blind Placebo-Controlled Trial of Plerixafor Plus Granulocyte Colony-Stimulating Factor Compared With Placebo Plus Granulocyte Colony-Stimulating Factor for Autologous Stem-Cell Mobilization and Transplantation for Patients With Non-Hodgkin's Lymphoma. J. Clin. Oncol. *27*, 4767–4773. https://doi.org/10.1200/JCO.2008.20.7209.

167. Kalatskaya, I., Berchiche, Y.A., Gravel, S., Limberg, B.J., Rosenbaum, J.S., and Heveker, N. (2009). AMD3100 Is a CXCR7 Ligand with Allosteric Agonist Properties. Mol. Pharmacol. *75*, 1240–1247. https://doi.org/10.1124/mol.108.053389.

168. Cao, T., Gu, Y., Yagmurlu, B., Yerraballa, H., Bertrand, S., Naya, L., Miller, K., Iv, M., Soltys, S., Patel, C., et al. (2024). A phase II study of plerixafor combined with whole brain

radiation therapy (WBRT) for patients with newly diagnosed glioblastoma. J. Clin. Oncol. *42*, 2075–2075. https://doi.org/10.1200/JCO.2024.42.16_suppl.2075.

169. Wen, P.Y. (2017). Phase I Study of Plerixafor (AMD3100) and Bevacizumab for Recurrent High-Grade Glioma (clinicaltrials.gov).

170. Neklyudova, O., Arlt, M.J.E., Brennecke, P., Thelen, M., Gvozdenovic, A., Kuzmanov, A., Robl, B., Botter, S.M., Born, W., and Fuchs, B. (2016). Altered CXCL12 expression reveals a dual role of CXCR4 in osteosarcoma primary tumor growth and metastasis. J. Cancer Res. Clin. Oncol. *142*, 1739–1750. https://doi.org/10.1007/s00432-016-2185-5.

171. Williams, S.A., Harata-Lee, Y., Comerford, I., Anderson, R.L., Smyth, M.J., and McColl, S.R. (2010). Multiple functions of CXCL12 in a syngeneic model of breast cancer. Mol. Cancer *9*, 250. https://doi.org/10.1186/1476-4598-9-250.

172. Lucchini, S., Nicholson, J.G., Zhang, X., Househam, J., Lim, Y.M., Mossner, M., Millner, T.O., Brandner, S., Graham, T., and Marino, S. (2025). A novel model of glioblastoma recurrence to identify therapeutic vulnerabilities. EMBO Mol. Med. *17*, 1325–1354. https://doi.org/10.1038/s44321-025-00237-z.

173. Zhao, D., Zhang, H., Uyar, R., Hossain, J.A., Miletic, H., Tonn, J.-C., Glass, R., and Kälin, R.E. (2021). Comparing Tumor Cell Invasion and Myeloid Cell Composition in Compatible Primary and Relapsing Glioblastoma. Cancers *13*, 3636. https://doi.org/10.3390/cancers13143636.

174. Lombard, A., Isci, D., Reuter, G., Di Valentin, E., Hego, A., Martin, D., Rogister, B., and Neirinckx, V. (2024). Development of an intraventricular adeno-associated virus-based labeling strategy for glioblastoma cells nested in the subventricular zone. Neuro-Oncol. Adv. *6*, vdae161. https://doi.org/10.1093/noajnl/vdae161.

175. De Gioia, R., Biella, F., Citterio, G., Rizzo, F., Abati, E., Nizzardo, M., Bresolin, N., Comi, G.P., and Corti, S. (2020). Neural Stem Cell Transplantation for Neurodegenerative Diseases. Int. J. Mol. Sci. *21*, 3103. https://doi.org/10.3390/ijms21093103.

176. Liu, Y., Zhou, F., Ali, H., Lathia, J.D., and Chen, P. (2024). Immunotherapy for glioblastoma: current state, challenges, and future perspectives. Cell. Mol. Immunol. *21*, 1354–1375. https://doi.org/10.1038/s41423-024-01226-x.

177. Todo, T., Ito, H., Ino, Y., Ohtsu, H., Ota, Y., Shibahara, J., and Tanaka, M. (2022). Intratumoral oncolytic herpes virus G47Δ for residual or recurrent glioblastoma: a phase 2 trial. Nat. Med. *28*, 1630–1639. https://doi.org/10.1038/s41591-022-01897-x.

178. Maruyama, Y., Sakurai, A., Noda, S., Fujiwara, Y., Okura, N., Takagi, T., Asano, J., and Honda, F. (2023). Regulatory Issues: PMDA – Review of Sakigake Designation Products: Oncolytic Virus Therapy with Delytact Injection (Teserpaturev) for Malignant Glioma. The Oncologist *28*, 664–670. https://doi.org/10.1093/oncolo/oyad041.

179. Khalsa, J.K., Cheng, N., Keegan, J., Chaudry, A., Driver, J., Bi, W.L., Lederer, J., and Shah, K. (2020). Immune phenotyping of diverse syngeneic murine brain tumors identifies immunologically distinct types. Nat. Commun. *11*, 3912. https://doi.org/10.1038/s41467-020-17704-5.

180. Kardani, K., Ghouse, S.M., Din Abdul Jabbar, M.A., Rajasubramanian, N., Sanchez Gil, J., Stemmer-Rachamimov, A., Soda, Y., Martuza, R.L., Hara, T., Wakimoto, H., et al. (2025). Immunocompetent murine glioblastoma stem-like cell models exhibiting distinct phenotypes. Neuro-Oncol. Adv. *7*, vdae215. https://doi.org/10.1093/noajnl/vdae215.

181. Wouters, R., Bevers, S., Riva, M., De Smet, F., and Coosemans, A. (2020). Immunocompetent Mouse Models in the Search for Effective Immunotherapy in Glioblastoma. Cancers *13*, 19. https://doi.org/10.3390/cancers13010019.

182. Bhatt, D.K., Janzen, T., Daemen, T., and Weissing, F.J. (2022). Modelling the spatial dynamics of oncolytic virotherapy in the presence of virus-resistant tumour cells. PLOS Comput. Biol. *18*, e1010076. https://doi.org/10.1371/journal.pcbi.1010076.

183. Franks, M.L., An, J.-H., and Leavenworth, J.W. (2024). The Role of Natural Killer Cells in Oncolytic Virotherapy: Friends or Foes? Vaccines *12*, 721. https://doi.org/10.3390/vaccines12070721.

184. Alvarez-Breckenridge, C.A., Yu, J., Price, R., Wojton, J., Pradarelli, J., Mao, H., Wei, M., Wang, Y., He, S., Hardcastle, J., et al. (2012). NK cells impede glioblastoma virotherapy via NKp30 and NKp46 natural cytotoxicity receptors. Nat. Med. *18*, 1827–1834. https://doi.org/10.1038/nm.3013.

185. Wang, S., Castro, B.A., Katz, J.L., Arrieta, V., Najem, H., Vazquez-Cervantes, G.I., Wan, H., Olson, I.E., Hou, D., Dapash, M., et al. B cell–based therapy produces antibodies that inhibit glioblastoma growth. J. Clin. Invest. *134*, e177384. https://doi.org/10.1172/JCI177384.

186. Schuessler, A., Smith, C., Beagley, L., Boyle, G.M., Rehan, S., Matthews, K., Jones, L., Crough, T., Dasari, V., Klein, K., et al. (2014). Autologous T-cell Therapy for Cytomegalovirus as a Consolidative Treatment for Recurrent Glioblastoma. Cancer Res. *74*, 3466–3476. https://doi.org/10.1158/0008-5472.CAN-14-0296.

187. Khader, S.A., Divangahi, M., Hanekom, W., Hill, P.C., Maeurer, M., Makar, K.W., Mayer-Barber, K.D., Mhlanga, M.M., Nemes, E., Schlesinger, L.S., et al. (2020). Targeting innate immunity for tuberculosis vaccination. https://doi.org/10.1172/JCI128877.

188. Sego, T.J., Aponte-Serrano, J., Ferrari Gianlupi, J., Heaps, S., Breithaupt, K., Brusch, L., Osborne, J., Quardokus, E., Plemper, R., and Glazier, J. (2020). A modular framework for multiscale multicellular spatial modeling of viral infection, immune response and drug therapy timing and efficacy in epithelial tissues https://doi.org/10.1101/2020.04.27.064139.

189. Charles A Janeway, J., Travers, P., Walport, M., and Shlomchik, M.J. (2001). Principles of innate and adaptive immunity. In Immunobiology: The Immune System in Health and Disease. 5th edition (Garland Science).

190. Reardon, D.A., Brandes, A.A., Omuro, A., Mulholland, P., Lim, M., Wick, A., Baehring, J., Ahluwalia, M.S., Roth, P., Bähr, O., et al. (2020). Effect of Nivolumab vs Bevacizumab in Patients With Recurrent Glioblastoma: The CheckMate 143 Phase 3 Randomized Clinical Trial. JAMA Oncol. *6*, 1003–1010. https://doi.org/10.1001/jamaoncol.2020.1024.

191. Aghi, M., Rabkin, S.D., and Martuza, R.L. (2007). Angiogenic Response Caused by Oncolytic Herpes Simplex Virus–Induced Reduced Thrombospondin Expression Can Be Prevented by Specific Viral Mutations or by Administering a Thrombospondin-Derived Peptide. Cancer Res. *67*, 440–444. https://doi.org/10.1158/0008-5472.CAN-06-3145.

192. Kurozumi, K., Hardcastle, J., Thakur, R., Shroll, J., Nowicki, M., Otsuki, A., Chiocca, E.A., and Kaur, B. (2008). Oncolytic HSV-1 Infection of Tumors Induces Angiogenesis and Upregulates CYR61. Mol. Ther. J. Am. Soc. Gene Ther. *16*, 1382–1391. https://doi.org/10.1038/mt.2008.112.

193. Saha, D., Rabkin, S.D., and Martuza, R.L. (2020). Temozolomide antagonizes oncolytic immunovirotherapy in glioblastoma. J. Immunother. Cancer *8*, e000345. https://doi.org/10.1136/jitc-2019-000345.

194. Gesundheit, B., Ben-David, E., Posen, Y., Ellis, R., Wollmann, G., Schneider, E.M., Aigner, K., Brauns, L., Nesselhut, T., Ackva, I., et al. (2020). Effective Treatment of Glioblastoma Multiforme With Oncolytic Virotherapy: A Case-Series. Front. Oncol. *10*, 702. https://doi.org/10.3389/fonc.2020.00702.

195. Bhatt, D.K., Janzen, T., Daemen, T., and Weissing, F.J. (2024). Effects of virus-induced immunogenic cues on oncolytic virotherapy. Sci. Rep. *14*, 28861. https://doi.org/10.1038/s41598-024-80542-8.

196. Stavrakaki, E., Everts, A., van den Hoogen, B.G., and Lamfers, M.L.M. (2025). The 16th International Oncolytic Virus Conference: Advancing oncolytic virotherapy by balancing anti-tumor and anti-viral immunity. Mol. Ther. Oncol. *33*, 200950. https://doi.org/10.1016/j.omton.2025.200950.